SANDIA REPORT
SAND89—2027 • UC—721
Unlimited Release
Printed December 1989

Performance Assessment Methodology Demonstration: Methodology Development for Evaluating Compliance With EPA 40 CFR 191, Subpart B, for the Waste Isolation Pilot Plant

Melvin G. Marietta, Sharla G. Bertram-Howery, D. R. (Rip) Anderson,
Kenneth F. Brinster, Robert V. Guzowski, Harold Iuzzolino, Robert P. Rechard

Prepared by
Sandia National Laboratories
Albuquerque, New Mexico 87185 and Livermore, California 94550
for the United States Department of Energy
under Contract DE-AC04-76DP00789

Issued by Sandia National Laboratories, operated for the United States Department of Energy by Sandia Corporation.

Available to DOE and DOE contractors from
Office of Scientific and Technical Information
PO Box 62
Oak Ridge, TN 37831

Prices available from (615) 576-8401, FTS 626-8401

Available to the public from
National Technical Information Service
US Department of Commerce
5285 Port Royal Rd
Springfield, VA 22161

NTIS price codes
Printed copy: A10
Microfiche copy: A01

SAND--89-2027

DE90 006421

SAND89-2027
Unlimited Release
Printed December 1989

PERFORMANCE ASSESSMENT METHODOLOGY DEMONSTRATION: METHODOLOGY DEVELOPMENT FOR EVALUATING COMPLIANCE WITH EPA 40 CFR 191, SUBPART B, FOR THE WASTE ISOLATION PILOT PLANT

Melvin G. Marietta
Sharla G. Bertram-Howery
D. R. (Rip) Anderson, Kenneth F. Brinster*, Robert V. Guzowski*,
Harold Iuzzolino**, Robert P. Rechard

Sandia National Laboratories
Albuquerque, NM 87185

ABSTRACT

This report describes a demonstration of the performance assessment methodology for the Waste Isolation Pilot Plant (WIPP) to be used in assessing compliance with the Environmental Protection Agency's Standard, *Environmental Radiation Protection Standards for the Management and Disposal of Spent Nuclear Fuel, High Level and Transuranic Radioactive Wastes* (40 CFR Part 191, Subpart B). This demonstration incorporates development and screening of potentially disruptive scenarios. A preliminary analysis of the WIPP disposal system's response to human intrusion scenarios produces preliminary complementary cumulative distribution functions (CCDFs) similar to those that will ultimately be used to assess the compliance of the WIPP with the Containment Requirements of the Standard. Preliminary estimates of scenario probabilities are used to construct two demonstration CCDFs. The conceptual model of the disposal system consists of geologic, hydrologic, and disposal system subsystems along with the physical and chemical processes associated with these subsystems. Parameter values defining the systems contain uncertainties and modeling approximations of such a disposal system contributes to those uncertainties. The WIPP compliance assessment methodology consists of a system of techniques and computer codes that estimate releases of radionuclides from the disposal system, incorporating analysis of the parameter uncertainties in the estimates. Demonstration CCDFs are presented, but are not yet credible enough to judge the probability of compliance of the WIPP with the EPA Standard. One CCDF, based primarily on conservative reference data and conservative conceptual models, exceeds EPA limits, and another CCDF that represents effects of possible engineered alternatives does not exceed EPA limits.

---

* Science Applications International Corporation
** Geo-Centers, Inc.

ACKNOWLEDGEMENTS

The authors gratefully acknowledge the scientists and engineers in the Waste Management Technology Department (6340) at Sandia National Laboratories for their assistance in developing and implementing the WIPP Compliance Assessment Methodology. The work of B. M. Butcher, E. J. Nowak, D. E. Munson, P. B. Davies, R. L. Beauheim, D. J. Borns, L. S. Gomez, L. H. Brush, R. L. Hunter, and other department staff, as well as M. S. Y. Chu of Waste Management System Division (6416) provides the basis for our efforts. W. Beyeler (SAIC), J. Schreiber (SAIC), D. Rudeen (NMERI) and R. McCurley (NMERI) contributed to the analyses.

We thank those whose review of the draft report provided insight and guidance for the final version:

Performance Assessment Peer Review Panel

- G. R. Heath, University of Washington
- R. J. Budnitz, Future Resources Associates, Inc.
- T. A. Cotton, J. K. Associates
- P. A. Domenico, Texas A & M University
- C. J. Mann, University of Illinois
- T. H. Pigford, University of California at Berkeley

Sandia National Laboratories

- J. E. Campbell, 6415
- R. D. Klett, 6341

The schedule for preparation and production of this *Methodology Demonstration* was demanding. We could not have met it without the support of Tech. Reps., Inc. personnel Debra Medina and John Stikar for editing; Darcy Pulliam, Chris Northrop and the Illustration Department for illustration and coordination; Debbie Rivard, Ona Bailey, Theresa Allen and Dolores Miera for word processing, and Debbie Marchand, Debbie Salgado, and the Production Department, all directed by Bob Jones of the Energy and Waste Management Department.

GLOSSARY

Access Fraction - Fractional volume of a saturated waste panel that is drained into an intrusion borehole in a specified time interval

ALGEBRA - Computer code that algebraically manipulates data in CAMDAT and **BLOT** - Mesh and curve plot code

Am - Americium

beta distribution - A useful model for random variates defined on a finite interval. The beta distribution permits representation of a wide variety of distributional shapes by selection of two shape parameters.

C2FINTRP - Computer code that interpolates boundary conditions from a coarse to fine mesh

CAM - Compliance Assessment Methodology

CAMCON - Compliance Assessment Methodology CONtroller

CAMDAT - Compliance Assessment Methodology DATa base

CCDF - Complementary cumulative distribution function

CCDFPLT - Computer code that calculates and plots the complementary cumulative distribution function

CFR - Code of Federal Regulations

CH-TRU Waste - Contact-Handled TRansUranic waste, packaged TRU waste whose external surface dose rate does not exceed 200 mrem per hour

Ci - Curie. A unit of radioactivity equal to the number of disintegrations per second of 1 pure gram of radium-226 (1 Ci = 3.7×10^{10} disintegrations/second)

cm - Centimeter

Darcy - A standard unit of permeability, and is defined by a medium for which a flow of 1 cm^3/s is obtained through a section of 1 cm^2, for a fluid viscosity of 1 cP and a pressure gradient of 1 atm/cm. One darcy is equal to 0.987×10^{-12} m^2.

DOE - The U. S. Department of Energy, established in 1978 as a successor to ERDA and the AEC

E1 - An event or scenario: intrusion of a borehole through a disposal panel into a pressurized brine occurrence in the Castile Formation

E2 - An event or scenario: intrusion of a borehole into a disposal panel.

E3 - An event: a withdrawal well into the Culebra Dolomite downgradient from the WIPP

E1E2 - A scenario: intrusion of a borehole through a disposal panel into a pressurized brine occurrence in the Castile Formation and another intrusion of a borehole into the same panel

E1E3 - A scenario: intrusion of a borehole through a disposal panel into a pressurized brine occurrence in the Castile Formation with a withdrawal well into the Culebra Dolomite downgradient from the WIPP

E1E2E3 - A scenario: intrusion of a borehole through a disposal panel into a pressurized brine occurrence in the Castile Formation and another intrusion of a borehole into the same panel with a withdrawal well into the Culebra Dolomite downgradient from the WIPP

E2E3 - A scenario: intrusion of a borehole into a disposal panel with a withdrawal well into the Culebra Dolomite downgradient from the WIPP

EPA - Environmental Protection Agency of the U.S. Government

F2CINTRP - Computer code that interpolates boundary conditions from a fine to coarse mesh

ft - Foot or feet

g - Gram(s)

GENMESH - Computer code that generates three-dimensional, finite-difference, meshes.

GENNET - Computer code that generates networks

GRIDGEOS - Computer code that interpolates observational hydrologic or geologic data onto computational meshes

HST3D - Computer code that simulates three-dimensional ground-water flow systems and heat and solute transport

Hydrodynamic Dispersion - A nonsteady, irreversible process, including molecular diffusion within the liquid phase and mechanical dispersion because of the presence of interconnected passages within the pore structure of the medium, by which a tracer mass mixes with its host liquid in a porous medium

karstification - Geologic process resulting in a topography formed over limestone dolomite or gypsum and characterized by sinkholes, caves, and underground drainage

kg - Kilogram(s)

km - Kilometer(s)

kriging - Geostatistical method for optimizing the estimation of a magnitude (e.g. hydrogeological parameters), which is distributed in space and is measured at a network of points

lb - Pound

LHS - Computer code that selects latin hypercube samples: A constrained Monte Carlo sampling scheme which samples n different values of a continuous random variate from n nonoverlapping intervals selected on the basis of equal probability

LOGNORMAL - The model for a random variable whose logarithm follows the normal distribution

LOGUNIFORM - The model for a random variable whose logarithm follows the uniform distribution

M - Molar (molarity): Concentration of a solution expressed as moles of solute per liter of solution.

MATSET - Computer code that sets material properties in CAMDAT

MB139 - Marker Bed 139: One of 45 siliceous or sulfatic units within the Salado Formation consisting of about 1 m of polyhalitic anhydrite and anhydrite. MB139 is located within the WIPP horizon.

MESHER3D - Computer code that generates three-dimensional grids/markers for finite difference or finite element codes

mg/ℓ - Milligrams per liter

mi - Mile(s)

Microdarcy (μd) - A unit of permeability (10^{-6} darcies)

Millidarcy (md) - A unit of permeability (10^{-3} darcies)

MPa - Megapascal (10^{6} Pa)

mrem - Millirem (10^{-3} rem)

nanodarcy - A unit of permeability (10^{-9} darcies)

NEA - Nuclear Energy Agency of the Office of Economic Cooperation and Development, Paris

NEFTRAN - Network flow and transport. Computer code that calculates flow and transport along one-dimensional legs comprising a flow network.

normal (or Gaussian) distribution - most widely used of all distributions providing a good representation for many physical variables. By the central limit theorem, if a random variable represents the effect of many small causes (addition of errors), its pdf is normal.

Np - Neptunium

PA - Performance assessment

Pa (pascal) - Basic unit of pressure produced by a force of 1 newton applied over an area of 1 m^2. One pound per square inch is equal to 6.895 x 10^3 Pa.

Pb - Lead

PCC/SRC - Computer code that calculates partial correlation and standardized regression coefficients

PDF - Probability density function of a continuous random variate x is the derivative with respect to x of the cumulative distribution function (the probability that x takes on a value equal to or less than some specified value of x). The pdf is generically called a distribution.

POSTHST - Post-processor computer code (translator) for HST3D

POSTLHS - Post-processor computer code (translator) for LHS

POSTSUTRA - Post-processor computer code (translator) for SUTRA

POSTSWIFT - Post-processor computer code (translator) for SWIFT II

PREHST - Pre-processor computer code (translator) for HST3D

PRELHS - Pre-processor computer code (translator) for LHS

PRENEF - Pre-processor computer code (translator) for NEFTRAN

PREPCC - Pre-processor computer code (translator) for PCC/SRC

PRESTEP - Pre-processor computer code (translator) for STEPWISE

PRESUTRA - Pre-processor computer code (translator) for SUTRA

PRESWIFT - Pre-processor computer code (translator) for SWIFT II

Pu - Plutonium

QA - Quality assurance

Ra - Radium

R_{acc} - Release of radioisotopes at the subsurface boundary of the accessible environment

rad - A basic unit of absorbed dose defined as an energy absorption of 100 erg/g of a specified material from any ionizing radiation.

R_c - Release of radioisotope-bearing cuttings and eroded material to the land surface during drilling of an intrusion borehole

rem - Roentgen equivalent man - a special unit of dose equivalent which is the product of absorbed dose, a quality factor which rates the biological effectiveness of the radiation types producing the dose, and other modifying factors (usually equal to one). If the quality and modifying factors are units, 1 rem is equal to 1 rad.

RESYSM - Repository/shaft system source term model

R_p - Release of radioisotope-bearing brine to the land surface through a withdrawal well in the Culebra Dolomite Member downgradient from the WIPP.

RH-TRU - Remotely-Handled TRansUranic waste. Packaged TRU waste whose external surface rate exceeds 200 mrem per hour, but not 1000 mrem per hour

SEIS - Supplemental environmental impact statement

SNL - Sandia National Laboratories

Stationarity - A stochastic process is said to be stationary in time (or space) if its set of associated pdfs (any statistical property) are invariant under arbitrary time (or space) translations

STEPWISE - Computer code that performs stepwise regression including rank regression

SUTRA - Finite-element simulation code that calculates saturated-unsaturated, fluid-density-dependent groundwater flow with energy transport or chemically reactive single-species solute transport

SWIFT II - Sandia Waste-Isolation Flow and Transport computer code that simulates saturated flow and heat, brine, and radionuclide chain transport in porous and fractured media

TC - A process for scenario construction - Unexpected climatic change

Th - Thorium

TRACKER - Code that tracks neutrally buoyant particles in a steady or transient flow

TS - A process for scenario construction - Conventional or solution mining of potash outside the land withdrawal boundary that results in areas of subsidence, which act as areas of recharge to underlying aquifers

U - Uranium

uniform distribution - A pdf that is a horizontal line, i.e. the model for the time of occurrence of an event that is equally likely to occur at any time during an interval.

WIPP - Waste Isolation Pilot Plant

CONTENTS

FIGURES

Page

TABLES

I. PURPOSE OF THE METHODOLOGY DEMONSTRATION

This report describes a demonstration of the performance assessment methodology for the Waste Isolation Pilot Plant (WIPP). The methodology is being developed for use in assessing compliance with the Environmental Protection Agency's (EPA) *Environmental Radiation Protection Standards for the Management and Disposal of Spent Nuclear Fuel, High-Level, and Transuranic Radioactive Wastes* (40 CFR Part 191, Subpart B) (U.S. EPA, 1985); hereafter called the Standard. The purpose of the methodology demonstration is to evaluate the performance of the computerized compliance assessment methodology (CAM) and the currently available computer codes. This has been accomplished by analyzing a "base case" scenario and other selected scenarios. Human-intrusion scenarios were identified early in the performance assessment (PA) program as being the critical set of scenarios for judging compliance. Therefore, scenarios analyzed here are selected as representative of the set of human-intrusion scenarios that would be used for the final compliance assessment.

Complementary cumulative distribution functions (CCDF) of the type that ultimately will be used to assess the status of compliance of the WIPP disposal system are compared to the Containment Requirements of the Standard (§ 191.13). The CCDFs in this report are only for demonstration purposes because they are constructed using incomplete scenarios, data, and models. These scenarios are expected to be representative of the final set, but they do not necessarily comprise a complete set. Final probabilities for these scenarios have not yet been assigned.

Some data sets are essentially complete and well understood, whereas other critically important data acquisition programs (e.g., radionuclide chemistry and gas generation) have just been initiated. Some computer codes that are used as modules within the CAM system are adequately sophisticated and have been partially validated, while others are still under development and cruder models have been used in the interim to approximate the final models. Therefore, the set of input parameters in these analyses is much smaller than the set of parameters to be sampled during the uncertainty analysis for the final performance assessment.

Remotely-handled transuranic (RH-TRU) waste is not considered in these preliminary uncertainty and sensitivity analyses because the inventory of individual radionuclides is not yet sufficiently accurate to support meaningful consequence analyses. The volume and curie (Ci) content of RH-TRU waste is small compared to contact-handled transuranic (CH-TRU) waste (Lappin et al., 1989), which is considered in this demonstration. Therefore, neither

the results nor the methodology demonstrated in this report is significantly affected by not including RH-TRU waste.

The CCDFs in this report may be considered as a "first look" at compliance, but should not be considered credible for judging the probability of compliance with EPA regulations. This report will be followed by a series of reports describing the systematic addition of computational modules to the CAM system and of parameters to the sampled set as their importance emerges from subsystem sensitivity analyses. That series of reports will quickly establish the WIPP Project's capability for assessing compliance using current data and understanding of the disposal system.

The methodology descriptions in this demonstration report are specific to the methodology demonstration; more complete descriptions are contained in another report, which is a forecast of the final compliance report's scope and format, produced in conjunction with this methodology demonstration (Bertram-Howery et al., 1989). That report will evolve into the final compliance report.

II. DEMONSTRATION APPROACH

The response of the disposal system to scenarios describing possible future conditions must be simulated in order to predict migration of radionuclides within the system and their release to the accessible environment. Simulation of disposal-system response requires characterization of the system and its components to determine important parameters. The Standard requires parameter uncertainty analysis using ranges and distributions for each parameter for which the value is uncertain. This chapter introduces the scenario development, disposal-system characterization, and parameter uncertainty analysis for the demonstration, followed by a brief discussion of the philosophy for compliance assessment methodology along with an overview description of that methodolgy. Also, inherent quality assurance of complex computer simulations, sensitivity analyses necessary to establish parameter importance, and potential need for multiple conceptual models to fully understand uncertainties associated with disposal systems are all briefly described.

SCENARIOS TO BE ANALYZED

For this preliminary analysis of the WIPP disposal system, preclassified events and processes (Cranwell et al., 1982a) are screened (Hunter, 1989) primarily on physical-reasonableness arguments. A total of 32 scenarios are constructed from the remaining events and processes through the use of a logic diagram. Screening of scenarios using physical-reasonableness arguments and elimination of duplicate scenarios reduces the number of potentially disruptive scenarios to 18, plus one for undisturbed conditions.

Scenarios consist of combinations of human-intrusion occurrences, extreme climatic change, and subsidence outside of the repository area resulting from potash mining. Additional screening criteria that are necessary but have not been used are probability of occurrence of each scenario and consequences (radionuclide release to the accessible environment) resulting from that occurrence. For consequence analysis, each scenario being analyzed is imposed upon the base-case scenario.

One product of constructing scenarios from logic diagrams is a base-case scenario. This scenario consists of geologic, hydrologic, and repository systems under conditions predicted to occur, including uncertainties, during the 10,000-yr regulatory period. Any event or process that is certain to occur is included in this base-case scenario. By definition, if the base-case scenario does not include human intrusions, it is then used to determine undisturbed performance. The preliminary scenario analysis of the WIPP disposal system (Bertram-Howery et al., 1989) indicates that the base-case

scenario does not contain human-intrusion events, and preliminary analyses of this scenario under expected conditions (Lappin et al., 1989) suggest that no releases of radionuclides to the accessible environment will occur in 10,000 years.

DISPOSAL SYSTEM CHARACTERIZATION

The disposal system consists of the repository, in which TRU radioactive waste will be stored, including the access shafts and drifts, and the surrounding geology and hydrology of the controlled area[1] (Figure 2-1). At the time of repository closure, all rooms and drifts in the repository as well as access shafts and drifts will have been backfilled with material specifically selected for each component of the disposal system. In addition, panel seals will have been emplaced in drifts and the underlying marker bed (MB139) at the locations indicated (Figure 2-2).

Characterization of the disposal system must provide the capability to model transport of radionuclides from rooms to the accessible environment. Pathways for this transport consist of migration through drifts or MB139 to shafts and upward to hydrostratigraphic units overlying the repository through which transport toward the accessible environment occurs. More direct pathways to the accessible environment at the surface above the repository or to the hydrostratigraphic units can be created as a result of human intrusion into the repository. The capability to model effects on the groundwater flow system of pressurized brine injection resulting from drilling into a pressurized brine occurrence must also be included.

The repository/shaft system can be described using a room component, a panel-seal component, an MB139-seal component, and a shaft-seal component (Bertram-Howery et al., 1989, Chapter II). Models of these components must include important processes and events that may affect groundwater flow and radionuclide transport. Models of the repository/shaft system's components have been assembled into a REpository/shaft SYstem Source term Model (RESYSM). The components of RESYSM consist of simple analytical to complex finite-element models depending on the amount of data available for the process, sensitivity of consequences to the process, or the capability to model the process given the present state of knowledge about it. These components can be used either individually or in combination depending on particular needs. The status of the various modeling aspects of each component of RESYSM is described elsewhere (Bertram-Howery et al., 1989, Chapter II).

1 The controlled area has not yet been defined. See Bertram-Howery and Hunter (1989), page II-2.

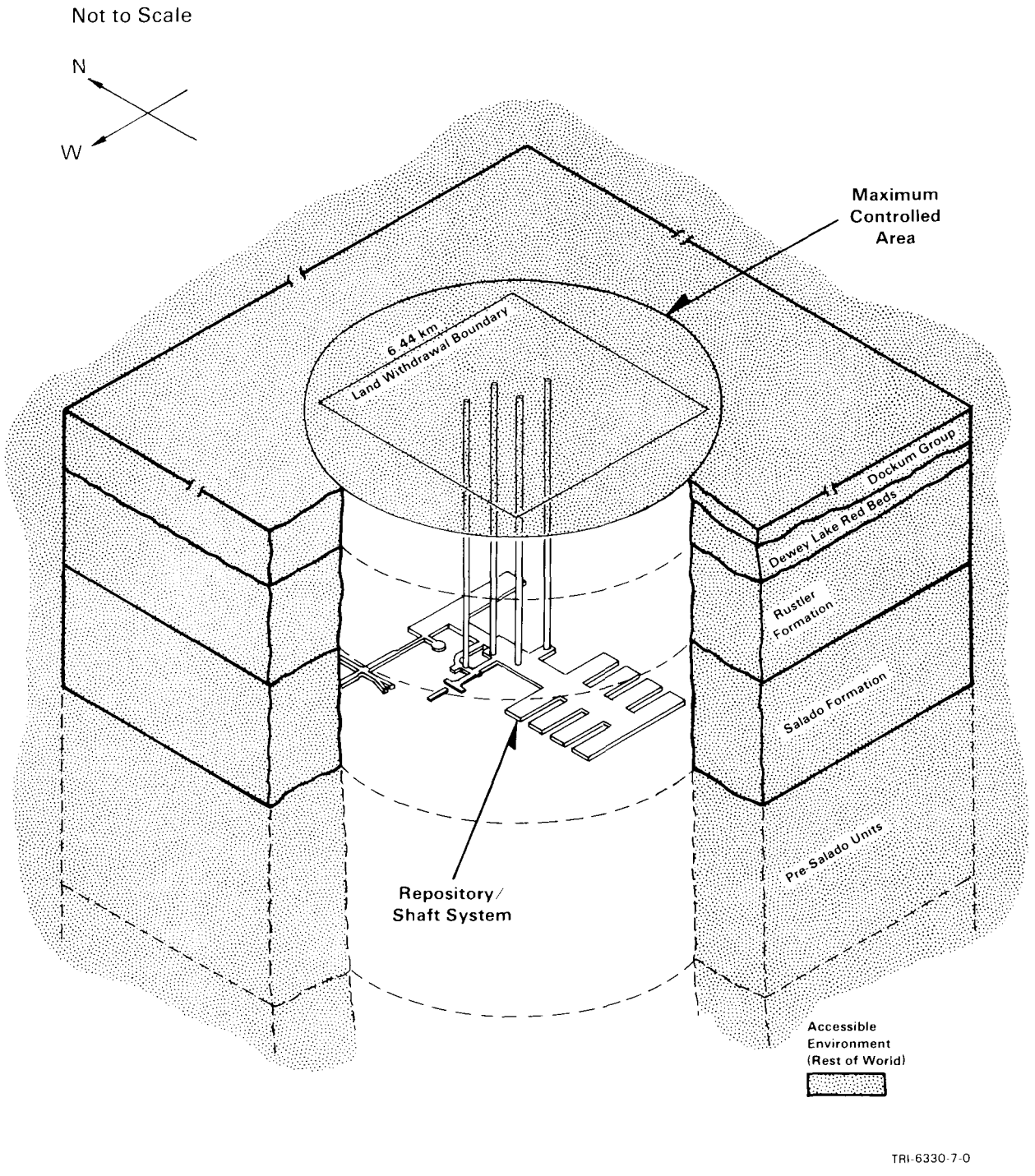

Figure 2-1. Disposal System: Repository/Shaft System and Controlled Area (Bertram-Howery and Hunter, 1989). The scale of the repository/shaft system is exaggerated.

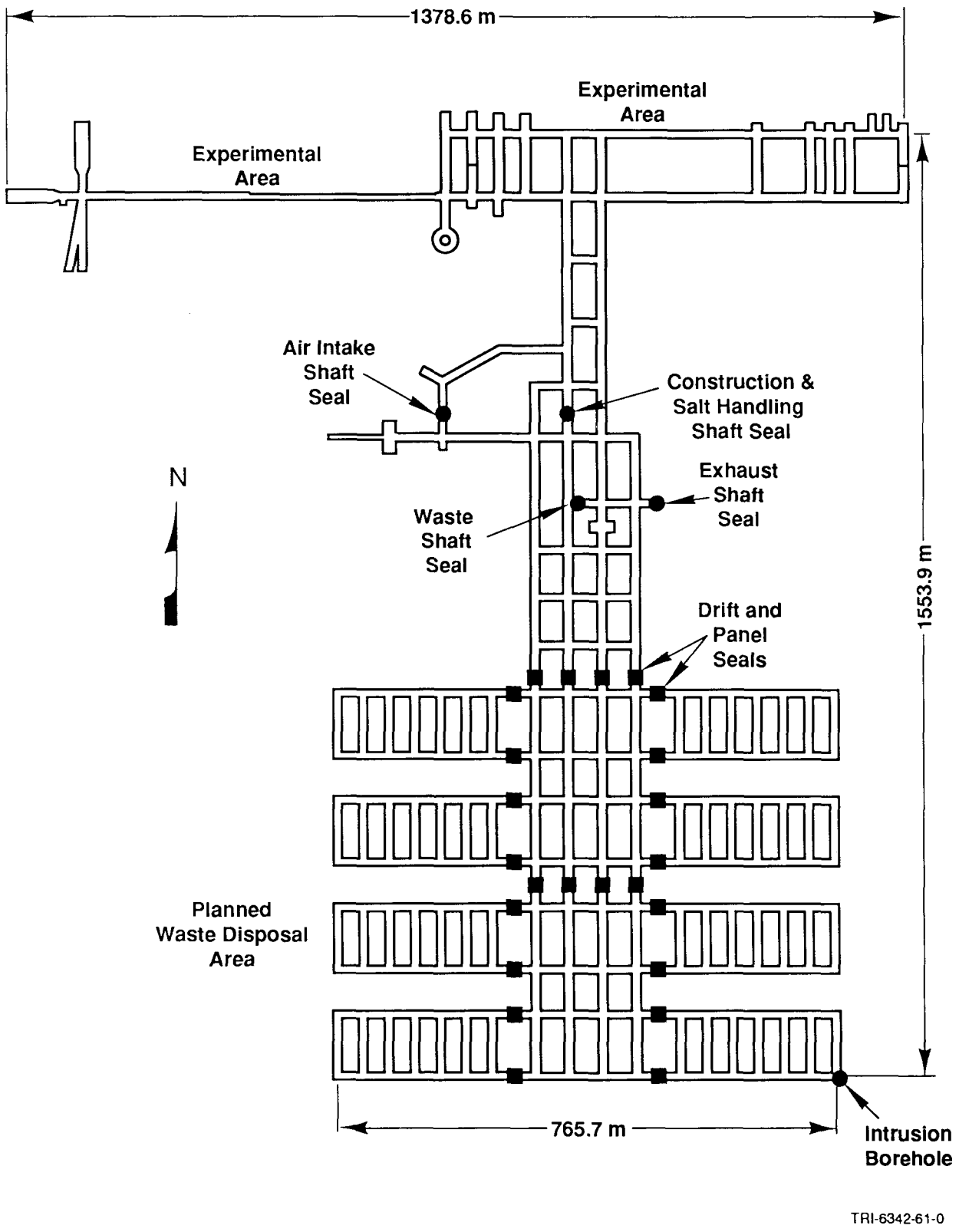

Figure 2-2. Location of Drift, Panel, and Shaft Seals (Modified from Lappin et al., 1989)

The SWIFT II (Sandia Waste-Isolation Flow and Transport) computer code is used to establish the groundwater flow field in the Culebra Dolomite Member (Figure 2-3) and to simulate injection of pressurized brine from the Castile Formation into the Culebra Dolomite Member. SWIFT II is a transient, three-dimensional code that solves equations for groundwater flow and radionuclide transport in both porous and fractured media. Fluid flow, heat transport, and dominant-species miscible displacement are used to establish the velocity field for radionuclide transport. The theory, implementation, data input, and basic limitations of the code are described elsewhere (Reeves et al., 1986a, 1986b). In this demonstration, SWIFT II is used to establish the flow field in the Culebra Dolomite both with and without injection of pressurized brine. The NEFTRAN code (NEtwork Flow and TRANsport; Campbell et al., 1981; Longsine et al., 1987) is used for radionuclide transport from the repository to the Culebra Dolomite Member and within the Culebra Dolomite to the accessible environment along particle trajectories determined using the flow fields from SWIFT II. Features of NEFTRAN pertinent to this demonstration have been summarized previously (Lappin et al., 1989, Appendix D).

Radionuclide migration is estimated downgradient 2.5 km (1.5 mi) and 5.0 km (3.0 mi) from the waste panels. These are approximate distances to the WIPP Project's proposed land withdrawal boundary and to the maximum allowable extent of the controlled area in the Standard (Figure 2-4).

PARAMETER UNCERTAINTY ANALYSIS AND THE STANDARD

Parameter values that define the geologic, hydrologic, and repository/shaft systems inherently contain uncertainty. These sources of data uncertainty are (1) incorrect or misapplied measurement techniques, (2) statistical reductions of measured data, (3) replacement of variable parameters with lumped parameters, (4) replacement of random parameters with deterministic parameters, and (5) misinterpretation of data (Cranwell and Bonano, 1987), as well as natural variability of the system. Modeling of these systems contributes additional sources of parameter uncertainty.

The need to consider uncertainty in predicted behavior, projected performance, and estimates of cumulative releases is recognized in the Standard in § 191.12(p), § 191.12(q)(3), § 191.13(b), and paragraphs 1 and 2 in Appendix B (U.S. EPA, 1985). Parameter uncertainty is mentioned only in paragraph 3 of that appendix, although parameter uncertainty is a major contributor to the other areas of uncertainty. Although uncertainties must be addressed, no guidance is provided in the Standard as to how this is to be accomplished.

The amount of variability in model results that can be attributed to the uncertainty or natural variability of the input data can be determined by a

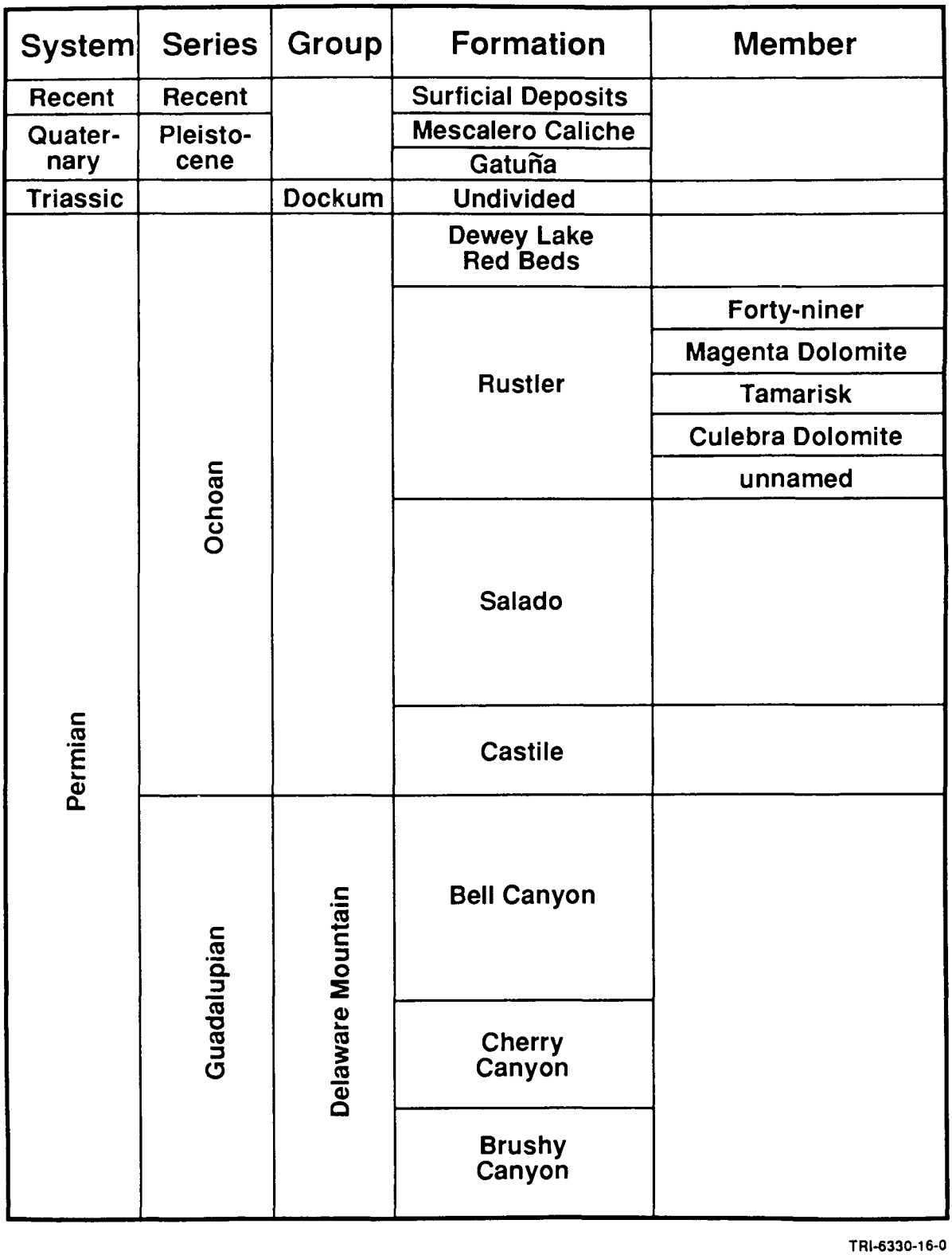

Figure 2-3. Generalized Stratigraphic Column of the Delaware Mountain Group and Younger Sedimentary Rocks Of and Near the WIPP Disposal System (Beauheim, 1987a).

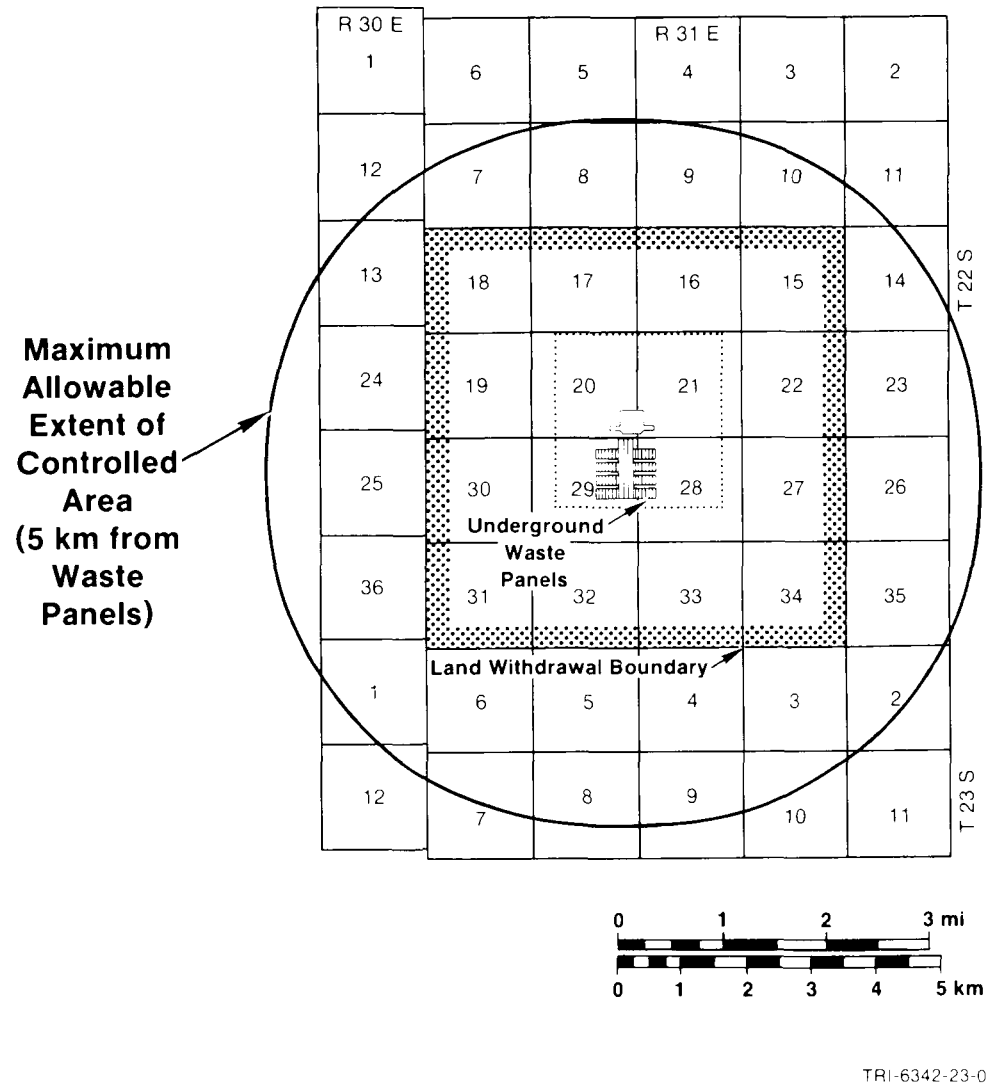

Figure 2-4. Location of the Underground Waste Panels Relative to the Proposed Land Withdrawal Boundary and the Maximum Allowable Extent of the Controlled Area Defined in the Standard (U.S. DOE, 1989b).

parameter uncertainty analysis. Several techniques that can be used to quantify parameter uncertainty are differential-analysis techniques, statistical methods, and stochastic modeling (Cranwell and Bonano, 1987). A study that compared several uncertainty and sensitivity analysis techniques concluded that latin hypercube sampling (LHS) with regression analysis provided the best overall results (Iman and Helton, 1985).

COMPLIANCE ASSESSMENT METHODOLOGY

The WIPP Project will assess compliance with the requirements of the Standard. The long-term performance requirements of Subpart B of the Standard are the focus of this methodology demonstration. For WIPP, two requirements must be met. The Containment Requirements (§ 191.13) limit cumulative releases of radioactive materials to the accessible environment for 10,000 years. The Individual Protection Requirements (§ 191.15) limit radiation doses to members of the public in the accessible environment for 1,000 years. First, the philosophy for assessing compliance of WIPP with these requirements is discussed. Second, a methodology for performing this assessment is briefly described.

PHILOSOPHY

The Containment Requirements

The Containment Requirements, § 191.13(a), specify that performance assessments must be used to determine whether cumulative releases to the accessible environment for 10,000 years after disposal from all significant processes and events that may affect the disposal system will meet specific release limits. Although the Standard does not specify how to demonstrate compliance, Appendix B suggests compliance can be determined by use of a CCDF. The WIPP performance assessment uses CCDFs to evaluate compliance (see Cranwell et al., 1982b; Pepping et al., 1983; Hunter et al., 1986; Campbell and Cranwell, 1988; and Rechard, 1989).

A performance assessment methodology consists of the following parts (Cranwell et al., 1982b; Hunter et al., 1986): (1) procedures for scenario development; (2) models for use in determining releases to the accessible environment; and (3) a procedure to assess compliance with the regulatory requirements.

Several different techniques have been proposed for development of scenarios. The basic steps are summarized as follows: (1) identifying a comprehensive list of events and processes that may affect the long-term isolation of the radioactive waste; (2) a classification of events and processes to aid in

completeness arguments; (3) a screening of events and processes based on well-defined criteria; (4) construction of scenarios by combining remaining events and processes; and (5) screening scenarios by well-defined criteria (Cranwell and Helton, 1980; Cranwell and Helton, 1981; Cranwell et al., 1982a). Appendix B of the Standard indicates that individual events and processes, and by implication their combined form as scenarios, do not have to be considered in performance assessment if their probability of occurrence is less than one chance in 10,000 of occurring in 10,000 years, or if their omission is not expected to change significantly the probability density function (pdf) for cumulative releases. Another screening criterion is the physical reasonableness of the event or process and of combinations of events and processes in scenarios for a specific disposal system.

The goal of the scenario-development procedure is to develop a comprehensive set of mutually exclusive scenarios that could result in release of radionuclides to the accessible environment. To initiate an analysis, physical processes being modeled are carefully defined, and conceptual and mathematical models are developed so that processes are described adequately over the range of conditions to be modeled. These models are relatively simplified representations of the real system. For these models to be credible, all phenomena and parameters that are shown to be important through sensitivity analyses must be included. All assumptions must be understood and accepted as reasonable.

An important aspect of model development and application is model verification and validation. Verification ensures that the model correctly performs the operations specified in the numerical procedures. Verification does not assess the physical correctness of the solution, therefore, a model is verified when it numerically solves the specified problem correctly. Model validation is the procedure that addresses physical correctness. Validation usually involves a test of the model output against available data to ensure that the model is a correct representation of natural processes or systems for which it is intended. Such tests evaluate both the mathematical and related conceptual models. Few models that describe environmental systems can ever be fully validated on the space and time scales of interest. Rather, model adequacy for the particular application is a subjective judgment of the analyst based on partial validation exercises.

In principle, models used for performance assessment can be either deterministic or stochastic. Deterministic models do not explicitly account for uncertainties, whereas stochastic models do. Models currently being considered for use in the WIPP performance assessment are all deterministic because stochastic models are not available. Additional error is introduced in deterministic calculations when processes that are actually stochastic are included as deterministic assumptions. Monte-Carlo sampling techniques can be

used with systems of deterministic models to perform stochastic analyses that evaluate effects of these uncertainties as demonstrated in this report.

The physical processes by which radioactive material can be released to the accessible environment are complex. As a result, models being used for the WIPP performance assessment are generally complex and results of consequence estimates have large uncertainties associated with them. In general, as stated above, uncertainty in consequence modeling has two components: model uncertainty and data uncertainty (Cranwell and Helton, 1981). Model uncertainty is partially addressed by verification and validation. However, there are always unquantifiable uncertainties associated with judging model adequacy. Because validation of environmental models on the time scales of interest is impossible, model uncertainty must ultimately be assessed by subjective judgments based on partial model validation. In WIPP performance assessment, data uncertainties are handled by first selecting ranges and distributions for each parameter and then using a statistical sampling procedure to select parameter values for each deterministic calculation. Many sampled values are used to generate a distribution of consequence values, and the range and distribution of these values reflect data uncertainty.

The Individual Protection Requirements

The Individual Protection Requirements (§ 191.15) specify that whole-body and critical-organ doses must be calculated for radionuclide releases to the accessible environment from all pathways assuming undisturbed conditions during the first 1,000 years after disposal. One product of scenario development for the Containment Requirements will be a scenario for undisturbed conditions. Techniques for analyzing this scenario are simple modifications of those required by the Containment Requirements. If releases to the accessible environment are predicted, compliance with the Standard will be evaluated using pathway and dosimetry models.

METHODOLOGY OVERVIEW

The WIPP compliance assessment methodology contains procedures and tools necessary for implementing the compliance assessment philosophy outlined under Philosophy. Modifying the three parts of a performance assessment listed above, the WIPP methodology (Rechard, 1989) consists of (1) disposal system and regional site characterization, (2) techniques for scenario development and probability estimates, (3) computer codes for consequence modeling, (4) statistical techniques for uncertainty and sensitivity analyses, and (5) a procedure that assembles the above results into a CCDF for compliance assessment. This methodology (Figure 2-5) was developed at Sandia National Laboratories (SNL) for high-level-waste disposal in repositories in bedded salt (Cranwell et al., 1982b), and basalt (Bonano et al., 1989)

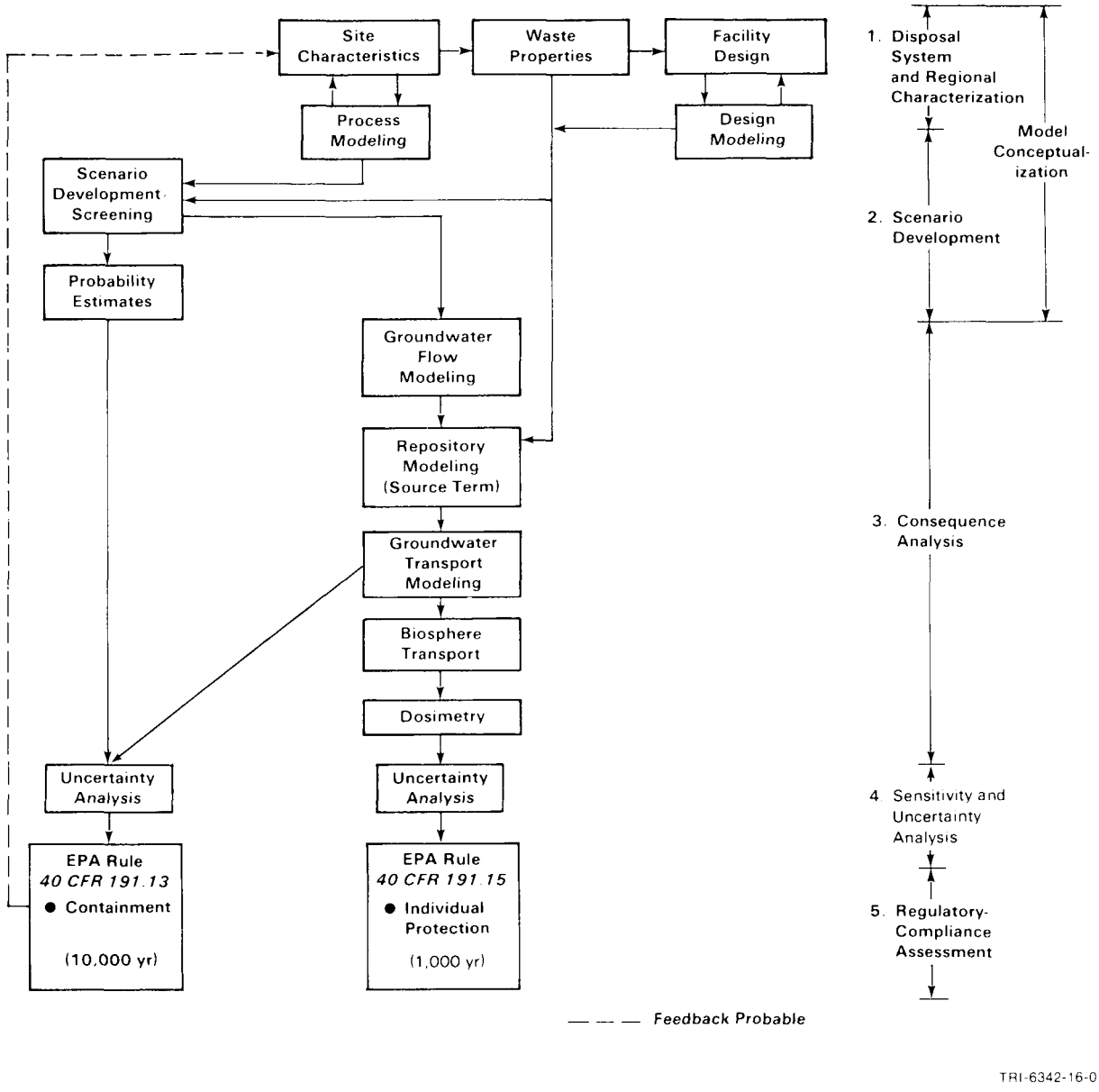

Figure 2-5. Compliance Assessment Methodology Structure (Modified from Rechard, 1989).

using generic data and for several locations in the subseabed (NEA, 1988) using empirical data.

The first step in the methodology is system description: characteristics of the controlled area, the repository, and the waste. Based on system description, those events and processes that may contribute to release of radionuclides from the repository and subsequent transport to the accessible environment are identified and screened. Once these events and processes have been developed into scenarios and these scenarios have been screened based on physical reasonableness and probability, a sequence of models is used to estimate the consequence of each scenario (Figure 2-6) (Rechard, 1989).

Physical and chemical processes simulated in consequence modeling for the Containment Requirements include: groundwater flow; repository resaturation from brine inflow; gas generation from corrosion and microbiological activity; room closure from salt creep; radionuclide transport in rooms, drifts, MB139, and shafts; and radionuclide transport in the hydrologic system. Additional processes simulated for the Individual Protection Requirements are radionuclide transport in the biosphere (i.e., surface and near-surface), and human uptake of radionuclides. Groundwater flow is simulated at regional and local scales for computational efficiency. Regional and local models are coupled in that the regional model provides boundary conditions to the local model. Each model can provide boundary conditions to the other for calibration. These hydrology models provide flow fields necessary to determine the quantity and time of radionuclide migration into the accessible environment (Rechard, 1989).

Given a groundwater-flow field and a radionuclide source from the repository model, radionuclide transport to the accessible environment can be simulated and transport along these flow paths can be calculated. Some scenarios for the WIPP performance assessment may require transient flow conditions. Consequence models usually produce a time-dependent discharge rate for each radionuclide at the accessible environment. The cumulative release of each radionuclide can be obtained by integrating the discharge rate over 10,000 years (Rechard, 1989).

For the Individual Protection Requirements, the biosphere-transport code simulates movement of radionuclides through the surface and near-surface environment and uptake by humans. This information is used to estimate whole-body and critical-organ doses (Rechard, 1989).

For the Containment Requirements, comparison with the Standard can be made by a probability-versus-consequence curve in the form of a CCDF. The CCDF of a value χ of consequence X indicates the probability of X having values greater than χ. Because consequence models currently being considered for use in WIPP

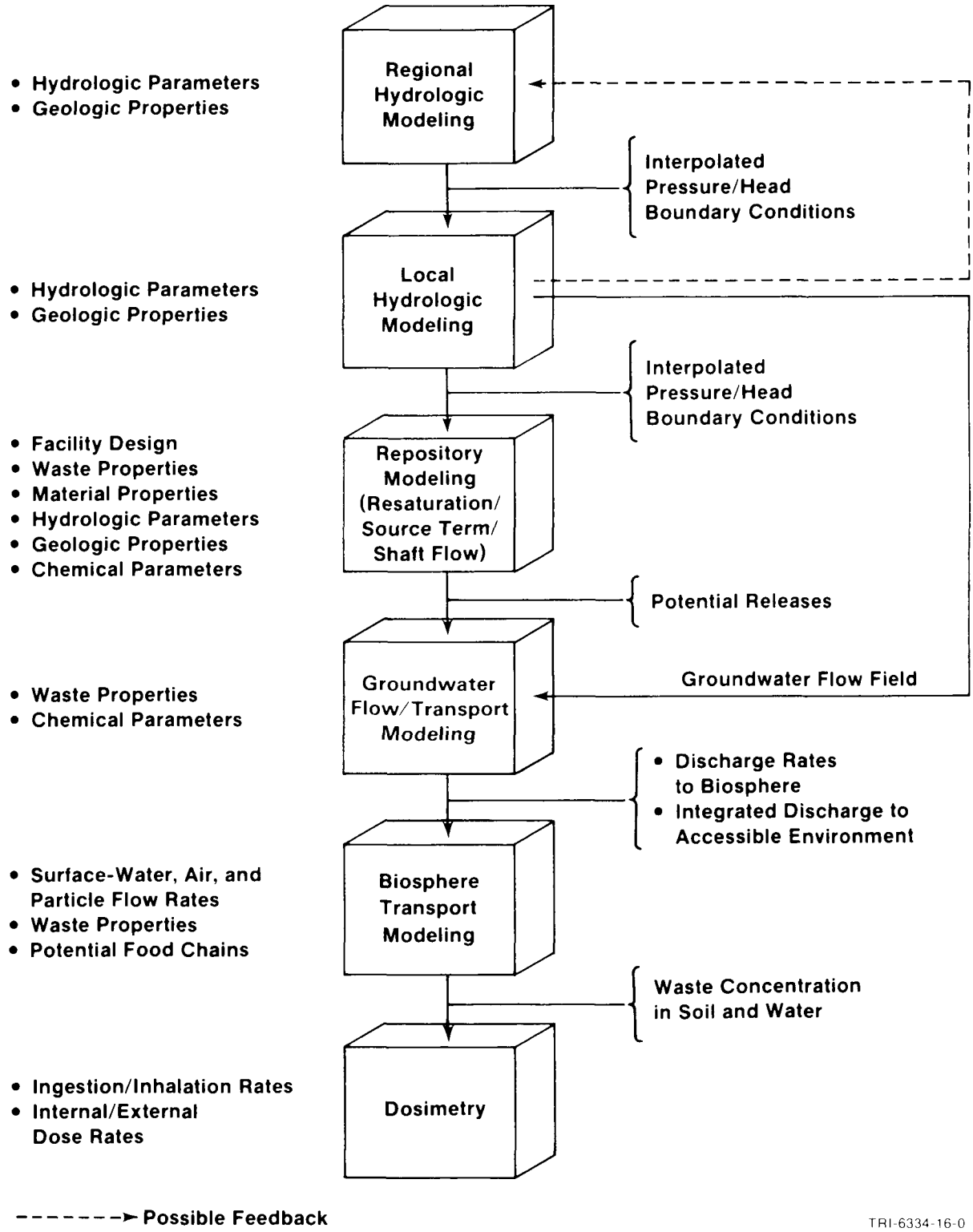

Figure 2-6. A Sequence of Codes for Consequence Modeling (Rechard, 1989).

performance assessment are deterministic models, the uncertainty of input data is handled by Monte Carlo sampling of the distribution for each parameter. These distributions are generated from observational data and rely to some extent on expert judgment. The following is a brief description of an approach to generating a CCDF using a Monte-Carlo sampling technique (Cranwell et al., 1982b; Pepping et al., 1983; Hunter et al., 1986; Campbell and Cranwell, 1988; and Rechard, 1989).

Appropriate ranges and distributions for model parameters are chosen for each significant scenario. This establishes a set of variables for characterizing data uncertainties over all scenarios. The distributions are statistically sampled to obtain sets of values (referred to as "input vectors"). For each scenario, m input vectors are generated. The same m input vectors are used for consequence analyses for each scenario, but all parameters may not be used in a single scenario analysis. Cumulative release to the accessible environment is the consequence calculated for each input vector, producing a distribution of cumulative releases for each scenario. A single CCDF is then generated by normalizing each consequence by the EPA limits for each significant scenario, ranking those normalized releases from largest to smallest, calculating the probability that a release is larger than some R_o from this ranking, weighting this probability by the probability of the associated scenario, summing over all significant scenarios, and plotting the result against R_o for each combination of R_o and the weighted sum of probabilities to obtain a probability versus consequence curve, usually plotted as a step function, that is the CCDF. If all portions of the CCDF curve (Figure 2-7) lie within the envelope of the EPA's Containment Requirements, compliance is indicated (Cranwell et al., 1982b; Pepping et al., 1983; Hunter et al., 1986; Campbell and Cranwell, 1988; and Rechard, 1989).

The compliance-assessment methodology will be implemented using a modular system of computer codes controlled by a computerized executive package. This system is referred to as the "Compliance Assessment Methodology CONtroller" (CAMCON). CAMCON contains translators that automatically translate output of one computer code into the appropriate input format needed for the next code. In this way, the executive controller can perform a computation for m input vectors through the entire set of modules with little operator intervention (Rechard, 1989).

CAMCON contains three data bases. The primary data base comprises observational data in a reduced form for quality assurance (QA) purposes. These data are transformed either by a combination of objective and subjective techniques, using interpolation or optimal-estimation procedures, or totally subjectively by expert judgment, into a secondary data base that can be accessed by the executive controller during a single run for m input vectors.

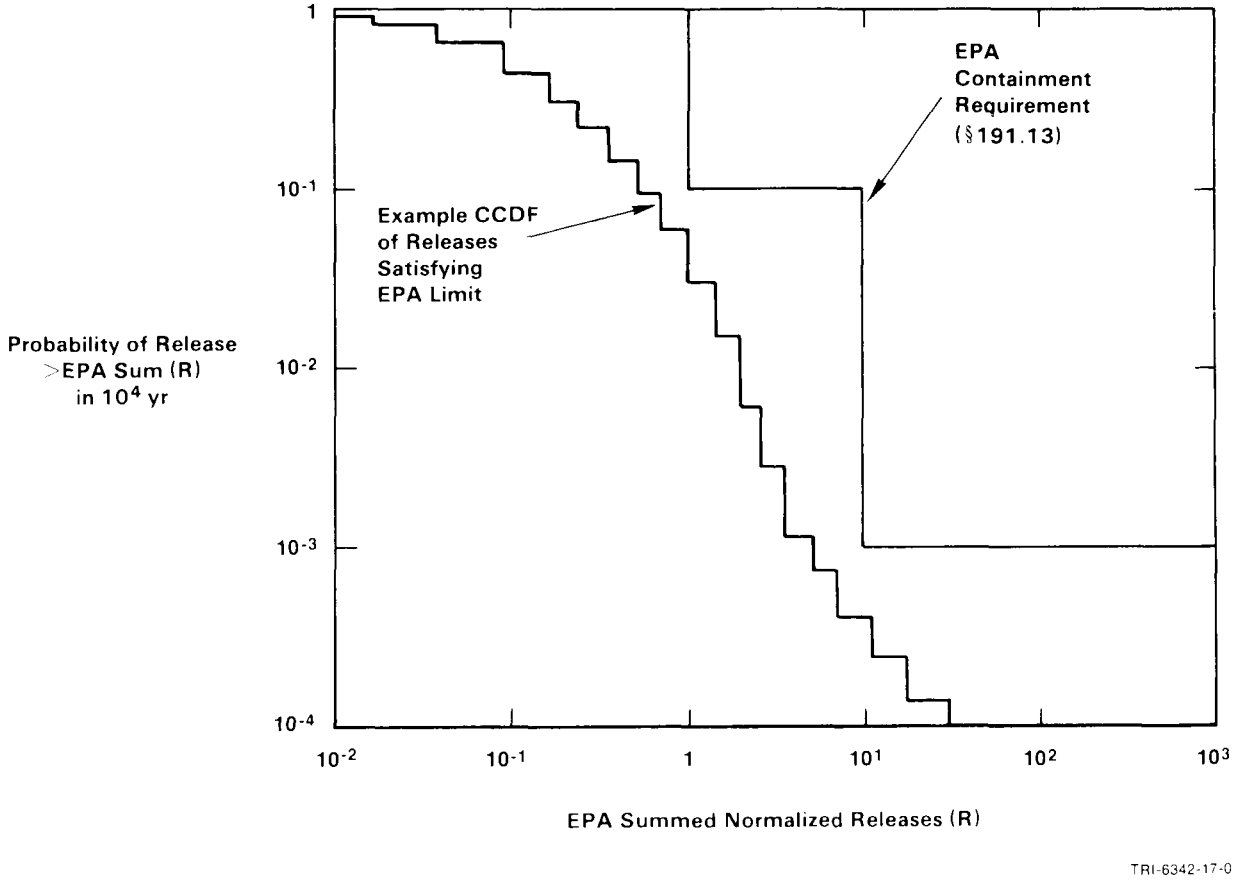

Figure 2-7. Hypothetical CCDF Illustrating Compliance with the Containment Requirements (Modified from Rechard, 1989).

During the calculation of cumulative release, the executive controller creates and writes to and from a computational data base that is generated anew for each input vector. An important feature of this system is that the executive controller automatically performs the calculation, data, and file management. This guarantees reproducibility for each computation, minimizes human error, and provides traceability for quality assurance purposes (Rechard, 1989).

QUALITY ASSURANCE

CAMCON: CONTROLLER FOR COMPLIANCE ANALYSIS

Based on the compliance-assessment procedure, an executive program to control consequence analyses has been constructed that meets two requirements: built-in flexibility and built-in QA. The best strategy for maintaining quality during repetitive systems-analysis calculations is to build QA into the executive program. CAMCON links distinct model components with little analyst intervention, tracks parameter uncertainty by Monte-Carlo techniques, uniquely records calculations so they can be repeated without misinterpretation, and produces a large number of intermediate diagnostics and final results. CAMCON also allows interpolation between modeling scales, permits iteration between computer modules for calibration of initial fields, aids in performing sensitivity analyses on subsystems and their components, and facilitates switching computer codes for the different modules (Rechard, 1989).

CAMDAT: COMPLIANCE ASSESSMENT METHODOLOGY DATA BASE

The computational data base, Compliance Assessment Methodology DATa (CAMDAT), uses a neutral file format with translators that provide a connection for data flow through the multicode system. Computational data base structure requires tracking codes that have added information to the data base to provide a trail for quality assurance by handling data from different types of codes (e.g., finite-difference, fluid-flow codes and finite-element, structural-analysis codes). These features require that any program that adds information to a file also identify itself by writing a record in the file. This helps the analyst to avoid misidentifying or misinterpreting a computer run when making repetitive calculations that produce similar results.

A logical data flow (e.g. CAMCON and CAMDAT) is necessary because the data flow and code linkage are complex in the algorithm used for assessing consequences of scenarios for the WIPP (Figure 2-8).

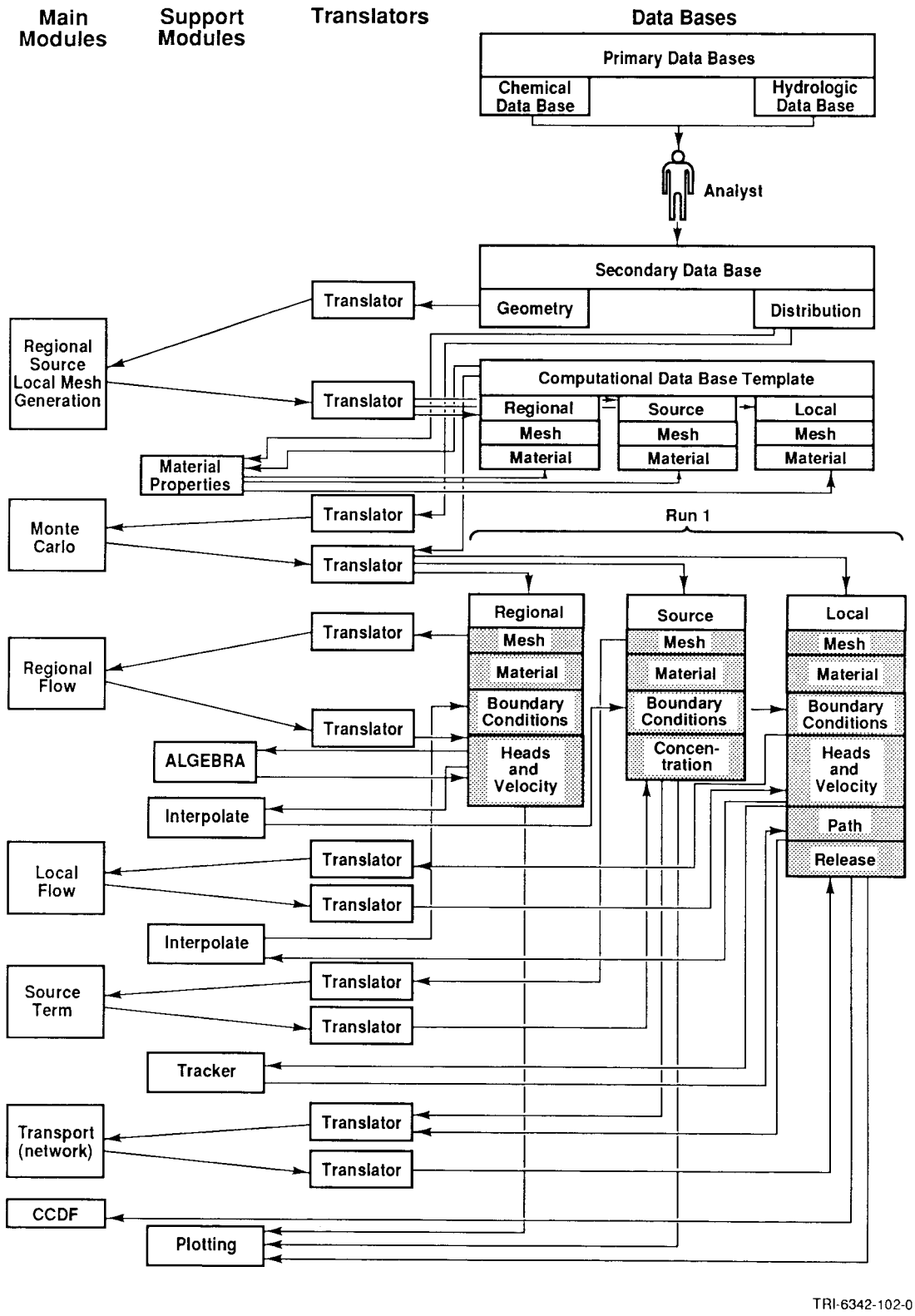

Figure 2-8. Algorithm for Logical Data Flow During Compliance Assessment (Rechard, 1989).

PARAMETER SENSITIVITY ANALYSIS

Parameter sensitivity analysis identifies important parameters by quantitatively estimating the variation in the results associated with variations in these parameters. This analysis can be performed on individual components of the system or on the system as a whole. Sensitivity analysis of an individual component provides understanding of an individual model and the processes it represents. An analysis of the whole system provides insight into the relative importance of modules and their processes within the whole system in determining the performance measure (release to the accessible environment). For nonstochastic models, sensitivity studies can be completed either by statistically sampling input parameter values and then using stepwise regression analysis of the output values as a function of input values, or by a deterministic approach using the explicit relationship between input and output in the computer codes. Key parameters are identified using either a direct method or the adjoint method.

Several sets of early sensitivity analyses were intended to provide guidance to experimental and design programs for individual components of the disposal system. Some of these analyses were concerned with processes within a room or panel both during and after consolidation following repository decommissioning. This work identified important interactions between brine inflow, gas generation, source term, and creep closure of the rooms. These early analyses are summarized elsewhere (Marietta and Anderson, in preparation). Other analyses demonstrated the importance of human-intrusion events, particularly pressurized brine injection, to the final CCDF and demonstrated the importance of the dual-porosity assumptions for the Culebra Dolomite in calculating releases to the accessible environment from human intrusion (Lappin et al., 1989). These results helped to identify a critical list of parameters for short-term and long-term performance of the WIPP.

Four sets of sensitivity analyses related to this report are presently underway. The first consists of a systems-level analysis for the undisturbed-performance scenario. This scenario is defined as the future state of the geologic, hydrologic, and repository/shaft systems under expected conditions during the next 10,000 years, including uncertainties of these conditions. This simple sensitivity analysis (Rechard et al., 1990, in preparation) examines parameter variations and correlations for the following parameters: hydraulic conductivities, porosities, and retardation factors for MB139, upper shaft seal, and lower shaft seal; and hydraulic conductivities, radionuclide solubility, and pressure in the waste panel.

The second set of sensitivity analyses is for human-intrusion scenarios (Chapter IV). These scenarios consist of combinations of three events: (1) a borehole into a waste-filled room, (2) a borehole through a room and into

pressurized brine in the Castile Formation, and (3) a withdrawal well downgradient from the repository. One combination of these events was analyzed earlier (Lappin et al., 1989), but an uncertainty analysis was not performed. Analyses consist of parameter variations for pressures in the waste panel; hydraulic conductivity in the rubble-filled borehole(s); hydraulic conductivity and radionuclide solubility in the waste panel; hydraulic conductivities, porosities, and retardation factors in the Culebra Dolomite Member; and time-of-intrusion events. Preliminary results are discussed below.

A third set of sensitivity analyses (Appendix A and Rechard et al., 1990, in preparation) on individual system components (see Appendix A) is based on parameter variations for: (1) amount of waste accessible to a borehole drilled into a waste-filled room as a function of material properties within the room and the rate of brine inflow from host rock; and (2) the amount of waste accessed by pressurized brine flowing toward an intrusion borehole in 10,000 years as a function of flow parameters and material properties within a room. Hydraulic conductivities of room contents are varied to establish criteria for possible engineered modifications to the repository and the waste.

The fourth sensitivity analysis assesses sensitivity of components within the repository/shaft system and of natural barriers (see Appendix A). The analysis includes: effect of panel seals; seals in MB139 and in shafts; and drift-backfill mixtures on the performance measure. Because the repository/shaft-system models are under development, results of this analysis are preliminary and will be updated when model development is complete.

CONCEPTUAL MODEL UNCERTAINTY

A conceptual model for a disposal system consists of the perceived geologic, hydrologic, and repository/shaft systems and the physical and chemical processes associated with these systems. Because of complexity in both natural and engineered systems and a limited amount and spatial distribution of available data for deciphering this complexity, full details of systems, processes, and interactions between processes are not completely understood. As a result, more than one conceptual model of the disposal system may be necessary to account for uncertainties in understanding these systems and processes.

Additional uncertainty is added to any particular conceptual model because of simplifications that must be made so that mathematical models can be used to approximate the "real world." An example of simplifications that may or may not be completely valid and may contribute to uncertainty in a conceptual model is lumping of stratigraphic units to form hydrologic units or

thermomechanically uniform units. Another example is assuming that Darcy flow occurs in extremely fine-grained sediments and crystalline sedimentary rocks.

Although conceptual-model uncertainty is not addressed specifically by analyses performed for this report, certain procedures will be followed regarding this topic in performance assessment. If major gaps in knowledge of the disposal system or processes occurring within the system cannot be resolved in a timely manner, and alternative conceptual models are outside the range covered by parameter variability within a single conceptual model, multiple conceptual models will be developed and performance-assessment calculations will be performed for each conceptual model. Whether these analyses will be combined and reported in a single CCDF or reported as a family of CCDFs will be decided later. Important issues to be considered in this decision are whether to (1) assign levels of confidence to different conceptual models and include them within the logic diagram for scenario construction, or (2) report the level of confidence in a CCDF for each conceptual model and map isopleths of uncertainty about a mean CCDF.

To compensate for uncertainty introduced by simplifying the conceptual model, assumptions will be made to increase the quantities of radionuclides transported, reduce the retardation of the radionuclides, and decrease groundwater travel times to the accessible environment. These simplifications will conservatively overestimate radionuclide releases.

Analyses in this demonstration clearly reflect the use of these assumptions to compensate for uncertainty in the conceptual model for groundwater flow and radionuclide transport. Lack of data for characterizing the Culebra Dolomite Member south of the WIPP leads to very conservative assumptions and results in extremely conservative predictions of groundwater travel times. These travel times are likely the fastest predictable within the conceptual model's uncertainty range. The probability that these are actual travel times has not been examined yet. A competing conceptual model predicts travel times to be as much as two orders of magnitude slower. Neither conceptual model incorporates radionuclide retardation, so the extreme of possible travel times is likely even slower. The uncertainty in groundwater flow and transport and the compensating conservatism make it virtually impossible to assess the influence of distance to the release point on the CCDFs constructed for this demonstration.

III. METHODOLOGY DEMONSTRATION

DEMONSTRATION SCENARIOS

UNDISTURBED PERFORMANCE SCENARIO

The Individual Protection Requirements of the Standard (§ 191.15 and § 191.16) call for the disposal system for TRU radioactive waste to be designed to limit doses to individuals for 1,000 years after disposal for the undisturbed performance of the disposal system. Although undisturbed performance is not mentioned in the Containment Requirements (§ 191.13), undisturbed performance is not precluded from the containment calculations. Undisturbed performance is the base case of the scenario-development methodology (Cranwell et al., 1982a; Bertram-Howery et al., 1989a).

As defined in the Standard (§ 191.12(p)), "'Undisturbed performance' means the predicted behavior of a disposal system, including the consideration of the uncertainties in predicted behavior, if the disposal system is not disrupted by human intrusion or the occurrence of unlikely natural events." No limitation on the duration of this performance is indicated in the definition. One product of the scenario-development methodology (Cranwell et al., 1982a) is a base-case scenario consisting of geologic, hydrologic, and repository/shaft systems at the time of closure along with all expected changes in these systems and the associated uncertainties for the 10,000 years of regulatory concern. For scenario development, expected changes are assumed to be a result of events and processes that are certain to occur. Because no future human-intrusion event (or any other human activity) after the assumed loss of institutional control of the disposal site can have a probability of occurrence of 1, the base-case scenario will not contain disruption of the disposal system by human intrusion. The Standard does not provide a definition of unlikely natural events to be excluded from undisturbed performance nor, by implication, likely natural events to be included. Because of the relative stability of the natural systems within the region of the WIPP disposal system, all naturally occurring events and processes that are expected to occur are part of the base-case scenario and are assumed to represent undisturbed performance. This scenario can be used for the Containment Requirements for the 10,000 years of regulatory concern, as well as for the Individual Protection Requirements for the 1,000 years of regulatory concern. However, different data sets may be required to define undisturbed performance of the WIPP disposal system if the time frame in the requirements is extended beyond 1,000 years.

After the repository is filled with waste, the disposal rooms and drifts in the panels are backfilled and panel seals are emplaced in the access drifts to

the panels (Figure 3-1). While excavations are open, the salt creeps inward because of the decrease in confining pressure on the salt around the rooms. The movement of floors upward into rooms and drifts fractures the more brittle anhydrite in MB139, which is directly beneath the excavations. The anhydrite is expected to fracture directly beneath excavated rooms and drifts but not beneath the pillars because of the overburden pressure on the pillars. To control potential radionuclide migration through MB139, seals are emplaced in MB139 directly beneath the panel seals (Stormont et al., 1987, Borns and Stormont, 1988). Access drifts and lower parts of shafts are backfilled with salt. Because of the high lithostatic pressures at the repository depth, salt creep is expected to exert sufficient pressure on the backfill to consolidate the material into low-conductivity seals with properties similar to those of host rock. Upper parts of the shafts are also backfilled with salt, but pressure exerted by salt creep on backfill is not expected to be sufficient to cause the same degree of consolidation as is expected in lower portions of the shafts.

Before the amount and direction of groundwater flow and radionuclide release from the repository can be finally determined, gas generation must be considered. However, gas generation and its effects on radionuclide release are not included in this demonstration because not enough is known about these phenomena. Some waste and some waste containers will be composed of organic material. Because microbes transported into the repository with the waste are expected to be viable under sealed-repository conditions (Brush and Anderson, 1988), organic material in the repository will biodegrade with concomitant generation of gases. In addition, moisture in the repository, either brought in with waste or seeping in from the Salado Formation, may corrode metals in the waste and metallic waste containers themselves. This corrosion also will generate gases. The time period over which gases will generate is not known. Both biodegradation and corrosion are dependent on availability of water. The humidity required for microbiological activity and whether or not saturated conditions are required for corrosion have not been established. Moisture and microbes in waste will generate some gas prior to waste emplacement in the repository. After emplacement, the amount and rate of gas generation will depend on such factors as microbe metabolisms; relationships between gas pressure, brine inflow, room closure, and backfill and waste consolidation; and the degree to which reactions attain completion.

For this methodology demonstration, radionuclide migration out of the repository and transport to the accessible environment depend on the existence of saturated conditions in the repository and along hypothesized flow paths. Although gas pressure resulting from microbiological activity and corrosion may prevent brine inflow from the Salado Formation, thereby preventing saturation of the backfill, waste, and possibly MB139, saturated conditions are assumed to exist from the time of final repository

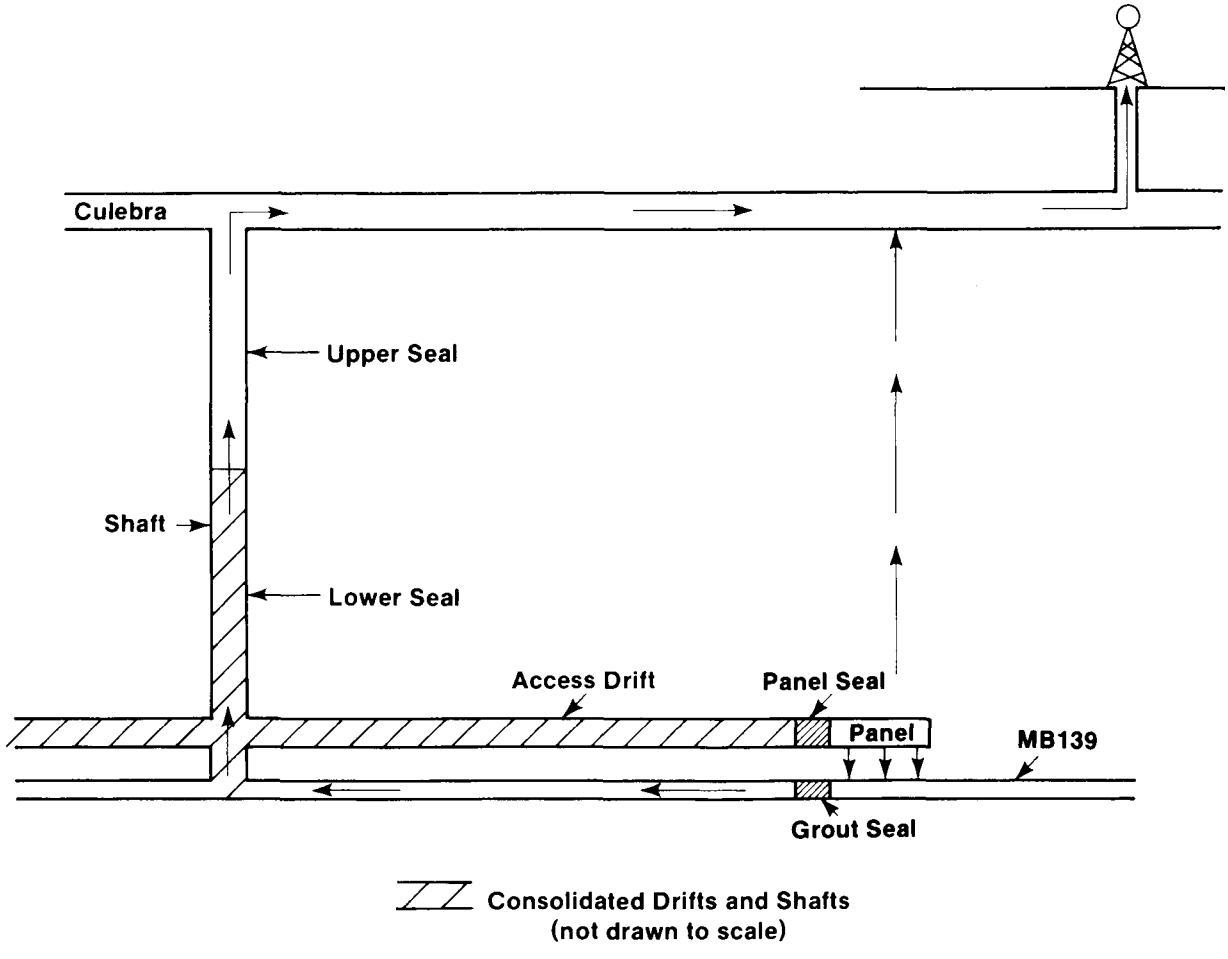

Figure 3-1. Conceptual Model Used in Simulating Undisturbed Performance (Lappin et al., 1989).

consolidation. As a result, radionuclide transport calculations span the entire 10,000 years.

Two pathways for groundwater flow and radionuclide transport likely will dominate the disposal system. In the first path, radionuclides enter MB139, either through fractures in salt or directly as a result of rooms and drifts intersecting the marker bed during construction or room closure. Because material in the upper shaft is expected to be poorly consolidated, the hydraulic pressure at the junction of the upper and lower parts of the shaft seals is assumed to approximate the pressure head of the Culebra Dolomite Member. As a result, the pressure gradient tends to force radionuclide-bearing groundwater from MB139 beneath the panel through the seal in the marker bed, along the fracture in MB139 to the base of the shaft, up the shaft to the Culebra Dolomite Member, and downgradient in the Culebra to the accessible environment and/or a pumping well for a livestock pond. Relative motion during salt creep and resulting backfill consolidation prevent MB139 from returning to its original position and the salt-creep induced fractures do not completely close. Flow is through MB139 instead of through the overlying access drift because of the substantially higher hydraulic conductivity in MB139 (Appendix A). Flow in MB139 is to the north through the seal rather than to the south down the pre-excavation hydraulic gradient within MB139, because the pressure drop to the north is greater after excavation, and the flow to the south would be impeded by extremely low permeability of the intact marker bed. Therefore, the horizontal path through MB139 to the accessible environment is not included for this demonstration but this path may be considered for other analyses. The other dominant path is assumed to be from the repository vertically through the intact Salado Formation toward the Culebra Dolomite Member (Lappin et al., 1989). This path has the largest pressure decline over the shortest distance of any path. In addition, large potential exists for radionuclides to leave the repository along this path because of the large horizontal cross-sectional area of the waste-bearing rooms and drifts in the repository. Two other pathways, one through the Salado and another through the consolidated drifts and panel seals, are less important than the pathway through MB139 (Lappin et al., 1989). Only the MB139 pathway is considered here.

The methodology can determine pathways to individuals and calculate doses to humans. Because undisturbed performance releases no radionuclides, these capabilities are not demonstrated for this scenario.

HUMAN INTRUSION SCENARIOS

Appendix B of the Standard provides guidance on a number of factors concerning human intrusion. In the section entitled "Institutional Controls," active controls are not allowed to prevent or reduce radionuclide releases for more

than 100 years after disposal. Passive institutional controls can be assumed to deter systematic and persistent exploitation and to reduce the likelihood of inadvertent intrusion, but these controls cannot eliminate the chance of inadvertent intrusion. The section on "Consideration of Inadvertent Human Intrusion into Geologic Repositories" suggests that exploratory drilling for resources can be the most severe form of human intrusion considered. The section on "Frequency and Severity of Inadvertent Human Intrusion into Geologic Repositories" suggests that the likelihood and consequence of drilling should be based on site-specific factors.

In keeping with the guidance, this demonstration includes scenarios that contain human-intrusion events. To derive these scenarios, a preliminary application to the WIPP disposal system of a scenario-development methodology (Cranwell et al., 1982a) is used (Bertram-Howery et al., 1989). The methodology has four basic steps: (1) listing events and processes that may affect release and/or transport of radionuclides, (2) screening events and processes based on well-defined criteria, (3) constructing scenarios from the remaining events and processes using a logic diagram, and (4) screening the scenarios based on well-defined criteria.

For the WIPP disposal system, an initial list of events and processes has been reduced to five by screening (Bertram-Howery et al., 1989; Hunter, 1989): (1) conventional or solution mining of potash outside the disposal system, resulting in areas of subsidence that permit recharge to underlying aquifers (Process TS), (2) unexpected climatic change (Process TC), (3) drilling a borehole through a disposal room or drift and into pressurized brine in the Castile Formation (Event E1), (4) drilling a borehole into a disposal room or drift (Event E2), and (5) pumping from a water well downgradient from the repository (Event E3). Using a logic diagram to construct scenarios (Figure 3-2) results in a comprehensive and mutually exclusive set of scenarios for the events and processes identified. Scenarios with no mechanism for radionuclide release and those with subsidence (TS) in the absence of extreme climatic change (TC) have been deleted from the diagram.

Intrusion Borehole into a Room or Drift (Scenario E2)

Scenario E2 consists of a single borehole that penetrates to or through a waste-filled room or drift in a panel (Figure 3-3). The borehole does not intersect pressurized brine or any other important source of water. The hole is abandoned after a plug is emplaced above the Culebra Dolomite Member.

After decomissioning of the repository, moisture in the waste or brine from the host rock allows microbiological activity and corrosion to occur, generating gas. Depending on rate of gas generation, amount of brine inflow, and rate of room closure, sufficient gas may be produced to fill available

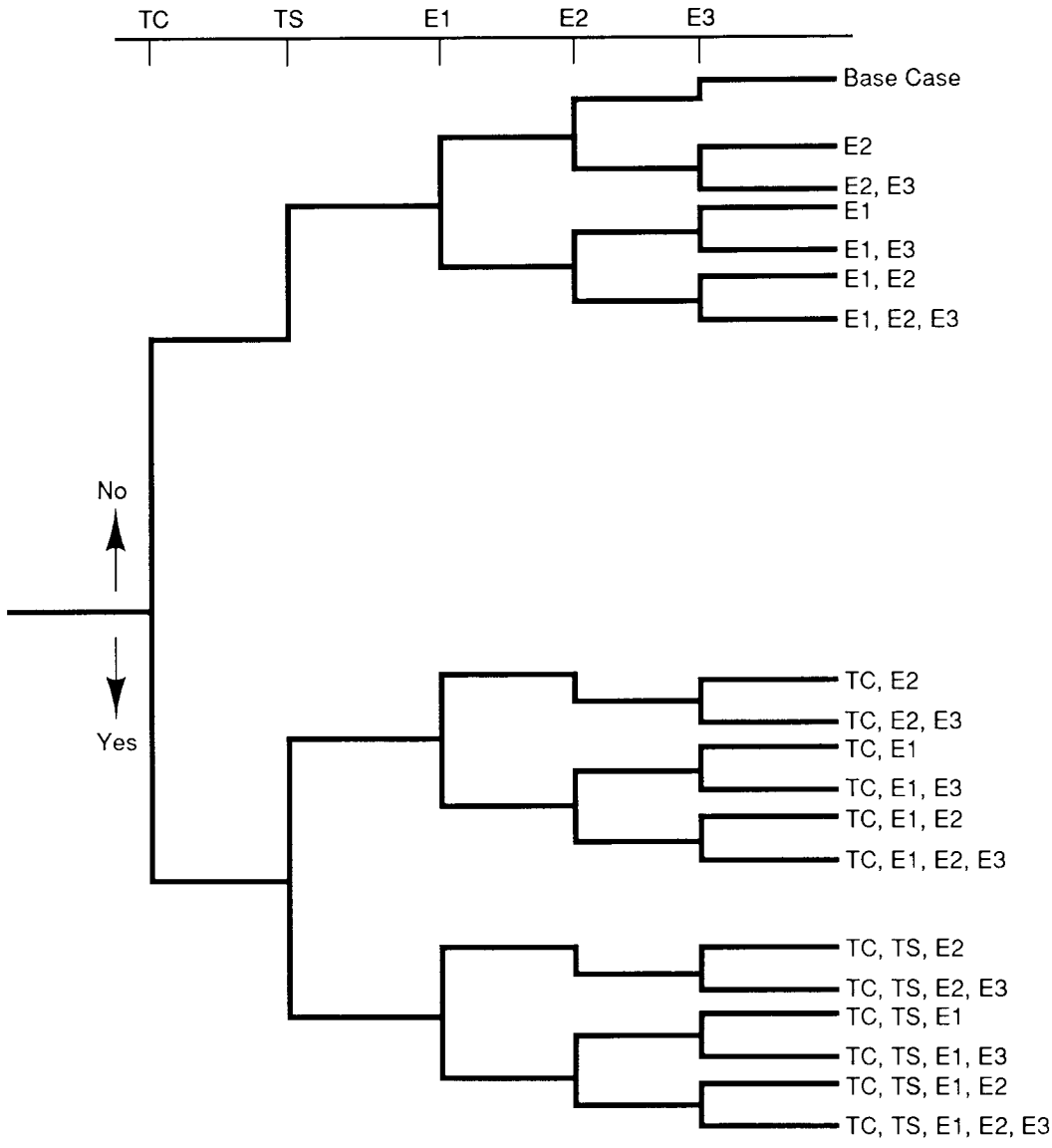

TC - Climatic Change
TS - Subsidence Resulting from Solution Mining of Potash
E1 - Drilling through Room and Brine Pocket
E2 - Drilling through or into a Room
E3 - Drilling Downgradient from Repository

TRI-6342-13-0

Figure 3-2. Logic Diagram for Constructing Demonstration Scenarios.

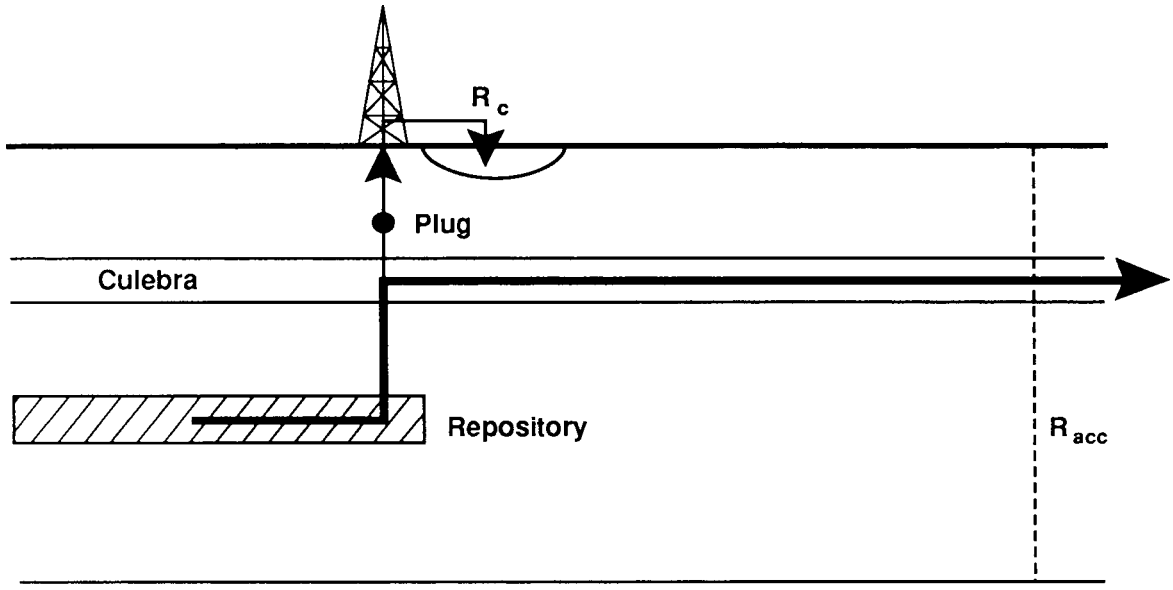

R_c = Release of Cuttings and Eroded Material

R_{acc} = Release at the Subsurface Boundary of the Accessible Environment

TRI-6342-216-0

Figure 3-3. Conceptual Model for Scenario E2. Arrows Indicate Assumed Direction of Flow.

pore space within rooms and drifts. Gas pressure may reach lithostatic. This gas may vent through an intruding borehole, thereby allowing the repository to resaturate. For this demonstration, gas generation is ignored and the repository is assumed to be saturated from the time of final consolidation, which is assumed to occur immediately after decommissioning. During drilling, radionuclides are released directly to the surface as the borehole penetrates a room or drift and intersects drums and boxes of waste. The waste that is ground up by the drill bit is transported to the surface by circulating drilling fluid. Additional material may be dislodged from walls of the borehole by the circulating fluid as drilling proceeds below the repository.

After drilling is completed, the hole is plugged. Because hydrostatic pressure in the Culebra Dolomite Member is less than assumed lithostatic pressure within the repository, the connection between repository and Culebra Dolomite results in a pressure gradient that allows the pressure in the repository to decrease toward, if not to, hydrostatic pressure. This process forces water from the repository into the Culebra Dolomite Member. After the pressure within the repository is sufficiently reduced, brine inflows from the host rock, assuming that pore pressure within the host rock is greater than hydrostatic. This inflow forces brine to flow up the borehole toward the Culebra Dolomite. The borehole plug for this scenario is located so that all flow up the borehole is diverted into the Culebra Dolomite Member.

Intrusion Borehole into a Room or Drift with a Withdrawal Well (Scenario E2E3)

Scenario E2E3 includes a borehole that penetrates a waste-filled room or drift, but does not intersect pressurized brine or other important sources of water (Scenario E2) (Figure 3-4). The hole is plugged above the Culebra Dolomite Member. This scenario also includes a withdrawal well into the Culebra Dolomite, 2.5 km (1.5 mi) downgradient (Scenario E3). The withdrawal well presumably supplies water to a livestock tank or pond. The location and the functional life of the well is dependent on salinity of the water in the Culebra Dolomite. A change in salinity of the water, such as might result from a contaminant plume reaching the location, could result in abandonment of the well.

This scenario is essentially the same as Scenario E2 described above, including release of radionuclides directly to the surface during drilling of the borehole into the room or drift. The addition of the withdrawal well downgradient from the repository provides another pathway for radionuclide transport through the Culebra Dolomite Member and to the surface. The amount of waste diverted in this manner is dependent on when the well is drilled and on the amount of water withdrawn from the well, concentration of radionuclides in the water, and duration of pumping (in part, a function of salinity of the water).

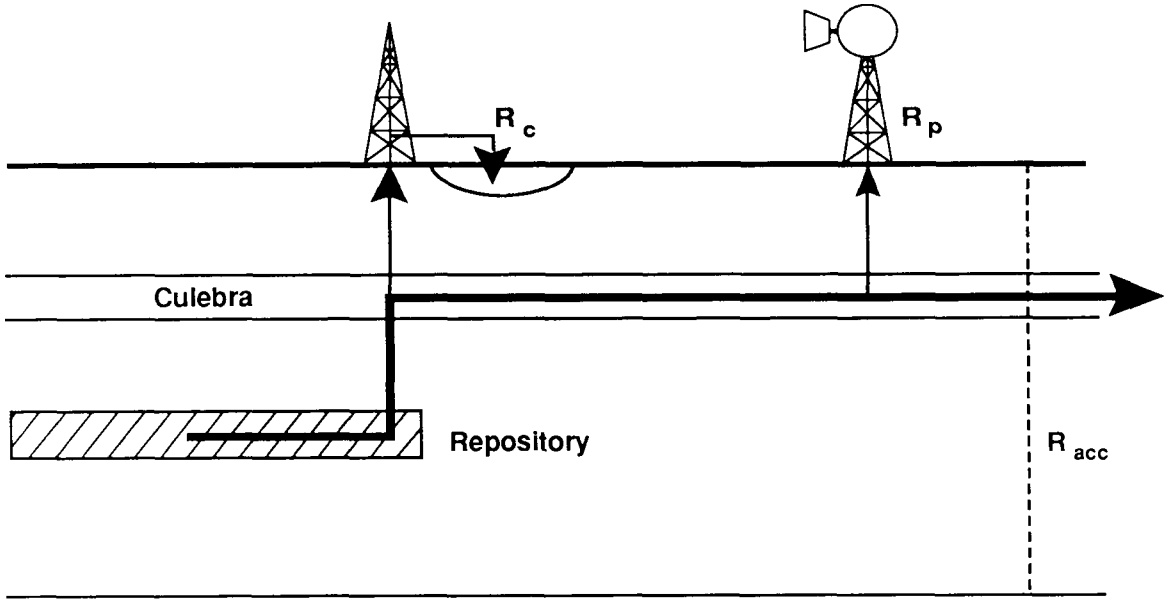

R_c = Release of Cuttings and Eroded Material
R_{acc} = Release at the Subsurface Boundary of the Accessible Environment
R_p = Release to Surface through Withdrawal Well

TRI-6342-219-0

Figure 3-4. Conceptual Model for Scenario E2E3. Arrows Indicate Assumed Direction of Flow.

Intrusion Borehole Through a Room or Drift into Pressurized Brine in the Castile Formation (Scenario E1)

Scenario E1 consists of a single borehole that penetrates through a waste-filled room or drift and continues into or through a pressurized brine occurrence in the Castile Formation (Figure 3-5) in which brine pressure is between hydrostatic and lithostatic for that depth. The borehole is plugged at a level above the Culebra Dolomite Member.

As in the scenarios described above, the repository for this scenario is assumed to be saturated from the time of final consolidation. A borehole that penetrates a room or a drift intersects containers of waste. This waste is incorporated into the drilling fluid and circulated directly to the mud pits at the surface. After the hole is plugged and abandoned, the brine pressure is assumed to be sufficient to drive flow up the borehole into the Culebra Dolomite Member. The rate of flow is dependent on the pressure difference between the Culebra Dolomite and the injected brine and on the hydraulic properties of materials in the borehole. Waste from the repository is incorporated into the brine by the circulation of the brine into the waste adjacent to the borehole. Upon reaching the Culebra Dolomite, the waste-bearing brine flows down the hydraulic gradient toward the 5.0-km (3.0-mi) boundary. Pressurized brine injection results in temporary alterations of the flow field in the Culebra Dolomite. Brine flow reduces the local residual pressure in the Castile Formation, thereby reducing the driving pressure of the flow. Eventually, brine stops flowing.

Intrusion Borehole Through a Room or Drift into Pressurized Brine in the Castile Formation, with a Withdrawal Well into the Culebra Dolomite Member (Scenario E1E3)

Scenario E1E3 consists of a borehole that penetrates a room or drift in the repository and also penetrates pressurized brine in the Castile Formation (Figure 3-6). In addition, a pumping well that supplies water to a livestock tank or pond is 2.5 km (1.5 mi) downgradient from the repository.

Radionuclides from the repository are released directly to the surface when the borehole penetrates the waste-filled room or drift. Waste is entrained in the drilling fluid and circulated to the surface. In addition, circulating drilling fluid washes particles off borehole walls in the repository or circulates through waste adjacent to the borehole. After the borehole penetrates pressurized brine in the Castile Formation, the hole is completed and a plug is emplaced above the Culebra Dolomite Member to force all flow up the borehole into the Culebra Dolomite. Brine pressure is assumed to be great enough to force the brine up into the Culebra Dolomite, where flow would be downgradient. Depending on the rate of flow through the borehole and the hydraulic properties of waste in the repository, the brine flowing up the borehole entrains waste or flows through the waste immediately adjacent to the

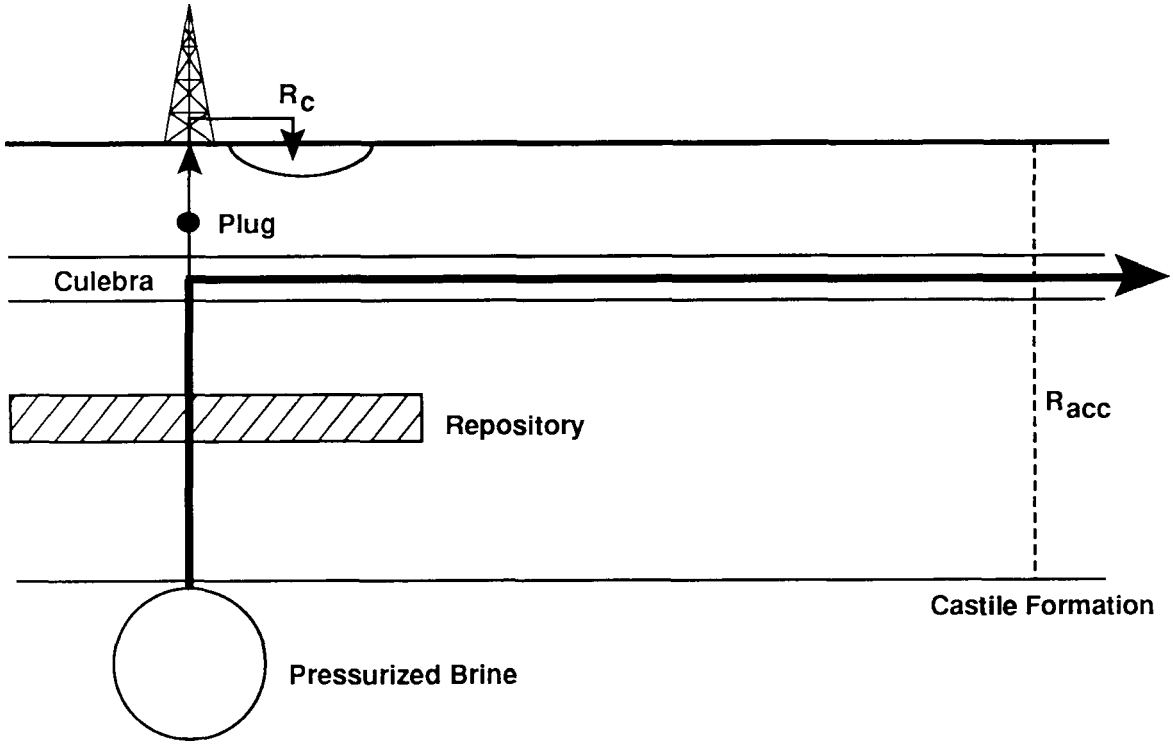

R_c = Release of Cuttings and Eroded Material
R_{acc} = Release at the Subsurface Boundary of the Accessible Environment

TRI-6342-215-0

Figure 3-5. Conceptual Model for Scenario E1. Arrows Indicate Assumed Direction of Flow.

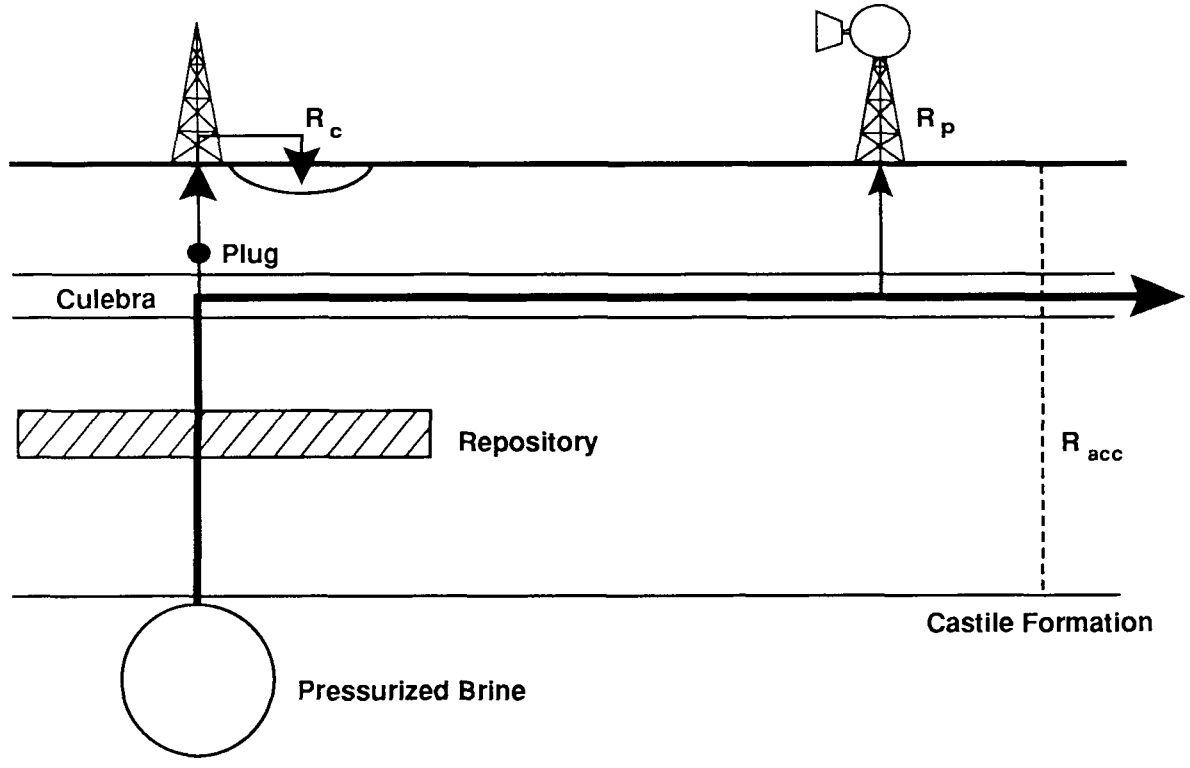

R_c = Release of Cuttings and Eroded Material
R_{acc} = Release at the Subsurface Boundary of the Accessible Environment
R_p = Release to Surface through Withdrawal Well

TRI-6342-218-0

Figure 3-6. Conceptual Model for Scenario E1E3. Arrows Indicate Assumed Direction of Flow.

hole and dissolves radionuclides from the waste. Upon reaching the Culebra Dolomite, radionuclides are transported downgradient. The amount of waste in the portion of the contaminant plume diverted to the surface by the pumping well depends on when the well is drilled, the volume of water withdrawn from the well, radionuclide concentrations in the water, and pumping duration.

Intrusion Borehole Through a Room or Drift into Pressurized Brine in the Castile Formation and Another Intrusion Borehole into the Same Panel (Scenario E1E2)

Scenario E1E2 consists of two boreholes that penetrate waste-filled rooms or drifts in the same panel. One borehole also penetrates pressurized brine in the Castile Formation, whereas the other borehole does not. The borehole that penetrates the pressurized brine is plugged between repository and Culebra Dolomite Member forcing into the room all the brine flowing up the borehole. The other borehole is plugged above the Culebra Dolomite Member, forcing into the Culebra Dolomite all the brine flowing up this borehole. The brine is assumed to be under a greater pressure than gas or fluid in rooms and drifts of the repository (Figure 3-7).

Radionuclides are released directly to the surface during drilling of the two holes that penetrate the waste-filled rooms or drifts. The radionuclides are incorporated into the drilling fluid and carried to the surface. Additional releases from this system are dependent on the sequence in which the holes are drilled. The plug in the borehole that penetrates the pressurized brine allows brine flowing up the hole to enter the repository but not leave the repository until the second hole penetrates the same panel. Once the second hole is drilled, a pathway is formed for brine from the pressurized brine occurrence to flow through rooms and/or drifts to this new hole and up to the Culebra Dolomite Member. Flow in the Culebra Dolomite is downgradient.

If the hole that does not penetrate pressurized brine is drilled first, gas and/or fluid pressure is relieved; this is followed by groundwater flow and radionuclide transport up the hole as a result of brine inflow into the panel from the host rock, possibly enhanced by creep closure of rooms and drifts. Flow is diverted into the Culebra Dolomite Member by the plug located above this unit. The subsequent drilling and plugging of the borehole that penetrates the pressurized brine results in flow through the facility and up the other borehole (Figure 3-7). After the driving pressure is depleted Scenario E1E2 reverts to Scenario E2, because the borehole that penetrates the pressurized brine no longer contributes to flow and transport.

When the two boreholes are drilled affects radionuclide releases. Sequence of drilling, time lapsed between drilling events, and distance between the two boreholes in the same panel all affect radionuclide migration. Flow through the rooms and drifts depends on hydraulic properties of materials placed in

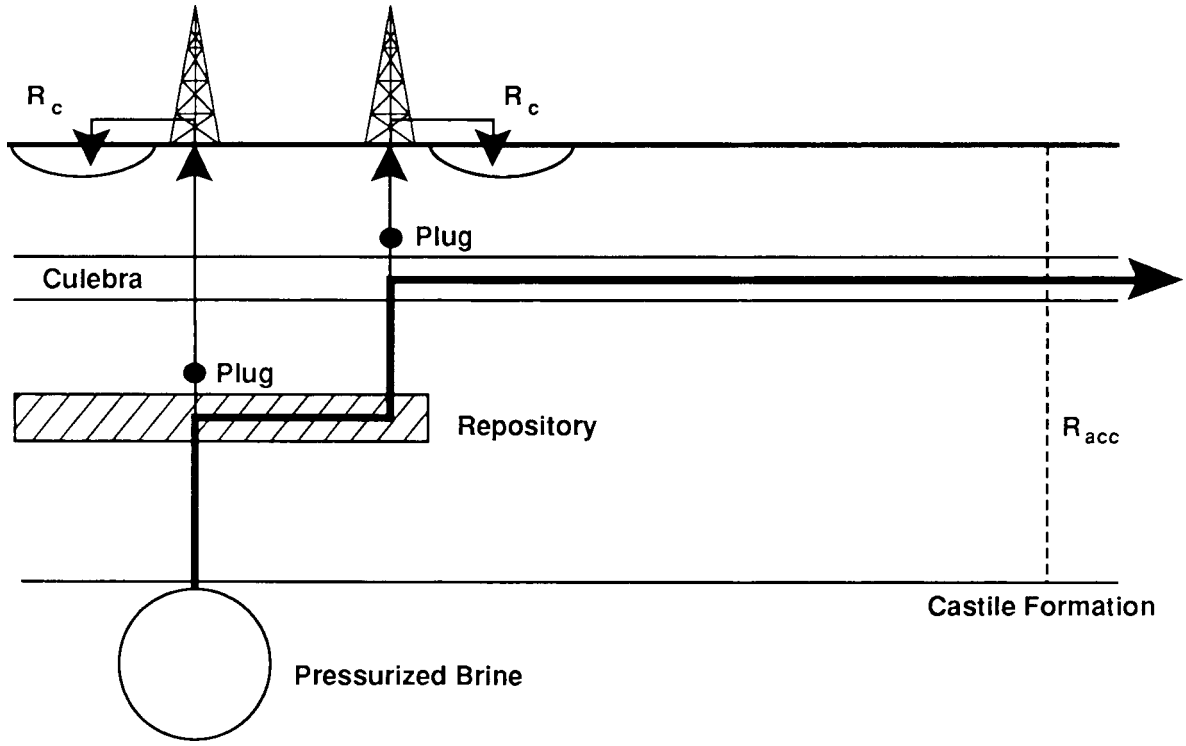

R_c = Release of Cuttings and Eroded Material

R_{acc} = Release at the Subsurface Boundary of the Accessible Environment

TRI-6342-217-0

Figure 3-7. Conceptual Model for Scenario E1E2. Arrows Indicate Assumed Direction of Flow.

these openings and on the pressure gradient between the holes. For some configurations, flow from one hole to the other may take longer than the regulatory period or take sufficiently long to allow significant decay of radionuclides in transport.

Intrusion Borehole Through a Room or Drift into Pressurized Brine in the Castile Formation with Another Borehole into the Same Panel and a Withdrawal Well into the Culebra Dolomite Member (Scenario E1E2E3)

Scenario E1E2E3 consists of three boreholes (Figure 3-8). Two boreholes are drilled into the waste-filled portions of the same panel. One borehole penetrates pressurized brine in the Castile Formation, and the other borehole does not penetrate pressurized brine or another important source of groundwater. The third borehole is a pumping well into the Culebra Dolomite Member, located 2.5 km (1.5 mi) downgradient from the waste panels. The portion of this scenario that concerns two boreholes through the same panel is identical to Scenario E1E2, and the same factors and considerations apply. A pumping well into the Culebra Dolomite at 2.5 km (1.5 mi) will divert to the surface a portion of the flow and any radionuclides in transport.

COMPLIANCE ASSESSMENT SYSTEM FOR THE DEMONSTRATION

SUMMARY OF THE HYDROGEOLOGY OF THE NORTHERN DELAWARE BASIN

The Los Medaños Study Area is in the north-central Delaware Basin, which is in the southern Pecos Valley section of the Great Plains physiographic province, between the high plains of West Texas and the Guadalupe and Sacramento Mountains in southeastern New Mexico. This Study Area covers a 40 x 40 km (25 x 25 mi) area and extends from Nash Draw; 20 km (12 mi) north of the Texas-New Mexico border in Eddy County, New Mexico eastward into Lea County, New Mexico (Figure 3-9).

The Los Medaños Study Area has two main geomorphological features: Nash Draw on the western part and dunes in the eastern part. Nash Draw is a broad [about 6.8 km (4.2 mi) wide], shallow topographic depression with no external surface drainage, extending 35 km (22 mi) from the Pecos River at Malaga Bend almost due north to the Maroon Cliffs. The draw is bounded on the east by Livingston Ridge and on the west by Quahada Ridge. The dunes are gently rolling hills that extend from Livingston Ridge eastward toward Lea County.

This section discusses the hydrostratigraphy of the Culebra Dolomite Member of the Rustler Formation in the Los Medaños Study Area. The compliance assessment system includes two hydrologic models, one for the "local" scale of the WIPP, and a three-dimensional regional domain that will be modeled in the future (Figure 3-9). Nash Draw is a hydrologic boundary for the regional model (Brinster, 1989; in preparation).

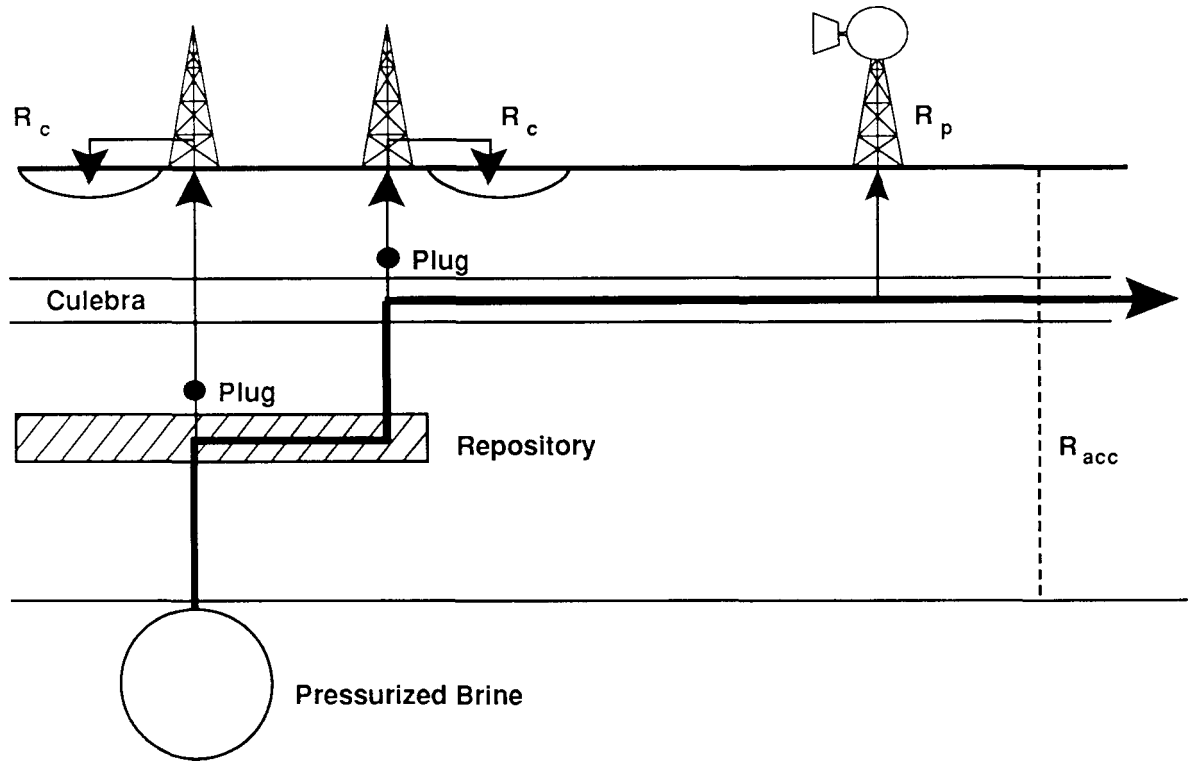

Figure 3-8. Conceptual Model for Scenario E1E2E3. Arrows Indicate Assumed Direction of Flow.

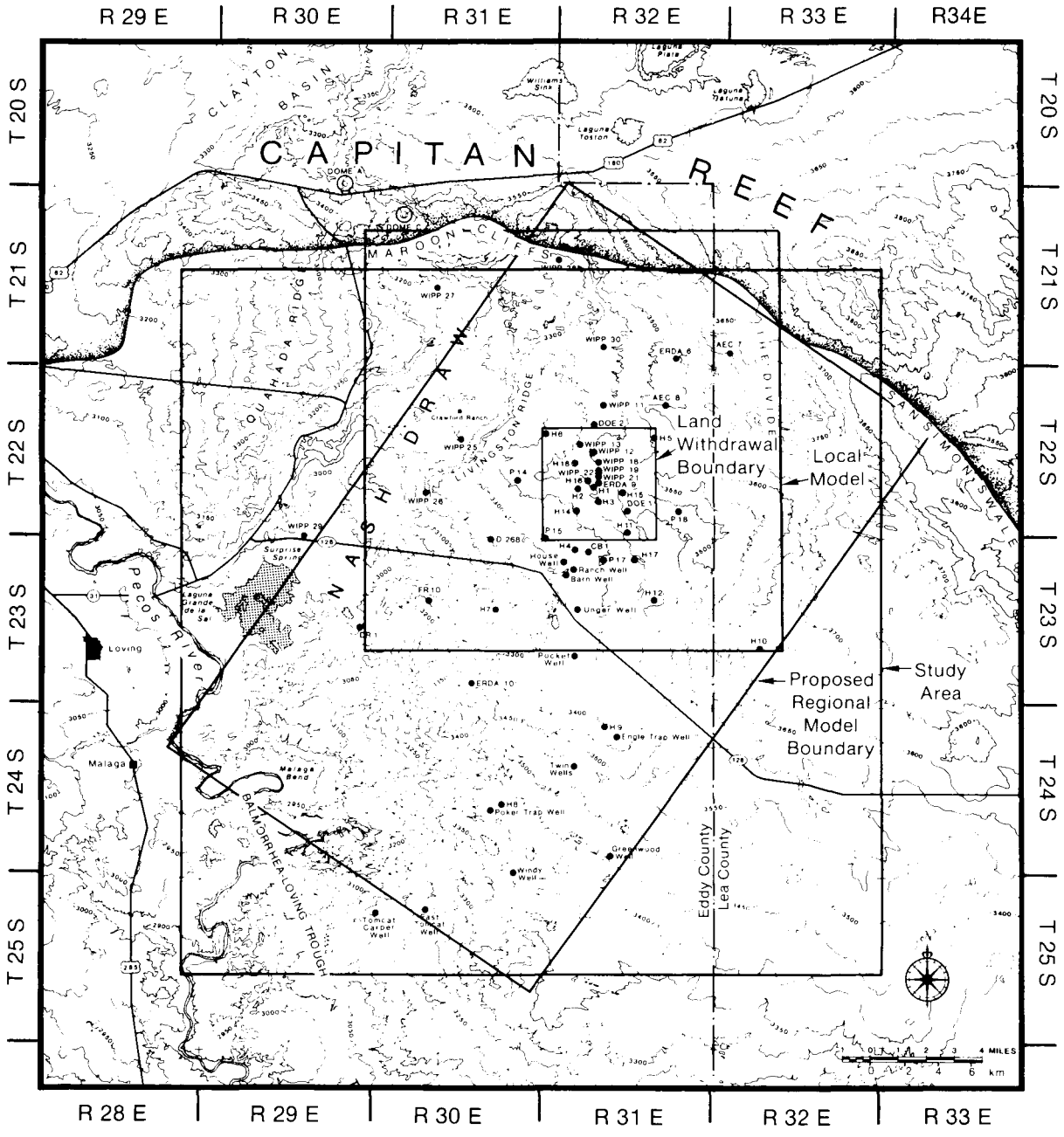

TRI-6342-144-0

Figure 3-9. Different Study Areas That Have Been Used for Regional (Brinster, 1989; in preparation) and Local (LaVenue et al., 1988) Models to Date.

Hydrogeology of the Rustler Formation

The Rustler Formation is of particular interest because the Culebra Dolomite Member may provide potential pathways for radionuclides from the WIPP repository to the accessible environment.

The Rustler Formation conformably overlies the Salado Formation and is the youngest unit of the Ochoan Series of evaporites (Figure 2-3). Composition of the Rustler is about 0.40 anhydrite, 0.30 halite, 0.20 siltstone and sandstone, and 0.10 anhydritic dolomite (Lambert, 1983). The Rustler Formation has been divided into four formally named members and a lower unnamed member on the basis of lithologies of units that outcrop along Nash Draw west of the WIPP (Vine 1963) (Figure 2-3).

Rustler Formation Aquitard Units

The lower unnamed member ranges in thickness from about 3 to 160 m (10 to 528 ft) and has a mean thickness of about 40 m (131 ft) (Table 3-1). It is about 36 m (118 ft) thick at the WIPP. Thickness of the unit is consistent across the Study Area with a slight thickening eastward which can be seen in a cross section of the Study Area. The unit is composed mostly of fine-grained silty sandstones and siltstones interbedded with anhydrite (gypsum at Nash Draw) in the western part of the Study Area with increasing amounts of halite in the eastern part of the Study Area.

The only drill-stem test in the unnamed lower member was at H-16 (Figure 3-10). Transmissivities of 2.9×10^{-10} and 2.4×10^{-10} m^2/s (2.2×10^{-4} and 2.7×10^{-4} ft^2/d) for the first and second buildup periods of a drill-stem test in a siltstone unit near the base of the unnamed member have been calculated (Beauheim, 1987c).

The Tamarisk Member ranges in thickness from about 10 m (33 ft) to 80 m (262 ft) in southeastern New Mexico (Table 3-1). It has a mean thickness of 40 m (131 ft) in the Study Area and is about 36 m (118 ft) thick at the WIPP. The Tamarisk consists of mostly anhydrite interbedded with thin layers of claystone and siltstone. The member outcrops along the southwestern part of Nash Draw.

Attempts were made to test a 2.4-m (7.8-ft) section of the Tamarisk Member, which consists of a claystone/mudstone/siltstone sequence overlain and underlain by anhydrite, in two wells, H-14 and H-16. Permeability of the Tamarisk Member was too low to yield a transmissivity value in either well, but transmissivity of the claystone sequence was estimated to be about two orders of magnitude less than values calculated for the unnamed lower member (Beauheim, 1987c).

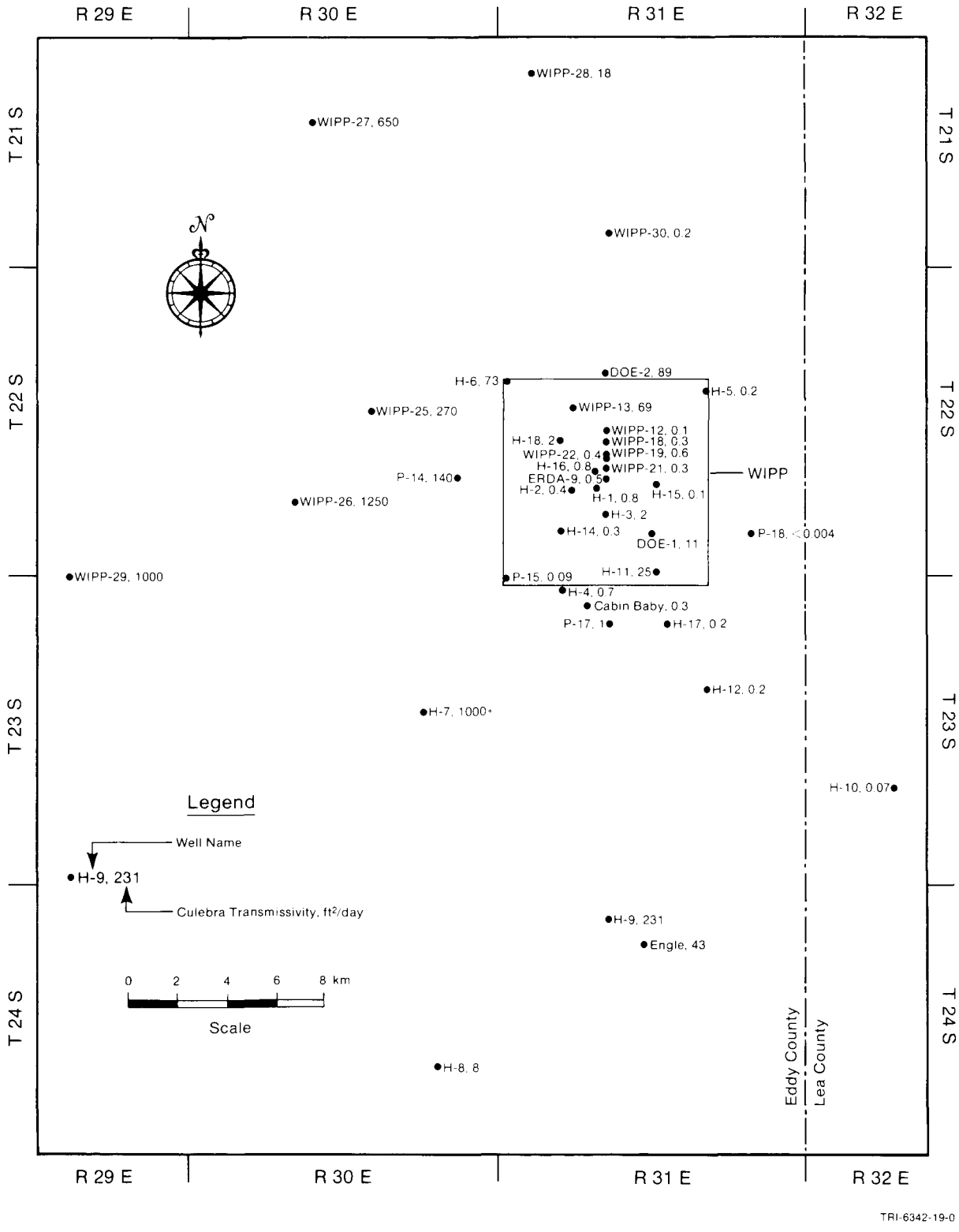

Figure 3-10. Wells Tested by the WIPP Project (Beauheim, 1988).

TABLE 3-1. MEAN THICKNESS OF RUSTLER FORMATION MEMBERS IN VICINITY OF THE WIPP AND NASH DRAW FOR 513 SAMPLES

Member	Mean Thickness (m)	Standard Deviation	Minimum Value (m)	Maximum Value (m)
Forty-niner Claystone	20.0	3.3	5.5	35.1
Magenta Dolomite	6.5	1.2	3.0	11.2
Tamarisk Claystone	39.5	15.0	7.6	84.4
Culebra Dolomite	7.5	1.42	3.0	13.7
Unnamed lower member	39.1	11.7	2.8	162.1

The uppermost member of the Rustler, the Forty-niner Member, consists of anhydrite interbedded with a layer of siltstone. The unit ranges in thickness from 6 to 35 m (20 to 115 ft) and has a mean thickness of 20 m (65 ft) (Table 3-1). At the WIPP, the unit is about 20 m (65 ft) thick, is of uniform thickness throughout the Study Area, and is consistent in structure with the lower units. Tests also were conducted on the Forty-niner Member in well H-14 on a claystone unit and on an upper anhydrite unit, and in well H-16 on a clayey unit. Forty-niner claystone in well H-14 and clay in well H-16 yielded estimated transmissivity values that ranged from 2.4×10^{-10} to 7.6×10^{-8} m^2/s (2.2×10^{-4} to 7.1×10^{-2} ft^2/d). The anhydrite permeability was judged to be too low to test in a short time (days) (Beauheim, 1987c).

Rustler Formation Hydrostratigraphic Units

Aquifers are defined as permeable, saturated geologic units that yield water under normal gradients in useful quantities. The hydraulic conductivity must be on the order of 10^{-6} m/s (~10^{-6} ft/s) or better (Freeze and Cherry, 1979). Under this definition, three units in the Rustler can be considered as marginal aquifers. Taken in a relative sense, though, these units have hydraulic conductivities that are several orders of magnitude greater than the intervening aquitards and thus are considered as hydrostratigraphic units here. The following summaries are for the Culebra Dolomite hydrostratigraphic unit (Mercer, 1983; Beauheim, 1987c; Lappin, 1988; Brinster, 1989 (in preparation); Davies, 1989). More detailed discussions of the other hydrostratigraphic units are available.

The Culebra Dolomite Member of the Rustler is microcrystalline grayish dolomite or dolomitic limestone with solution cavities (Vine, 1963). The Culebra Dolomite, where present, ranges in thickness from 3 to 14 m (10 to 46 ft) and has a mean thickness of about 7 m (23 ft) (Table 3-1). In the Study Area, the Culebra Dolomite has a relatively uniform thickness. The Culebra Dolomite dips fairly steeply to the northeast 0.01 m/m northeast of the WIPP

but in the western part of the Study Area the Culebra is relatively flat lying 0.001 m/m. Outcrops of the Culebra occur in the southern part of Nash Draw and along the Pecos River.

Hydrologic Properties of the Culebra Hydrostratigraphic Unit

More is known about the hydrologic properties of the Culebra Dolomite Member than any other unit in the Study Area. The following discussion of hydrologic properties is a summary of work to date (Mercer and Orr, 1977; Mercer and Orr, 1979; Mercer, 1983; Beauheim, 1987b; LaVenue et al., 1988). A comprehensive data base has been compiled for the Culebra Dolomite Member (see Table 3-2).

In the vicinity of the WIPP the mean thickness of the unit is 7.7 m (~25 ft) (LaVenue et al., 1988). Transmissivity ranges from 10^{-3} m^2/s (~10^3 ft^2/d) in the Nash Draw vicinity to 10^{-9} m^2/s (~10^{-3} ft^2/d) east of the WIPP. A potentiometric map of calculated freshwater heads shows that regional flow changes from a southerly direction at the WIPP to a southwesterly direction in Nash Draw (Figure 3-11).

A porosity value of 0.20 has been used for the single-porosity conceptualization and for the matrix porosity of the dual-porosity conceptualization (Haug et al., 1987). A value of 0.20 was considered (Haug et al., 1987) to be representative of porosities ranging from 0.07 to 0.30, obtained from laboratory analyses of 3-cm (1-in) plugs taken from core samples. Total porosities of 0.144 and 0.137 and effective porosities of 0.078 and 0.111 for two blocks of dolomite taken from depths of 154 m (504 ft) and 157 m (513 ft) from the access shaft excavation for Project Gnome were reported (Cooper and Glanzman, 1971).

The quality of Culebra water is marginal and usage of this water is restricted mostly to stock watering; none is used for domestic purposes. Total dissolved solids range from 3,200 to 420,000 mg/ℓ at test holes H-8b and P-18, respectively. Fluid density ranges from 1.000 to 1.153 g/cm^3 (Table 3-2) (Density of P-18 waters has not been measured but is probably >1.153 g/cm^3).

Summary of Hydrologic Modeling

Two modeling studies conducted in the WIPP vicinity are used as a basis for local scale modeling (Haug et al., 1987; LaVenue et al., 1988). The earlier model study's objectives were to (1) document a hydrologic data base for the Culebra Dolomite Member at the WIPP; (2) conceptualize the hydrology and develop a modeling strategy; and (3) present the approach to model calibration and the modeling results for the Culebra Dolomite before it was disturbed by

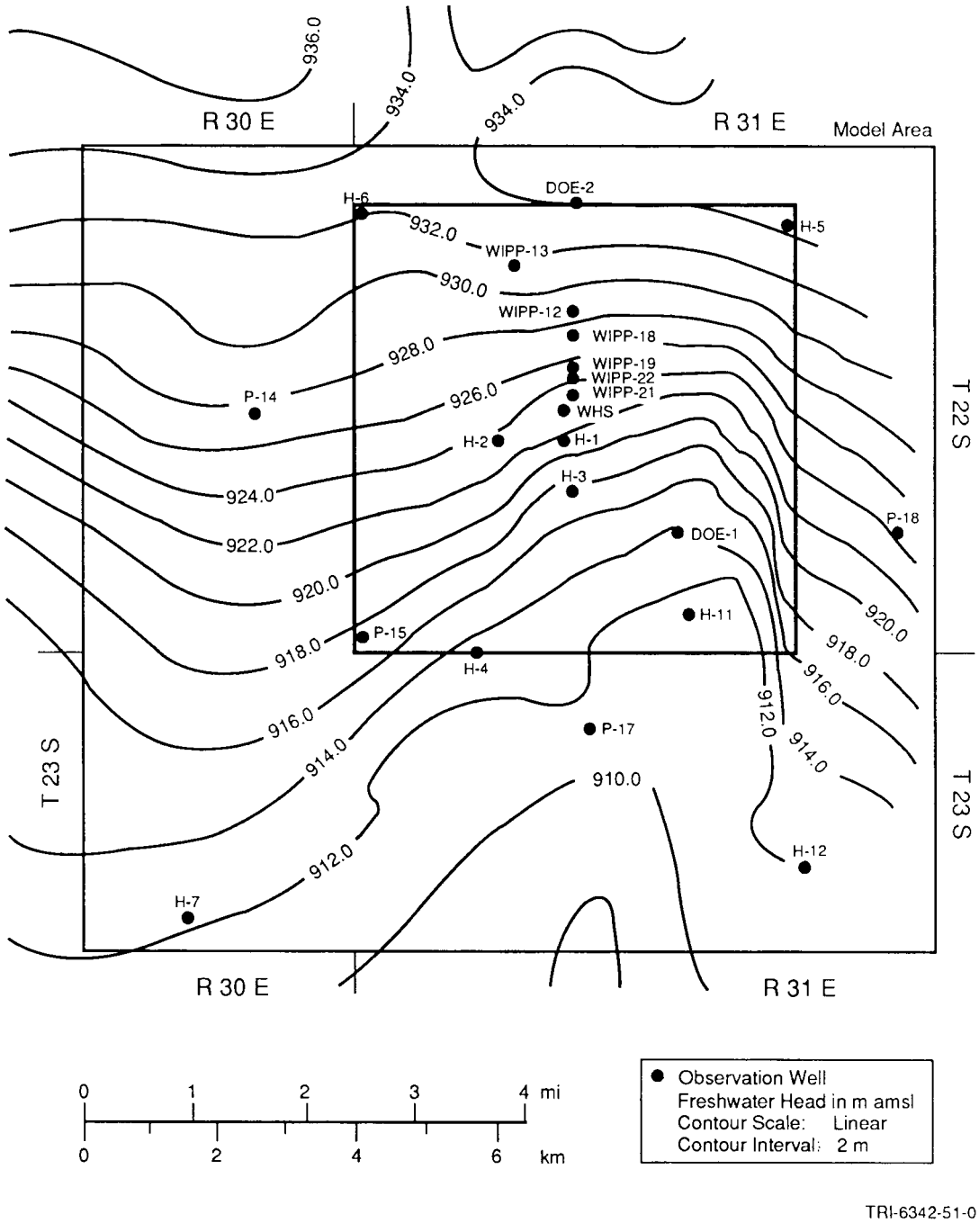

Figure 3-11. Best Estimate of the Undisturbed Freshwater Heads in the Culebra Dolomite Member (From Haug et al., 1987).

TABLE 3-2. CULEBRA DOLOMITE DATA BASE USED FOR TWO-DIMENSIONAL CULEBRA MODEL (LaVenue et al., 1988)

Well	Transmissivity (m^2/s)	Water Level (m)	Density (g/cm^3)	Thickness (m)	Storativity
H1	7.56×10^{-7}	921.6	1.022	7.0	1×10^{-4}
H2	5.61×10^{-7}	923.5	1.009	6.1	1×10^{-9}
H3	2.47×10^{-6}	917.1	1.036	7.3	.
H4	1.02×10^{-6}	913.3	1.016	7.7	1×10^{-9}
H5	1.52×10^{-7}	933.5	1.102	7.2	1×10^{-5}
H6	7.95×10^{-5}	932.3	1.039	7.0	.
H7	1.11×10^{-3}	912.6	1.001	11.3	.
H8	8.86×10^{-6}	911.8	1.000	7.9	.
H9	1.73×10^{-4}	907.0	1.001	9.1	.
H10	7.56×10^{-8}	920.8	1.047	9.4	1×10^{-4}
H11	2.76×10^{-5}	912.5	1.078	7.6	.
H12	1.84×10^{-7}	913.5	1.093	8.2	.
H14	3.29×10^{-7}	915.0	1.008	8.2	.
H15	1.32×10^{-7}	918.0	1.153	6.7	.
H16	7.56×10^{-7}	.	.	7.6	.
H17	2.16×10^{-7}	917.5	1.103	7.8	.
DOE1	1.19×10^{-5}	915.0	1.088	7.0	.
DOE2	9.61×10^{-5}	935.4	1.041	6.7	.
P14	2.30×10^{-4}	927.0	1.017	6.7	.
P15	9.26×10^{-8}	916.4	1.015	6.7	1×10^{-4}
P17	1.38×10^{-6}	912.6	1.061	7.6	1×10^{-6}
P18	1.87×10^{-9}	.	.	8.8	.
ERDA9	5.08×10^{-7}	.	.	7.0	.
CABIN1	3.02×10^{-7}	911.2	.	7.9	.
ENGLE	4.64×10^{-5}	.	1.001	6.7	.
USGS1	5.54×10^{-4}	909.0	.	7.8	.
WIPP12	3.24×10^{-8}	932.2	.	7.6	.
WIPP13	7.45×10^{-5}	934.0	1.043	7.0	.
WIPP18	3.24×10^{-7}	930.0	.	6.7	.
WIPP19	6.48×10^{-7}	.	.	6.4	.
WIPP21	2.70×10^{-7}	.	.	7.3	.
WIPP22	4.00×10^{-7}	.	.	6.7	.
WIPP25	2.92×10^{-4}	931.0	1.008	7.7	.
WIPP26	1.35×10^{-3}	917.5	1.012	7.0	.
WIPP27	7.02×10^{-4}	937.5	.	7.9	.
WIPP28	1.95×10^{-5}	938.1	1.032	7.9	.
WIPP29	1.00×10^{-3}	905.4	.	9.1	.
WIPP30	3.24×10^{-7}	934.7	1.041	7.0	1×10^{-4}

pumping and for the transient conditions caused by the pumping. The latter study's objectives were similar: (1) developing the data base for the Culebra Dolomite; (2) conceptualizing the model; and (3) presenting calibration techniques and results. The former study area is 12.24 × 11.7 km (4.73 × 4.52 mi), encompassing an area of 143.21 km^2 (55.30 mi^2). The latter study area was extended to 24 × 25 km (15 × 16 mi) and covers an area of 600 km^2 (232 mi^2).

The more recent study (LaVenue et al., 1988) is used in this demonstration. Data for the SWIFT II computer code (Table 3-2) were obtained from reports on basic data, hydrologic data, interpretations, water quality, and geochemistry (LaVenue et al., 1988, Appendices A through G).

The following is a brief description of the SWIFT II computer code and the modeling approach (Haug et al., 1987; LaVenue et al., 1988 ; Reeves et al., 1986a and 1986b; Ward et al., 1984). SWIFT II is a transient, three-dimensional, finite-difference code that solves coupled equations for flow and transport in singly or doubly porous geologic media. The processes solved with SWIFT II are: fluid flow, heat transport, brine migration transport, and trace-species miscible displacement (radionuclide transport). Steady-state and transient-flow simulations employ the steady-state and transient flow equations with variable fluid density. Fluid densities are fixed over space; thus, brine transport is not calculated. By fixing fluid densities, densities observed today are maintained and can be used in calculating formation pressures and flow directions (LaVenue et al., 1988). The double-porosity option in SWIFT II is not used (Haug et al., 1987) because on the large scale, dual-porosity effects are negligible.

The expanded model area minimizes effects of boundaries on transient modeling results for multipad pumping tests at H-3 and H-13 (LaVenue et al., 1988). Model gridding is finer where the density of data is greater near the center of the model area. Grid size increases outward by less than a factor of two in order to maintain numerical stability. The model is one layer thick (z direction) and 26 grid blocks wide (x direction) by 44 grid blocks long (y direction) (Table 3-3). A mean thickness of 7.7 m (~25 ft) is used for each block. SWIFT II has an option of using the exact elevation of each grid block utilized. Elevations are calculated from borehole data using a kriging code (Figure 3-12). Physical constants used (Haug et al., 1987) include some constants, such as heat capacity, that have no effect on flow results because the equation for heat is not solved (Table 3-4).

The transmissivity data base for the Culebra Dolomite Member (Table 3-2) is based on numerous test analyses reported in the literature describing hydrologic parameters (LaVenue et al., 1988). The transmissivity data taken from the literature are evaluated by judging the scale the test covered. For example, a slug test covers a smaller volume of porous medium than does a pumping test. This interpretation is used to determine values of transmissivity relative to model scale. Kriging techniques are used in determining the transmissivity surface (LaVenue et al., 1988). Kriged transmissivities for the Culebra (Figure 3-13) generally decrease easterly from Nash Draw. SWIFT II requires hydraulic conductivities over the domain. Values are calculated by dividing kriged transmissivities by kriged thicknesses for each grid block.

Mean storativity is estimated to be between 1×10^{-5} and 5×10^{-4} with a range over five orders of magnitude (Table 3-2) (LaVenue et al., 1988). A porosity of 0.16 is used in the model and for travel time calculations. Formation fluid density for the model region is estimated using kriging techniques on

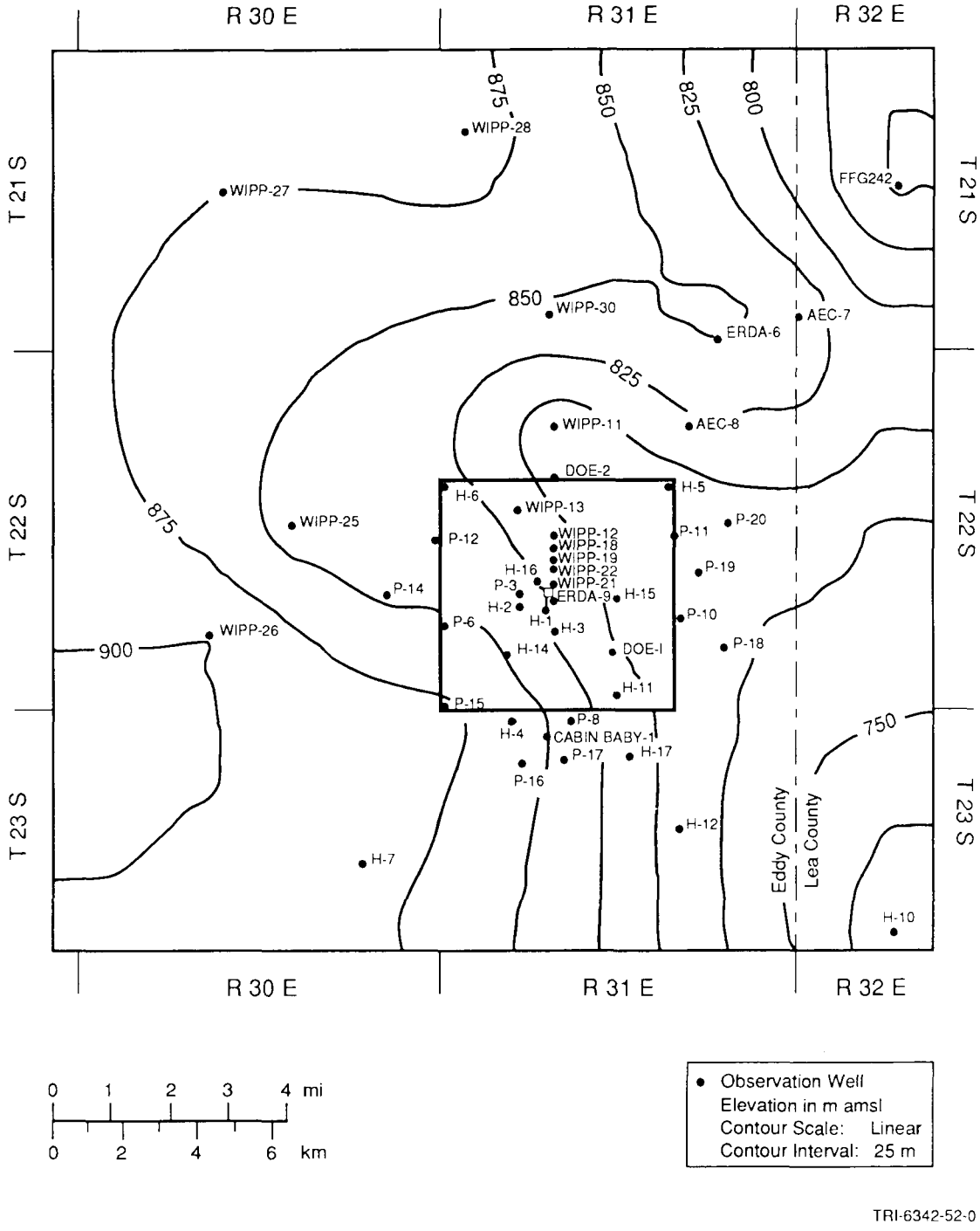

Figure 3-12. Center-of-Culebra Kriged Elevations Over Modeled Region (Reproduced From LaVenue et al., 1988).

TABLE 3-3. COORDINATES AND DIMENSIONS OF MODEL AREA AND GRID BLOCKS (LaVenue et al., 1988)

UTM* Coordinates of the Model-Area Corners		
Southwest corner	35 72 000 m N	6 00 000 m E
Southeast corner	35 72 000 m N	6 24 000 m E
Northeast corner	35 97 000 m N	6 24 000 m E
Northwest corner	35 97 000 m N	6 00 000 m E
Dimensions of the Model Area		
East - West	24.0 km (14.9 mi)	
North - South	25.0 km (15.6 mi)	
Area	600.0 km^2 (231.7 mi^2)	
Grid Block Dimensions (m)		
From West to East	2700, 2600, 2200, 1100, 1000, 700, 600, 700, 600, 350, 200, 200, 200, 200, 150, 150, 150, 250, 450, 500, 600, 800, 1000, 2000, 2300, 2300.	
From South to North	2000, 1000, 1000, 1000, 800, 500, 300, 300, 400, 520, 320, 320, 320, 240, 260, 260, 260, 190, 140, 140, 140, 160, 140, 140, 190, 300, 360, 220, 220, 220, 340, 220, 140, 120, 220, 400, 700, 1000, 1400, 1600, 1800, 1600, 1600, 1500.	

*Universal Transverse Mercator

the density data. Geochemical evidence indicates that the fluid density should be fixed over the Study Area using the appropriate SWIFT II option because fluid density over the region is not at steady-state and therefore cannot be used for steady-state calibration (LaVenue et al., 1988).

Initial undisturbed pressures expressed in equivalent freshwater heads are estimated using the same kriging techniques used for fluid density and

TABLE 3-4. PHYSICAL CONSTANTS USED IN THE CULEBRA MODEL (LaVenue et al., 1988)

Fluid Properties		Reference
Temperature	25 °C	INTERA (1986)
Compressibility	4.53×10^{-10} m^2/N (25°C)	Langguth and Voight (1980)
Thermal Expansion Factor	2.07×10^{-4} °C^{-1}	Kuchling (1982)
Heat Capacity	4.18×10^{3} J/kg °C	Kuchling (1982)
Viscosity	1.0×10^{-3} Pa s	Haug et al. (1987)
Density		
Freshwater	1000 kg/m^3	Haug et al. (1987)
Brine	2000 kg/m^3	Haug et al. (1987)
Rock Properties		
Compressibility	1.1×10^{-9} m^2/N	Freeze and Cherry (1979)
Heat Capacity	$8.0 \times 10^{+2}$ J/kg°C	Kuchling (1982)
Density	2500 kg/m^3	Kuchling (1982)
Transport Properties		
Longitudinal Dispersivity	50.0 m	Haug et al. (1987)
Transverse Dispersivity	2.5 m	Haug et al. (1987)
Molecular Diffusivity in Geologic Medium	1.6×10^{-10} m^2/s	Bear (1972), Lerman (1979)

transmissivity (LaVenue et al., 1988). Flow in the vicinity of the WIPP is generally to the south.(Figure 3-11). In the north-central and central part of the Study Area, gradients are steeper and are consistent with the low transmissivities (Figure 3-13). The gradient is also low to the south in areas near wells H-4, CB-1, P-17, and H-17 where transmissivites are low (Figure 3-13). "Pilot points" were introduced modifying transmissivity values in the area to calibrate the model (LaVenue et al., 1988). The modification of the aquifer transmissivity values ranged from 3 x 10^{-5} to 2 x 10^{-4} m/s (9 to 57 ft/d) to increase the groundwater flux and to level out the calculated potentiometric surface.

Model inputs using SWIFT II are taken directly from tables (Table 3-4) or calculated using kriged data. Water pressures at the model-boundary grid blocks (Table 3-5) are calculated using maps of the equivalent freshwater head

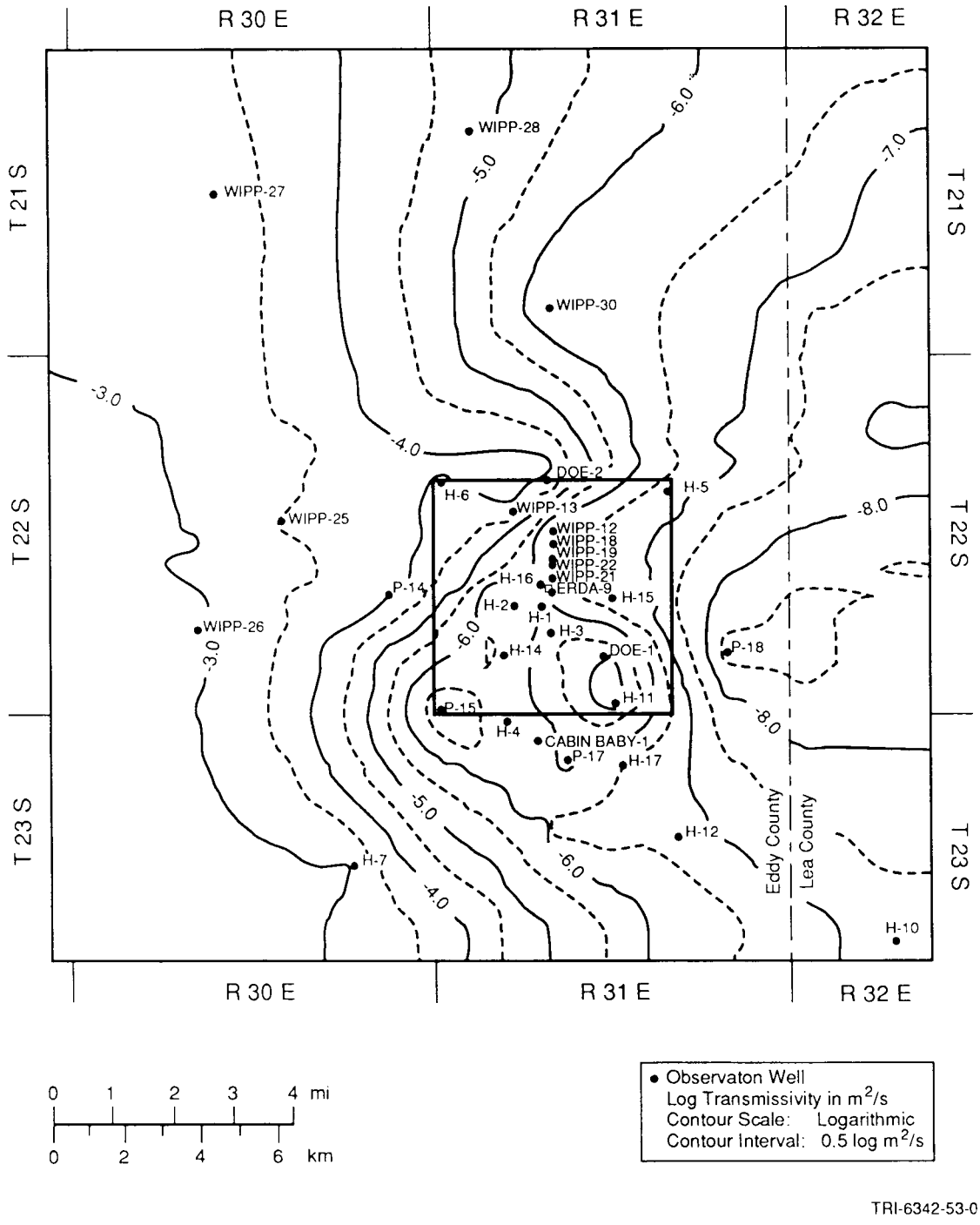

Figure 3-13. Kriged Transmissivities (Reproduced from LaVenue et al., 1988)

TABLE 3-5. BOUNDARY CONDITIONS FOR STEADY-STATE CALIBRATED CULEBRA MODEL (LaVenue et al., 1988)

Model Indices I	J	K	Grid Block Center Elevation (m)	Freshwater Head (m)	Fluid Density (kg/m^3)
Western Boundary					
1	1	1	897.5	910.0	1000.0
1	2	1	899.8	910.6	1000.0
1	3	1	901.2	911.0	1000.0
1	4	1	902.1	911.4	1001.5
1	5	1	902.6	911.8	1001.5
1	6	1	901.8	912.0	1002.2
1	7	1	901.9	912.4	1002.7
1	8	1	901.9	912.8	1003.0
1	9	1	901.8	913.2	1003.3
1	10	1	901.6	913.6	1003.5
1	11	1	901.2	914.0	1003.7
1	12	1	900.7	914.4	1003.5
1	13	1	900.0	914.8	1003.4
1	14	1	899.3	915.2	1003.3
1	15	1	898.6	915.6	1003.1
1	16	1	897.7	916.0	1002.9
1	17	1	896.2	916.8	1002.7
1	18	1	895.2	917.6	1002.4
1	19	1	894.5	918.3	1002.3
1	20	1	893.9	919.1	1002.1
1	21	1	893.2	919.8	1001.9
1	22	1	892.5	920.6	1001.7
1	23	1	891.8	921.3	1001.5
1	24	1	891.2	922.1	1001.3
1	25	1	890.4	922.9	1001.2
1	26	1	889.2	923.6	1000.9
1	27	1	887.7	924.4	1000.6
1	28	1	886.4	925.1	1000.4
1	29	1	885.0	925.9	1000.3
1	30	1	884.1	926.6	1000.2
1	31	1	883.0	927.5	1000.1
1	32	1	881.9	928.2	1000.0
1	33	1	881.3	929.0	1000.0
1	34	1	880.9	929.7	1000.0
1	35	1	880.4	930.5	1000.0
1	36	1	879.5	931.2	1000.0
1	37	1	878.3	932.1	1000.0
1	38	1	877.1	934.0	1000.0
1	39	1	876.2	934.5	1000.0
1	40	1	876.8	936.0	1000.0
1	41	1	878.3	938.0	1000.0
1	42	1	880.9	939.0	1000.0
1	43	1	883.8	940.0	1000.0

TABLE 3-5. BOUNDARY CONDITIONS FOR STEADY-STATE CALIBRATED CULEBRA MODEL (LaVenue et al., 1988) (Concluded)

Model Indices I	J	K	Grid Block Center Elevation (m)	Freshwater Head (m)	Fluid Density (kg/m^3)
Northern Boundary					
1	44	1	886.4	942.4	1000.0
2	44	1	884.7	941.7	1000.9
3	44	1	879.9	941.0	1009.7
4	44	1	881.1	941.1	1016.7
5	44	1	881.9	941.2	1021.2
6	44	1	882.3	941.4	1027.7
7	44	1	882.0	941.5	1031.8
8	44	1	880.6	941.7	1036.2
9	44	1	877.8	941.9	1040.8
10	44	1	875.1	942.0	1044.3
11	44	1	873.2	942.1	1046.5
12	44	1	871.7	942.2	1048.1
13	44	1	870.1	942.2	1049.7
14	44	1	868.5	942.3	1051.3
15	44	1	867.1	942.3	1052.8
16	44	1	865.8	942.4	1054.1
17	44	1	864.5	942.4	1055.4
18	44	1	862.8	942.5	1053.4
19	44	1	859.7	942.6	1056.3
20	44	1	855.3	942.7	1063.1
21	44	1	850.1	942.8	1068.5
22	44	1	843.1	943.0	1076.4
23	44	1	833.4	943.3	1086.3
24	44	1	815.6	943.7	1105.4
25	44	1	785.9	944.3	1134.7
26	44	1	755.3	946.0	1163.0
Southern Boundary					
2	1	1	893.2	910.0	1000.0
3	1	1	886.9	910.0	1000.0
4	1	1	880.5	910.0	1000.9
5	1	1	874.7	910.0	1004.7
6	1	1	869.1	910.0	1008.7
7	1	1	864.2	910.0	1012.9
8	1	1	858.9	910.0	1017.4
9	1	1	855.3	910.0	1022.4
10	1	1	850.6	910.0	1026.8
11	1	1	847.8	910.0	1029.3
12	1	1	845.7	910.0	1031.1
13	1	1	843.3	910.0	1035.0
14	1	1	841.3	910.0	1036.8
15	1	1	839.3	910.0	1038.3
16	1	1	837.6	910.0	1039.7
17	1	1	835.8	910.3	1041.1
18	1	1	833.4	910.5	1043.0
19	1	1	829.1	911.0	1045.7
20	1	1	823.1	911.5	1047.7
21	1	1	815.8	912.0	1051.7
22	1	1	806.2	912.5	1055.9
23	1	1	793.4	913.0	1060.0
24	1	1	771.9	914.0	1062.9
25	1	1	740.7	918.0	1060.6
26	1	1	709.3	920.1	1055.1

and fluid density. Hydraulic conductivity, fluid density, and block center elevation are calculated for each grid block using the kriging interpolator.

An earlier model calibration is summarized here (LaVenue et al., 1988). Calibration proceeded from north to south with several regions changed simultaneously to reduce computer time. Increasing freshwater heads in the north required "drains" to be introduced in the south by increasing transmissivities. Freshwater-head boundary conditions (Table 3-5) were used in the SWIFT II simulation to obtain the calibrated steady-state heads (Figure 3-14). Darcy-velocity values and flow directions (Figure 3-15) were results of assumptions made in calibrating the model. Flow was southerly south of the WIPP because of density effects and increased transmissivity in the vicinity of the "pilot points."

Travel times (Table 3-6) were calculated for seven particles in the flow field (Figure 3-15). In those calculations, three particles from Nash Draw and four from within the WIPP boundary were tracked (Figure 3-16). Particles A, B, and C were predicted to travel along Nash Draw and not go through the WIPP. Particle D moved away from the WIPP and eventually exited at the southern boundary of the model area. Particle E traveled through the low-transmissivity zone east of the repository. Particles F and G traveled in the high-transmissivity zone. Particle G, tracked from a point almost at the center of the repository, reached the model boundary in 36,000 years, passing the WIPP boundary at about 13,000 years. The travel time was attributed to the lower transmissivities in the vicinity of H-11 (LaVenue et al., 1988).

The four main conclusions of the reference study for steady-state modeling are repeated here (LaVenue et al., 1988). These conclusions are quoted without comment. They are the basis for the demonstration calculations within the Culebra Dolomite Member.

> The calibrated transmissivity distribution contains the same general trend over the model area as the observed transmissivities with predominantly lower transmissivities ($<1 \times 10^{-7}$ m^2/s) east of the WIPP-site boundary, intermediate transmissivities in the central part of the model area (1×10^{-6} to 1×10^{-4} m^2/s), and high transmissivities ($>1 \times 10^{-3}$ m^2/s) in the western part of the model area representing Nash Draw. Local differences to the general trend are present west of WIPP-30 and WIPP-27 and between H-17 and P-17. The transmissivities in these areas were increased to reduce the differences between the calculated and observed heads to below the uncertainties of the observed heads. The high-transmissivity feature between H-17 and P-17 is less transmissive than a similar feature proposed in Haug et al. (1987).

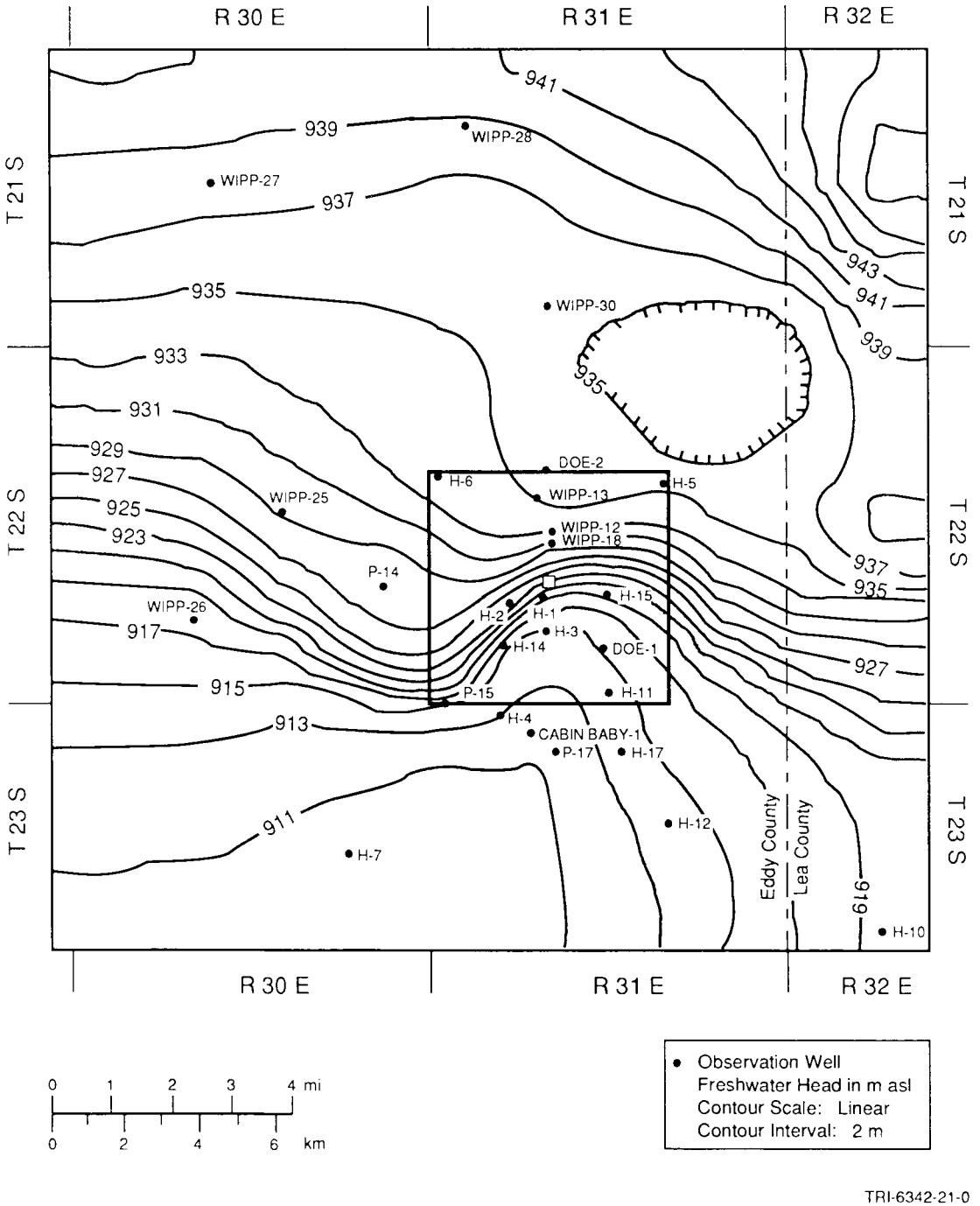

Figure 3-14. Steady-State Calibrated Heads (Reproduced from LaVenue et al., 1988).

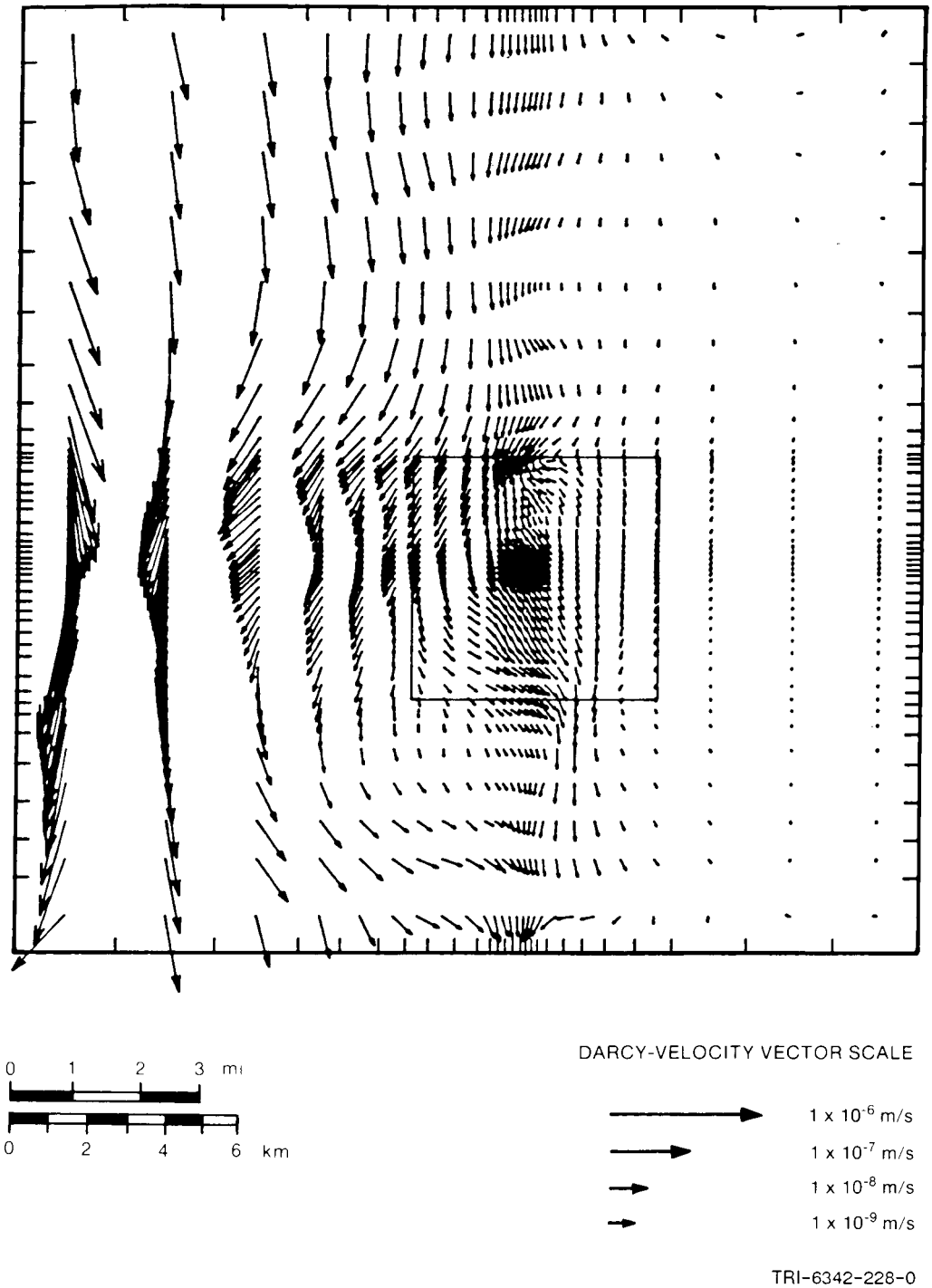

Figure 3-15. Steady-State Darcy-Velocity Vectors (Reproduced from LaVenue et al., 1988).

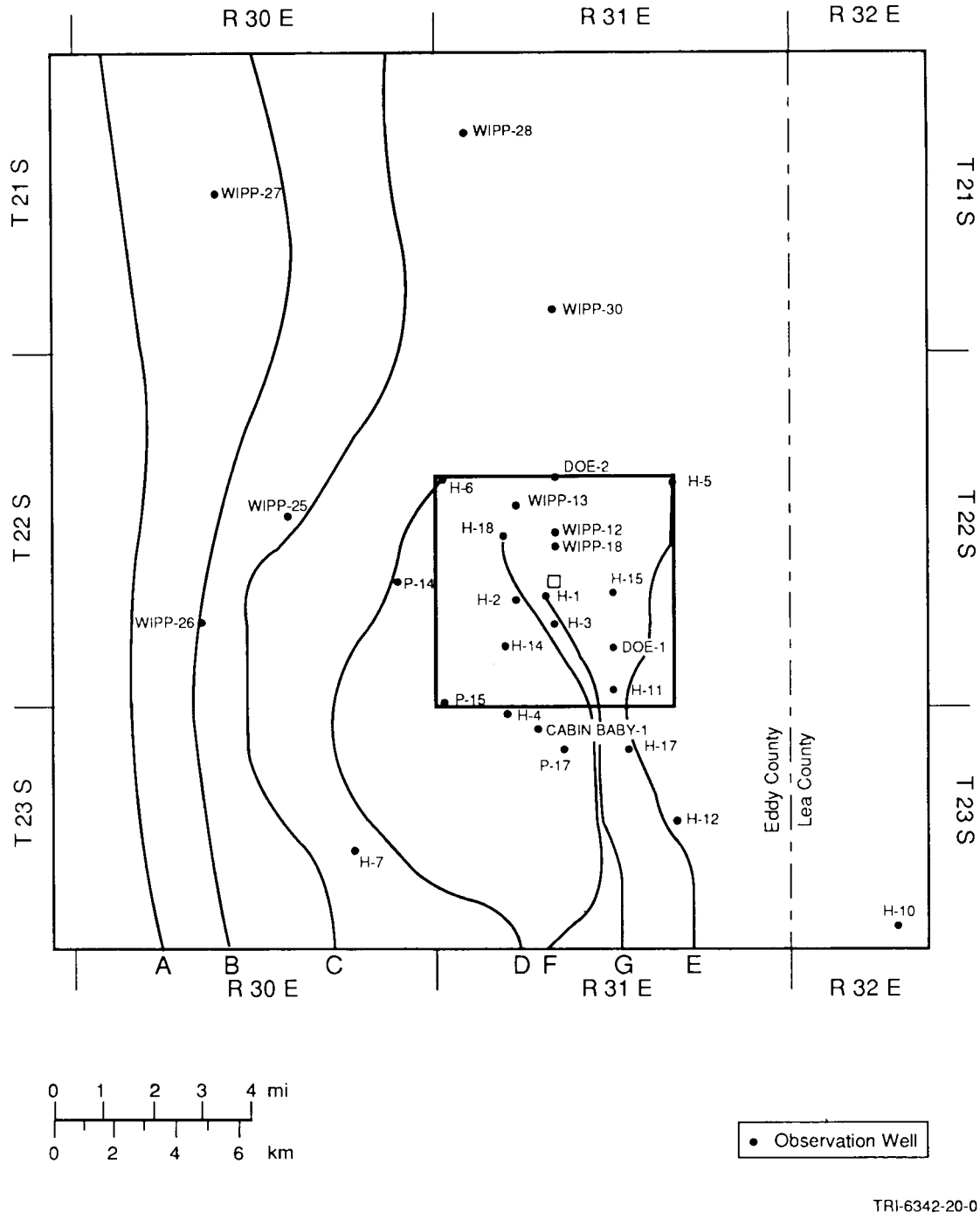

Figure 3-16. Calculated Particle Travel Paths in the Model Region (LaVenue et al., 1988).

TABLE 3-6. CALCULATED PARTICLE TRAVEL TIMES IN YEARS OVER PATHS ILLUSTRATED IN FIGURE 3-8 (LaVenue et al., 1988)

Particle A	4.5×10^2
Particle B	9.8×10^2
Particle C	2.8×10^3
Particle D	1.6×10^4
Particle E	1.4×10^6
Particle F	5.8×10^4
Particle G	3.6×10^4

The steady-state calibrated freshwater heads illustrate low-hydraulic gradients (1×10^{-4} m/m) north of the WIPP-site boundary between WIPP-28 and DOE-2 and south of the WIPP-site boundary between H-17 and H-7. Higher gradients (4×10^{-3} m/m) occur in the central part of the model area.

The model-calculated groundwater-flow directions are predominantly south to southwest. The largest volume of groundwater enters the model area through the northern model boundary and enters the high-transmissivity area along the western part of the model representing Nash Draw. A significant portion of the groundwater within the WIPP site boundaries passes through the high-transmissivity zone south of H-11 and exits the southern boundary of the model area east of H-7. The model-calculated flow directions support conclusions from previous modeling and isotopic studies that the groundwater chemistry is not at steady state with respect to groundwater flow.

The calculated Darcy velocities range over six orders of magnitude in the model area. The highest velocities (1×10^{-7} to 1×10^{-6} m/s) occur in the western portion of the model area representing Nash Draw. Darcy velocities within the WIPP-site boundary range from approximately 5×10^{-10} m/s in the vicinity of the shafts to 1×10^{-9} m/s in the high-transmissivity zone south of the H-11. Darcy velocities of 1×10^{-12} m/s occur east of the WIPP-site boundary.

CALIBRATION OF GROUNDWATER MODELS FOR THE DEMONSTRATION

A primary objective of the WIPP hydrologic investigations is to provide an estimate of potential travel paths for any portion of the radionuclide inventory migrating into water-bearing units above the facility. Interaction of the groundwater, matrix, and radionuclides along those paths then may be evaluated to assess release to the accessible environment.

To meet this objective, groundwater-flow models are being developed to accurately represent the pertinent hydrologic features accessible to radionuclides escaping the facility under natural and perturbed conditions. Gradients and conductivities from this representation can be used to provide advective migration paths. The purpose of model calibration for performance assessment is to find those sets of hydrologic parameters consistent with observations of the relevant groundwater systems, so that plausible migration paths may be identified and an understanding of the hydrologic system achieved with reasonable certainty.

This section contains some general considerations for model calibration, and a description of the method of calibration to be used in performance assessment modeling.

General Considerations for Calibration

Hydrologic properties of the hydrostratigraphic units overlying the repository have been inferred from interpretation of well tests at many locations at and surrounding the WIPP site (Beauheim, 1987a,b,c). These interpretations provide local estimates of average or effective parameter values, but do not define parameter values over the entire domain of interest. Parameter values and boundary conditions that are indeterminate from well-test results may be estimated from observations of the potentiometric surface. Model calibration is systematically adjusting hydrologic parameters and boundary conditions to bring the calculated potentiometric surface into agreement with the observed potentiometric surface.

Method of Calibration for Site Characterization Models

As discussed above, the regional flow model used in the WIPP performance assessment will include all major hydrostratigraphic units in the Rustler Formation. Most prior investigations have focused on the Culebra Dolomite Member of the Rustler Formation as most likely to provide a pathway for migration of radionuclides away from the disposal system under worst-case conditions. An earlier model constructed as a part of WIPP site characterization incorporates the most complete set of hydrologic data available for the Culebra Dolomite (LaVenue et al., 1988). The calibration method used, however, is not specific to the model, nor to the modeled unit. That calibration procedure (LaVenue et al., 1988), therefore, will be the reference method for calibration of the performance assessment model.

In the reference approach to calibration, dimensions of parameter space (necessary for a well-posed parameter estimation problem) are reduced by assuming stationarity (no trend) of the random field, by assuming that the

mean parameter field belongs to a certain class of functions (e.g., intrinsic random functions), and by assuming a linear relationship between the parameter value at any point and the value at nearby measured points. The assumption of stationarity is essential for identification of variance structure, to which the solution is expected to be sensitive. The six orders of magnitude variation in transmissivity of the Culebra has been attributed to fracturing. Because flow mechanisms are fundamentally different between fractured and intact dolomite, the degree and scale of parameter variability within fractured and unfractured portions of the Culebra can be expected to be unrelated.

An independent covariance estimation and interpolation procedure (kriging) is used to generate the distribution of the potentiometric surface. For a given discretization of the domain (model grid), kriging provides an estimate of the parameter values for each model block, an estimate of potentiometric surface elevation for each block, and a measure of estimation error. In addition, kriging reproduces observed point values, so that the interpolated parameter surface is always consistent with prior estimates of parameter values. Any simulated potentiometric surface can be compared to the interpolation of the observed potentiometric surface, with the estimated error of interpolation used to assess the significance of discrepancies.

Interpolated parameters are determined solely by fixed point values and covariance identified from them. In order to improve the agreement between observed and simulated potentials within the framework of kriging, it is necessary to alter either the covariance or the data used in the interpolation. The first option is unattractive, as the influence of parameter covariance on simulated potentials may not be readily anticipated, and may not be local to the areas of greatest discrepancy in potential. In a region where undersampling has resulted in a paucity of data, observed parameter data have been supplemented with artificial observations or "pilot points" (LaVenue et al., 1988; Haug et al., 1987). The parameter surface was selectively and locally altered to improve agreement between simulated and observed potentials.

REPOSITORY/SHAFT SYSTEM OVERVIEW FOR THE DEMONSTRATION

Undisturbed Conditions

The NEFTRAN computer code is used to simulate undisturbed performance of the disposal system. This code simulates steady-state groundwater flow and radionuclide transport under saturated conditions by subdividing the flow field into a network of one-dimensional "legs." Darcy flow is assumed to be valid for all porous materials along the flow path, although a dual-porosity option exists for fractured media. Mass is conserved at each junction. These

legs may be configured to represent multidimensional flow fields. Radionuclide transport is simulated using a distributed velocity method in which an average velocity is calculated for each isotope from the isotopic velocities in all the legs along the flow path. A generalized flow network (Figure 3-17) for NEFTRAN simulations of undisturbed performance indicates assumed flow direction (arrows) along each leg (uncircled numbers) and nodes (circled numbers).

The relationship between legs in the network and the conceptual model is as follows: Leg 2 represents the seal in MB139; Leg 3 represents MB139 between the seal and base of the shaft; Leg 4 represents the lower, well-consolidated waste-shaft seal (the largest of the four shafts); Leg 5 represents the upper, less well-consolidated shaft seal; Legs 6, 8, and 9 represent the Culebra Dolomite; and Leg 7 represents the intact Salado Formation between the repository and Culebra Dolomite. Leg 1 represents the repository and is included to establish flow toward the seal in MB139, and Leg 10 represents existing flow through the Culebra Dolomite Member. A stock well into the Culebra Dolomite is represented by Node 9. Options in this computer code treat the Culebra Dolomite as either a single-porosity medium or a dual-porosity medium. Because undisturbed performance of the disposal system prevents migration of radionuclides to the Culebra Dolomite Member within 10,000 years, flow in the Culebra Dolomite Member is not simulated (Lappin et al, 1989).

Radionuclide-transport calculations include pathways through Legs 1, 2, 3, 4, 5, 6, 8, and 9, and through Legs 7, 8, and 9. Because NEFTRAN integrates nuclide arrivals at a particular node and not at intermediate nodes, and arrival times to certain nodes along the path through MB139 and the shaft are extremely long, separate simulations are required to determine migration through the shaft to the Culebra Dolomite (Node 6), to the junction of the upper and lower shaft seals (Node 5), to the base of the shaft (Node 4), and at the end of the MB139 seal (Node 3). For the path directly from the repository to the Culebra Dolomite, separate simulations are required to estimate radionuclide migration to Node 7 (Lappin et al., 1989).

The flow network is driven by the pressure gradient between the waste panels (Node 1) and the Culebra Dolomite Member (Node 6). Node 1 pressure conservatively is assumed to be lithostatic (14.8 MPa) and the Node 6 pressure is 1.0 MPa. Pressure is not sampled during the Monte Carlo analysis. The entire system is assumed to be saturated, and one-dimensional Darcy flow is calculated along each leg. Transport of radionuclides is calculated to each node along the pathway to the Culebra.

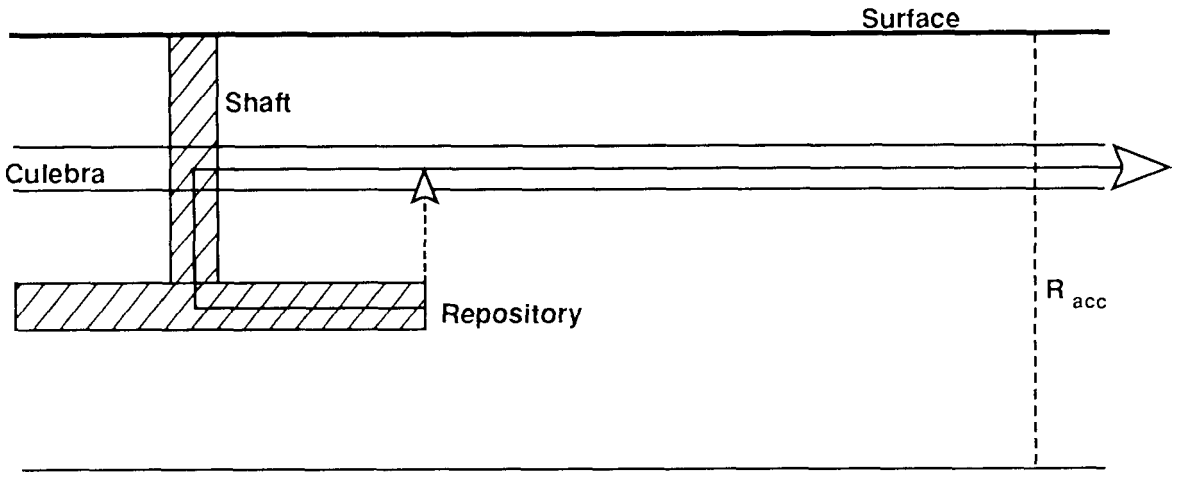

Conceptual Model

R_{acc} = Release at the Subsurface Boundary of the Accessible Environment

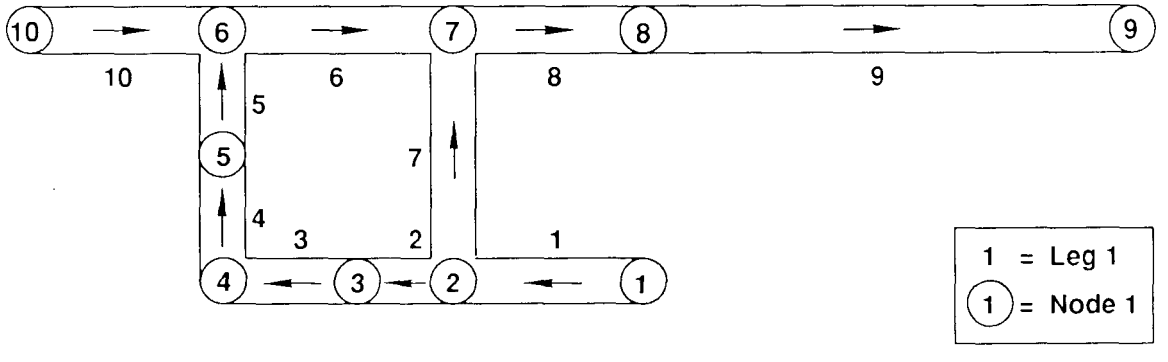

Flow Network

TRI-6342-199-0

Figure 3-17. Conceptual Model and Network for the Undisturbed Disposal System (after Lappin et al., 1989).

Human Intrusion Scenarios: NEFTRAN Simulations

The flow network for NEFTRAN simulations of human intrusion scenarios changes slightly with each scenario. Prior to uncertainty analysis, the NEFTRAN simulations are calibrated by comparing with particle travel times calculated using SWIFT II (Table 3-6) and the conductivity field from earlier studies (LaVenue et al., 1988).

The NEFTRAN flow network (Figure 3-18) for Scenario E1 is as follows: Leg 1 represents the room; Leg 2 represents the segment of the rubble-filled borehole between the Castile Formation and the repository; Leg 3 represents the segment of the hole between the repository and the Culebra Dolomite Member; Leg 4 represents a relatively low-conductivity zone surrounding the repository area and within the Culebra Dolomite above; and Legs 5 and 6 represent higher conductivity zones within the Culebra. Node 6 is 2.5 km (1.5 mi) and Node 7 is 5.0 km (3.0 mi) downgradient from the waste panels. The flow network is driven by pressure gradients between Nodes 1 and 7 and between Nodes 3 and 7. Node 1 pressure is assumed to be between hydrostatic (6 MPa) and lithostatic (15 MPa), and is sampled during the uncertainty analysis. Node 3 pressure is conservatively set at 16 MPa, which is the maximum observed brine pressure (Lappin et al., 1989, Tables 3-19 and E-4).

The NEFTRAN flow network for Scenario E2 (Figure 3-19) is as follows: Leg 1 represents the repository; Leg 2 represents the borehole; Leg 3 represents a zone of relatively low hydraulic conductivity surrounding the repository and in the Culebra Dolomite Member above; and Legs 4 and 5 represent zones of higher conductivity in the Culebra Dolomite. Node 5 is 2.5 km (1.5 mi) downgradient from the waste panels, and Node 6 is 5.0 km (3.0 mi) downgradient from the waste panels.

The NEFTRAN flow network (Figure 3-20) for Scenario E1E2 is as follows: Leg 1 represents the repository; Leg 2 represents the segment of the borehole between the Castile Formation and the repository; Leg 3 represents the segment of the open borehole connecting the repository and the Culebra Dolomite Member; Legs 4, 5, and 6 represent different hydraulic-conductivity zones in the Culebra. Leg 4 represents a zone of relatively low conductivity that overlies and surrounds the repository area; Leg 5 represents a higher conductivity zone that extends approximately 2.5 km (1.5 mi) downgradient (Node 6); and Leg 6 represents a possibly higher conductivity zone that extends beyond 5.0 km (3.0 mi) downgradient (Node 7). Scenario E1E2 is a variation of Scenario E1 because Legs 2, 1, and 3 are in series with pressurized brine circulating from the E1 borehole through the room to the E2 borehole. The pressure gradient driving the flow is between Nodes 3 and 7.

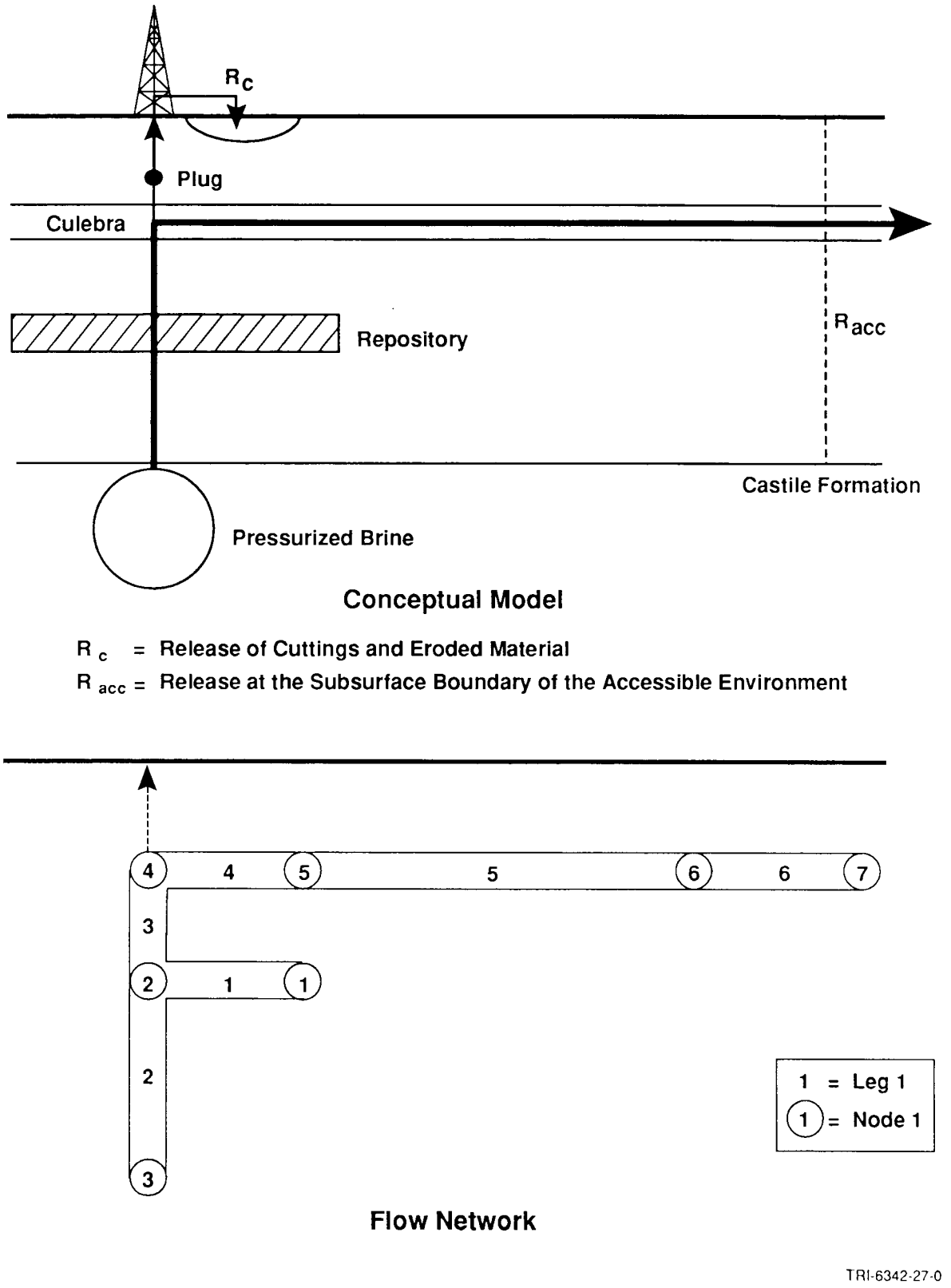

Figure 3-18. Conceptual Model and Flow Network for Scenario E1. Arrows Indicate Assumed Direction of Flow.

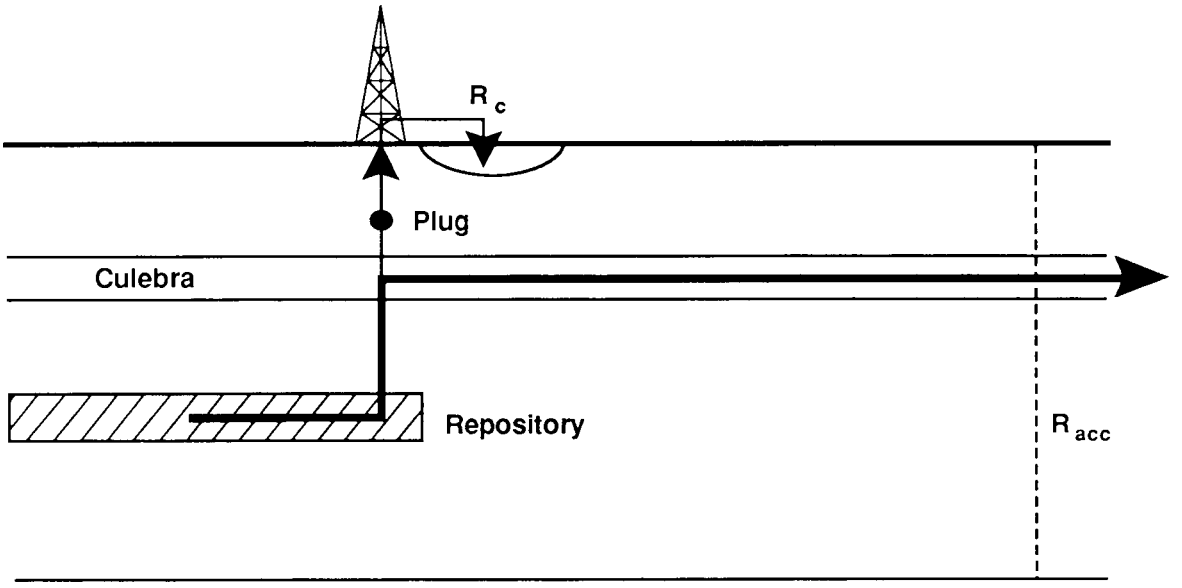

Conceptual Model

R_c = Release of Cuttings and Eroded Material

R_{acc} = Release at the Subsurface Boundary of the Accessible Environment

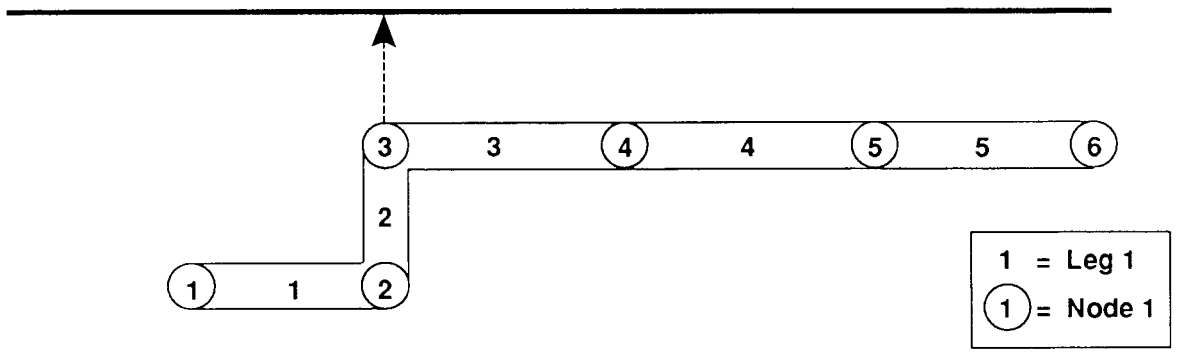

Flow Network

TRI-6342-28-0

Figure 3-19. Conceptual Model and Flow Network for Scenario E2. Arrows Indicate Assumed Direction of Flow.

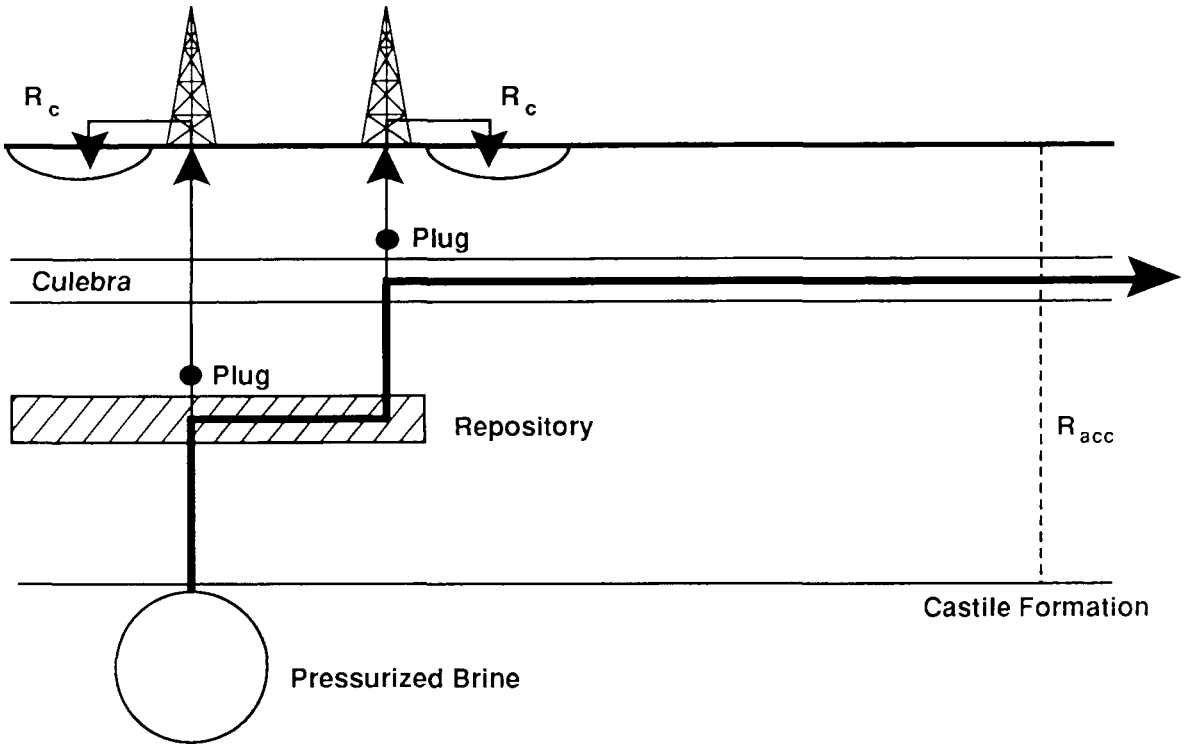

Conceptual Model

R_c = Release of Cuttings and Eroded Material

R_{acc} = Release at the Subsurface Boundary of the Accessible Environment

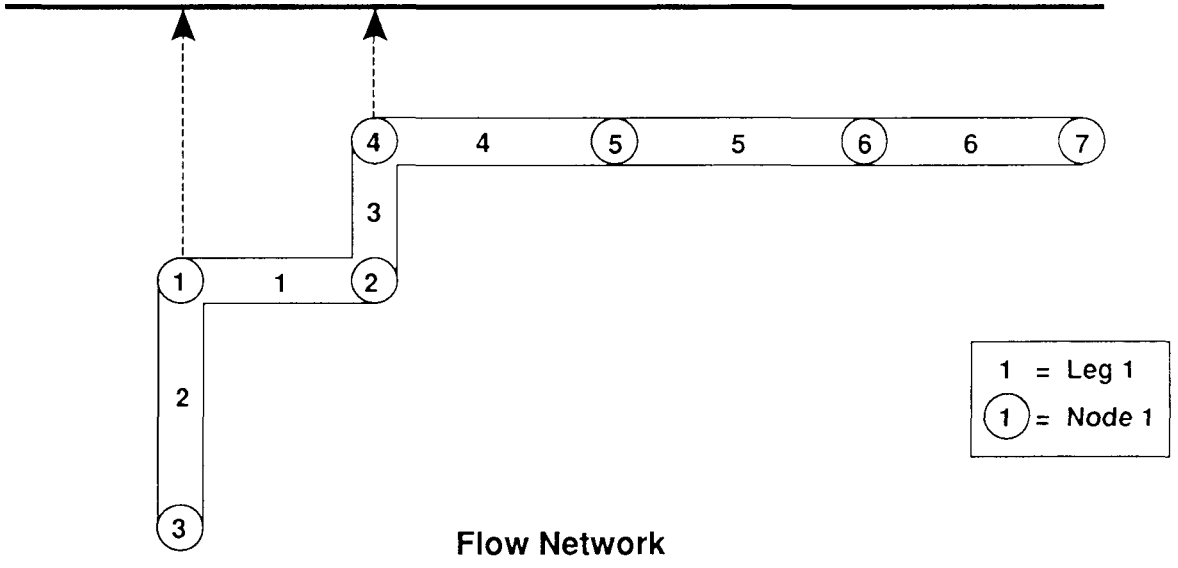

Flow Network

TRI-6342-29-0

Figure 3-20. Conceptual Model for Scenario E1E2. Arrows Indicate Assumed Direction of Flow.

The NEFTRAN flow network (Figure 3-21) for Scenario E1E3 is the same as for Scenario E1 with the addition of Leg 7, which represents the pumping well 2.5 km (1.5 mi) downgradient from the waste panels. The amount of waste diverted by this well depends on when the well is drilled, and on volume of water pumped from the well, radionuclide concentrations in the water, and duration of pumping.

The NEFTRAN flow network (Figure 3-22) for Scenario E2E3 is essentially the same as for Scenario E2. An additional leg (Leg 6) is added from Node 5 to the surface to represent a withdrawal well 2.5 km (1.5 mi) downgradient from the waste panels. Node 7 is 5.0 km (3.0 mi) downgradient from the waste panels.

The NEFTRAN flow network (Figure 3-23) for Scenario E1E2E3 is the same as for Scenario E1E2, except for the addition of Leg 7, which represents the pumping well at 2.5 km (1.5 mi).

Scenarios E1, E2, and E1E2 include removal of cuttings and eroded radioactive material to the surface during the drilling process. It is estimated that no more than the contents of three drums would be removed during one drilling procedure (Lappin et al., 1989). Rather than include this estimate in uncertainty analysis for the demonstration, the contents of three drums for each borehole drilled into a waste panel was added directly to the integrated discharge to the accessible environment for each input vector and each radionuclide.

Scenarios that include Event E3 are simple variations of Scenarios E1, E2, and E1E2. The withdrawal well is assumed to be at Node 6 regardless of water quality, and to produce water for one year (Lappin et al., 1989). The volume of water removed from the Culebra Dolomite is more than the volume supplied by Leg 5, in this demonstration, so the calculated radionuclide concentration is diluted by uncontaminated flow from the Culebra Dolomite. Concentration after dilution is not important for calculating integrated discharge. The number of curies removed to the surface during the one-yr lifetime of the well must be estimated, and added (along with curies in the cuttings and eroded material releases) to the integrated discharge at 5.0 km (3.0 mi). Radionuclides pumped to the surface, which is part of the accessible environment, will add to the integrated discharge only if those radionuclides would not have been counted anyway at the 5.0-km (3.0-mi) point. Travel times through Leg 6 of the Culebra Dolomite are relatively fast, because fracture flow is assumed. Therefore, the withdrawal well is assumed to be active only during the last modeled time step (>50 years). In this case, release through the pumping well adds to any releases at 5.0 km (3.0 mi).

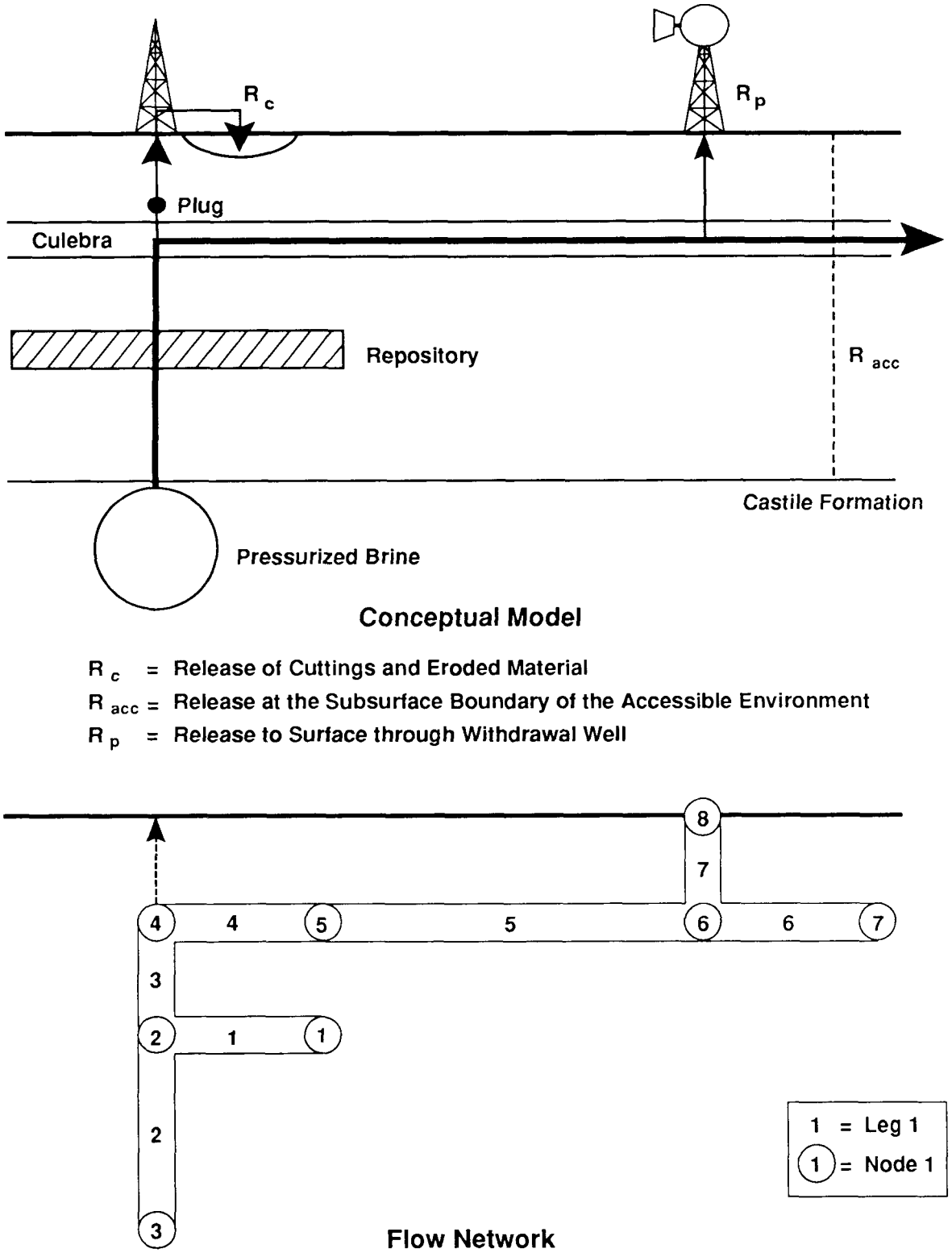

Figure 3-21. Conceptual Model and Flow Network for Scenario E1E3. Arrows Indicate Assumed Direction of Flow.

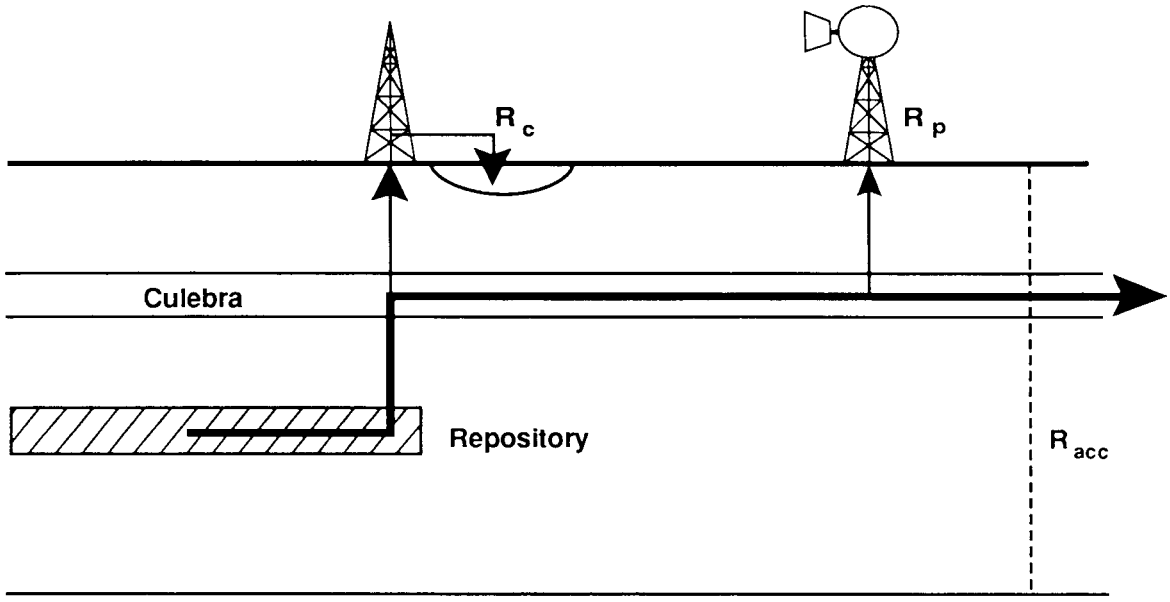

Conceptual Model

R_c = Release of Cuttings and Eroded Material
R_{acc} = Release at the Subsurface Boundary of the Accessible Environment
R_p = Release to Surface through Withdrawal Well

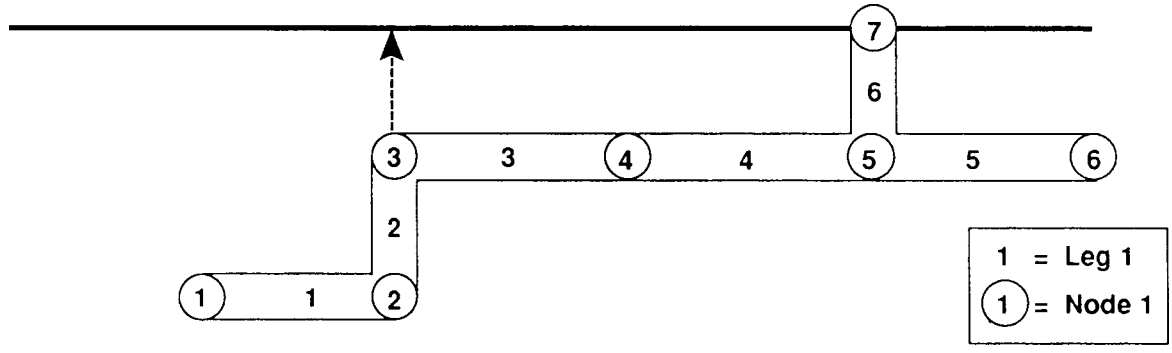

Flow Network

TRI-6342-31-0

Figure 3-22. Conceptual Model and Flow Network for Scenario E2E3. Arrows Indicate Assumed Direction of Flow.

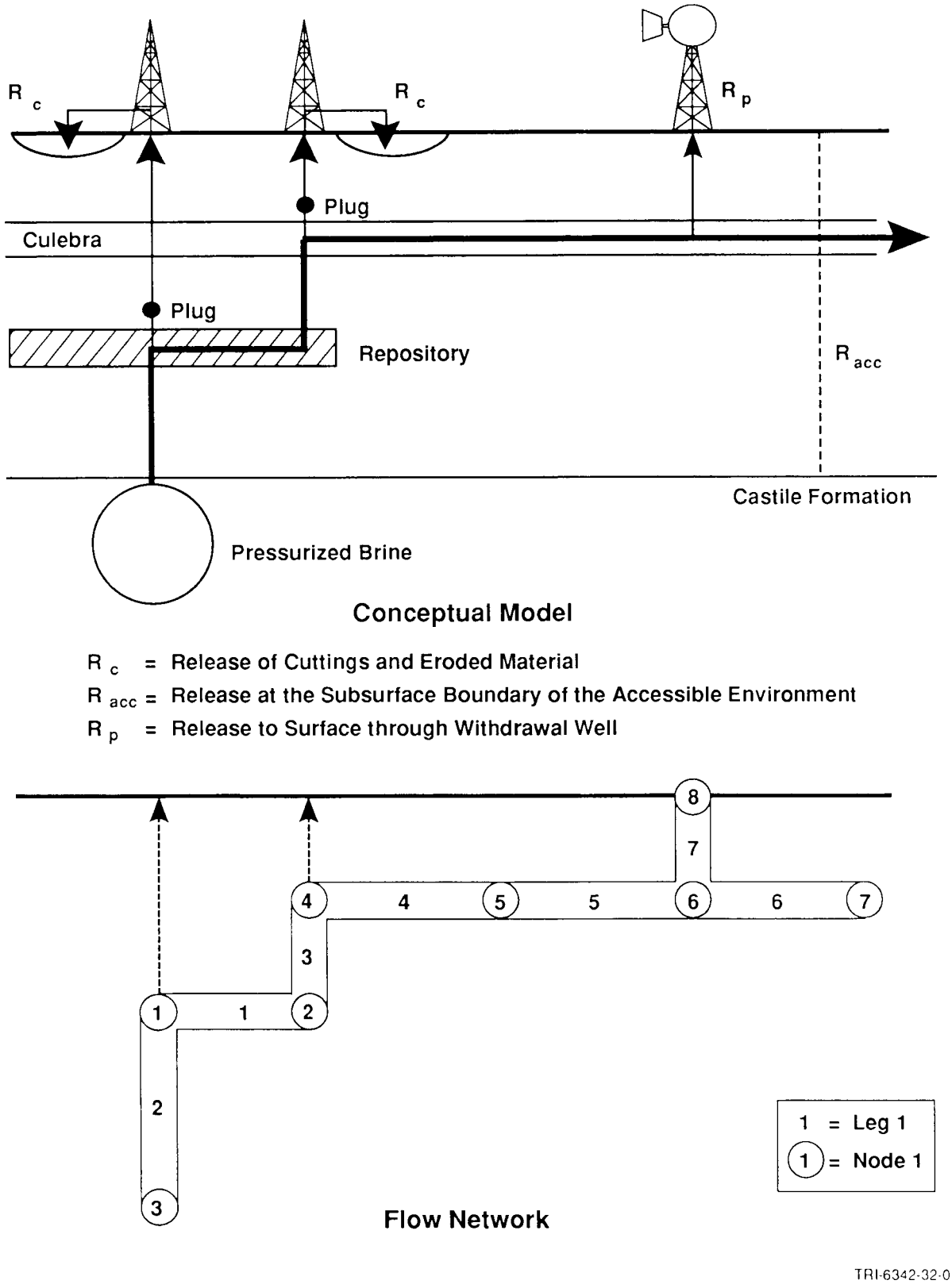

Figure 3-23. Conceptual Model for Scenario E1E2E3. Arrows Indicate Assumed Direction of Flow.

Network models for Scenarios E1, E2, and E1E2 are applied only during uncertainty analysis. Releases from cuttings, eroded material, and withdrawal wells are added directly to integrated releases through the Culebra Dolomite Member that are calculated by NEFTRAN.

Human Intrusion Scenarios: SWIFT/NEFTRAN Simulations

Scenario E1 also was simulated using the CAMCON system with SWIFT II and previously determined conductivity fields (LaVenue et al., 1988). In this procedure, conductivity contour plots are divided into zones of constant conductivity. Conductivity is averaged to estimate an expected value for each zone. A range for each zone is assigned by assuming variation is an order of magnitude in either direction about the mean. Lognormal distributions are constructed for each zone. A conductivity for each zone is sampled during the uncertainty analysis. This change eliminates legs for Culebra Dolomite from NEFTRAN networks for the sampling step. It does not affect legs for the intruding borehole and room. Using CAMCON with both SWIFT II and NEFTRAN involves (1) calculating a flow field with SWIFT II based on the sampled conductivity values (2) calculating a particle trajectory to the 5.0-km (3.0-mi) release point within the flow field and (3) calculating transport of radionuclides with NEFTRAN along this trajectory. This procedure is repeated for each of the 50 input vectors.

Source Term for the Demonstration

A source term based on the modified inventory (Table 3-7) (Lappin et al., 1989) and simplified chains (Table 3-8) is used in the NEFTRAN transport analysis (Lappin et al., 1989). Only the CH-TRU waste is considered in this demonstration.

The concentration of plutonium and americium in any brine that resaturates WIPP disposal rooms, estimated to be 10^{-6} molar (M) (Appendix E) is the solubility-limited source term for the transport analysis (Lappin et al., 1989). This is an intermediate value (on a logarithmic scale) of the range of radionuclide concentrations (10^{-3} to 10^{-9} M) currently used for sensitivity studies of the source term. The intermediate value and the range are estimates. To construct a distribution with these estimates, the intermediate value is used as the median for a loguniform distribution. It is shown in Chapter IV that the calculated CCDF is sensitive to the estimates and distribution selection.

Concentrations are solubility limited. All brine in the waste disposal rooms and drifts is assumed to be in direct contact with MB139 through fractures in floors underlying excavations. For human-intrusion events, the amount of radionuclides entering a borehole depends on the volume of brine within waste

TABLE 3-7. MODIFIED CH-TRU WASTE INVENTORY (Lappin et al., 1989, Table 4-2b)

Radionuclide	$t_{1/2}$ (yr)	Curies	Grams
^{238}Pu	8.77×10^{1}	3.90×10^{6}	2.28×10^{5}
^{239}Pu	2.41×10^{4}	4.25×10^{5}	6.84×10^{6}
^{240}Pu	6.54×10^{3}	1.05×10^{5}	4.61×10^{5}
^{233}U	1.59×10^{5}	7.72×10^{3}	8.15×10^{5}
^{234}U	2.44×10^{5}	0	0
^{235}U	7.04×10^{8}	3.7×10^{-1}	1.71×10^{5}
^{236}U	2.34×10^{7}	0	0
^{241}Am	4.32×10^{2}	7.75×10^{5}	2.26×10^{5}
^{237}Np	2.14×10^{6}	8.02	1.14×10^{4}
^{229}Th	7.43×10^{3}	0	0
^{230}Th	7.70×10^{4}	0	0
^{226}Ra	1.60×10^{3}	0	0
^{210}PB	2.23×10^{1}	0	0

TABLE 3-8. SIMPLIFIED RADIONUCLIDE CHAINS (Lappin et al., 1989, Table 4-3)

(1) $^{240}Pu \rightarrow {}^{236}U$

(2) $^{241}Am \rightarrow {}^{237}Np \rightarrow {}^{233}U \rightarrow {}^{229}Th$

(3) $^{238}Pu \rightarrow {}^{234}U \rightarrow {}^{230}Th \rightarrow {}^{226}Ra \rightarrow {}^{210}Pb$

(4) ^{239}Pu

Note: The inventory to be used for the above four chains is listed in Table 3-7.

panels and accessible to that borehole. A whole panel is assumed to be accessible to circulating Castile Formation pressurized brine and long-term brine inflow from the host rock (Lappin et al., 1989). Preliminary calculations indicate that this assumption is conservative even for the least favorable parameter value selection (Appendix A).

ROOM MODEL FOR THE DEMONSTRATION

Undisturbed Conditions

The room model for undisturbed performance is represented in the NEFTRAN generalized network (see Figure 3-17) as Leg 1. This leg is a one-dimensional flow model driven by room pressure with conductivity and porosity values assumed to be uniform throughout panels. To be consistent with assumptions in earlier work (Appendix B and Lappin et al., 1989), a solubility-limited, well-mixed cell is used for the source model. Because NEFTRAN assumes Darcy flow, it is necessary to assume that the room is saturated. Gas cannot be included within NEFTRAN. Transport out of the saturated room is assumed to begin immediately upon decommissioning of the repository. This analysis does not consider the possibility that for some initial period, the repository will remain dry because of gas generation. For the Individual Protection Requirements' time of 1,000 years, to assume that this time period is zero is conservative.

Distributions are fit to minimum, maximum, and expected or median values (see Table 3-9) for conductivity, porosity, and solubility according to the philosophy described under Selected Distributions and Parameter Ranges and Appendix C. No engineered modifications are considered in the analyses of undisturbed conditions, because no radionuclides escape from the facility as it is currently designed in either 1,000 or 10,000 years.

Human Intrusion Scenarios

The room model for human intrusion is represented as a single leg in the NEFTRAN generalized network. Additional cases are calculated for the E1 human-intrusion scenario. These are (1) Case $E1_a$: ranges and expected values (Table 3-10) (Appendix B) for undisturbed conditions with a 2.5-km (1.5-mi) boundary, (2) Case $E1_b$: as Case $E1_a$, but with a 5.0-km (3.0-mi) boundary, (3) Case $E1_c$: as Case $E1_b$, but with solubility changed by decreasing its range of uncertainty, yet maintaining the same median value, (4) Case $E1_d$: as Case $E1_b$, but with room parameters (conductivity and porosity) changed to show the effect of possible engineered modifications, (5) Case $E1_e$: a combination of Cases $E1_c$ and $E1_d$ where solubility and room parameters changed simultaneously, (6) Case $E1_f$: as Case $E1_b$, but with SWIFT/NEFTRAN system and 15 sampled zones of conductivity in the Culebra, and (7) Case $E1_g$: as Case $E1_e$, but with SWIFT/NEFTRAN system and 15 sampled zones of conductivity in the Culebra.

TABLE 3-9. REFERENCE DATA BASE FOR NEFTRAN SIMULATION OF UNDISTURBED CONDITIONS

Variable	Distribution	Range	Units	Expected Value* or Median**
		Marker Bed 139 Pathway: Sampled Parameters		
Room Pressure	Uniform	[6.0,15.0]	MPa	10.5
Solubility	Loguniform	$[10^{-9},10^{-3}]$	Molar	10^{-6}
Room Conductivity	Beta	$[10^{-11},10^{-6}]$	m/s	10^{-7}
MB139 Seal Conductivity	Lognormal	$[10^{-12},4 \times 10^{-10}]$	m/s	2×10^{-11}
MB139 Seal Porosity	Normal	[0.02,0.04]		0.03
Lower Shaft Seal Conductivity	Lognormal	$[3 \times 10^{-14},10^{-11}]$	m/s	5×10^{-12}
Lower Shaft Seal Porosity	Beta	[0.001,0.08]		0.05
Upper Shaft Seal Conductivity	Lognormal	$[10^{-7},10^{-3}]$	m/s	10^{-5}
Upper Shaft Seal Porosity	Normal	[0.1,0.3]		0.20
MB139 Retardation (Pu,Th)	Beta	[1.0,10.0]		4.7
MB139 Retardation (Am)	Beta	[1.0,10.0]		1.9
Lower Shaft Seal Retardation (Pu,Th,Am)	Beta	[1.0,10.0]		5.2
Lower Shaft Seal Retardation (Np)	Beta	[1.0,10.0]		1.4
Upper Shaft Seal Retardation (Pu,Th,Am)	Beta	[1.0,10.0]		1.7
		Marker Bed 139 Pathway: Unsampled Parameters		
MB139 Retardation (U,Np,Ra,Pb)				1.0
Lower Shaft Seal Retardation (U,Ra,Pb)				1.0
Upper Shaft Seal Retardation (Np)				1.1
Upper Shaft Seal Retardation (U,Ra,Pb)				1.0

*Lappin et al., 1989
**Median value is listed for loguniform and lognormal distributions

TABLE 3-9. REFERENCE DATA BASE FOR NEFTRAN SIMULATION OF UNDISTURBED CONDITIONS (Concluded)

Variable	Distribution	Range	Units	Expected Value* or Median**
Salado Pathway Parameters				
Salado Conductivity		2.9×10^{-14}	m/s	
Salado Porosity				0.001
Salado Retardation (Pu,Am,Th)			m^2	231.0
Salado Retardation (Np)			m^2	24.0
Salado Retardation (U,Ra,Pb)			m^2	3.3

Marker Bed 139 Pathway Constant Parameter Values

Legs:	Repository	Marker Bed Seal	Marker Bed	Lower Shaft Seal	Upper Shaft Seal	Culebra Leg	Culebra Leg	Culebra Leg	Culebra Upgradient
Length (m)	91.4	30	366	200	200	430	1030	3444	400
Area (m^2)	38.9	5.57	5.57	29.2	29.2	800	800	800	800
Rock Density (kg/m^3)	2720	2720	2720	2720	2720	2720	2720	2720	2720
Fluid Density (kg/m^3)	1186	1186	1186	1186	1186	1092	1092	1092	1092

*Lappin et al., 1989
**Median value is listed for loguniform and lognormal distributions

PANEL AND MB139 SEAL MODELING

Undisturbed Conditions

Travel times have been calculated (Lappin et al., 1989) from waste panels to the Culebra Dolomite Member via three pathways: through MB139 and shaft seals, through consolidated drifts and panel/shaft seals, and through the Salado Formation. In that study, the marker bed route dominated because the marker bed's fracture porosity (Table 3-9) was used. Panel seals were assumed to consolidate to within 0.05 of host rock permeability. Travel times through the Salado were greater than a million years. Therefore, transport along the marker bed pathway is used for this demonstration.

TABLE 3-10. REFERENCE DATA BASE FOR NEFTRAN SIMULATION OF HUMAN INTRUSION SCENARIOS

Variable	Distribution	Range	Units	Expected Value* or Median**
Time of Release	Uniform	[0.0,10^4]	yrs	5×10^3
Solubility	Loguniform	[10^{-9},10^{-3}]	Molar	10^{-6}
Alternative Solubility	Loguniform	[10^{-8},10^{-4}]	Molar	10^{-6}
Room Conductivity	Beta	[10^{-11},10^{-6}]	m/s	10^{-7}
Alternative Room Conductivity	Beta	[10^{-14},10^{-10}]	m/s	10^{-11}
Room Porosity	Normal	[0.15,0.21]		0.18
Alternative Room Porosity	Lognormal	[0.05,0.20]		0.10
Borehole conductivity	Lognormal	[10^{-6},10^{-4}]	m/s	10^{-5}
Borehole porosity	Normal	[0.10,0.30]		0.20
Culebra conductivity Leg 4	Lognormal	[10^{-7},10^{-5}]	m/s	10^{-6}
Culebra conductivity Leg 5	Lognormal	[10^{-8},10^{-6}]	m/s	10^{-7}
Culebra conductivity Leg 6	Lognormal	[10^{-8},10^{-6}]	m/s	10^{-7}
Culebra porosity Leg 4	Lognormal	[0.00015,0.015]		0.0015
Culebra porosity Leg 5	Lognormal	[0.00015,0.015]		0.0015
Culebra porosity Leg 6	Lognormal	[0.00015,0.015]		0.0015

Marker Bed MB139 Pathway: Retardation Factors*

		Legs			
Radioisotope	Repository	Lower Borehole	Culebra from Borehole	Culebra to 2.5 km	Culebra to 5.0 km
^{240}Pu	1.0	1.74	1.12	1.12	1.12
^{236}U	1.0	1.007	1.001	1.001	1.001
^{241}Am	1.0	1.74	1.12	1.12	1.12
^{237}Np	1.0	1.07	1.001	1.001	1.001
^{233}U	1.0	1.007	1.001	1.001	1.001
^{229}Th	1.0	1.74	1.12	1.12	1.12
^{238}Pu	1.0	1.74	1.12	1.12	1.12
^{234}U	1.0	1.007	1.001	1.001	1.001
^{230}Th	1.0	1.74	1.12	1.12	1.12
^{226}Ra	1.0	1.007	1.006	1.006	1.006
^{210}Pb	1.0	1.007	1.006	1.006	1.006
^{239}Pu	1.0	1.74	1.12	1.12	1.12

*Lappin et al., 1989
**Median value is listed for loguniform and lognormal distributions

TABLE 3-10. REFERENCE DATA BASE FOR NEFTRAN SIMULATION OF HUMAN INTRUSION SCENARIOS (Concluded)

Marker Bed MB139 and Salado Formation Pathway Constant Parameter Values*

Legs:	Repository	Lower Borehole	Upper Borehole	Culebra Leg 1	Culebra to 2.5 km	Culebra to 5.0 km
Length (m)	300.0	270.0	440.0	300.0	2140.0	2560.0
Area (m^2)	38.9	0.01	0.02	800.0	800.0	800.0
Rock Density (kg/m^3)	2720	2720	2720	2720	2720	2720
Fluid Density kg/m^3	1186	1186	1186	1092	1092	1092
Node Pressure:	10.5 MPa Repository 16.0 MPa Castile Brine Occurrence 0.92 MPa Culebra at 5 km					

* Lappin et al., 1989

A seal in MB139 underlies each panel seal. Only the northernmost seals are considered in the demonstration. Because the northern equivalent panel (the drifts containing waste directly behind the northernmost seals) is the closest to the shafts, this panel is used for the demonstration. One MB139 seal is assumed to be 30 m (99 ft) long with 5.8-m^2 (62.5-ft^2) cross-sectional area. Minimum, maximum, and expected or median values (Table 3-9) for MB139-seal conductivity and porosity are used (Lappin et al., 1989). Distributions are fit to these data as described below under Selected Distributions and Parameter Ranges and Appendix C. These estimates use current seal design (Lappin et al., 1989; Tyler et al., 1988).

DRIFTS AND MB139 MODELING

Undisturbed Conditions

All excavations are assumed to be underlain by open fractures in MB139. Backfilled drifts are expected to consolidate to within 0.05 of the Salado Formation density. The dominant pathway is assumed to be through MB139 (Lappin et al., 1989, and Appendix A). It is not realistic to assume that drifts and seals are fully consolidated and saturated for transport calculations using Darcy flow assumptions that begin at the time of repository decommissioning. The time for resaturation of the facility is still unknown because effects of gas generation have not been defined. However, for Individual Protection Requirements, these assumptions are conservative.

The flow path through MB139 is represented by Leg 3 in Figure 3-17. The length and cross-sectional area of this leg are 366 m (1,207 ft) and 1.0 m^2 (11.0 ft^2), respectively. Distributions for MB139 conductivity and porosity (Lappin et al., 1989) are not sampled during the demonstration because few data are available to estimate ranges under consolidated conditions with gas present.

SHAFT SEAL SYSTEM

Undisturbed Conditions

The shaft seal system is divided into lower and upper seals (Lappin et al., 1989). The lower seal is expected to consolidate and is the primary barrier to pressure-driven flow upward from the facility. The upper seal is a temporary barrier to protect the lower seal from downward flow of water from overlying aquifers. The upper seal is designed to be an effective barrier while the lower seal consolidates. The upper seal gradually degrades as the concrete in its structural members deteriorates. The lower seal consolidates to near host-rock density. The upper seal does not consolidate to this extent, and, therefore, does not represent as significant a barrier to pressure-driven upward flow from the facility.

Legs 4 and 5 represent the lower and upper seals. The length and cross-sectional area of each leg is 200 m (660 ft) and 29.2 m^2 (314.2 ft^2). Minimum, maximum, and expected or median values (Table 3-9) for conductivity and porosity are used for each leg (Lappin et al., 1989). Distributions are fit to these data as described below under Selected Distributions and Parameter Ranges and in Appendix C. These estimates are for the current shaft-seal design (Lappin et al., 1989; Tyler et al., 1988).

RADIONUCLIDE TRANSPORT FOR THE DEMONSTRATION

Calibration of SWIFT II is described above in Summary of the Hydrogeology of the Northern Delaware Basin. A calibrated simulation is used to calculate flow fields for the transport of radionuclides in the Culebra Dolomite Member of the Rustler Formation. The insight obtained from data synthesis and assimilation using optimal estimation techniques for the calibration is utilized in calculating these flow fields for radionuclide transport. This section describes the methodology that is employed. The results are discussed in Chapter IV.

A previously calculated flow field (LaVenue et al., 1988) is used to calculate particle trajectories from several drop-point locations within the model domain (see Figure 3-16). Drop point G near well H-1 is used as a "base case" path because its initial point lies above the approximate center of the WIPP.

The path of the neutrally-buoyant particle is superimposed on a contour plot (Figure 3-24) of the steady-state calibrated log transmissivities. This path and the particle travel time to a point 5.0 km (3.0 mi) downgradient from well H-3 provide a calibration scale for the NEFTRAN legs. For the calculations using only NEFTRAN, the drop point, which represents the intrusion borehole for scenarios E1, E1E3, E2, and E2E3, is located at the southeastern corner of the waste panels (Figure 2-2). For scenarios E1E2 and E1E2E3, the second intrusion borehole is assumed to be located one room-length from the first. The particle trajectory is calculated using a SWIFT II flow-field simulation that is based on the calibrated fields (Figure 3-24).

The particle trajectory (Figure 3-24) can be divided into three conductivity zones (Table 3-4) that approximate the changes in transmissivity along this trajectory. The flow for undisturbed conditions is then calculated by NEFTRAN using lithostatic pressure the waste panel and hydrostatic pressure 5.0 km (3.0 mi) downgradiant in the Culebra Dolomite Member. A similar approach is used for human intrusion analyses except that the first conductivity zone (Table 3-10) represents an initial region of larger conductivity because of Castile Formation brine injection from the intrusion borehole. Flow through all three zones is calculated using fracture-flow, single-porosity assumptions (Lappin et al., 1989 and Table 3-10).

For comparison with the above simplified conductivity field, average hydraulic conductivities near the particle pathway are calculated using calibrated values for 15 different zones (Figure 3-25). These average values are assumed to be expected values (see Appendix C). Each zone is assigned a range of one order of magnitude change on each side of the mean. A beta distribution is constructed for the conductivity in each zone. The observed trends of decreasing conductivity from east to west and north to south are maintained. Each distribution is sampled by LHS during the uncertainty analysis using CAMCON and SWIFT II is run for each input vector generated by LHS. A flow field is processed by CAMCON for each of the 50 input vectors. During these runs, each flow field is used to calculate a mean hydraulic conductivity for a single NEFTRAN leg that calculates radionuclide transport. Each case comprises 50 individual simulations of transport for each radionuclide.

DOSE PATHWAYS AND HUMAN DOSES FOR THE INDIVIDUAL PROTECTION REQUIREMENTS

For undisturbed conditions, results described in Chapter IV along with other analyses (Lappin et al., 1989) predict that radionuclides will not be released to the accessible environment or to the biosphere in the first 1,000 years after decommissioning. Therefore, dose pathways for radionuclide transport and human doses are not considered in this demonstration.

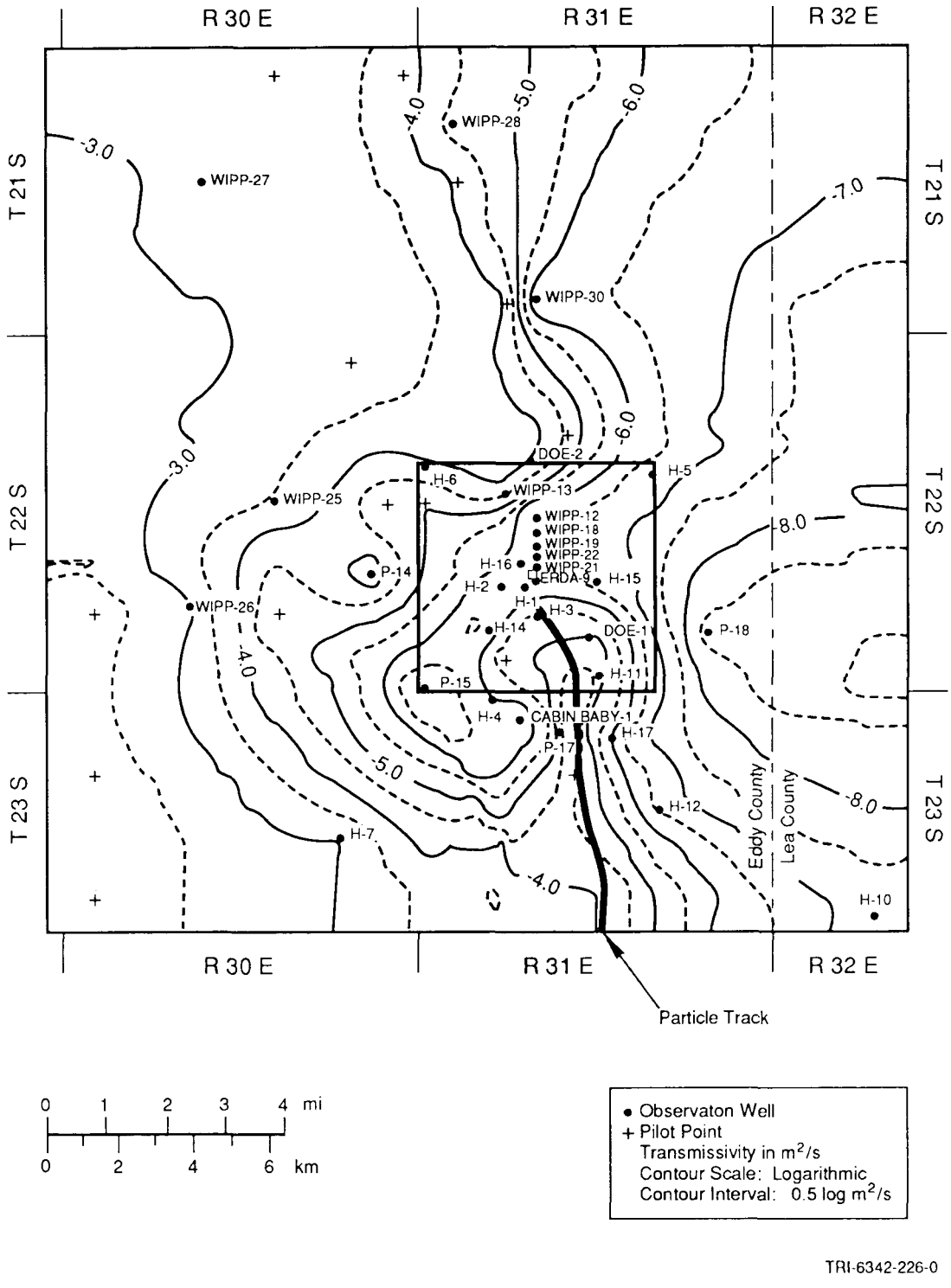

Figure 3-24. Steady-State Calibrated Log Transmissivities Through the Flow Path from Well H-3 to the Boundary (Modified from LaVenue et al., 1988).

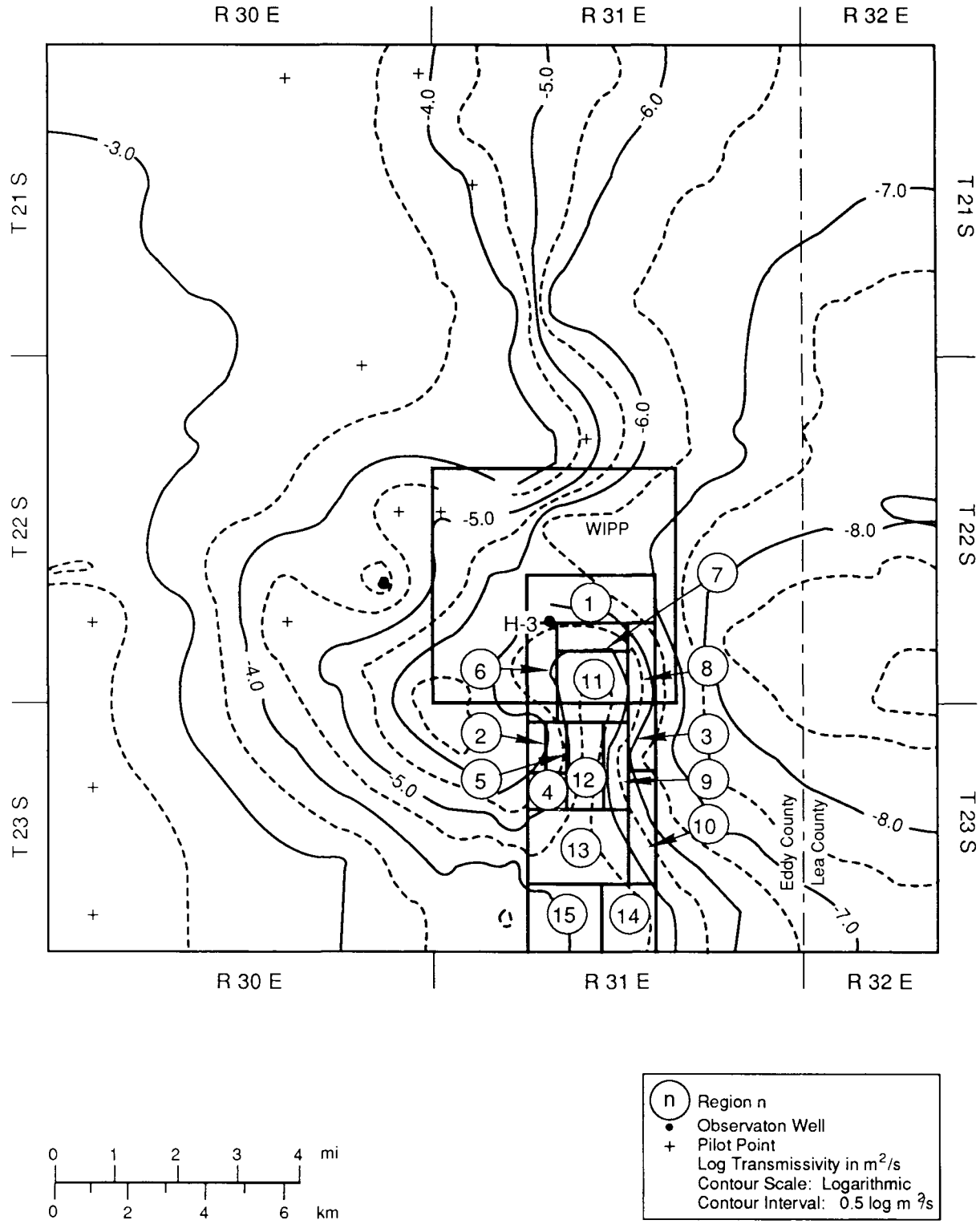

Figure 3-25. Sampled Conductivity Zones Superimposed on the Particle Track from Well H-3 to the Model Boundary (Modified from LaVenue et al., 1988).

CAMCON: COMPLIANCE ASSESSMENT METHODOLOGY CONTROLLER

Primary Data Base for the Demonstration

The primary data base contains the measured field and laboratory data gathered during characterization of the disposal system and surrounding region (Rechard, 1989; Bertram-Howery et al., 1989). Currently, the primary structural data base is complete. The primary chemical data base is nearly complete, and the geohydrologic data base is still being assembled from numerous data reports. Interpreted data (Lappin et al., 1989; LaVenue et al., 1988) are used as a starting point for the secondary data base.

Secondary Data Base for the Demonstration

The secondary data base embodies the conceptual model of the disposal system (Rechard, 1989; Bertram-Howery et al., 1989). Interpretations vary from objective/subjective interpolation to subjective extrapolation. Literature, data, and professional judgment bridge gaps in observational data and established reference properties (Lappin et al., 1989). The selection of parameters to vary and their distributions and ranges are described in Compliance Assessment System for the Demonstration, above.

Status of CAMCON

The status of CAMCON is described in the CAMCON user's manual (Rechard et al., 1989). The following computer program modules, grouped by category, are available:

1. Mesh generation module
   - GENMESH: Three-dimensional, finite-difference, mesh generator code
   - GENNET: Network generator code
   - MESHER3D: mesh generator code

2. Monte Carlo sampling module
   - LHS: Latin hypercube sampling code (Iman et al., 1980a; Iman and Shortencarier, 1984)
     - PRELHS: Pre-processor (translator) for LHS
     - POSTLHS: Post-processor (translator) for LHS

3. Regional and local hydrologic modules
   - SUTRA: Finite-element simulation code for saturated or unsaturated, fluid-density dependent, groundwater flow with energy transport or chemically reactive single-species solute transport (Voss, 1984)
     - PRESUTRA: Pre-processor (translator) for SUTRA
     - POSTSUTRA: Post-processor (translator) for SUTRA

- SWIFT II: Sandia Waste Isolation Flow and Transport code for fractured media which solves transient, three-dimensional coupled equations for fluid flow, heat transport, brine miscible displacement, and radionuclide miscible displacement (Reeves et al., 1986a, 1986b)
  - PRESWIFT: Pre-processor (translator) for SWIFT II
  - POSTSWIFT: Post-processor (translator) for SWIFT II
- HST3D: Code for simulating heat and solute transport in three-dimensional groundwater systems (Kipp, 1987)
  - PREHST: Pre-processor (translator) for HST3D
  - POSTHST: Post-processor (translator) for HST3D

4. Repository/shaft module (to be developed from RESYSM)
   - A NEFTRAN version is available

5. Transport module
   - NEFTRAN: Network flow and transport code (Longsine et al., 1987)
     - PRENEF: Pre-processor (translator) for NEFTRAN
   - See also SUTRA, SWIFT II, and HST3D

6. Containment calculation module
   - CCDFPLT: Code for calculating and plotting the complementary cumulative distribution function

7. Statistical module
   - STEPWISE: Stepwise regression code (Iman et al., 1980b)
     - PRESTEP: Pre-processor (translator) for STEPWISE
   - PCC/SRC: Code for calculating partial correlation and standardized regression coefficients (Iman et al., 1985)
     - PREPCC: Pre-processor (translator) for PCC/SRC

8. Support modules
   - ALGEBRA: Code that algebraically manipulates data in CAMDAT (Gilkey, 1988)
   - BLOT: Mesh and curve plot code (Gilkey and Glick, 1989)
   - C2FINTRP: Code for interpolating boundary conditions from a coarse to fine SWIFT mesh
   - F2CINTRP: Code for interpolating boundary conditions from a fine to coarse SWIFT mesh
   - GRIDGEOS: Code for interpolating from observational hydrologic or geologic data to a computational mesh
   - MATSET: Code for setting material properties in CAMDAT
   - TRACKER: Code for tracking neutrally bouyant particles

This series of computer codes provides a nearly complete compliance assessment system for WIPP. In addition to a repository/shaft module, future CAMCON development work will include numerous minor modifications to the translators and support modules to fine tune the system. Other groundwater and/or radionuclide-transport codes may be added. A code to simulate multiphase fluid flow will be acquired or developed for the repository/shaft module.

SELECTED DISTRIBUTIONS AND PARAMETER RANGES

Minimum, maximum, and expected or median values for most parameters required for the demonstration were taken from an earlier study (Lappin et al., 1989). However, distributions for these parameters do not appear in that report, because only expected and degraded cases described by specific choices for the value of each parameter were considered (Appendix B). The probability of occurrence of parameters selected for uncertainty analysis is based on the construction of a probability density function (pdf) for each parameter that is sampled. This section discusses the philosophy used in this demonstration for constructing these pdfs.

Input parameter values are uncertain because of sparse data, measurement errors, and natural and design variability. A pdf is a functional description of the probabilistic nature of these parameters. To construct pdfs, certain information must be known about the parameter values. Most physical parameters have minima and maxima. If something is known about the phenomenon through actual measurements, an expected value might be assigned. In this case, the expected value is not a statistically defined property, but is an assumption based on limited or sparse data (Kaplan and Yarrington, 1989). The coefficient of variation, defined as the ratio of the standard deviation to the expected value, is a measure of the inherent variability of a property that is independent of sample size. It can be used in a probabilistic sense to estimate a standard deviation if analog data are available. For example, the coefficient of variation for the matrix porosity of a unit within a tuffaceous bed can be estimated based on analog data from different soil classes (Kaplan and Yarrington, 1989). If the analyst assumes the minimum, maximum, and expected values of the uncertain parameter and a coefficient of variation, a beta distribution which maximize uncertainty (Harr, 1987) can be fit that constrains the outcome of repeated experiments. With less information, other distributions may still be fit. The analyst's assumptions are based on available data, physical meaning of the variable, behavior of analog systems, and subjective expert judgment.

The philosophy for selecting pdfs for probabilistic descriptions of the parameters that are sampled during the demonstration calculations is directed more toward including a variety of distributions (Tables 3-9 and 3-10 and Appendix C) than toward choosing a final set of distributions. Therefore,

uniform, normal, loguniform, lognormal, and beta distributions are all represented (Appendix C). No attempt to use time-to-failure models is made for the time of intrusion so neither exponential nor gamma distributions are included. The computed results may be sensitive to the choice of distribution but an analysis of these sensitivities was not performed for this demonstration.

MONTE CARLO ANALYSES USING A LATIN HYPERCUBE SAMPLING TECHNIQUE

Uncertainty analyses are summarized for undisturbed conditions for the Individual Protection Requirements and the seven scenarios described above for the Containment Requirements. A latin hypercube sampling (LHS) technique (Iman and Shortencarrier, 1984) is used to sample the parameter PDFs, and repetitive deterministic calculations are performed using CAMCON to produce distributions of the consequence (e.g., integrated discharge) and, after including estimated scenario probabilities, CCDFs. Tables of the sampled parameter values are contained in Appendix D.

IV. RESULTS OF METHODOLOGY DEMONSTRATION

The results of the methodology demonstration for undisturbed performance and for six human-intrusion scenarios are presented in this chapter. Undisturbed performance is simulated using the base-case scenario; human intrusion is simulated using the base case and Scenarios E1, E2, E1E2, E1E3, E2E3 and E1E2E3 (Figure 4-1) with preliminary estimates of the probability of occurrence for each scenario. The scenarios are all described in Chapter III.

UNDISTURBED PERFORMANCE

Three evaluations of undisturbed performance are reported here. These are (1) one simulation, referred to as IA, using reference (best-estimate) parameter values (Appendix B); (2) one simulation, IB, using parameter values degraded from the best estimate (Appendix B); and (3) fifty simulations using LHS-sampled values for uncertainty analysis of the parameters.

Uncertainty analysis of undisturbed performance is based on pdfs representing the most realistic estimates of minimum, maximum, and expected or median values and distributions of parameters (Table 3-11 and Appendix C). Monte Carlo samples of each parameter's pdf are used for 50 simulations of system performance.

In these simulations, no radionuclides move out of the repository/shaft system during 1,000 years of regulatory concern. Because of this slow rate of radionuclide movement, simulations were extended to 50,000 yr to assess system performance. Even at this longer time interval, no radionuclides travel as far as the middle of the shaft-seal system. As a result, the following discussion considers radionuclide migration to the base of the shaft (NEFTRAN Node 4, Figure 3-17) and through the MB139 seal below the repository (NEFTRAN Node 3, Figure 3-17).

For the purposes of this demonstration, the repository is assumed to be consolidated and all legs in the network along the flow path are assumed to be saturated from the time of repository decommissioning. This conservative assumption results in radionuclide migration throughout the 50,000 years simulated.

RADIONUCLIDE MIGRATION

Of the twelve radionuclides tracked for this demonstration, uranium-233, uranium-234, and thorium-229, in decreasing order, dominate migration to the base of the shaft (NEFTRAN Node 4, Figure 3-17), based on the average curies

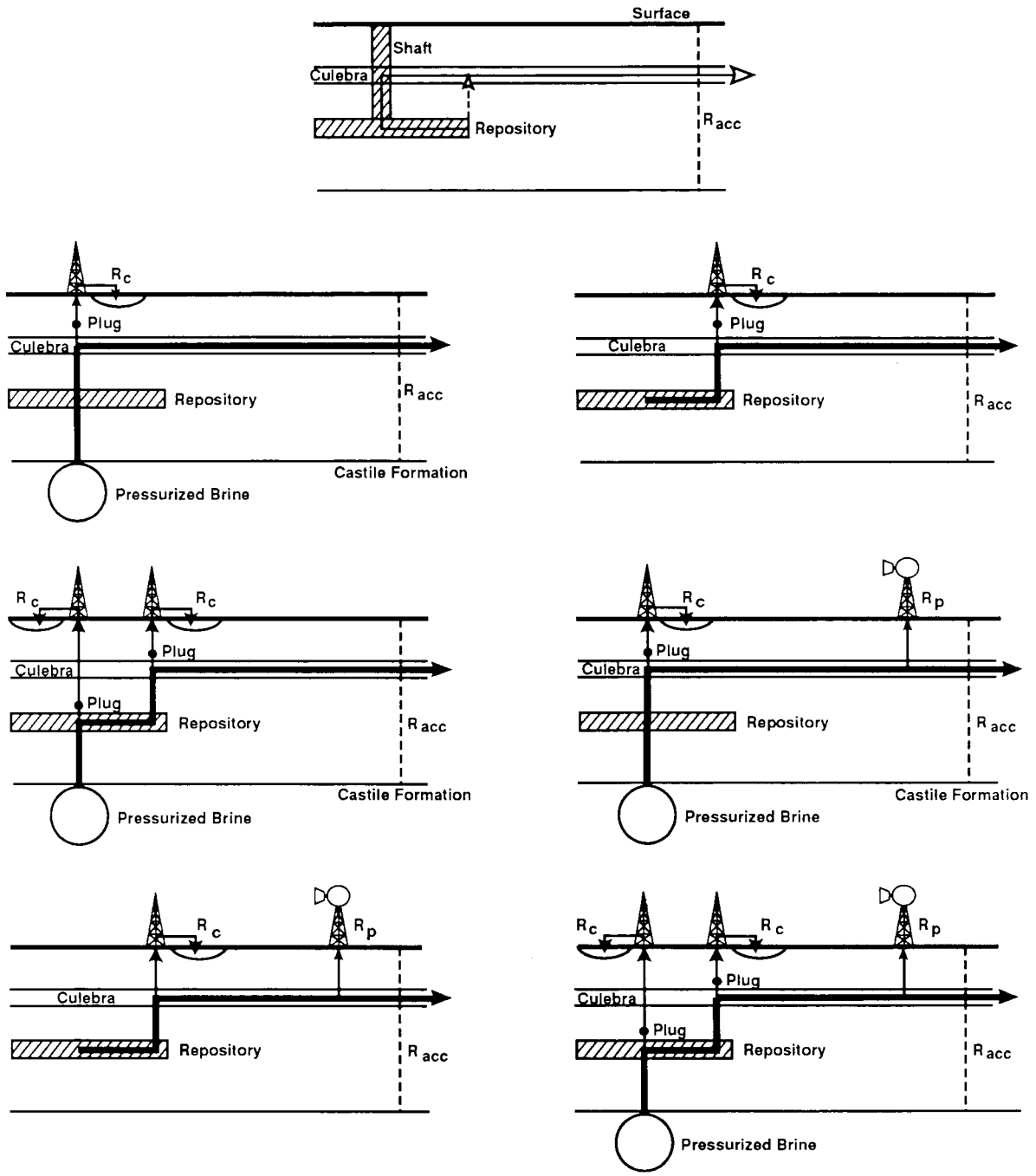

R_c = Release of Cuttings and Eroded Material
R_{acc} = Release at the Subsurface Boundary of the Accessible Environment
R_p = Release to Surface through Withdrawal Well

TRI-6342-33-0

Figure 4-1. Conceptualizations of Seven Demonstration Scenarios.

per radionuclide for the 50 simulations. For each radionuclide, the distribution appears exponential, although only 19 simulations result in more than 1×10^{-10} Ci arriving at the base of the shaft (Figure 4-2). The results for these simulations vary over ranges of 11 to 13 orders of magnitude depending on the radionuclide, indicating that the sampled parameter values have a profound effect. For some parameters, the values for degraded conditions (IB) are not an end-point value of the parameter's range. For example, migration through degraded seals (IB) is less than migration for some of the 50 simulations in the uncertainty analysis (Table 4-1). Therefore, degraded parameter values are not always the least-favorable choice and outlying (low-probability) sampled values can result in greater migration of radionuclides (Figure 4-2).

The dominant radionuclides migrating through the MB139 seal (NEFTRAN Node 3 Figure 3-17) are, in decreasing order, plutonium-239, plutonium-240, thorium-229, and americium-241 (Figure 4-3 and Table 4-2). The nonuniform distributions result from the relatively large frequency for migration of certain quantities of each radionuclide. Whereas the quantities tend to be in the same range to only slightly larger than at the base of the shaft, the frequencies are much greater.

DOSE CONSIDERATIONS

For undisturbed conditions simulated in this demonstration, radionuclides do not migrate out of the repository/shaft system even when the simulations are extended to 50,000 years instead of the 1,000 years required by the Standard. As a result, dose estimates are not required.

Numerous conservative assumptions used in developing the conceptual model for undisturbed conditions result in projected radionuclide migrations much greater than are expected for more realistic assumptions. Moreover, additional disposal-system characterization, including gas generation, is not expected to produce data that will significantly alter the no-release result of this analysis. Because no releases are expected to occur, no dose estimates will be necessary for undisturbed conditions for the final performance assessment.

HUMAN INTRUSION

The demonstration results for the human-intrusion scenarios are based on simulations representing the most realistic estimates of minimum, maximum, and expected or median values and distributions of parameters for properties of the borehole fill, room, backfill, and waste, and for the fracture-flow conceptual model of the Culebra Dolomite Member (Table 3-10; also see Appendix B and Lappin et al., 1989). For the purposes of this demonstration, the

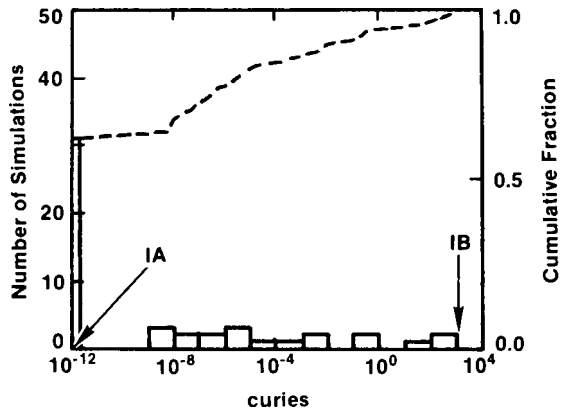

a. Uranium-233

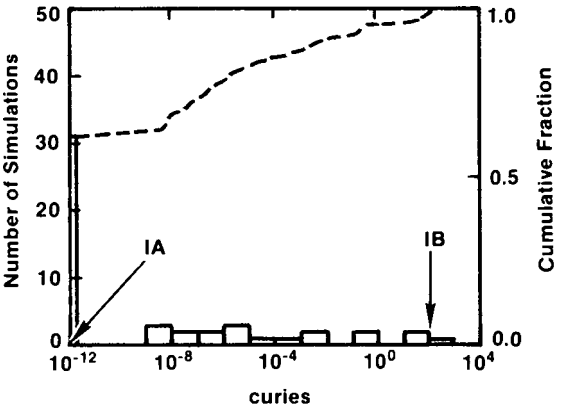

b. Uranium-234

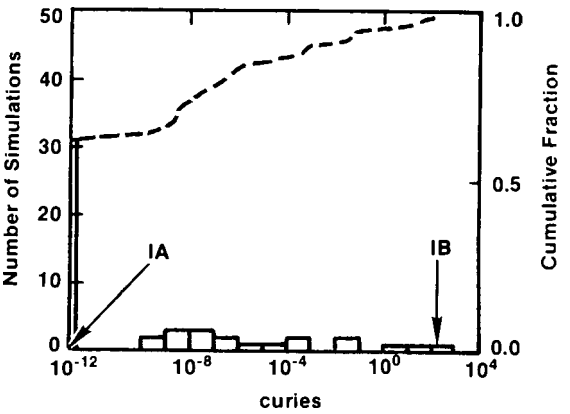

c. Thorium-229

TRI-6342-167-0

Figure 4-2. Histograms of Frequency of Simulations in which Quantities of Radioisotopes Migrate to the Base of the Shaft in 50,000 yr, Showing the Cumulative Fractional Density of Simulations, for Undisturbed Performance.

TABLE 4-1. CUMULATIVE CURIES (≥0.000005) MIGRATING TO THE BASE OF THE SHAFT IN 50,000 YR FOR UNDISTURBED PERFORMANCE

Simulation	PU-240	U-236	AM-241	NP-237	U-233	TH-229
IA	.	.	.	.	.	.
IB	175.42	2.8814	.00105	16.372	708.15	182.39
1	.	.	.	.	.	.
2	.	.	.	.	.	.
3	.	.	.	.	.	.
4	.	.	.	.	.	.
5	.	.	.	.	.	.
6	.	.00009	.	.00117	.00827	.00069
7	.	.	.	.	.	.
8	.	.	.	.	.	.
9	.	.	.	.	.	.
10	.	.	.	.	.	.
11	.	.	.	.	.	.
12	.	.	.	.	.00001	.
13	.	.	.	.	.	.
14	.	.	.	.00006	.00039	.00003
15	.	.	.	.	.	.
16	.	.	.	.	.	.
17	.	.	.	.	.	.
18	.	.	.	.	.	.
19	.	.	.	.	.	.
20	.	.00001	.	.00027	.00441	.00035
21	.	.	.	.	.	.
22	.	1.6650	.	12.108	421.65	60.852
23	.	.	.	.	.	.
27	.	.	.	.	.00003	.
28	.	.	.	.	.	.
29	.	.	.	.	.	.
30	.	.	.	.	.	.
31	.	.00373	.	.04132	.32091	.05056
32	.	.	.	.	.	.
33	.	.	.	.	.	.
34	.	.	.	.	.	.
35	.	.00205	.	.02256	.18224	.03277
36	.	.	.	.	.	.
37	.	.	.	.	.	.
38	.	.	.	.	.	.
39	.	.	.	.	.	.
40	.	.	.	.	.	.
41	.	.	.	.	.	.
42	.	.	.	.	.	.
43	10.124	2.8866	.00006	16.334	705.91	169.30
44	.	.	.	.	.	.
45	.	.	.	.	.	.
46	.	.56381	.	4.7398	47.243	7.3531
47	.	.	.	.	.	.
48	.	.	.	.	.	.
49	.	.	.	.	.	.
50	.	.	.	.	.	.
$Average_{50}$	.20249	.10243	.	.66494	23.506	4.7518

TABLE 4-1. CUMULATIVE CURIES (≥0.000005) MIGRATING TO THE BASE OF THE SHAFT IN 50,000 YR FOR UNDISTURBED PERFORMANCE (Concluded)

Simulation	PU-238	U-234	TH-230	RA-226	PB-210	PU-239
IA	.	.	.	.	.	.
IB	.	135.71	10.852	39.269	40.789	1109.0
1	.	.	.	.	.	.
2	.	.	.	.	.	.
3	.	.	.	.	.	.
4	.	.	.	.	.	.
5	.	.	.	.	.	.
6	.	.00652	.00008	.00036	.00038	.
7	.	.	.	.	.	.
8	.	.	.	.	.	.
9	.	.	.	.	.	.
10	.	.	.	.	.	.
11	.	.	.	.	.	.
12	.	.00001	.	.	.	.
13	.	.	.	.	.	.
14	.	.00035	.	.00001	.00001	.
15	.	.	.	.	.	.
16	.	.	.	.	.	.
17	.	.	.	.	.	.
18	.	.	.	.	.	.
19	.	.	.	.	.	.
20	.	.00175	.00002	.00005	.00005	.
21	.	.	.	.	.	.
22	.	97.397	2.7231	11.215	10.367	.
23	.	.	.	.	.	.
27	.	.00002	.	.	.	.
28	.	.	.	.	.	.
29	.	.	.	.	.	.
30	.	.	.	.	.	.
31	.	.24827	.00585	.01588	.01711	.
32	.	.	.	.	.	.
33	.	.	.	.	.	.
34	.	.	.	.	.	.
35	.	.14228	.00356	.00727	.00717	.
36	.	.	.	.	.	.
37	.	.	.	.	.	.
38	.	.	.	.	.	.
39	.	.	.	.	.	.
40	.	.	.	.	.	.
41	.	.	.	.	.	.
42	.	.	.	.	.	.
43	.	133.23	9.7563	37.838	37.276	56.004
44	.	.	.	.	.	.
45	.	.	.	.	.	.
46	.	33.202	.82222	2.6658	2.7534	.00001
47	.	.	.	.	.	.
48	.	.	.	.	.	.
49	.	.	.	.	.	.
50	.	.	.	.	.	.
$Average_{50}$	.	5.2847	.26622	1.0349	1.0084	1.1201

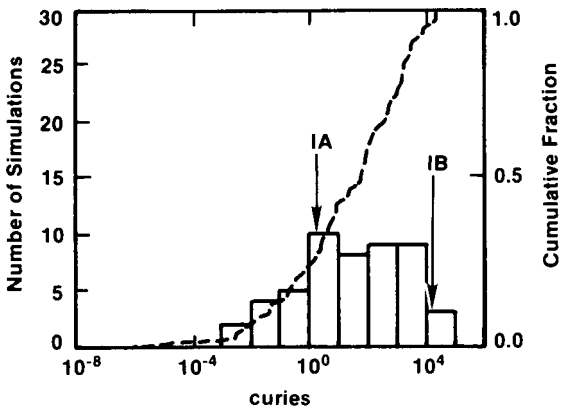

a. Plutonium-239

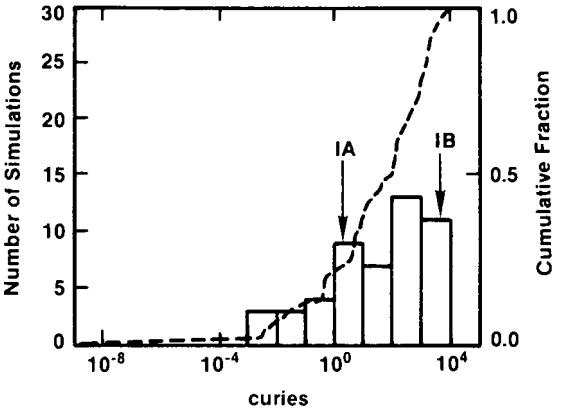

b. Plutonium-240

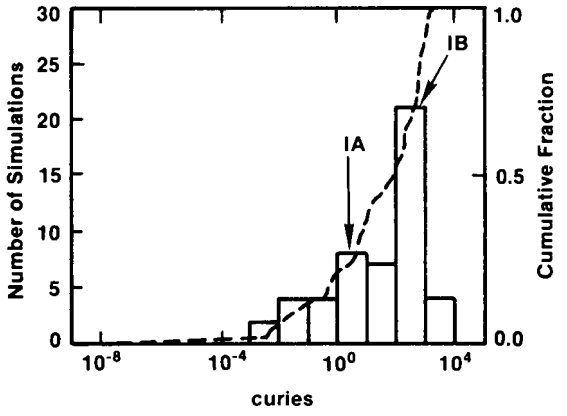

c. Thorium-229

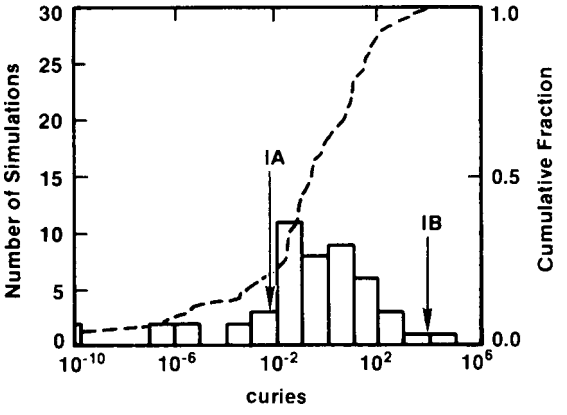

d. Americium-241

TRI-6342-168-0

Figure 4-3. Histograms of Frequency of Simulations in which Quantities of Radioisotopes Migrate to the Base of the Shaft in 50,000 yr, Showing the Cumulative Fractional Density of Simulations, for Undisturbed Performance.

TABLE 4-2. CUMULATIVE CURIES (≥0.000005) MIGRATING THROUGH THE MARKER BED SEAL OF THE SHAFT IN 50,000 YR FOR UNDISTURBED PERFORMANCE

Simulation	PU-240	U-236	AM-241	NP-237	U-233	TH-229
IA	17.104	.04569	.00709	.32266	3.5152	21.323
IB	6278.9	1.1746	9177.1	14.594	733.85	743.75
1	4.7824	.00773	.02805	.05886	.63040	5.1576
2	93.215	.17694	.23180	1.2673	14.180	108.06
3	.08086	.00011	.00119	.00090	.00931	.08515
4	.00682	.00006	.	.00047	.00400	.01182
5	.02077	.00024	.	.00186	.01609	.04095
6	4.5577	.00216	1.1152	.02145	.24956	4.2132
7	13.189	.01983	.08362	.14897	1.6362	14.085
8	108.46	.39169	.03226	2.8016	31.143	169.96
9	25.334	.05604	.02537	.39844	4.3322	29.059
10	10.697	.01121	.23701	.08923	1.0021	10.821
11	9.9455	.02925	.00236	.20666	2.1767	12.186
12	.43839	.00028	.05051	.00264	.02938	.41859
13	3.5192	.00617	.01528	.04683	.49574	3.8532
14	756.78	.93143	25.942	7.9548	96.717	1164.5
15	1441.3	2.3261	59.422	15.858	264.14	1218.5
16	.43032	.00038	.02462	.00331	.03574	.42490
17	1.0689	.00086	.06802	.00751	.08270	1.0427
18	363.20	.80617	1.6850	6.1839	71.851	551.59
19	1048.5	2.4439	7.5527	14.072	357.56	634.39
20	3926.1	1.8288	237.64	16.301	729.59	497.23
21	.00324	.00001	.	.00007	.00065	.00386
22	6400.1	1.1454	2958.0	15.823	745.96	425.28
23	124.28	.30899	.13591	2.1943	24.688	168.76
24	40.201	.25687	.00041	1.8112	19.752	51.282
25	810.74	2.2996	3.3024	12.668	306.38	517.21
26	133.99	.20123	.81647	1.4794	16.876	149.59
27	2.9846	.00251	.16202	.02140	.23849	2.9350
28	2439.7	2.2331	46.314	16.208	694.02	637.86
29	621.23	.99014	9.0915	8.0650	96.334	938.27
30	1502.6	2.4488	15.541	15.247	556.94	709.33
31	224.85	.11803	26.825	1.0881	13.144	210.67
32	.47661	.00057	.00880	.00463	.04925	.49174
33	189.61	.99876	.02647	5.7643	109.87	163.60
34	37.608	.05661	.21568	.41839	4.6845	40.056
35	1640.9	2.1783	114.70	16.067	257.95	1462.9
36	7.1665	.00959	.07310	.07418	.81319	7.5058
37	4.3561	.00521	.06366	.04123	.45277	4.4879
38	858.60	1.8510	9.1449	13.768	187.22	810.72
39	1288.7	2.2316	5.1818	14.280	590.86	532.91
40	88.148	.12362	.58106	.91268	10.388	93.505
41	.42282	.00274	.	.01997	.18918	.65653
42	318.61	.35742	7.3826	2.8192	33.502	376.85
43	7830.7	.74287	10255.	14.357	754.41	300.50
44	1785.7	2.4201	41.559	16.044	493.85	934.49
45	.01595	.00005	.00001	.00039	.00365	.01970
46	2936.6	2.1098	951.65	16.214	425.17	1853.9
47	7.2759	.02711	.00039	.18953	1.9634	9.4724
48	117.22	.09554	4.4065	.77605	9.1451	114.58
49	463.97	1.7767	.42491	9.5011	226.62	327.18
50	.00314	.00001	.	.00010	.00087	.00411
$Average_{50}$	753.77	.68063	295.69	5.0257	143.15	305.41

TABLE 4-2. CUMULATIVE CURIES (≥0.000005) MIGRATING THROUGH THE MARKER BED SEAL OF THE SHAFT IN 50,000 YR FOR UNDISTURBED PERFORMANCE (Concluded)

Simulation	PU-238	U-234	TH-230	RA-226	PB-210	PU-239
IA	.	2.4248	7.0204	7.4776	7.1563	14.373
IB	3296.1	138.16	3.7631	.75033	.70553	10939.
1	.	.43189	1.2636	3.5116	3.2520	2.9646
2	.	9.7298	23.624	23.501	23.780	64.985
3	.	.00649	.01871	.06967	.07347	.04542
4	.	.00293	.00781	.00808	.00811	.01289
5	.	.01173	.03130	.03167	.03108	.04872
6	.02825	.16885	.51322	9.5861	9.4941	1.5327
7	.	1.1189	3.2933	9.3846	10.147	7.8477
8	.	21.604	12.724	12.209	11.684	128.94
9	.	2.9867	8.6017	10.081	10.352	18.934
10	.00003	.67935	2.0284	10.491	11.031	5.2322
11	.	1.5113	4.3210	4.8675	5.0098	8.9050
12	.00023	.02005	.05999	.67311	.64143	.16965
13	.	.34036	.99308	2.4757	2.2095	2.2872
14	.04358	64.793	37.192	32.130	29.603	527.46
15	.10578	130.10	26.435	22.150	20.115	1450.4
16	.00004	.02451	.07254	.52286	.55638	.19304
17	.00013	.05645	.16845	1.3749	1.3683	.45862
18	.00003	49.101	26.388	24.451	22.904	338.22
19	.00008	123.39	25.168	22.733	22.287	1721.2
20	.40534	136.09	11.089	8.5913	8.3470	18443.
21	.	.00046	.00128	.00207	.00207	.00270
22	174.79	138.67	4.1617	2.0749	2.0747	20081.
23	.	17.017	18.952	18.856	19.062	108.69
24	.	13.691	5.5328	5.3724	5.3965	72.818
25	.00001	113.40	25.203	23.204	23.032	1424.0
26	.00002	11.507	30.542	28.970	27.705	81.880
27	.00032	.16259	.48459	3.7353	3.7829	1.3050
28	.00172	133.75	16.734	14.153	13.760	7643.6
29	.00189	65.355	33.592	31.564	31.889	496.82
30	.00029	129.40	22.101	20.020	20.440	2922.6
31	.49687	8.7893	26.857	88.025	83.856	79.440
32	.	.03440	.10002	.44064	.41163	.25038
33	.	47.191	12.816	12.057	12.010	440.60
34	.	3.1857	9.3927	16.108	15.994	22.394
35	.48366	130.85	26.222	21.281	20.932	1462.8
36	.	.55386	1.6367	5.7967	5.1750	4.0063
37	.	.30893	.91344	3.9059	3.6908	2.2922
38	.00055	115.28	29.710	26.771	25.745	938.10
39	.	117.05	22.099	19.971	19.680	7329.5
40	.00002	7.0905	20.688	23.851	22.223	50.736
41	.	.13490	.37144	.38284	.37911	.65173
42	.00957	22.632	39.001	34.674	31.189	177.63
43	2215.4	138.76	1.9561	.56088	.54313	23842.
44	.00470	132.65	20.430	17.406	16.647	2617.5
45	.	.00264	.00724	.01009	.00998	.01475
46	58.019	134.24	15.989	8.7605	7.8896	2654.9
47	.	1.3728	3.8361	3.9537	3.9111	7.6185
48	.00905	6.1706	18.562	48.665	48.908	50.476
49	.	85.304	20.975	19.320	18.782	978.19
50	.	.00064	.00172	.00210	.00210	.00335
$Average_{50}$	48.996	42.334	12.257	13.975	13.560	1924.3

repository is assumed to be consolidated and all legs in the network along the flow path are assumed to be saturated from the time of repository decommissioning.

For each human-intrusion scenario, uncertainty analysis consists of 50 simulations of the disposal system's response to the sampled set of parameter values. Each set of parameter values called a "Monte Carlo input vector," results from Monte Carlo sampling using a latin hypercube sampling technique of the pdfs assigned to the data ranges for the parameters. A separate simulation using the most realistic estimates of the parameter values is referred to as IIA. A previous simulation of a single human-intrusion scenario using degraded parameter values (Appendix B) resulted in a normalized release of 5.1 (U.S. DOE, 1989a). This value is indicated on the CCDFs as IIC. Twelve radionuclides in four simplified chains are tracked for each simulation.

RADIONUCLIDE MIGRATION

This section presents results of analyses that predict radionuclide migration from the repository/shaft system through the Culebra Dolomite Member to a point in the Culebra Dolomite either 2.5 or 5.0 km (1.5 or 3.0 mi) downgradient from the repository. The extremely conservative fracture-flow conceptual model predicts relatively rapid migration downgradient. Using NEFTRAN to mimic fracture flow results in extremely conservative predictions.

Scenario E1

Scenario E1 consists of a borehole that penetrates a room or drift in the repository and also penetrates pressurized brine in the Castile Formation. Seven cases are analyzed for this scenario. The first five cases are used to establish certain parameter values, ranges, or distributions for the demonstration. Analyses of the first five, referred to as Cases $E1_a$ through $E1_e$, use the NEFTRAN module in CAMCON. Analyses of two other cases, $E1_f$ and $E1_g$, which correspond to Cases $E1_b$ and $E1_e$, use the SWIFT/NEFTRAN system within CAMCON to include sampling on additional conductivity zones in the Culebra Dolomite Member.

Cases $E1_f$ and $E1_g$ investigate somewhat more realistic modeling of transport by imposing the SWIFT II hydraulic conductivities and resultant gradient on the NEFTRAN legs corresponding to the Culebra Dolomite Member. The sampling technique is described in Chapter II under Radionuclide Transport for the Demonstration. The results of each set of 50 simulations are used in constructing two CCDFs for comparison to Case $E1_b$ and Case $E1_e$. This transport modeling technique was not used for the demonstration.

Case $E1_a$. This analysis uses reference data (Table 3-10; also see Appendix B and Lappin et al., 1989) to estimate radionuclide transport 2.5 km (1.5 mi) downgradient from the waste panels. The 50 Monte Carlo input vectors for the uncertainty analysis are selected from data distributions that include parameter values corresponding to degraded conditions (Appendix B). Input variables include properties of repository components, borehole fill, and the Culebra Dolomite Member; along with the intrusion time, which is sampled over a uniform distribution for 10,000 years. The radionuclides dominating transport 2.5 km (1.5 mi) downgradient are, in decreasing order, plutonium-239, plutonium-240, americium-241, and uranium-233. For these radionuclides the quantities transported vary over a range of 9 to 12 orders of magnitude across the 50 simulations. There is considerable variation in the distribution for each radionuclide, although certain quantities occur with a relatively large frequency (Figure 4-4 and Table 4-3). Because of the choice of reference data, the conservative assumptions made in the conceptual model, and the 2.5-km (1.5 mi) transport distance, Case $E1_a$ of Scenario E1 exceeds the limits in the Standard (Figure 4-5).

Case $E1_b$. The conceptual difference between this case and Case $E1_a$ is that radionuclides are transported 5.0 km (3.0 mi) instead of 2.5 km (1.5 mi) from the waste panels. This change adds approximately 2.5 km to the transport distance in the Culebra Dolomite Member. The three radionuclides dominating this case are, in decreasing order, plutonium-239, plutonium-240, and uranium-233. This result differs from Case $E1_a$ in that the americium-241 has been replaced by uranium-233. The frequencies of migration for plutonium-239 differ significantly from those for plutonium-240 and uranium-233 (Figure 4-6 and Table 4-4). Although migration to 5.0 km (3.0 mi) still exceeds limits in the Standard, the curve has shifted slightly (Figure 4-7). The greater distance for radionuclide transport appears to have little affect on migration, because of the short travel times in the Culebra resulting from the simplistic representation of fracture flow in the model combined with assumed minimal radionuclide retardation. More realistic modeling of transport in fracture flow (e.g., Case $E1_f$) and incorporation of conceptual model uncertainty should significantly increase this shift. Correlating parameter values with results indicates that among the parameters sampled, the time-of-the-intrusion event, along with solubility, room properties, and borehole-fill properties account for two-thirds of the variability in the results. Because solubility and room properties can be influenced by engineered modifications, they are investigated in variations of Case $E1_b$.

Case $E1_c$. Except for the uncertainty in the solubility of the radionuclides located in the rooms and drifts, this case is identical to Case $E1_b$. The range of the solubility uncertainty in Cases $E1_a$ and $E1_b$ (10^{-9} to 10^{-3} M; see Appendix E) decreases (10^{-8} to 10^{-4} M), although the type of distribution remains the same. The minimum, maximum, and median values for solubility are

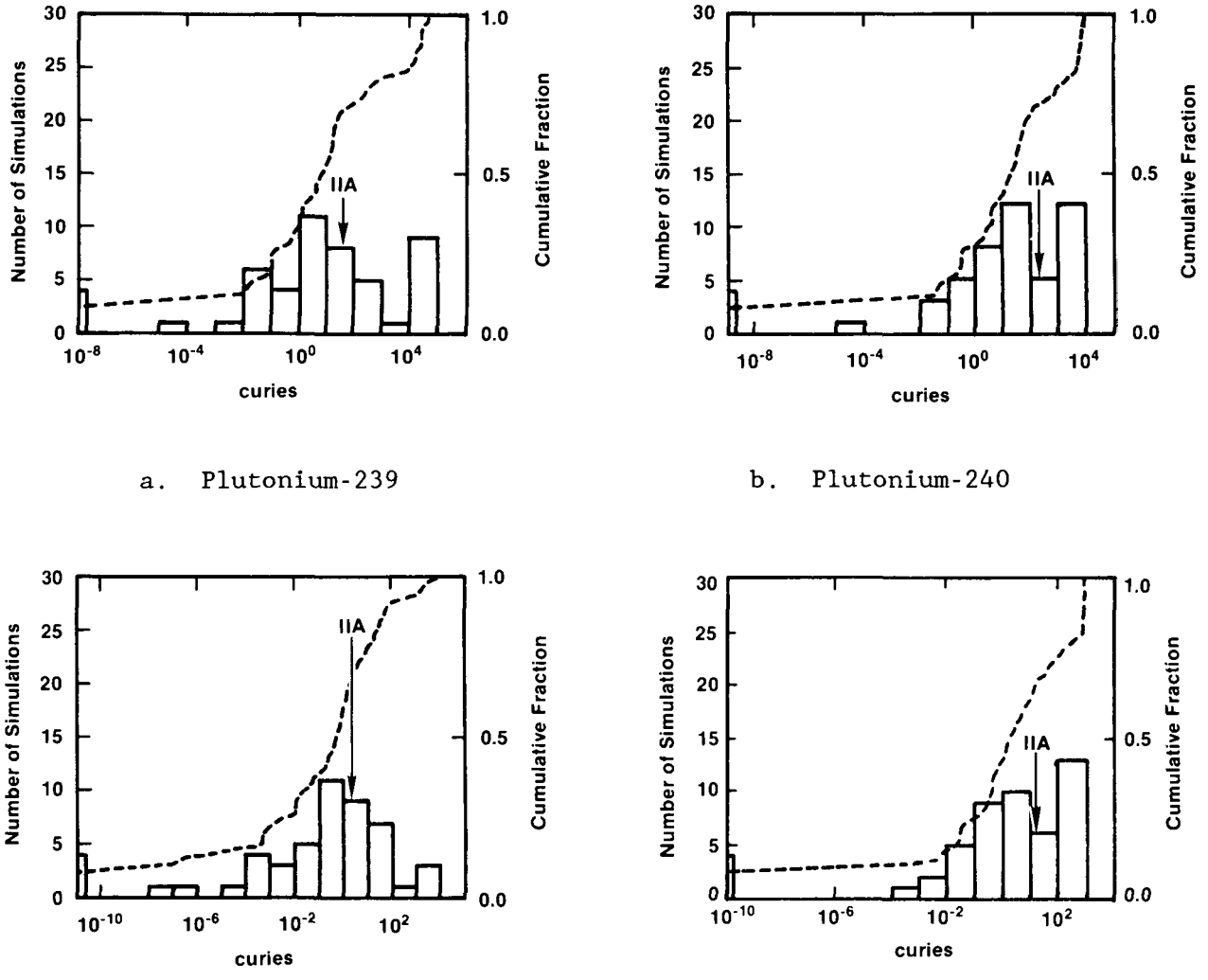

Figure 4-4. Histograms of Frequency of Simulations in which Quantities of Radioisotopes Migrate 2.5 km (1.5 mi) Downgradient from the Waste Panels in 10,000 yr, Showing the Cumulative Fractional Density of Simulations, for Human Intrusion Scenario E1, Case $E1_a$.

TABLE 4-3. CUMULATIVE CURIES (≥0.000005) MIGRATING 2.5 KM (1.5 MI) DOWNGRADIENT FROM THE WASTE PANELS AFTER 10,000 YR FOR HUMAN INTRUSION SCENARIO E1, CASE $E1_a$

Simulation	PU-240	U-236	AM-241	NP-237	U-233	TH-229
IIA	155.25	.10347	4.0827	1.0834	14.619	293.01
1	113.89	.27502	.00050	2.8267	38.149	28.023
2	12.532	.00811	.04408	.08510	1.1431	22.394
3	.	.	.	.	.	.
4	.22484	.00014	.69960	.00180	.01996	.40046
5	5560.0	1.3805	6.2255	16.397	752.16	334.71
6	4.0183	.00253	.48896	.02709	.36216	7.1367
7	31.158	.03529	.06474	.34112	4.5219	58.469
8	6348.4	1.1605	45.555	16.399	756.45	277.12
9	.29885	.00023	.79671	.00402	.03197	.58264
10	.	.	.	.	.	.
11	25.219	.01756	1.0331	.18287	2.4407	45.274
12	.29434	.00021	.41699	.00258	.02891	.52847
13	2.2333	.00477	.00044	.04873	.65129	4.1204
14	1.3885	.00151	.36112	.02666	.19476	2.9947
15	63.327	.09311	.00206	.96668	12.945	92.009
16	719.44	.45386	2.2818	4.8280	64.724	509.72
17	13.635	.00868	.19803	.09263	1.2418	24.236
18	4.0417	.00306	7.4147	.04489	.42061	7.7614
19	7330.0	.88635	817.00	16.251	761.87	192.22
20	122.99	.08607	.82376	.89950	12.061	220.17
21	4.0860	.00339	.01789	.03475	.46547	7.3861
22	19.267	.01100	.32012	.12028	1.6092	33.988
23	6143.5	1.2163	23.783	16.392	755.21	286.88
24	306.80	.28257	15.935	2.9727	37.288	371.47
25	.05611	.00187	.	.01686	.27065	.02063
26	5036.7	1.5265	1.1477	16.392	749.35	363.58
27	4.9525	.00291	25.739	.03353	.42555	8.9200
28	.03208	.00003	.00001	.00036	.00482	.05749
29	700.32	.82496	.01002	8.1380	110.64	232.39
30	48.138	.02935	62.952	.32796	4.2415	87.465
31	8208.3	.64009	2115.7	15.987	764.54	143.25
32	.	.	.	.	.	.
33	2.0621	.00159	2.3888	.02242	.21680	3.8740
34	1299.9	1.0105	1175.3	12.245	140.26	483.43
35	.28905	.00018	4.0181	.00256	.02663	.55407
36	.32754	.00040	.03548	.00667	.05133	.64447
37	.03729	.00004	.00934	.00051	.00584	.06844
38	4500.3	1.6774	.21018	16.388	746.24	394.54
39	.	.	.	.	.	.
40	56.722	.11707	.00041	1.2209	16.372	25.520
41	2791.1	1.7151	.00922	14.837	344.32	372.77
42	8.2023	.00574	.63328	.06013	.79572	14.737
43	29.659	.02084	15.654	.23292	2.9050	54.515
44	15.568	.01008	.15167	.10607	1.4179	27.839
45	5055.4	1.5219	1.2553	16.393	750.10	349.67
46	46.238	.06963	.00095	.71850	9.5923	52.795
47	.00003	.	.	.00001	.00013	.00007
48	7793.1	.75636	8130.6	14.777	763.45	174.57
49	41.990	.04986	2.7000	.67857	6.3490	90.142
50	6295.8	1.1750	40.858	16.399	756.23	278.24
$Average_{50}$	1375.2	.34177	250.06	4.2786	167.44	113.74

TABLE 4-3. CUMULATIVE CURIES (≥0.000005) MIGRATING 2.5 KM (1.5 MI) DOWNGRADIENT FROM THE WASTE PANELS AFTER 10,000 YR FOR HUMAN INTRUSION SCENARIO E1, CASE $E1_a$ (Concluded)

Simulation	PU-238	U-234	TH-230	RA-226	PB-210	PU-239
IIA	.	9.4947	10.647	4.6309	4.5279	45.321
1	.	24.672	.92872	.94693	.93931	23.055
2	.	.74527	2.3165	3.6385	3.6550	3.6316
3	.	.	.	.	.	.
4	.	.01299	.04107	1.5082	1.5288	.06452
5	.	137.92	6.9588	1.3965	1.3112	14157.
6	.	.23613	.71936	8.2681	8.3532	1.1357
7	.	2.9612	6.5576	6.1386	6.0652	10.829
8	.	138.43	5.4951	.98426	.91286	23330.
9	.	.02095	.06371	1.7823	1.8176	.09119
10	.	.	.	.	.	.
11	.	1.5935	4.8252	6.6766	6.4671	7.4996
12	.	.01885	.05593	1.8785	1.8621	.08718
13	.	.42515	.46941	.55804	.53901	.52655
14	.	.13590	.37821	3.1819	3.0748	.48572
15	.	8.4373	2.5832	2.0617	1.9930	19.383
16	.	42.171	10.725	2.7991	2.6366	204.12
17	.	.80919	2.4426	6.5164	6.6788	3.8574
18	.	.27471	.84491	8.6696	8.9282	1.2254
19	.00014	139.16	3.1873	1.3138	1.2869	13011.
20	.	7.8348	10.256	5.0941	4.9411	36.166
21	.	.30346	.80024	1.8176	1.8702	1.2383
22	.	1.0473	3.3193	8.2754	8.1946	5.2861
23	.	138.18	6.0057	.34518	.25612	35901.
24	.	24.362	8.5695	6.3127	6.3041	101.48
25	.	.14016	.00090	.00209	.00196	.01772
26	.	137.50	8.2005	1.4815	1.3748	22428.
27	.	.27618	.87082	17.668	17.808	1.3590
28	.	.00314	.00598	.00837	.00841	.00935
29	.	70.603	7.1021	5.3402	5.3148	225.58
30	.	2.7637	8.7563	8.7449	8.7325	13.483
31	.00844	139.33	2.5649	.58375	.55038	37119.
32	.	.	.	.	.	.
33	.	.14141	.42843	6.8795	7.1154	.63635
34	.20245	93.018	7.8902	3.8356	3.7484	390.61
35	.07664	.01776	.05500	2.3303	2.3776	.08053
36	.	.03358	.08467	1.1006	1.0503	.11895
37	.	.00382	.00789	.25107	.25380	.01193
38	.	137.12	9.3588	3.5977	3.4650	10157.
39	.	.	.	.	.	.
40	.	10.670	.76312	.70369	.68266	14.243
41	.	123.55	9.9552	2.6927	2.5310	910.72
42	.	.52000	1.5721	6.0456	5.8551	2.4368
43	.	1.8966	5.7747	8.0392	8.3103	8.7686
44	.	.92486	2.8849	5.3796	5.4245	4.5243
45	.	137.57	8.0068	4.0911	4.0185	24416.
46	.	6.2600	1.5156	1.2496	1.2546	14.344
47	.	.00008	.00001	.00087	.00084	.00001
48	6.0539	139.60	1.8642	.30123	.27693	7494.3
49	.	4.1539	6.9680	6.4014	6.5149	15.275
50	.	138.41	5.5371	1.4830	1.4394	22260.
$Average_{50}$	.12683	36.285	3.3542	3.3675	3.3545	4245.9

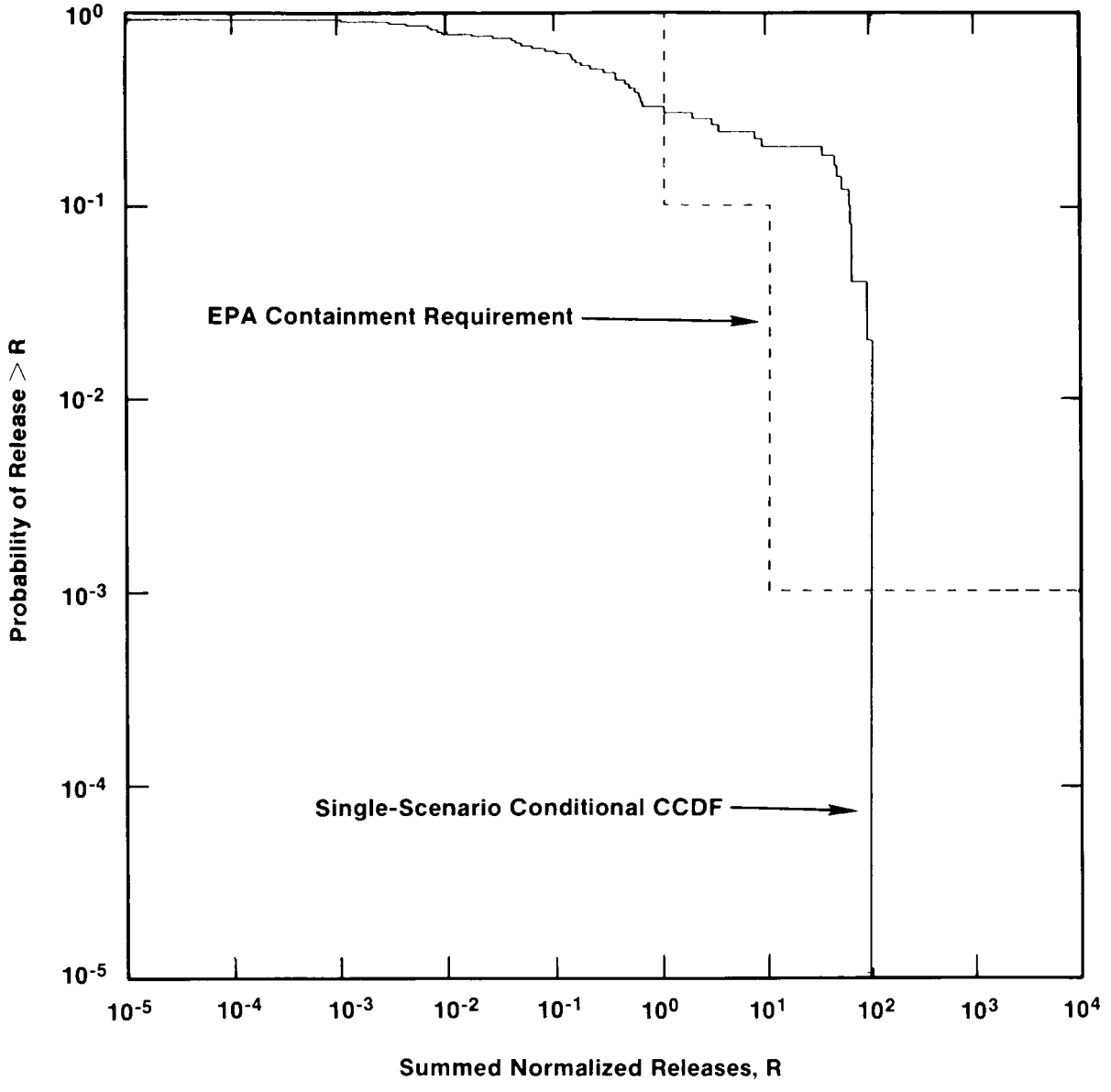

TRI-6342-188-0

Figure 4-5. CCDF for 50 Simulations of One Scenario, Case $E1_a$ of Scenario E1, for Radionuclide Migration 2.5 km (1.5 mi) Downgradient from the Waste Panels. Given that the Scenario Occurs, the Probability that the CCDF is within the EPA Limit is 0.68.

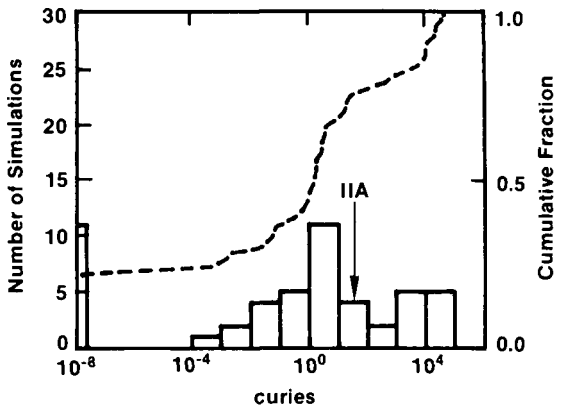

a. Plutonium-239

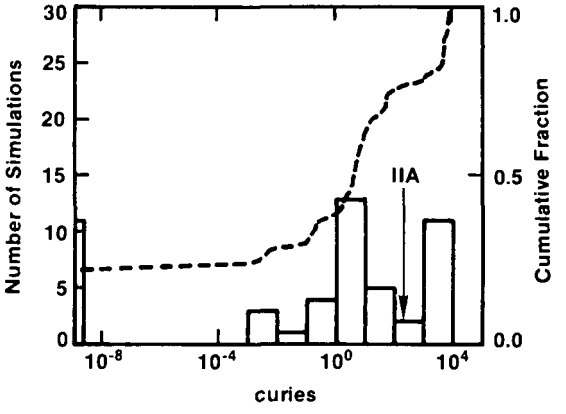

b. Plutonium-240

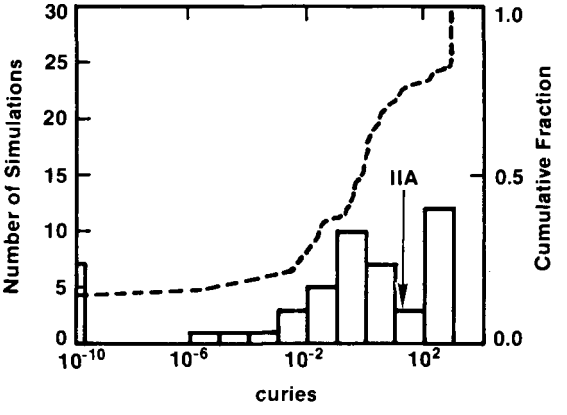

c. Uranium-233

TRI-6342-170-0

Figure 4-6. Histograms of Frequency of Simulations in which Quantities of Radioisotopes Migrate 5.0 km (3.0 mi) Downgradient from the Waste Panels in 10,000 yr, Showing the Cumulative Fractional Density of Simulations, for Human Intrusion Scenario E1, Case $E1_b$ (Case $E1_a$ with Distance Increased).

TABLE 4-4. CUMULATIVE CURIES (≥0.000005) MIGRATING 5.0 KM (3.0 MI) DOWNGRADIENT FROM THE WASTE PANELS AFTER 10,000 YR FOR HUMAN INTRUSION SCENARIO E1, CASE $E1_b$ (CASE $E1_a$ WITH DISTANCE INCREASED)

Simulation	PU-240	U-236	AM-241	NP-237	U-233	TH-229
IIA	108.67	.08462	.99413	.85789	11.626	208.52
1	.00354	.00024	.	.00258	.03449	.00260
2	2.9393	.00284	.00664	.02895	.38765	5.3423
3	.	.	.	.	.	.
4	.09045	.00008	.04536	.00127	.01103	.16602
5	4600.7	1.6491	.30100	16.389	746.94	385.83
6	3.6192	.00228	.27811	.02409	.32167	6.4524
7	3.6343	.01046	.00361	.10287	1.3435	7.1659
8	6101.5	1.2292	20.938	16.398	755.31	288.49
9	.17018	.00019	.03756	.00351	.02388	.35578
10	.	.	.	.	.	.
11	4.5259	.00640	.01972	.06316	.82164	8.5458
12	.11442	.00012	.03436	.00165	.01527	.21127
13	.	.00003	.	.00034	.00453	.00016
14	1.2255	.00144	.16899	.02589	.18483	2.7057
15	9.9214	.02017	.00020	.20682	2.7652	15.790
16	.62528	.00805	.00004	.08167	1.0815	1.2971
17	5.5432	.00501	.02815	.05132	.68599	10.044
18	2.1331	.00233	.30273	.03738	.29940	4.3881
19	3202.8	1.6865	.12636	16.317	727.76	362.05
20	113.31	.07856	.53228	.81298	10.860	203.57
21	.00525	.00006	.00001	.00058	.00771	.01018
22	11.988	.00826	.05963	.08671	1.1609	21.445
23	5995.9	1.2587	16.036	16.399	754.85	294.74
24	43.541	.10205	.04959	1.1315	12.565	96.661
25	.	.	.	.	.	.
26	4041.9	1.8047	.04260	16.383	743.64	414.06
27	4.7131	.00282	20.444	.03335	.40932	8.5182
28	.	.	.	.00003	.00043	.00001
29	48.997	.14947	.00038	1.5072	20.191	22.060
30	47.438	.02940	56.852	.32890	4.2406	86.412
31	7681.1	.78773	687.42	16.276	762.70	176.27
32	.	.	.	.	.	.
33	1.7277	.00147	1.0245	.02123	.19686	3.2909
34	1093.6	.96646	386.65	11.702	130.58	425.45
35	.21197	.00017	.57054	.00302	.02330	.42066
36	.00123	.00002	.00001	.00036	.00260	.00294
37	.	.	.	.	.	.
38	4391.0	1.7072	.14461	16.387	745.57	400.37
39	.	.	.	.	.	.
40	.	.	.	.	.	.
41	989.56	.53730	.00172	4.5422	151.59	122.97
42	7.7345	.00548	.45204	.05741	.75381	13.948
43	27.369	.02007	9.4281	.22313	2.7538	50.856
44	7.8388	.00657	.03904	.06698	.89307	14.227
45	4617.6	1.6436	.32066	16.390	747.67	373.57
46	.	.	.	.	.00003	.
47	.	.	.	.	.	.
48	7404.2	.86533	3087.7	15.797	762.13	195.74
49	4.9871	.01648	.00543	.29229	2.0178	13.025
50	5765.5	1.3236	8.9786	16.398	753.81	306.47
$Average_{50}$	1124.8	.31880	85.982	3.6915	156.93	86.858

TABLE 4-4. CUMULATIVE CURIES (≥0.000005) MIGRATING 5.0 KM (3.0 MI) DOWNGRADIENT FROM THE WASTE PANELS AFTER 10,000 YR FOR HUMAN INTRUSION SCENARIO E1, CASE $E1_b$ (CASE $E1_a$ WITH DISTANCE INCREASED) (Concluded)

Simulation	PU-238	U-234	TH-230	RA-226	PB-210	PU-239
IIA	.	7.5582	9.4983	6.0760	5.9401	33.975
1	.	.02251	.00014	.00038	.00033	.00116
2	.	.25297	.59659	.88537	.87262	.91545
3	.	.	.	.	.	.
4	.	.00719	.01958	.44028	.42880	.02960
5	.	137.25	8.9599	5.3980	5.3477	7694.7
6	.	.20978	.66280	6.0089	6.0831	1.0411
7	.	.88093	.97511	1.4858	1.4733	1.3722
8	.	138.23	6.0254	1.9214	1.8529	21404.
9	.	.01564	.04543	.67116	.67148	.06008
10	.	.	.	.	.	.
11	.	.53782	1.1036	1.6657	1.7016	1.6155
12	.	.00997	.02537	.55596	.58306	.03818
13	.	.00296	.00001	.00100	.00112	.
14	.	.12821	.35402	2.4659	2.4394	.44327
15	.	1.8032	.46205	.53667	.54079	3.1264
16	.	.70760	.07289	.21412	.22407	.23666
17	.	.44753	1.1070	2.3916	2.3630	1.7055
18	.	.19586	.56373	2.7193	2.7693	.75589
19	.	136.53	9.0426	7.3466	7.2381	1969.8
20	.	7.0565	10.054	5.6190	5.5262	34.033
21	.	.00503	.00117	.01317	.01313	.00172
22	.	.75627	2.2408	4.2119	4.2518	3.5036
23	.	138.15	6.2777	.93962	.85372	35823.
24	.	8.2386	3.8180	4.2358	4.2061	18.821
25	.	.	.	.	.	.
26	.	136.78	10.338	6.4761	6.4127	8331.2
27	.	.26568	.84139	15.160	15.361	1.3075
28	.	.00028	.	.00047	.00052	.
29	.	13.143	.75204	.94708	.90974	15.836
30	.	2.7633	8.6959	8.7638	8.7596	13.352
31	.00004	139.10	3.3515	1.2413	1.1942	36504.
32	.	.	.	.	.	.
33	.	.12846	.38001	4.9588	5.0575	.55526
34	.00093	86.818	7.9166	4.8448	4.7813	346.70
35	.00001	.01562	.04622	1.2906	1.3324	.06491
36	.	.00171	.00042	.01363	.01343	.00051
37	.	.	.	.	.	.
38	.	137.03	9.5947	4.1734	4.0119	8382.2
39	.	.	.	.	.	.
40	.	.	.	.	.	.
41	.	37.794	3.2881	1.1821	1.1452	490.42
42	.	.49272	1.5131	5.4097	5.4426	2.3344
43	.	1.7986	5.5285	7.4809	7.5145	8.2895
44	.	.58306	1.5809	2.7811	2.8642	2.4322
45	.	137.27	8.8758	5.5924	5.3927	17856.
46	.	.00002	.	.	.	.
47	.	.	.	.	.	.
48	.05381	139.41	2.4441	.71993	.69075	7045.0
49	.	1.3245	1.8503	2.3199	2.3608	2.3623
50	.	138.05	6.5619	3.1301	3.0730	18417.
$Average_{50}$	.00110	30.884	2.5193	2.5243	2.5152	3287.6

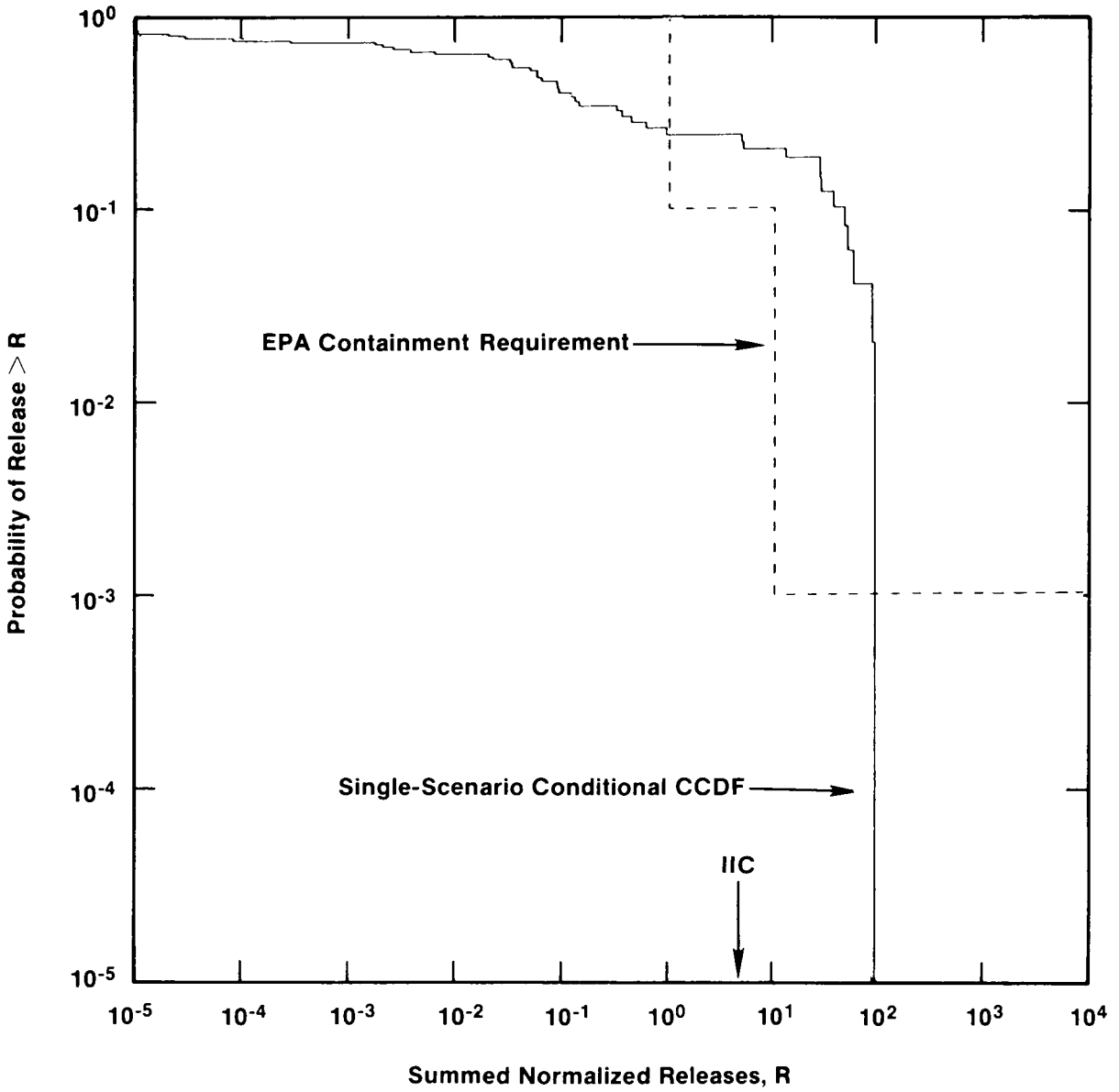

TRI-6342-189-0

Figure 4-7. CCDF for 50 Simulations of One Scenario Case $E1_b$ of Scenario E1, for Radionuclide Migration 5.0 km (3.0 mi) Downgradient from the Waste Panels. Given that the Scenario Occurs, the Probability that the CCDF is within the EPA Limit is 0.76.

estimated because data are not available. Reducing the range of solubility values represents a decrease in the uncertainty in this parameter. Uncertainty caused by natural variability within the consolidated waste and backfill materials is also included. The four radionuclides dominating releases for this case are, in decreasing order, plutonium-240, plutonium-239, uranium-233 and thorium-229. This result differs from Case El_b in that plutonium-240 is transported in the largest quantities. The results for plutonium-240 and uranium-233 are similar to those in Case El_b (Figure 4-8 and Table 4-5). As in the previous two cases, transport 5.0 km (3.0 mi) downgradient exceeds the limits in the Standard (Figure 4-9). The change in the range of radionuclide solubility results in only a moderate shift of the CCDF toward the limits, because the median value of solubility remains the same.

Case El_d. Except for room properties, this case is the same as Case El_b. Changing the room properties (permeability and porosity) reflects possible modifications to the room contents and waste (such as supercompaction and grouting). For Case El_d, the range of hydraulic-conductivity values is on the order of 10^{-14} to 10^{-10} m/s ($\sim 10^{-14}$ to 10^{-10} ft/s) with a mean of 10^{-11} m/s ($\sim 10^{-11}$ ft/s) and the range of porosity values is 0.05 to 0.20 with a median of 0.10. For comparison, the reference value of the mean hydraulic conductivity for the room is on the order of 10^{-7} m/s ($\sim 10^{-7}$ ft/s) (Table 3-10; see also Lappin et al., 1989). The four radionuclides dominating this case are in decreasing order, thorium-229, plutonium-240, americium-241, and plutonium-239 (Figure 4-10 and Table 4-6). This result differs from the preceding cases in that thorium-229, which has not previously dominated, now migrates in the largest quantities. Plutonium-239 is reduced in importance. For Case El_d, americium-241 migrates in the third largest quantities, as it did for reference conditions (Case El_b). The distributions in the histograms for thorium-229 and plutonium-240 are similar, especially in the results that occur with large frequencies, while the americium-241 distribution lacks the distinct large frequencies. The assumed changes in room properties produce a CCDF that is within the limits in the Standard (Figure 4-11). The shift in the CCDF, resulting from changes in room properties, is large when compared to the earlier cases and suggests that room properties have an important effect on radionuclide migration.

Case El_e. This case is a combination of Cases El_c and El_d. Both the narrower range in radionuclide-solubility values and the modified room properties are used. The three radionuclides dominating transport are, in decreasing order, thorium-229, plutonium-240, and americium-241 (Figure 4-12 and Table 4-7) with radium-226 and lead-210 within a factor of four of thorium. Because the change in room properties has great influence on total transport and this change is included in Case El_e, the same three radionuclides dominate the results. Correlating parameter values with results indicates that among

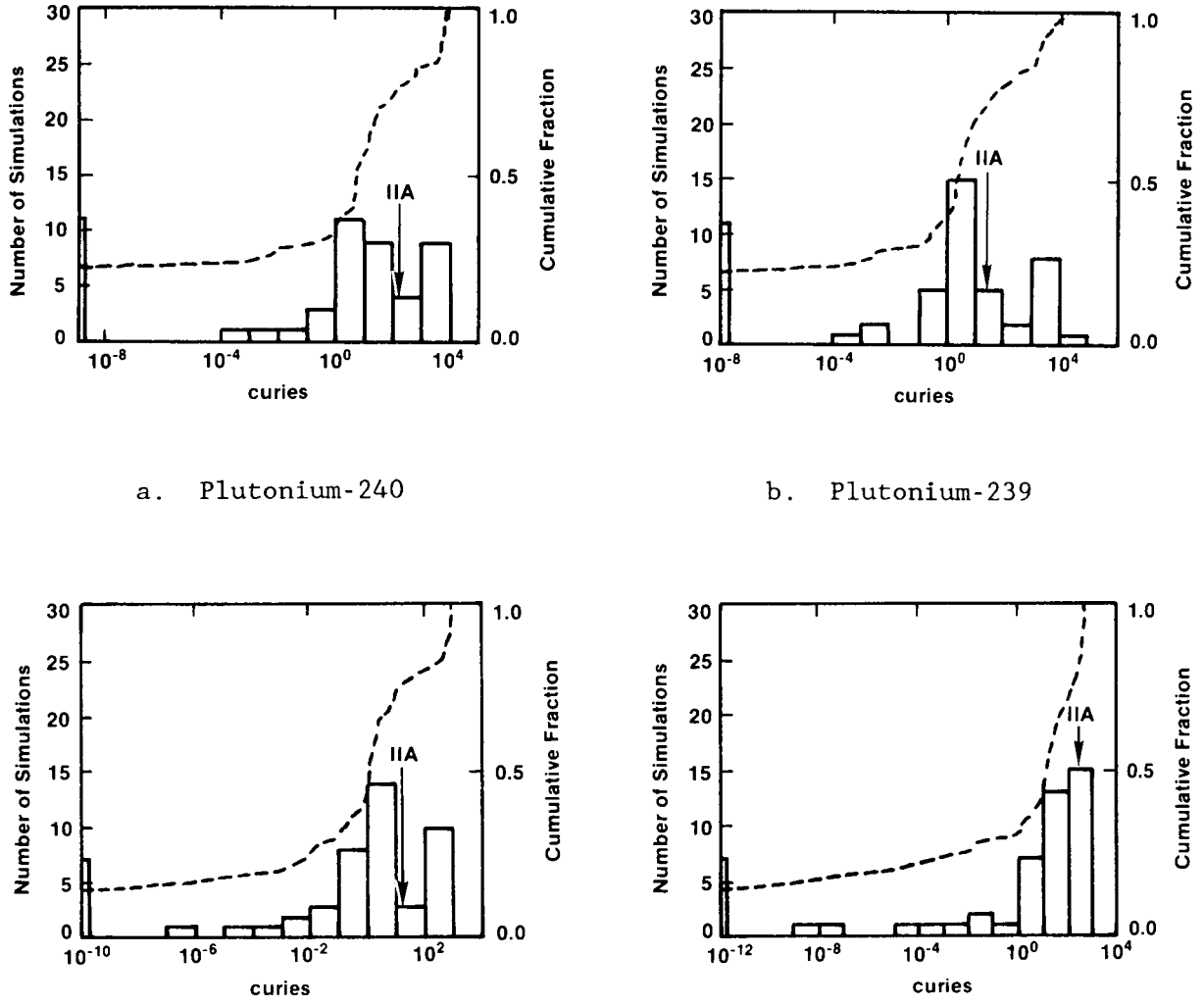

Figure 4-8. Histograms of Frequency of Simulations in which Quantities of Radioisotopes Migrate 5.0 km (3.0 mi) Downgradient from the Waste Panels in 10,000 yr, Showing the Cumulative Fractional Density of Simulations, for Human Intrusion Scenario E_1, Case $E1_c$ (Case $E1_b$ with Radionuclide Solubility Range Narrowed).

TABLE 4-5. CUMULATIVE CURIES (≥0.000005) MIGRATING 5.0 KM (3.0 MI) DOWNGRADIENT FROM THE WASTE PANELS AFTER 10,000 YR FOR HUMAN INTRUSION SCENARIO E1, CASE $E1_c$ (CASE $E1_b$ WITH RADIONUCLIDE SOLUBILITY RANGE NARROWED)

Simulation	PU-240	U-236	AM-241	NP-237	U-233	TH-229
IIA	108.67	.08462	.99413	.85789	11.626	208.52
1	.00068	.00005	.	.00050	.00664	.00112
2	6.1218	.00591	.00664	.06018	.80522	11.126
3	.	.	.	.	.	.
4	.74503	.00069	.07374	.00750	.09054	1.3653
5	3933.4	1.7696	.30100	16.387	468.32	403.43
6	13.346	.00839	.27811	.08910	1.1873	23.809
7	3.9978	.01152	.00361	.11317	1.4824	7.9197
8	5545.5	1.3846	20.938	16.397	751.14	372.44
9	1.3374	.00146	.24056	.02482	.18767	2.7907
10	.	.	.	.	.	.
11	4.7435	.00671	.01972	.06616	.86231	8.9773
12	.75375	.00077	.04699	.00822	.10052	1.3918
13	.	.00002	.	.00022	.00293	.00011
14	5.0611	.00596	.58752	.09923	.76404	11.190
15	4.0125	.00818	.00020	.08343	1.1187	7.3938
16	.27261	.00350	.00004	.03574	.47340	.56503
17	9.0352	.00817	.02815	.08362	1.1182	16.367
18	7.3258	.00800	.78298	.11575	1.0292	15.041
19	578.90	.99075	.12636	14.630	191.20	145.61
20	134.56	.09358	.53228	.96096	12.876	242.20
21	.01030	.00011	.00001	.00113	.01511	.01993
22	22.809	.01572	.05963	.16475	2.2055	40.765
23	5865.6	1.2951	16.036	16.399	753.78	318.13
24	30.016	.07026	.04959	.83464	8.6536	70.052
25	.	.	.	.	.	.
26	3174.8	1.8168	.04260	16.368	400.34	379.13
27	27.044	.01627	45.509	.18191	2.3553	48.980
28	.	.	.	.00005	.00072	.00001
29	11.805	.03603	.00038	.36516	4.8654	20.136
30	98.202	.06090	68.046	.66926	8.7713	179.19
31	6920.9	1.0003	687.42	16.276	759.82	231.89
32	.	.	.	.	.	.
33	5.2921	.00450	2.1488	.05866	.60146	10.066
34	598.13	.52670	259.37	6.6506	71.225	433.49
35	2.1025	.00168	4.3018	.02693	.23104	4.1708
36	.00474	.00008	.00004	.00137	.01000	.01129
37	.	.	.	.	.	.
38	3880.7	1.7912	.14461	16.385	413.64	430.03
39	.	.	.	.	.	.
40	.	.	.	.	.	.
41	301.35	.19118	.00172	2.0073	26.934	114.88
42	18.518	.01312	.45204	.13620	1.8047	33.407
43	62.250	.04553	9.4281	.48445	6.2725	115.54
44	13.510	.01129	.03904	.11506	1.5360	24.494
45	4265.7	1.7409	.32066	16.389	650.15	415.34
46	.	.	.	.	.00001	.
47	.	.	.	.	.	.
48	5557.4	1.3813	3087.7	15.792	604.39	414.92
49	5.1979	.01712	.00564	.30349	2.0958	13.598
50	5181.1	1.4869	8.9786	16.397	749.41	390.47
$Average_{50}$	925.83	.31662	84.281	3.5034	118.04	99.206

TABLE 4-5. CUMULATIVE CURIES (≥0.000005) MIGRATING 5.0 KM (3.0 MI) DOWNGRADIENT FROM THE WASTE PANELS AFTER 10,000 YR FOR HUMAN INTRUSION SCENARIO E1, CASE $E1_c$ (CASE $E1_b$ WITH RADIONUCLIDE SOLUBILITY RANGE NARROWED) (Concluded)

Simulation	PU-238	U-234	TH-230	RA-226	PB-210	PU-239
IIA	.	7.5582	9.4983	6.0760	5.9401	33.975
1	.	.00434	.00005	.00033	.00028	.00022
2	.	.52541	1.2423	1.2734	1.2531	1.9069
3	.	.	.	.	.	.
4	.	.05924	.16120	2.0308	1.9738	.24357
5	.	137.10	9.4238	5.7186	5.6664	1310.0
6	.	.77099	2.4494	5.9870	6.0320	3.8335
7	.	.97154	1.0737	1.6167	1.6034	1.5102
8	.	138.14	6.3019	2.0173	1.9457	3767.7
9	.	.12249	.35674	2.8039	2.8018	.47162
10	.	.	.	.	.	.
11	.	.56432	1.1591	1.7182	1.7550	1.6935
12	.	.06565	.16717	1.5910	1.6676	.25150
13	.	.00191	.00001	.00078	.00087	.
14	.	.53140	1.4596	3.1204	3.0823	1.8360
15	.	.73257	.45020	.53206	.53627	1.2679
16	.	.30863	.06762	.21033	.22023	.10354
17	.	.72931	1.8033	2.7180	2.6851	2.7776
18	.	.67316	1.9320	3.5759	3.6231	2.5964
19	.	115.06	7.5933	6.6348	6.5281	270.16
20	.	8.3670	10.058	5.5180	5.4241	40.459
21	.	.00987	.00230	.01656	.01647	.00337
22	.	1.4391	4.2542	4.5837	4.5952	6.6549
23	.	138.14	6.3246	.94688	.86034	13378.
24	.	5.6727	3.7284	4.1716	4.1430	12.977
25	.	.	.	.	.	.
26	.	136.60	10.515	6.6155	6.5513	1052.0
27	.	1.5353	4.8591	11.874	11.967	7.5312
28	.	.00047	.	.00050	.00056	.
29	.	3.1828	.61960	.87859	.84475	3.8193
30	.	5.7255	11.339	4.1394	4.0309	27.594
31	.00004	139.06	3.4836	1.3034	1.2545	7156.4
32	.	.	.	.	.	.
33	.	.39260	1.1627	5.1908	5.2792	1.7003
34	.00052	47.677	8.5174	5.4658	5.4012	189.97
35	.00002	.15164	.45799	8.3904	8.6596	.64377
36	.	.00657	.00162	.01708	.01683	.00198
37	.	.	.	.	.	.
38	.	136.92	9.9624	4.3458	4.1780	1208.1
39	.	.	.	.	.	.
40	.	.	.	.	.	.
41	.	17.562	3.1571	1.1613	1.1261	87.057
42	.	1.1785	3.6206	5.8391	5.8414	5.5945
43	.	4.0942	9.9714	6.6136	6.5836	18.866
44	.	1.0035	2.7202	3.3000	3.3775	4.1851
45	.	137.19	9.1360	5.7831	5.5770	1834.0
46	.	.00001	.	.	.	.
47	.	.	.	.	.	.
48	.05381	139.03	3.7591	1.2224	1.1787	1782.8
49	.	1.3754	1.8631	2.3311	2.3721	2.4626
50	.	137.96	6.8590	3.2929	3.2335	3101.4
$Average_{50}$	.00109	29.213	3.0403	2.6910	2.6777	705.77

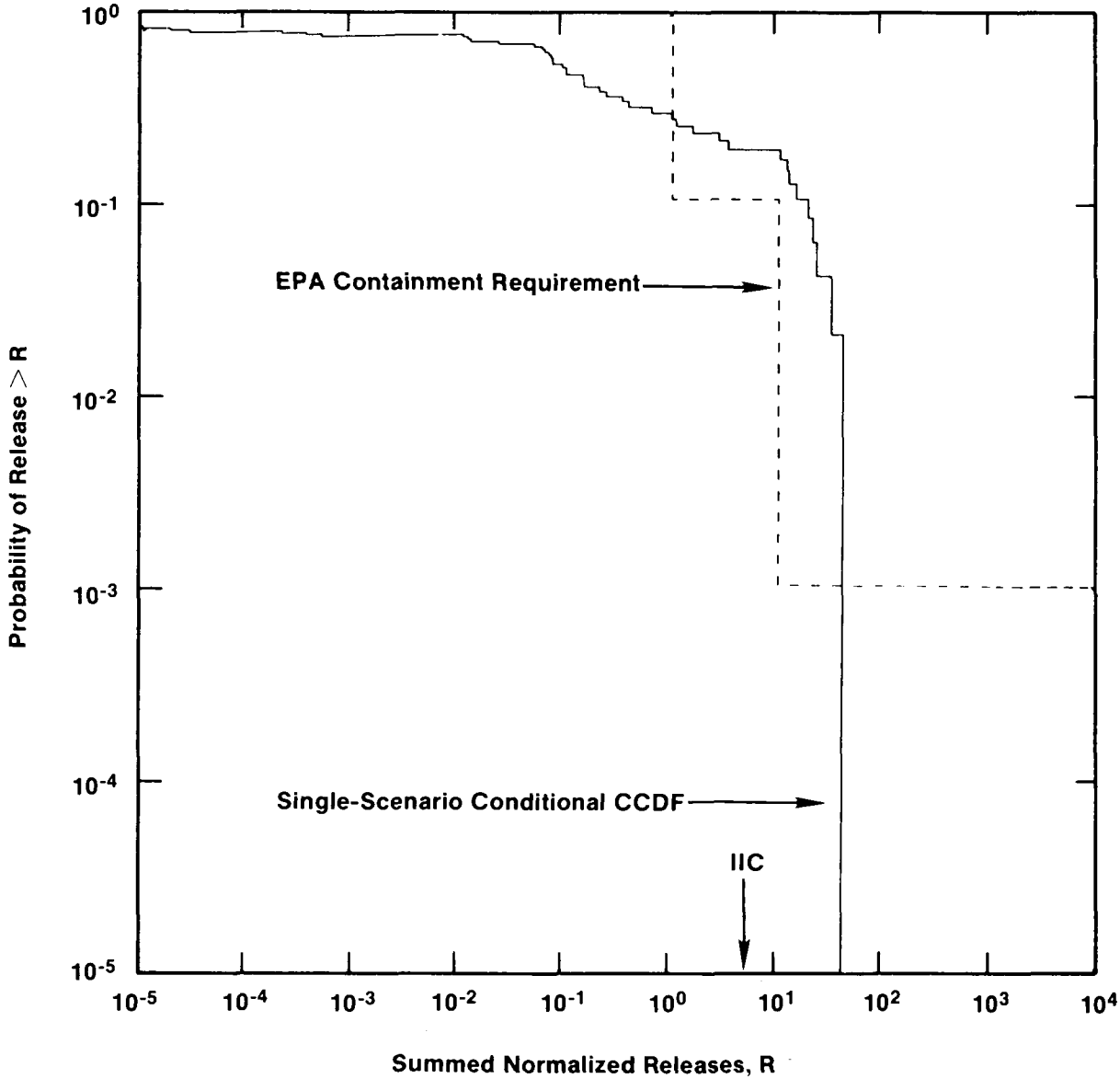

Figure 4-9. CCDF for 50 Simulations of One Scenario, Case $E1_c$ of Scenario E1, for Radionuclide Migration 5.0 km (3.0 mi) Downgradient from the Waste Panels (Case $E1_b$ with Radionuclides Solubility Range Narrowed). Given that the Scenario Occurs, the Probability that the CCDF is within the EPA Limit is 0.76.

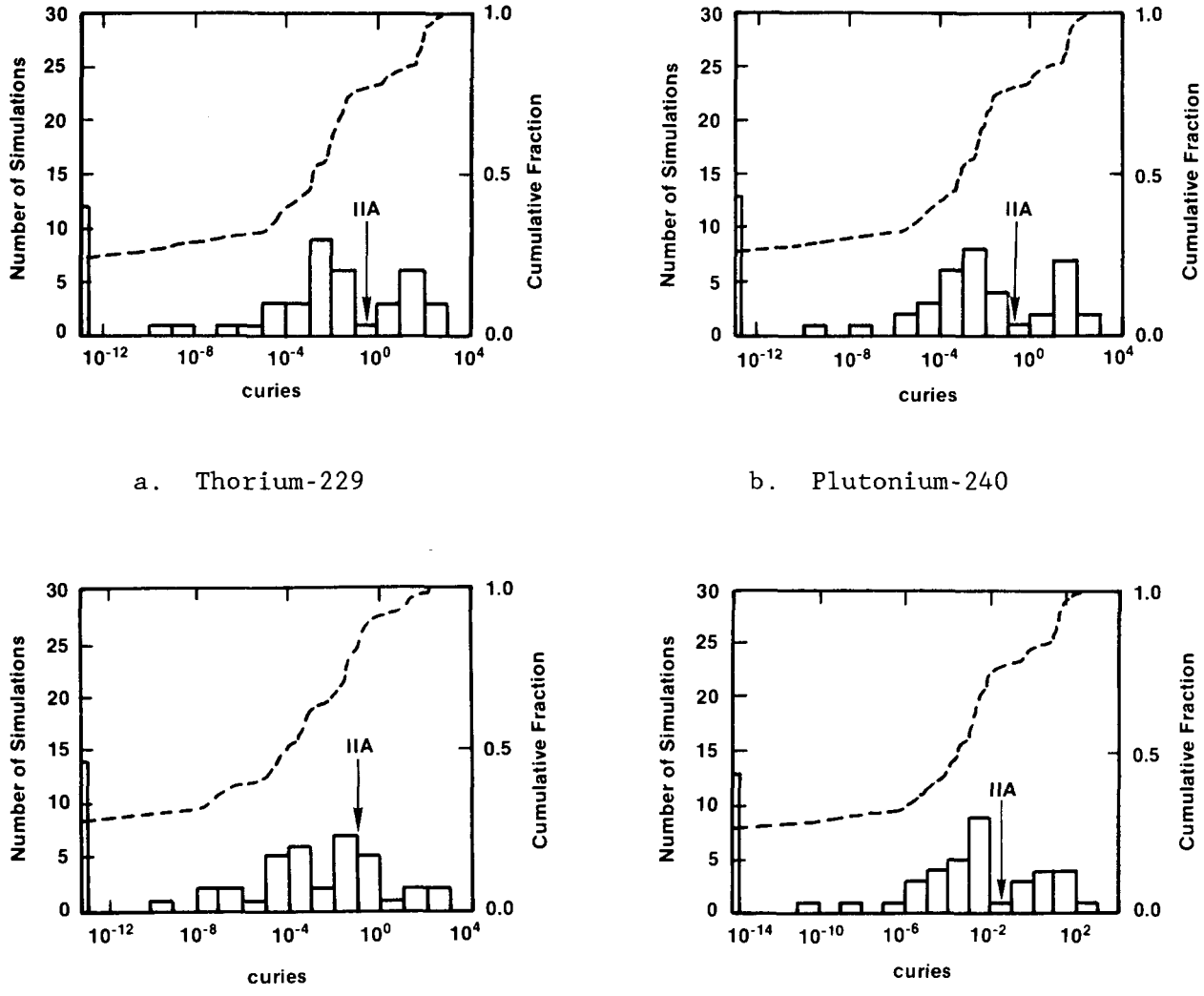

Figure 4-10. Histograms of Frequency of Simulations in which Quantities of Radioisotopes Migrate 5.0 km (3.0 mi) Downgradient from the Waste Panels in 10,000 yr, Showing the Cumulative Fractional Density of Simulations, for Human Intrusion Scenario E1, Case $E1_d$ (Case $E1_b$ with Permeability and Porosity of Room Decreased).

TABLE 4-6. CUMULATIVE CURIES (≥0.000005) MIGRATING 5.0 KM (3.0 MI) DOWNGRADIENT FROM THE WASTE PANELS AFTER 10,000 YR FOR HUMAN INTRUSION SCENARIO E1, CASE $E1_d$ (CASE $E1_b$ WITH PERMEABILITY AND POROSITY OF ROOM DECREASED)

Simulation	PU-240	U-236	AM-241	NP-237	U-233	TH-229
IIA	.16250	.00014	.11676	.00221	.01908	.31482
1	.	.	.	.	.	.
2	.00035	.	.00047	.00002	.00017	.00065
3	.	.	.	.	.	.
4	.00006	.	.00002	.	.00001	.00011
5	28.936	.02794	.12875	.27716	3.6641	53.866
6	.00362	.	.02536	.00004	.00034	.00648
7	.00002	.	.	.00001	.00008	.00004
8	40.197	.02599	17.885	.28359	3.6728	73.395
9	.00050	.	.00003	.00001	.00008	.00108
10	.	.	.	.	.	.
11	.00074	.	.00005	.00004	.00031	.00144
12	.00003	.	.00001	.	.	.00005
13	.	.	.	.	.	.
14	.00226	.	.00009	.00006	.00040	.00523
15	.	.	.	.00001	.00008	.00001
16	.	.	.	.	.	.
17	.00812	.00001	.00923	.00015	.00121	.01483
18	.00406	.00001	.00023	.00010	.00067	.00868
19	2.1703	.01489	.00071	.27145	1.8609	6.2214
20	.06551	.00005	.10703	.00081	.00706	.11847
21	.	.	.	.	.	.
22	.00694	.00001	.02736	.00008	.00072	.01245
23	499.48	.29595	13.895	3.1861	42.865	548.30
24	.00755	.00004	.00001	.00082	.00564	.01895
25	.	.	.	.	.	.
26	19.747	.02384	.01631	.23612	3.1436	36.696
27	.00313	.	.05302	.00003	.00027	.00567
28	.	.	.	.	.	.
29	.00001	.	.	.00002	.00029	.00002
30	.01912	.00001	.22696	.00020	.00175	.03485
31	111.66	.08454	112.53	1.0690	11.639	219.00
32	.	.	.	.	.	.
33	.00073	.	.00053	.00001	.00009	.00141
34	1.0037	.00096	.65130	.01702	.12797	2.1150
35	.00015	.	.00029	.	.00002	.00031
36	.	.	.	.	.	.
37	.	.	.	.	.	.
38	57.054	.04335	.08810	.44369	5.9345	102.88
39	.	.	.	.	.	.
40	.	.	.	.	.	.
41	.76678	.00071	.00097	.00741	.09917	1.3716
42	.01631	.00001	.03284	.00023	.00171	.02960
43	.02023	.00002	.04480	.00030	.00212	.03782
44	.00442	.	.00572	.00008	.00061	.00809
45	19.112	.01887	.16223	.18766	2.4498	35.888
46	.	.	.	.	.	.
47	.	.	.	.	.	.
48	43.061	.03177	115.56	.43415	4.4571	84.633
49	.00040	.	.	.00006	.00039	.00114
50	31.525	.02444	5.4265	.26604	3.3091	58.876
$Average_{50}$	17.098	.01187	5.3374	.13365	1.6649	24.471

TABLE 4-6. CUMULATIVE CURIES (≥0.000005) MIGRATING 5.0 KM (3.0 MI) DOWNGRADIENT FROM THE WASTE PANELS AFTER 10,000 YR FOR HUMAN INTRUSION SCENARIO E1, CASE $E1_d$ (CASE $E1_b$ WITH PERMEABILITY AND POROSITY OF ROOM DECREASED) (Concluded)

Simulation	PU-238	U-234	TH-230	RA-226	PB-210	PU-239
IIA	.	.01241	.03636	.84822	.85912	.05261
1	.	.	.	.	.	.
2	.	.00011	.00007	.00723	.00753	.00010
3	.	.	.	.	.	.
4	.	.00001	.00001	.00029	.00031	.00002
5	.	2.3945	6.4914	6.1513	5.9821	9.6797
6	.	.00022	.00068	.02377	.02415	.00106
7	.	.00005	.	.00096	.00093	.00001
8	.	2.3963	7.5754	8.1630	8.1542	11.606
9	.	.00006	.00015	.00166	.00163	.00019
10	.	.	.	.	.	.
11	.	.00020	.00019	.00594	.00615	.00024
12	.	.	.00001	.00014	.00014	.00001
13	.	.	.	.	.	.
14	.	.00030	.00074	.00724	.00726	.00088
15	.	.00005	.	.00169	.00198	.
16	.	.	.	.00001	.00001	.
17	.	.00079	.00169	.05530	.05670	.00258
18	.	.00044	.00120	.01349	.01340	.00154
19	.	1.2257	.41915	.62378	.60307	.59053
20	.	.00459	.01313	.37568	.38021	.02013
21	.	.	.	.	.	.
22	.	.00047	.00133	.04589	.04755	.00206
23	.	27.969	11.013	2.1703	2.0283	139.12
24	.	.00370	.00309	.02918	.02708	.00183
25	.	.	.	.	.	.
26	.	2.0459	4.4013	4.3426	4.4168	6.6711
27	.	.00018	.00056	.02335	.02371	.00087
28	.	.	.	.	.	.
29	.	.00019	.	.00060	.00051	.
30	.	.00114	.00353	.14099	.14493	.00542
31	.00001	7.5635	10.032	5.3999	5.3059	33.931
32	.	.	.	.	.	.
33	.	.00006	.00017	.00336	.00342	.00024
34	.	.08835	.25293	3.7003	3.7552	.33069
35	.	.00001	.00003	.00084	.00085	.00005
36	.	.	.	.	.	.
37	.	.	.	.	.	.
38	.	3.8766	9.6316	6.1990	6.0963	17.301
39	.	.	.	.	.	.
40	.	.	.	.	.	.
41	.	.06472	.14296	.27077	.27425	.23433
42	.	.00112	.00331	.08732	.08539	.00507
43	.	.00139	.00423	.10860	.10616	.00629
44	.	.00040	.00093	.02735	.02835	.00141
45	.	1.6019	4.3859	4.8573	4.9582	6.4689
46	.	.	.	.	.	.
47	.	.	.	.	.	.
48	.01043	2.9275	8.8650	6.3753	6.4093	12.633
49	.	.00031	.00020	.00178	.00172	.00008
50	.	2.1597	6.5844	6.9659	6.8526	9.8233
$Average_{50}$	.00021	1.0866	1.3966	1.1236	1.1161	4.9688

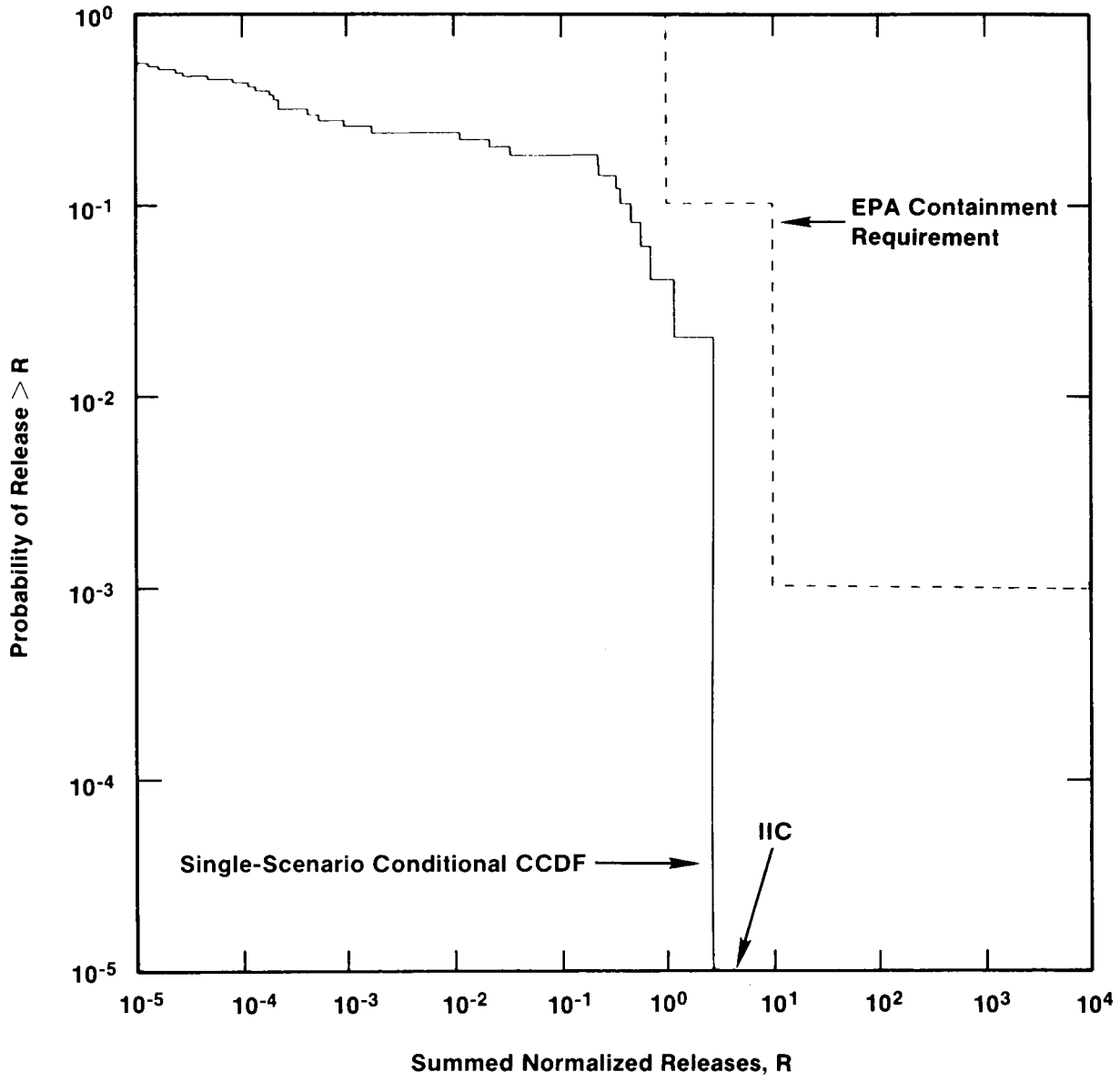

Figure 4-11. CCDF for 50 Simulations of One Scenario, Case El_d of Scenario E1, for Radionuclide Migration 5.0 km (3.0 mi) Downgradient from the Waste Panels (Case El_b with Permeability and Porosity of Room Decreased). Given that the Scenario Occurs, the Probability that the CCDF is within the EPA Limit is 1.00.

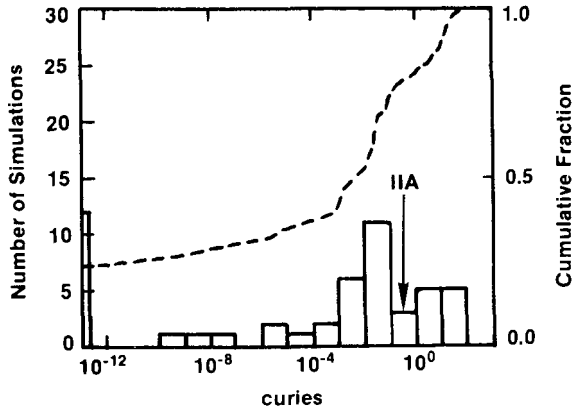

a. Thorium-229

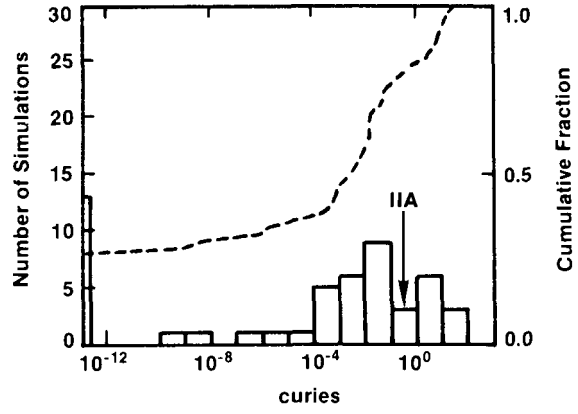

b. Plutonium-240

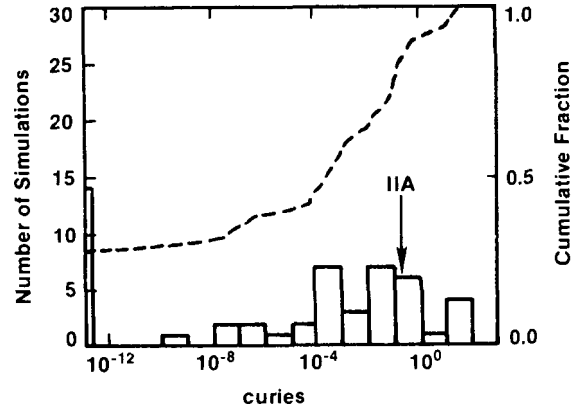

c. Americium-241

TRI-6342-173-0

Figure 4-12. Histograms of Frequency of Simulations in which Quantities of Radioisotopes Migrate 5.0 km (3.0 mi) Downgradient from the Waste Panels in 10,000 yr, Showing the Cumulative Fractional Density of Simulations, for Human Intrusion Scenario E1, Case $E1_e$ (Case $E1_b$ with Radionuclide Solubility Range Narrowed and Permeability and Porosity of Room Decreased).

TABLE 4-7. CUMULATIVE CURIES (≥0.000005) MIGRATING 5.0 KM (3.0 MI) DOWNGRADIENT FROM THE WASTE PANELS AFTER 10,000 YR FOR HUMAN INTRUSION SCENARIO E1, CASE $E1_e$ (CASE $E1_b$ WITH RADIONUCLIDE SOLUBILITY RANGE NARROWED AND WITH PERMEABILITY AND POROSITY OF ROOM DECREASED)

Simulation	PU-240	U-236	AM-241	NP-237	U-233	TH-229
IIA	.16250	.00014	.11676	.00221	.01908	.31482
1	.	.	.	.	.	.
2	.00074	.	.00047	.00003	.00036	.00136
3	.	.	.	.	.	.
4	.00050	.	.00019	.00001	.00007	.00093
5	4.9298	.00476	.12875	.04883	.62417	9.1712
6	.01335	.00001	.06630	.00014	.00126	.02389
7	.00002	.	.	.00001	.00009	.00004
8	7.0802	.00457	11.569	.05437	.64684	12.914
9	.00389	.00001	.00024	.00010	.00064	.00846
10	.	.	.	.	.	.
11	.00078	.	.00006	.00005	.00032	.00151
12	.00018	.	.00006	.	.00003	.00034
13	.	.	.	.	.	.
14	.00933	.00001	.00036	.00025	.00167	.02164
15	.	.	.	.	.00003	.
16	.	.	.	.	.	.
17	.01323	.00001	.01184	.00022	.00197	.02417
18	.01395	.00002	.00081	.00034	.00231	.02976
19	.29870	.00204	.00010	.03760	.25555	.85557
20	.07779	.00006	.12138	.00094	.00837	.14095
21	.	.	.	.	.	.
22	.01320	.00001	.03518	.00014	.00136	.02367
23	53.243	.03174	13.895	.34347	4.5783	95.323
24	.00520	.00003	.00001	.00056	.00388	.01305
25	.	.	.	.	.	.
26	2.5102	.00302	.01631	.03015	.39637	4.6436
27	.01798	.00001	.25578	.00016	.00158	.03259
28	.	.	.	.	.	.
29	.	.	.	.00001	.00007	.00001
30	.03959	.00003	.42646	.00039	.00361	.07226
31	14.273	.01085	24.639	.15396	1.4860	27.874
32	.	.	.	.	.	.
33	.00223	.	.00163	.00004	.00027	.00430
34	.54894	.00052	.37603	.00954	.06980	1.1587
35	.00152	.	.00287	.00003	.00017	.00305
36	.	.	.	.	.	.
37	.	.	.	.	.	.
38	8.2531	.00627	.08810	.06403	.86208	14.930
39	.	.	.	.	.	.
40	.	.	.	.	.	.
41	.13602	.00013	.00097	.00131	.01762	.24379
42	.03904	.00003	.06268	.00051	.00409	.07089
43	.04600	.00004	.09388	.00066	.00483	.08592
44	.00762	.00001	.00948	.00014	.00105	.01392
45	1.9629	.00194	.16223	.02206	.25185	3.6737
46	.	.	.	.	.	.
47	.	.	.	.	.	.
48	10.882	.00806	37.497	.11695	1.1314	21.429
49	.00042	.	.	.00006	.00040	.00119
50	5.3127	.00412	2.9109	.05124	.55677	9.9192
$Average_{50}$	2.1947	.00157	1.8475	.01877	.21830	4.0542

TABLE 4-7. CUMULATIVE CURIES (≥0.000005) MIGRATING 5.0 KM (3.0 MI) DOWNGRADIENT FROM THE WASTE PANELS AFTER 10,000 YR FOR HUMAN INTRUSION SCENARIO E1, CASE $E1_e$ (CASE $E1_b$ WITH RADIONUCLIDE SOLUBILITY RANGE NARROWED AND WITH PERMEABILITY AND POROSITY OF ROOM DECREASED) (Concluded)

Simulation	PU-238	U-234	TH-230	RA-226	PB-210	PU-239
IIA	.	.01241	.03636	.84822	.85912	.05261
1	.	.	.	.	.	.
2	.	.00023	.00015	.01503	.01565	.00020
3	.	.	.	.	.	.
4	.	.00005	.00011	.00240	.00252	.00017
5	.	.40767	1.1054	2.7292	2.6657	1.6479
6	.	.00082	.00250	.08784	.08922	.00389
7	.	.00006	.00001	.00106	.00103	.00001
8	.	.42173	1.3320	10.349	10.474	2.0431
9	.	.00044	.00117	.01302	.01282	.00147
10	.	.	.	.	.	.
11	.	.00021	.00020	.00621	.00643	.00025
12	.	.00002	.00004	.00090	.00090	.00006
13	.	.	.	.	.	.
14	.	.00121	.00307	.02994	.03005	.00366
15	.	.00002	.	.00119	.00139	.
16	.	.	.	.00001	.00001	.
17	.	.00129	.00275	.09005	.09232	.00420
18	.	.00151	.00411	.04634	.04603	.00530
19	.	.17120	.15344	.25110	.24192	.08099
20	.	.00544	.01551	.44794	.45335	.02393
21	.	.	.	.	.	.
22	.	.00089	.00252	.08718	.09034	.00392
23	.	2.9863	9.4269	7.9307	7.8948	14.835
24	.	.00255	.00213	.02284	.02124	.00126
25	.	.	.	.	.	.
26	.	.25973	.56052	1.2461	1.2786	.84236
27	.	.00103	.00325	.13476	.13669	.00503
28	.	.	.	.	.	.
29	.	.00005	.	.00057	.00048	.
30	.	.00236	.00729	.29193	.30008	.01120
31	.00001	.96690	3.0308	8.5068	8.5550	4.3078
32	.	.	.	.	.	.
33	.	.00017	.00051	.01031	.01047	.00074
34	.	.04894	.13820	2.3106	2.3451	.18120
35	.	.00012	.00035	.00834	.00840	.00048
36	.	.	.	.	.	.
37	.	.	.	.	.	.
38	.	.56024	1.6168	3.9055	3.9292	2.4934
39	.	.	.	.	.	.
40	.	.	.	.	.	.
41	.	.01149	.02539	.21983	.22424	.04160
42	.	.00267	.00793	.20903	.20441	.01214
43	.	.00315	.00960	.24716	.24162	.01431
44	.	.00069	.00160	.04710	.04882	.00243
45	.	.16464	.44890	2.2714	2.3589	.66446
46	.	.	.	.	.	.
47	.	.	.	.	.	.
48	.01043	.74921	2.2513	10.669	10.970	3.1968
49	.	.00032	.00021	.00186	.00179	.00009
50	.	.36363	1.1102	6.0252	5.9565	1.6542
$Average_{50}$	.00021	.14274	.42530	1.1644	1.1742	.64166

those variables sampled, solubility and room properties account for about two-fifths of the variability in output. Including time-of-the-intrusion event and borehole-fill properties accounts for about three-fifths of the variability in the results. The CCDF for this case is also within the limits set by the Standard, because of the influence of the change in room properties (Figure 4-13).

Case El_f (Case El_b with SWIFT II Generated Inputs). The dominating radionuclides, in decreasing order, for Case El_b are plutonium-239, plutonium-240 and uranium-233; the CCDF (Figure 4-7) exceeds the limits in the Standard. Case El_f uses the same data as Case El_b except for conductivities in the Culebra Dolomite Member. For Case El_f the same two plutonium radioisotopes dominate transport 5.0 km (3.0 mi) downgradient from the waste panels, but uranium-233 is replaced by americium-241 (Table 4-8). The transported quantities for Case El_f are less than for Case El_b. The CCDF still exceeds the limits in the Standard (Figure 4-14) but the maximum summed normalized release (30) is one-third of the release (90) for Case El_b.

Case El_g (Case El_e with SWIFT II Generated Inputs). The dominating radionuclides, in decreasing order, for Case El_e are thorium-229, plutonium-240, and americium-241; the CCDF (Figure 4-13) is within the limits in the Standard. Case El_g uses the same data as Case El_e except for the method of sampling. The room's hydraulic conductivity range is on the order of 10^{-14} to 10^{-10} m/s ($\sim 10^{-14}$ to 10^{-10} ft/s) [expected value 10^{-11} m/s ($\sim 10^{-11}$ ft/d)]. The room's porosity range is 0.05 to 0.20 (median value 0.10). For Case El_g, americium-241 and thorium-229 dominate transport 5.0 km (3.0 mi) downgradient with plutonium-240 following fifth behind radium-226 and lead-210 (Table 4-9). The quantities are less than for Case El_e. The CCDF for Case El_g (Figure 4-15) is within the limits of the Standard (Figure 4-13). The maximum summed normalized release for Case El_g (0.2) is slightly greater than one-third of the sum (0.5) for Case El_e.

When NEFTRAN is run using an average hydraulic conductivity from SWIFT II and an average gradient calculated from the flow field simulated by SWIFT II, the summed normalized releases are less than when NEFTRAN alone is used. The decrease in summed normalized releases is represented as a downward shift in the CCDF, illustrating the effect of a slightly more realistic modeling approach.

Conclusion. The seven cases for Scenario E1 are sensitivity analyses of certain parameter variations for a single scenario. Each case assumes that Scenario E1 actually occurs in the 10,000-yr period following repository decommissioning. This scenario, if it occurs, should result in releases

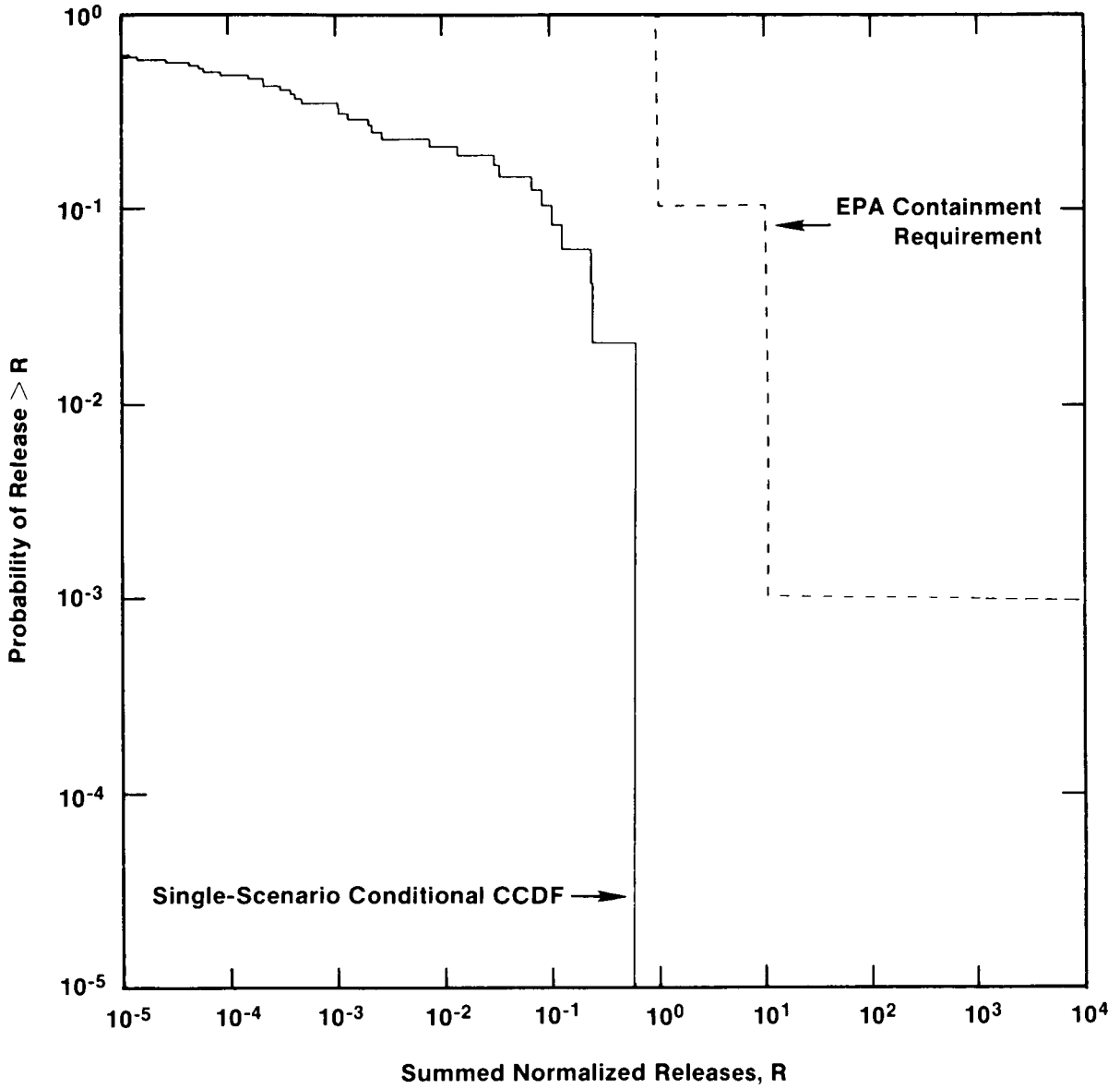

Figure 4-13. CCDF for 50 Simulations of One Scenario, Case $E1_e$ of Scenario E1, for Radionuclide Migration 5.0 km (3.0 mi) Downgradient from the Waste Panels (Case $E1_b$ with Radionuclide Solubility Range Narrowed and Permeability and Porosity of Room Decreased). Given that the Scenario Occurs, the Probability that the CCDF is within the EPA Limit is 1.00.

TABLE 4-8. CUMULATIVE CURIES (≥0.000005) MIGRATING 5.0 KM (3.0 MI) DOWNGRADIENT FROM THE WASTE PANELS AFTER 10,000 YR FOR HUMAN INTRUSION SCENARIO E1, CASE $E1_f$ (CASE $E1_b$ WITH SWIFT II HYDRAULIC CONDUCTIVITIES FOR THE CULEBRA DOLOMITE MEMBER)

Simulation	PU-240	U-236	AM-241	NP-237	U-233	TH-229
IA	109.73	.08539	.93076	.86672	11.723	210.78
1	.72195	.07062	.00504	.02686	10.442	1.4848
2	.	.	.	.	.	.
3	75.087	.02154	81.780	1.5697	2.8118	393.19
4	492.45	.05449	.13370	.58337	5.3947	258.84
5	41.457	.00810	.00278	.00175	.05925	.45022
6	10.356	.06772	.02711	.26695	9.2623	3.5431
7	9.8713	1.1450	1.2129	1.8188	579.26	208.74
8	.	.	.	.	.	.
9	.	.	.	.	.	.
10	943.18	.41553	10.036	16.168	58.993	504.63
11	15.772	.29617	2.8615	.83196	43.281	62.689
12	5867.7	.45480	345.25	2.7612	13.776	457.43
13	.	.	.	.	.	.
14	.00053	.00020	.	.00114	.02759	.00516
15	.48038	.00511	.01304	1.4321	.76034	2.3880
16	14.252	.03200	.02725	.26330	4.5603	1.5022
17	5220.7	1.0486	3.7769	16.397	142.91	20.711
18	5392.8	.32428	102.63	16.398	16.683	44.545
19	.	.	.	.	.	.
20	28.336	.03653	1.6595	.19507	4.9144	333.64
21	1253.0	.56214	.02123	.00529	55.453	26.741
22	23.345	.00695	.00426	.00205	.02673	.34469
23	2.9397	.02486	.00137	.00150	3.5635	.79405
24	83.850	.01961	.47568	13.937	1.4343	80.054
25	58.002	.03782	2245.1	10.954	5.4020	49.098
26	.	.	.	.	.	.
27	26.280	.00599	.01187	1.4235	.63832	36.806
28	.	.	.	.	.	.
29	154.12	.02830	14.345	9.0512	2.4139	28.330
30	.37000	.00138	.00018	.02766	.18196	.36704
31	30.292	1.8016	244.63	15.314	764.17	150.37
32	16.798	.07009	52.400	5.7312	10.185	377.54
33	1260.3	.32022	52.491	13.338	44.968	358.87
34	304.10	1.8120	14873.	5.7542	516.27	439.07
35	59.903	.02205	.15743	16.386	2.6901	346.03
36	1970.3	.09822	50.134	16.443	1.5294	1.8429
37	.12525	.01835	.00019	.03213	2.6363	1.4260
38	240.77	.06915	32.197	.45315	7.4398	414.92
39	344.55	.11391	49.986	.19741	15.221	137.61
40	76.212	1.4607	2.2809	5.8985	690.42	175.89
41	1.4425	.00128	.00208	6.3732	.28182	1.0182
42	61.539	.04506	558.25	2.8875	6.5077	557.47
43	.03808	.01066	.02170	.70455	1.5802	72.546
44	.17428	.00124	.00143	.38802	.18137	37.633
45	.	.	.	.	.	.
46	.11028	.00528	.00003	.00152	.77964	.16040
47	5.0721	.00619	.00034	.00197	.90536	4.6658
48	2233.7	.17669	718.76	6.5603	3.6585	6.6383
49	3.0752	.01907	4.4934	.08551	2.7643	28.235
50	746.10	.77130	8.4992	.29970	105.55	397.45
$Average_{50}$	541.39	.22982	389.13	3.8193	62.800	120.51

TABLE 4-8. CUMULATIVE CURIES (≥0.000005) MIGRATING 5.0 KM (3.0 MI) DOWNGRADIENT FROM THE WASTE PANELS AFTER 10,000 YR FOR HUMAN INTRUSION SCENARIO E1, CASE $E1_f$ (CASE $E1_b$ WITH SWIFT II HYDRAULIC CONDUCTIVITIES FOR THE CULEBRA DOLOMITE MEMBER) (Concluded)

Simulation	PU-238	U-234	TH-230	RA-226	PB-210	PU-239
IA	.	7.6210	9.4668	6.1190	6.0808	34.412
1	.	6.7928	.10723	.45952	.46517	.22704
2	.	.	.	.	.	.
3	.	1.8227	10.312	4.8156	4.7324	22.330
4	.	3.5041	10.099	4.8534	4.7717	146.37
5	.	.03859	.05504	.31199	.31305	14.200
6	.	6.0602	.31949	.43341	.42979	4.6332
7	.	137.78	7.3112	5.3810	5.4268	4.1379
8	.	.	.	.	.	.
9	.	.	.	.	.	.
10	.	38.285	10.360	3.4758	3.3603	271.05
11	.	28.210	7.4398	6.8969	6.9872	5.6448
12	.00011	9.0850	9.3986	5.9244	5.8919	2756.8
13	.	.	.	.	.	.
14	.	.01813	.00046	.00110	.00117	.00028
15	.	.48615	.27558	.99327	.97605	.15787
16	.	2.9662	.14192	1.5154	1.5469	4.5896
17	.	92.774	1.8526	10.091	10.087	5697.7
18	.21423	11.882	4.7129	7.7276	7.5894	1679.5
19	.	.	.	.	.	.
20	.	3.2005	7.8933	6.5664	6.4653	9.8167
21	.	36.146	2.7652	2.8955	2.8622	441.60
22	.	.01743	.04674	.24640	.25432	8.7815
23	.	2.3221	.07116	.22996	.21715	1.0119
24	.	.81341	7.3468	6.7071	6.7138	29.811
25	.01366	3.4898	5.1506	8.5329	8.6676	17.182
26	.	.	.	.	.	.
27	.	.40864	4.1154	3.2057	3.2073	8.2376
28	.	.	.	.	.	.
29	.	1.5158	3.3020	5.7705	5.9366	50.413
30	.	.11836	.04432	.13880	.14522	.08124
31	.08573	139.50	2.1730	.59814	.57209	8.7586
32	.	6.6788	8.3592	6.5183	6.3428	5.6516
33	.	29.181	10.784	3.0937	2.9581	357.10
34	10.190	139.89	3.2435	.79472	.75273	86.901
35	.	1.6458	8.7893	6.2764	6.1877	19.482
36	.	.93329	.19190	8.0778	8.1601	597.83
37	.	1.7288	.18258	.27266	.24558	.02545
38	.	4.8515	8.9338	6.3287	6.3020	78.256
39	.00005	9.8902	10.250	4.9038	4.7872	101.87
40	.	138.18	4.2344	3.3199	3.3078	27.474
41	.	.08996	.16620	.35493	.36808	.67041
42	.00001	4.2193	10.859	4.1493	4.0289	17.887
43	.	1.0244	6.9888	5.8817	5.7685	.01263
44	.	.11511	1.4231	2.0156	1.8871	.05991
45	.	.	.	.	.	.
46	.	.50695	.01520	.04486	.04543	.03363
47	.	.58797	.47219	.17261	.16769	1.4547
48	.00006	2.4603	.73889	6.6086	6.6327	711.45
49	.	1.8166	3.3978	5.2404	5.1813	1.0378
50	.	68.695	8.9640	5.9289	5.9611	242.09
$Average_{50}$	.21008	18.795	3.6658	3.1551	3.1341	268.65

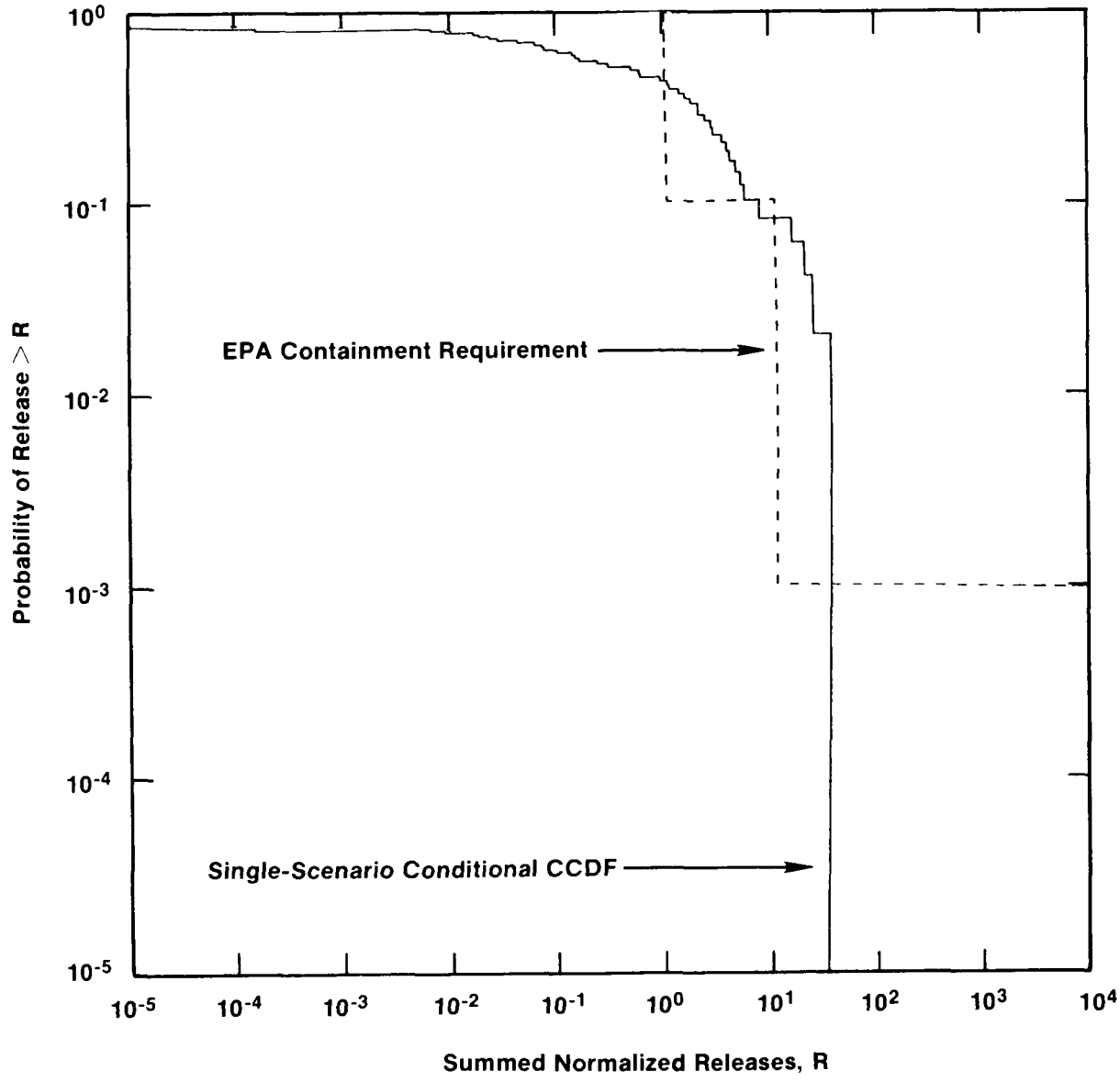

Figure 4-14. CCDF for 50 Simulations of One Scenario, Case $E1_f$ of Scenario E1, for Radionuclide Migration 5.0 km (3.0 mi) Downgradient from the Waste Panels (Case $E1_b$ with SWIFT II Hydraulic Conductivies for the Culebra Dolomite Member). Given that the Scenario Occurs, the Probability that the CCDF is within the EPA Limit is 0.60.

TABLE 4-9. CUMULATIVE CURIES (≥0.000005) MIGRATING 5.0 KM (3.0 MI) DOWNGRADIENT FROM THE WASTE PANELS AFTER 10,000 YR FOR HUMAN INTRUSION SCENARIO E1, CASE $E1_g$ (CASE $E1_e$ WITH SWIFT II HYDRAULIC CONDUCTIVITIES FOR THE CULEBRA DOLOMITE MEMBER)

Simulation	PU-240	U-236	AM-241	NP-237	U-233	TH-229
IIA	.16276	.00014	.10573	.00224	.01909	.31592
1	.00025	.00002	.00014	.00002	.00263	.00033
2	.	.	.	.	.	.
3	.10544	.00004	.30082	.00207	.00563	.40382
4	.23182	.00005	.08541	.00065	.00526	.18735
5	.00035	.	.	.	.00002	.00002
6	.00280	.00004	.	.00034	.00537	.00187
7	.02675	.00230	.00043	.00563	.33238	.16410
8	.	.	.	.	.	.
9	.	.	.	.	.	.
10	.28957	.00015	.22689	.00387	.02092	.33920
11	.05353	.00046	.04301	.01200	.06634	.17776
12	8.4833	.00111	1.3809	.01798	.06079	40.155
13	.	.	.	.	.	.
14	.	.	.	.	.	.
15	.00034	.	.00157	.00043	.00055	.00128
16	.00938	.00002	.00818	.00034	.00310	.00226
17	3.7130	.00049	1.6441	.00718	.06112	.03987
18	1.8445	.00022	.23343	.03855	.01958	.09540
19	.	.	.	.	.	.
20	.03037	.00004	.00173	.00039	.00553	.34188
21	.11163	.00017	.00013	.00005	.01969	.01087
22	.00006	.	.	.	.00001	.00001
23	.00002	.	.	.	.00021	.00002
24	.14752	.00007	.00459	.01341	.00610	.18802
25	.06698	.00005	4.1232	.00992	.00651	.07672
26	.	.	.	.	.	.
27	.01871	.00001	.00150	.00113	.00154	.02926
28	.	.	.	.	.	.
29	.43723	.00015	.09480	.01720	.01477	.18406
30	.	.	.	.	.	.
31	.07890	.00656	.87501	.01076	.97409	.54356
32	.11374	.00033	.13298	.01875	.04654	4.4334
33	.62468	.00022	3.7274	.00694	.03043	.33541
34	.32331	.00147	61.483	.03099	.21757	2.7934
35	.02124	.00001	.00253	.00357	.00146	.22152
36	.27986	.00002	1.2427	.01058	.00119	.00331
37	.	.	.	.	.00001	.
38	.40591	.00019	.09086	.00270	.02172	3.2520
39	.21118	.00009	.13768	.00044	.01248	.14653
40	.11279	.00215	.00244	.00604	.31154	.10546
41	.00391	.00001	.	.00661	.00122	.00468
42	.06985	.00005	2.3303	.00369	.00768	.51971
43	.00013	.00001	.00353	.00054	.00149	.02458
44	.	.	.	.00002	.00003	.00013
45	.	.	.	.	.	.
46	.	.	.	.	.	.
47	.00146	.	.00028	.	.00021	.00171
48	1.9475	.00027	3.1301	.04200	.01458	.05239
49	.00860	.00003	.00519	.00031	.00455	.05052
50	.36557	.00040	.35321	.00679	.05336	.93676
$Average_{50}$	.40284	.00034	1.6334	.00564	.04676	1.1165

TABLE 4-9. CUMULATIVE CURIES (≥0.000005) MIGRATING 5.0 KM (3.0 MI) DOWNGRADIENT FROM THE WASTE PANELS AFTER 10,000 YR FOR HUMAN INTRUSION SCENARIO E1, CASE $E1_g$ (CASE $E1_e$ WITH SWIFT II HYDRAULIC CONDUCTIVITIES FOR THE CULEBRA DOLOMITE MEMBER) (Concluded)

Simulation	PU-238	U-234	TH-230	RA-226	PB-210	PU-239
IIA	.	.01242	.03672	.83140	.83655	.05300
1	.	.00171	.00003	.05584	.04813	.00008
2	.	.	.	.	.	.
3	.	.00366	.04368	.09293	.09331	.03205
4	.	.00342	.02023	.17613	.17774	.07039
5	.	.00001	.	.00252	.00262	.00012
6	.	.00351	.00019	.01117	.01154	.00050
7	.	.21779	.01665	.18959	.19821	.01247
8	.	.	.	.	.	.
9	.	.	.	.	.	.
10	.	.01358	.03488	1.4475	1.4674	.08410
11	.	.04318	.02362	.07193	.07271	.02057
12	.	.05789	4.7211	5.9900	6.2007	2.7811
13	.	.	.	.	.	.
14	.	.	.	.	.	.
15	.	.00035	.00015	.08387	.08240	.00012
16	.	.00202	.00025	.24851	.24333	.00313
17	.	.03968	.00393	2.6138	2.6506	1.0672
18	.00011	.01878	.01044	1.3175	1.3504	.56669
19	.	.	.	.	.	.
20	.	.00360	.04543	.21087	.21777	.01115
21	.	.01285	.00124	.05317	.05126	.03522
22	.	.	.	.00268	.00281	.00002
23	.	.00014	.	.00258	.00274	.00001
24	.	.00383	.02597	.83225	.83068	.05625
25	.00002	.00443	.00823	1.7602	1.7958	.02023
26	.	.	.	.	.	.
27	.	.00100	.00339	.15349	.16144	.00607
28	.	.	.	.	.	.
29	.	.00949	.02261	.18147	.18923	.15020
30	.	.	.	.00009	.00008	.
31	.00037	.63483	.05375	2.9102	2.9677	.02316
32	.	.03115	.57104	1.1210	1.1408	.04057
33	.	.01975	.03390	1.2141	1.1994	.17862
34	.00908	.14259	.28580	5.2074	5.2763	.09347
35	.	.00093	.02679	1.1875	1.1772	.00715
36	.	.00073	.00036	.01510	.01515	.08628
37	.	.00001	.	.	.	.
38	.	.01520	.39893	.76654	.79451	.13842
39	.00001	.00817	.01566	.70766	.71966	.06362
40	.	.20410	.00878	.06502	.06787	.04380
41	.	.00106	.00086	.02408	.02244	.00199
42	.	.00499	.05440	2.5482	2.6081	.02060
43	.	.00096	.00305	.23849	.24056	.00004
44	.	.00002	.00002	.00022	.00023	.
45	.	.	.	.	.	.
46	.	.	.	.	.	.
47	.	.00014	.00017	.01262	.01280	.00042
48	.	.01537	.00623	1.7930	1.7834	.64689
49	.	.00303	.00644	.20933	.21320	.00306
50	.	.03470	.11371	.10340	.10413	.12399
$Average_{50}$	.00019	.03117	.13124	.67244	.68389	.12780

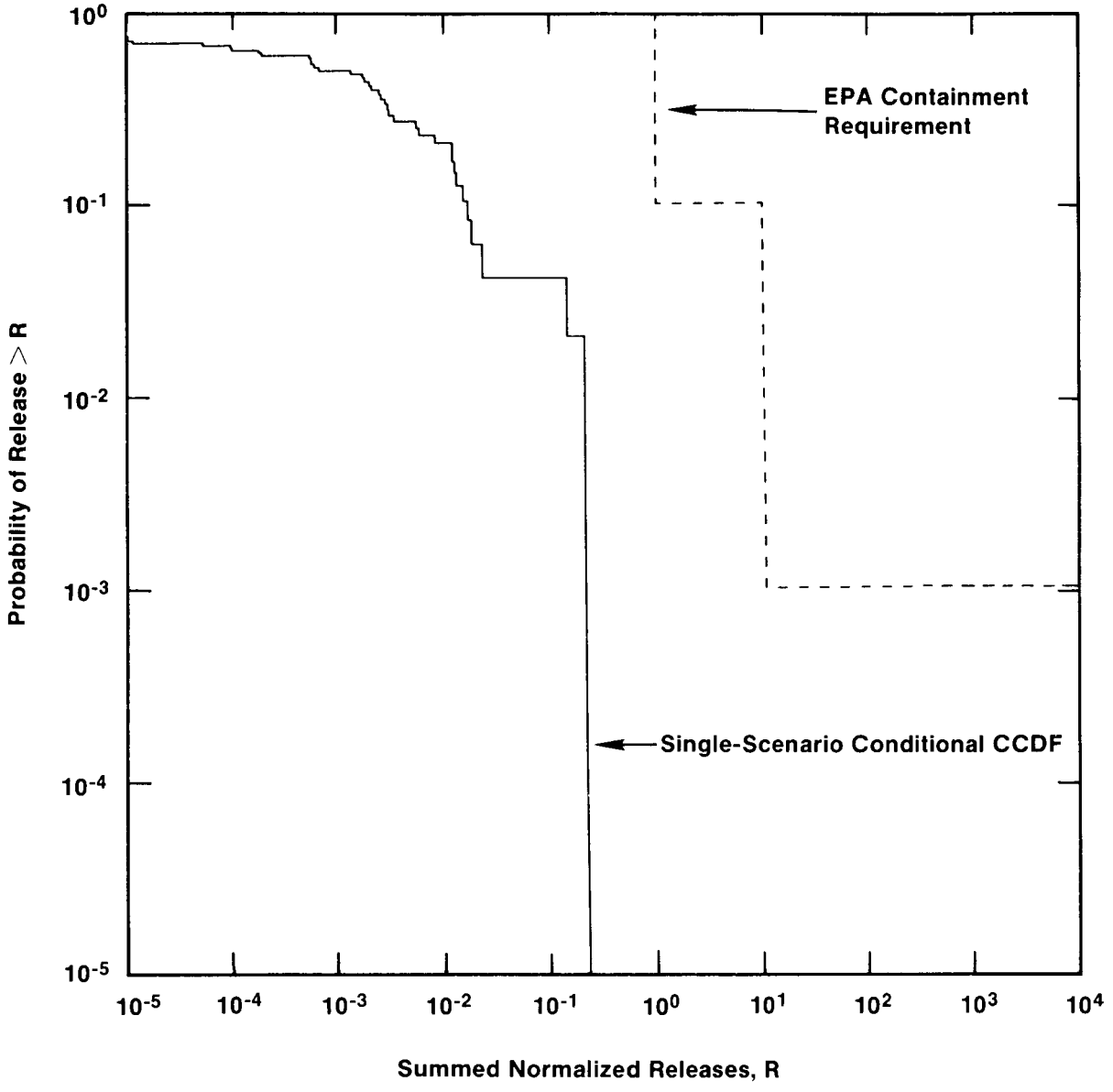

Figure 4-15. CCDF for 50 Simulations of One Scenario, Case $E1_g$ of Scenario E1, for Radionuclide Migration 5.0 km (3.0 mi) Downgradient from the Waste Panels (Case $E1_e$ with SWIFT II Hydraulic Conductivities for the Culebra Dolomite Member). Given that the Scenario Occurs, the Probability that the CCDF is within the EPA Limit is 1.00.

larger than those that might result from other human-intrusion scenarios that could occur. The purpose of these one-scenario analyses is to bound the problem and rank the influence of parameters and radionuclides on that bound. Simple correlation of parameter values with results indicates that time-of-the-intrusion event, borehole-fill properties, solubility, and room properties are important. From these seven cases, two sets of parameter pdfs are selected for the demonstration, one reflecting the current repository design and data for the reference conceptual model (Lappin et al., 1989) and the other representing effects of modifying the waste and disposal room.

Scenario E2

This scenario consists of a borehole penetrating a room or drift in the repository. Transport 5.0 km (3.0 mi) downgradient from the waste panels is predicted by the NEFTRAN code for each of 50 simulations of the disposal system's response to the scenario, using Monte Carlo input vectors selected from parameter distributions. The driving force for radionuclide transport from the repository, up the borehole, and into the Culebra Dolomite is the fluid pressure in the host rock. For this preliminary analysis, a pressure of 10.5 MPa is used (see Appendix B; also Lappin et al., 1989). This value is approximately halfway between lithostatic pressure and hydrostatic pressure at the repository depth. The true pressure variation is not estimated in this demonstration (see Appendix A).

Scenario E1E2

This scenario consists of two boreholes intersecting a room or drift in the same panel in the repository. Whereas one of the boreholes continues through the repository to intersect pressurized brine in the Castile Formation, the other borehole does not. Because of the modeled configuration of the seals, brine flows upward from the brine pocket, through a room or drift, and up the other borehole to the Culebra Dolomite Member. Both boreholes must be in the same panel in order to assure a hydraulic connection between the holes. The driving force for flow through the panel is the pressure difference between the brine encountered in the Castile Formation and the Culebra Dolomite Member at the release point. For calculational convenience, the two intrusion boreholes are assumed to be drilled at the same time.

Scenario E1E3

This scenario is the same as Scenario E1, except that a withdrawal well located 2.5 km (1.5 mi) downgradient from the repository diverts flow from the Culebra Dolomite Member to the surface.

Scenario E2E3

This scenario is the same as Scenario E2, except that a withdrawal well located 2.5 km (1.5 mi) downgradient from the repository diverts flow from the Culebra to the surface.

Scenario E1E2E3

This scenario consists of all three of the events included in the other scenarios. Two boreholes penetrate the rooms or drifts in a panel of the repository, and one hole extends into pressurized brine in the Castile Formation. A withdrawal well 2.5 km (1.5 mi) downgradient from the repository diverts flow from the Culebra to the surface.

PRELIMINARY CCDF

The sensitivity analysis of Scenario E1 shows that changes in the pdfs for room parameters will affect the CCDF; therefore, two cases, Reference Design and Modified Design, are analyzed for all seven scenarios, and a single CCDF is presented for each case. Reference Design corresponds to Case $E1_b$ data and distributions, and Modified Design corresponds to Case $E1_e$ data and distributions.

Items requiring special consideration when determining radionuclide releases 5.0 km (3.0 mi) downgradient from the waste panels are the pumping well at 2.5 km (1.5 mi), the cuttings that would be brought to the surface if a borehole penetrates a waste-filled room or drift, and the probability of occurrence of each scenario. Both the well and the cuttings release radionuclides that must be included with any releases resulting from transport in the Culebra Dolomite Member to determine integrated releases. These releases to the surface were not considered in the sensitivity analyses using Scenario E1, but are included in the following seven-scenario demonstration analyses. Furthermore, the probability of occurrence of the scenarios must be considered in constructing a CCDF. The summed normalized releases for the scenarios and their probabilities of occurrence are combined into a single CCDF to determine whether the releases exceed the release limits established by the Standard.

Appendix A to the Standard establishes the release limits for all the regulated radionuclides. Table 1 in that appendix gives the limit for cumulative releases to the accessible environment for 10,000 years after disposal for each radionuclide per unit of waste. Note 1(e) to Table 1 defines the unit of waste as an amount of TRU wastes containing 1×10^6 Ci of alpha-emitting transuranic radionuclides with half-lives greater than 20

years. Note 2(b) describes how to develop release limits for a TRU waste disposal system: the release limits are the quantities in Table 1 multiplied by the units of waste. Note 6 describes the manner in which the release limits are to be used to determine compliance with the Containment Requirements: for each radionuclide released, the ratio of the cumulative release to the total release limit for that radionuclide must be determined; the ratios for all radionuclides released are then summed for comparison to the requirements. Thus, the quantity of a radionuclide that may be safely released under the Standard depends on the quantities of all other nuclides projected to be released, but cannot exceed its own release limit. This summed normalized release cannot exceed one for release probabilities greater than 0.1 and cannot exceed 10 for release probabilities greater than 0.001. Releases that occur with probabilities less than 0.001 are not regulated (Bertram-Howery and Hunter, 1989).

For example, Table 1 in Appendix A to the Standard lists the release limits for plutonium-239 and americium-241 as 100 Ci each per waste unit; for a repository with a waste unit of one and a release that contained only those two nuclides, the sum of the two must not be greater than 100 Ci unless the probability of the release is less than 0.1 and must not be greater than 1,000 Ci unless the probability is less than 0.001. For the WIPP, the maximum possible number of waste units for the design capacity is about 15; however, all radioactivity in the waste cannot be included in the waste unit because all radioactivity is not from "alpha-emitting transuranic radionuclides with half-lives greater than 20 years." The waste unit for this demonstration is 5.08. Regardless of the waste unit, all regulated radionuclides must be included in release calculations (Bertram-Howery and Hunter, 1989).

PUMPING WELL (E3)

A pumping well is included in some of the scenarios in this analysis so that deterministic calculations previously published (U.S. DOE, 1989a; Lappin et al., 1989) can be compared with the demonstration. To estimate a withdrawal rate, the pumping well is assumed to be a livestock well. At 2.5 km (1.5 mi), this assumption is not realistic because brine in the Culebra Dolomite Member at this location is too saline for cattle consumption, but the analysis provides a conservative example of a capability that may be employed at other locations in the final compliance assessment. Water losses at the livestock well from consumption by eight cattle and by evaporation, offset by gains from precipitation, result in a net daily loss of 0.46 m^3 (~16.24 ft^3) (Lappin et al., 1989). This is more than is in the stream tube in the Culebra leg of the computer model. To account for this well, the entire flow within the Culebra stream tube is conservatively assumed to be diverted up the well for one year (Lappin et al., 1989). The simulation estimates radionuclide transport to 5.0 km (3.0 mi) and integrated discharge over 10,000 years. A second simulation

estimates radionuclide transport to the well at 2.5 km (1.5 mi) for the same time. The year's releases from the well at 2.5 km (1.5 mi) are added to the releases at 5.0 km (3.0 mi).

BOREHOLE CUTTINGS

When a borehole is drilled into a room or a drift filled with waste, the bit grinds up any material that it encounters. This material mixes with the drilling mud and is transported to the mud pits at the surface. As the drill goes deeper, the drilling mud that circulates from the bit to the surface mixes with any porous waste along the borehole, transporting radionuclides in the waste to the surface. An analysis of the amount of waste material that could be transported to the surface by these mechanisms indicated less than the contents of three drums could reach the surface in the drilling mud (Lappin et al., 1989). To determine integrated release for each human-intrusion scenario, the average radionuclide inventory in three drums is added to the other releases at 5.0 km (3.0 mi) for each borehole that penetrates a room or drift.

SCENARIO PROBABILITIES

The probability of occurrence of each scenario must be determined to construct a CCDF. Assuming that the events and processes used in the logic diagram to construct scenarios define all possible future states of the repository and natural systems, the scenario probability can be determined by combining the probability of occurrence of the events and processes in the scenario with the probability of non-occurrence of the events and processes that are not included in the scenario. The sum of the scenario probabilities in the logic diagram is one. The scenario probabilities determined for this report are preliminary and somewhat arbitrary. For this reason, these probabilities are for demonstration purposes only and should not be used for compliance assessment.

The likelihood that an exploratory borehole for oil or gas will intersect a waste-filled room or drift must be determined for Events E1 and E2. A uniform distribution for the time-of-the-intrusion event is chosen in the absence of guidance from the Standard. An exponential distribution may be more appropriate for single-intrusion-event scenarios, because its hazard function is equal to a constant (i.e., the probability of intrusion during a specified time interval is the same whether the repository has been closed for one year or 500 years). Using a uniform distribution over a 10,000-yr interval for intrusion time is inconsistent with probability estimates based on drilling frequencies over a subinterval. Such questions will be resolved in a way that is also consistent with regulatory guidance for institutional control and passive markers. This report is intended to demonstrate the performance-

assessment methodology and not to resolve these questions. In addition, the possibility of multiple boreholes of a particular type (e.g., Scenarios E1, E2, or E3) will be considered once the probability of drilling each type of borehole is formally determined. The approach to determining these probabilities will affect the number of boreholes into and downgradient from the repository.

The Standard suggests that passive markers can deter systematic and persistent exploitation of the site and reduce the likelihood of human intrusion. Based on this guidance, exploratory drilling will be considered but developmental drilling will not. The degree to which the markers can decrease the probability of drilling has not been determined and cannot be factored into the probability estimates at this time. Locating potentially important minerals above the repository will not require drilling through the repository level. For these reasons, mineral exploration is not a consideration in the preliminary probability estimates. Reserves of oil and gas at the WIPP site remain a statistical possibility (Brausch et al., 1982).

The techniques for estimating probability of drilling include (1) drilling rate versus the duration of this rate, (2) borehole spacing as defined by state regulations, and (3) expert judgment based on geologic setting and economic considerations. A technique based on drilling rate versus duration of the rate provides a preliminary estimate of probability for use in this demonstration report. Final drilling rates and other parameter values and distributions associated with future drilling and intrusion by future societies will be selected by expert judgment.

For this demonstration, a drilling rate of 3.0×10^{-3} holes/yr/km^2 is used (U.S. EPA, 1985, see Appendix B; Cranwell et al., 1982a, see Appendix C). Exploratory drilling is assumed to extend at least 500 years beyond the loss of administrative control of the WIPP site and only one intrusion event of each type is considered.

Based on the drilling rate, duration, and waste-panel area [0.5 km^2 (0.2 mi^2); U.S. DOE, 1988], 0.75 boreholes can be drilled into the repository. Because waste occupies about 0.23 of the waste-panel area, the probability of the borehole hitting a room or drift is 0.17 (Event E2 in Figure 4-16). Nearly one half of the repository may be underlain by pressurized brine in the Castile Formation (The Earth Technology Corporation, 1988). For random drilling, the probability of a borehole hitting either a room or drift and pressurized Castile brine is 0.085 (Event E1 in Figure 4-16).

For the boreholes in Events E1 and E2 intersecting the same panel, the probability of one of these events must be reduced. Because the repository consists of eight panels plus two equivalent panels (10 panels total), the

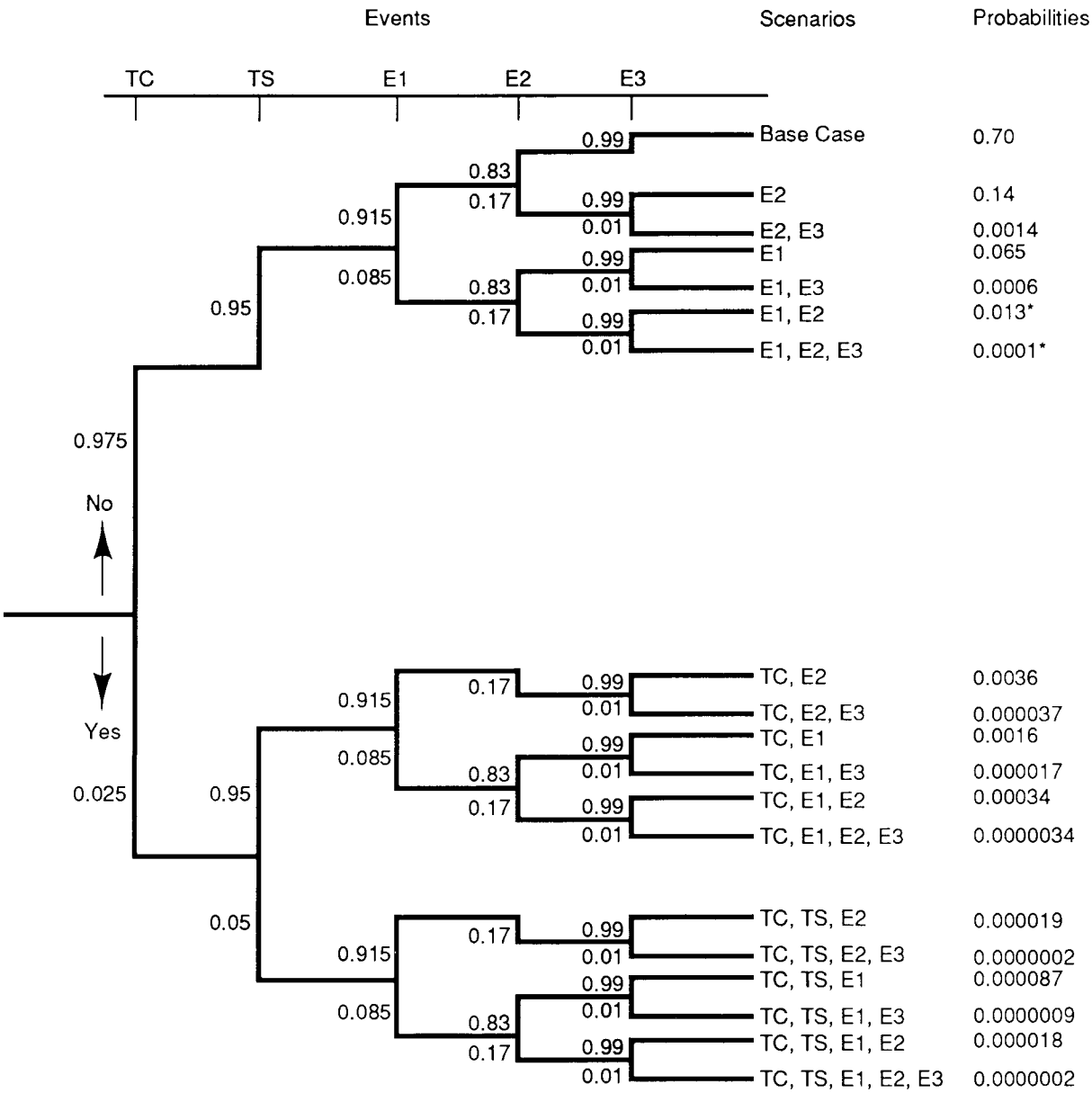

TC - Climatic Change
TS - Subsidence Resulting from Solution Mining of Potash
E1 - Drilling through Room and Brine Pocket
E2 - Drilling through or into a Room
E3 - Drilling Downgradient from Repository

* The probabilities used for the Reference Design and Modified Design cases for E1E2 and E1E2E3 were 0.0013 and 0.00001 since E1 and E2 are assumed to penetrate the same panel.

TRI-6342-22-0

Figure 4-16. Logic Diagram Showing Development of Preliminary Scenario Probabilities.

probability of a borehole hitting a particular panel is one-tenth the probability of hitting a room or drift anywhere in the repository. For this reason, Event E2 is assigned a probability of occurrence of 0.017 of hitting the same panel as Event E1 when these two events are in the same scenario.

For the pumping well (Event E3 in Figure 4-16), there is no suitable water for personal use in the Culebra Dolomite in the 5.0 km (3.0 mi) downgradient from the repository, but water suitable for livestock presently occurs just within 5.0 km (3.0 mi) (Lappin et al., 1989). This condition is not likely to change in the future. For consistency with the previous work (U.S. DOE, 1989a; Lappin et al., 1989) and future use for safety assessments, the pumping well is included in scenario development. The probability of Event E3 is assigned a value of 0.01.

Subsidence to the surface associated with potash mining (Process TS in Figure 4-16) has been observed in the Delaware Basin. The likelihood of future potash mining in the distant future is speculative. Based on the presence of known potash resources to the north-northeast of the WIPP site (Brausch et al., 1982) the likelihood of mining and associated subsidence is assigned a value of 0.05.

Climatic change is certain. Over the next 10,000 years, the WIPP site is likely to be subjected to both drier and wetter conditions. The range of these possible conditions has not been determined. Without consideration of when they might occur, the range of possible climatic conditions is assumed to have a normal distribution. If the expected range is the complete range of climatic conditions, climatic change is part of the base-case scenario by definition. For this demonstration, the range is assumed to be greater than the expected range; climatic changes greater than two standard deviations from the mean of the distribution are considered to be extreme changes. Whether this criterion satisfies the intent of the Standard for unlikely processes is not known.

Extreme climatic change is included in this demonstration. Natural variability in a parameter ordinarily would not be used to define an event or process for inclusion in scenario development. Because no justification is likely to be found for retaining extreme conditions, the process of extreme climatic change probably will be discarded as scenario development progresses. As a result, natural climatic variability over the complete range of expected climatic conditions for the time periods of interest must be a part of the uncertainty analysis for each scenario considered in constructing the CCDF. The probability of extreme climatic change over 10,000 years for this demonstration is based on the assumed normal distribution of all possible conditions. If extreme conditions constitute the part of the distribution beyond two standard deviations from the mean, these extreme conditions have a

probability of occurrence of approximately 0.050. Because half of this probability is for wetter conditions and half for drier and only wetter conditions have the potential to degrade the performance of the site; the probability of extreme wetter conditions (Process TC in Figure 4-16) is 0.025.

The calculation of scenario probabilities using the probabilities for TC, TS, E1, E2, and E3 is straightforward (Figure 4-16). The sum of the probabilities of the scenarios in a complete logic diagram is always one. Some scenarios were deleted (e.g. TS, E3, TSE3, ...,). These deleted scenarios still have non-zero probabilities so the sum of probabilities of retained scenarios is less than one.

PRELIMINARY CCDFs FOR THE DEMONSTRATION

The preliminary CCDFs (Reference Design and Modified Design) include the base case and the six human-intrusion scenarios (Figure 4-17). The base case represents undisturbed conditions for which no releases are predicted. The human-intrusion releases include contributions 5.0 km (3.0 mi) downgradient in the Culebra Dolomite Member and at the surface from drill cuttings from either one or two boreholes and from a pumping well 2.5 km (1.5 mi) downgradient from the repository as appropriate for the particular scenario. Including the cuttings results in releases for every simulation of each scenario. For those simulations with none or small radionuclide migration, the addition of the cuttings significantly increases the integrated releases. However, for those simulations with more radionuclide migration than the contents of a few drums, the addition of the cuttings does not affect the CCDF. Including the releases from the pumping well does not affect the CCDF, because of the relatively small contribution from this source to the integrated release. Incorporating probability estimates for scenarios in the CCDF shifts the curve noticeably downward from the CCDFs in Cases $E1_b$ and $E1_e$. This emphasizes the importance of the probability estimates in determining compliance with the Standard.

As suggested by the single-scenario sensitivity analyses for E1, the Modified Design CCDF is shifted downward away from EPA limits compared to the Reference Design CCDF because distributions for room parameters are changed. The Reference Design analysis uses reference data (Appendix B and Lappin et al., 1989) while the Modified Design analysis uses distributions on room parameters that represent possible engineered modifications plus decreased uncertainty in estimated solubility values. For the seven scenarios analyzed, Scenarios E1 and E2 are equally important contributors to the Reference Design CCDF, considering their estimated probabilities of occurrence differ by a factor of two. For the Modified Design, Scenario E1 is clearly the dominant scenario because the changes in room parameter distributions significantly decrease flow through the contents of the waste room. If the effects of preliminary

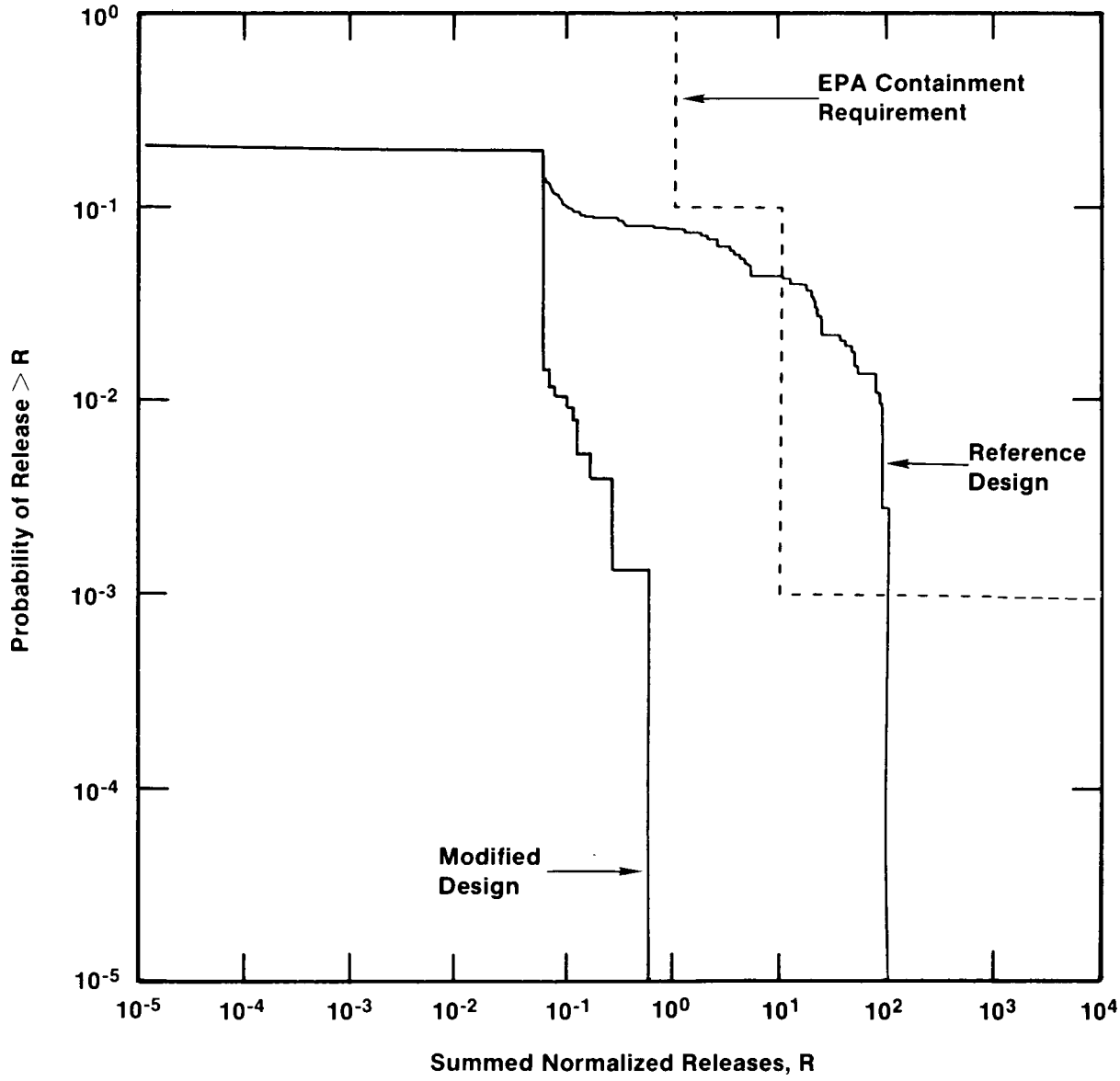

Figure 4-17. Two Demonstration CCDFs, each Constructed from 50 Simulations Per Scenario for Seven Scenarios (Base Case, E1, E2, E1E2, E1E3, E2E3, and E1E2E3 with Estimated Probabilities 0.70, 0.065, 0.14, 0.0013, 0.0006, 0.0014, and 0.00001, Respectively), Showing the Effect on the Reference Conceptual Model of Modifying the Room and the Waste. The Probabilities that the CCDFs are within the EPA Limit are 0.66 Reference Design and 1.000 Modified Design.

probability estimates are ignored, it is clear that the CCDF for the Reference Design exceeds the EPA limits and the CCDF for the Modified Design is within the limits. Gas generation is not considered in either design analysis.

A complete compliance assessment must consider levels of confidence associated with the CCDFs presented. One consideration is the variation in the CCDF resulting from different replications of the LHS samples. This variation has been shown to be very small (Iman, 1981; 1982) A more difficult consideration is assigning levels of confidence to the distributions and models used in the calculations. This requires subjective, expert judgment by both project investigators and external review panels. These judgments are beyond the scope of this demonstration and are not included.

A complete compliance assessment must also consider competing conceptual models and unquantifiable uncertainties in mathematical models. In this demonstration and in earlier analyses (Lappin et al., 1989), conservatism is substituted for uncertainty in the groundwater flow and radionuclide transport conceptual model. The range of uncertainty in predicted groundwater travel times, which may be greater than two orders of magnitude, will be incorporated in future analyses of radionuclide transport to the proposed land withdrawal boundary and the maximum-allowable controlled-area boundary for the WIPP. Unquantifiable uncertainties in mathematical models will be assessed using subjective judgment.

V. CONCLUSIONS

This demonstration produces complementary cumulative distribution functions (CCDFs) similar to those that will ultimately be used to assess the compliance of the WIPP with the Containment Requirements of the EPA Standard (§ 191.13). The CCDFs in this report are constructed for demonstration purposes only, using incomplete scenarios, data, and models. The scenarios used are representative of the final set, but they do not necessarily comprise a complete set. Final probabilities for these scenarios have not yet been determined. Estimates of scenario probabilities are used to construct CCDFs for this demonstration. Some data analyses are essentially complete while other critically important data acquisition programs have just been started. Some computer modules within the CAMCON system are partially validated, while crude models are used in place of others still under development. Therefore, the set of input parameters that could be sampled for these uncertainty analyses is much smaller than the final set of parameters that will be sampled for the final uncertainty analysis.

The demonstration analysis for undisturbed conditions indicates no releases from the repository in either the 1,000-yr period for Individual Protection Requirements (§ 191.15) or the 10,000-yr period for Containment Requirements (§ 191.13). In lieu of releases, transport through the MB139 seal and through MB139 to the bottom of the lower shaft seal are evaluated. The fact that no releases occur indicates that no dose calculations are needed for demonstrating compliance with Individual Protection Requirements. Furthermore, this long-term isolation under undisturbed conditions confirms the early project choices of repository design and location, for an essentially gas-free repository. The effect of gas on long-term performance is yet to be determined, but is not expected to change this conclusion.

Seven single-scenario uncertainty analyses that are conditional on that scenario occurring (Table 5-1) are included in a sensitivity analysis of the bounding scenario, E1. By changing initial distributions (Case $E1_b$) including minimum, maximum, and expected or median values, the influence of solubility, room conductivity, and room porosity on the CCDF is assessed. Decreasing the range of solubility (Case $E1_c$), which changes the loguniform distribution, moves the CCDF downward toward EPA limits. Representing possible waste/backfill modifications (Case $E1_d$) by changing room hydraulic conductivity and porosity, which changes their distributions, moves the CCDF farther inside the EPA limits. Changing solubility, room hydraulic conductivity, and room porosity together (Case $E1_e$) generates a CCDF that is well within the EPA limits, and is representative of possible engineered alternatives and achievable understanding of room chemistry. Therefore, Cases $E1_b$ and $E1_e$ are bounding scenario cases for two conceptual models of interest:

TABLE 5-1. REFERENCE PARAMETERS VARIED FOR SENSITIVITY AND UNCERTAINTY ANALYSES FOR SCENARIO E1

		Parameters Changed from Reference Parameters (Lappin et al., 1989)			
Case	Release Point	Solubility	Room Conductivity	Room Porosity	Culebra Conductivity
E1a	2.5 km				
E1b	5.0 km				
E1c	5.0 km	X			
E1d	5.0 km		X	X	
E1e	5.0 km	X	X	X	
E1f	5.0 km				X
E1g	5.0 km	X	X	X	X

(1) reference design data (Lappin et al., 1989); and (2) reference design data modified to assess possible engineering alternatives and better understanding of room chemistry.

Two additional variations on these single-scenario cases are considered. Case $E1_a$ assesses the influence on the CCDF of the path length in the Culebra Dolomite Member. For the models in this demonstration, the conservative representation of important processes that affect flow and transport mask the effects of the change from 2.5 to 5.0 km (1.5 to 3.0 mi). Better representation of these processes is expected to provide a more precise assessment of radionuclide transport along the path in the Culebra. Cases $E1_f$ and $E1_g$ assess the influence of increased realism in the computational module for Culebra hydrology and transport. Using SWIFT II instead of NEFTRAN and sampling fracture-flow hydraulic conductivity on 15 two-dimensional zones instead of along three one-dimensional legs moves the CCDF for Case $E1_f$ downward closer to the EPA limits than the CCDF for Case $E1_b$. The same approach moves the CCDF for Case $E1_g$ downward so that the CCDF is even more within the EPA limits than the CCDF for Case $E1_e$. This downward change indicates the conservatism inherent in the NEFTRAN simulations. As other conservative assumptions are relaxed toward increased realism (Appendix A) throughout the modeling system, the trend should continue for the CCDF to move well within the limits in the Standard.

Two cases, Reference Design and Modified Design, are evaluated for the methodology demonstration. These seven-scenario preliminary analyses, (Table 5-2) extend the conditional single-scenario Cases, $E1_b$ and $E1_e$. The Reference Design analyses correspond to Case $E1_b$ data and the Modified Design analysis corresponds to Case $E1_e$ data. Releases to the surface in the form of cuttings

TABLE 5-2. REFERENCE PARAMETERS VARIED FOR THE DEMONSTRATION ASSESSMENT WITH E1, E2, E1E2, E1E3, E2E3, E1E2E3, AND BASE CASE SCENARIOS

	Parameters Changed from Reference Parameters (Lappin et al., 1989)			
Demonstration Cases	Release Point	Solubility	Room Conductivity	Room Porosity
Reference Design	5.0 km + Surface			
Modified Design	5.0 km + Surface	X	X	X

and eroded particles from the drilling process and pumping at a withdrawal well were included in both analyses. Preliminary probabilities for the seven scenarios were estimated so that a single CCDF could be constructed for each case. Including scenario probabilities shifts the CCDF downward compared to conditional single-scenario CCDFs. Because Scenario E1 is the bounding scenario, CCDFs for the design analyses are similar to the conditional single-scenario CCDFs in that the Reference Design exceeds EPA limits while the Modified Design does not. These results are not influenced by the arbitrary estimates of scenario probabilities. The shifts away from EPA limits reflect decreased releases resulting from changes in the parameter distributions for solubility, room conductivity, and room porosity. Scenario E1 is the important scenario for the Modified Design while Scenarios E1 and E2 are both important for the Reference Design. Plutonium, americium, uranium, and thorium are important contributors to the CCDFs with plutonium-239 dominating the Reference Design while plutonium-238 dominates the Modified Design.

Solubility, room conductivity, and porosity are the most important parameters considered here that can be addressed by engineered alternatives and experimental programs. Time-of-the-intrusion event and borehole-fill conductivity and porosity are also important parameters. The effects of gas generation cannot be evaluated yet and are not included in these analyses. The analysis of undisturbed conditions demonstrates long-term isolation of the waste, but analysis of human-intrusion scenarios results in a non-zero probability of exceeding EPA limits for the Reference Design. Clearly, the problem of demonstrating compliance with EPA regulations must focus on human-intrusion events. Moreover, under the Standard promulgated by the EPA in 1985, engineered modifications and better understanding of room chemistry may ensure that EPA limits are not exceeded.

The CCDFs calculated in this report are for demonstration purposes only. They may be considered as a "first" look at compliance but should not be considered credible enough to judge the probability of compliance of the WIPP with the Standard. The preliminary, Reference Design CCDF is based primarily on the reference conceptual models and data (Lappin et al., 1989) and exceeds the limits in the Standard. However, results of varying just two room parameters (hydraulic conductivity and porosity) clearly indicate that the CCDF will not exceed EPA limits if engineered alternatives can achieve these modified parameter distributions.

REFERENCES

Bear, J., 1972, *Dynamics of Fluids in Porous Media,* Dover, New York, NY.

Beauheim, R.L., 1987a, *Interpretation of the WIPP-13 Multipad Pumping Test of the Culebra Dolomite at the Waste Isolation Pilot Plant (WIPP) Site,* SAND87-2456. Sandia National Laboratories, Albuquerque, NM.

Beauheim, R.L., 1987b. *Analysis of Pumping Tests of the Culebra Dolomite Conducted At the H-3 Hydropad at the Waste Isolation Pilot Plant (WIPP) Site,* SAND86-2311. Sandia National Laboratories, Albuquerque, NM.

Beauheim, R.L., 1987c. *Interpretations of Single-Well Hydraulic Tests Conducted At and Near the Waste Isolation Pilot Plant (WIPP) Site, 1983-1987,* SAND87-0039. Sandia National Laboratories, Albuquerque, NM.

Beauheim, R.L., 1988. *Scale Effects in Well Testing in Fractured Media,* SAND87-1955C. For presentation at the Fourth Canadian/American Conference on Hydrogeology: Fluid Flow, Heat Transfer, and Mass Transport in Fractured Rocks, Banff, Alberta, Canada.

Bertram-Howery, S.G., M.G. Marietta, D.R. Anderson, K.F. Brinster, L.H. Brush, L.S. Gomez, R.V. Guzowski, and R.P. Rechard, 1989. *Draft Forecast of the Final Report for the Comparison to 40 CFR Part 191, Subpart B for the Waste Isolation Pilot Plant,* SAND88-1452. Sandia National Laboratories, Albuquerque, NM.

Bertram-Howery, S.G., and R.L. Hunter, Eds., 1989. *Preliminary Plan for Disposal-System Characterization and Long-Term Performance Evaluation of the Waste Isolation Pilot Plant,* SAND89-0178. Sandia National Laboratories, Albuquerque, NM.

Bonano, E.J., P.A. Davis, L.R. Shipers, K.F. Brinster, W.E. Beyeler, C.D. Updegraff, E.R. Shepherd, L.M. Tilton, and K.K. Wahi, 1989. *Demonstration of a Performance Assessment Methodology for High-Level Radioactive Waste Disposal in Basalt Formations,* SAND86-2325 (NUREG/CR-4759). Sandia National Laboratories, Albuquerque, NM.

Borns, D.J., and J.C. Stormont, 1988. *An Interim Report on Excavation Effect Studies at the Waste Isolation Pilot Plant: The Delineation of the Disturbed Rock Zone,* SAND87-1375. Sandia National Laboratories, Albuquerque, NM.

Brausch, L.M., A.K. Kuhn, and J.K. Register, 1982. *Natural Resources Study. Waste Isolation Pilot Plant (WIPP) Project. Southeastern New Mexico,* WTSD-TME-3156. U.S. Department of Energy, Albuquerque, NM.

Brinster, K.F., 1989 (in preparation). *Preliminary Geohydrologic Conceptual Model of the Los Medaños Region near the Waste Isolation Pilot Plant (WIPP) for the Purpose of Performance Assessment,* SAND89-7147. Sandia National Laboratories, Albuquerque, NM.

Brush, L.H., and D.R. Anderson, 1988. "Appendix A.2--Effects of Microbial Activity on Repository Chemistry, Radionuclide Speciation, and Solubilities in WIPP Brines," in Lappin, A.R., R.L. Hunter, D.P. Garber, and P.B. Davies, eds., 1989. *Systems Analysis, Long-Term Radionuclide Transport, and Dose Assessments, Waste Isolation Pilot Plant (WIPP), Southeastern New Mexico; March 1989,* SAND89-0462. Sandia National Laboratories, Albuquerque, NM.

Campbell, J.E., D.E. Longsine, and R.M. Cranwell, 1981. *Risk Methodology for Geologic Disposal of Radioactive Waste: The NWFT/DVM Computer Code User's Manual,* SAND81-0886, NUREG/CR-2081. Sandia National Laboratories, Albuquerque, NM.

Campbell, J.E., and R.M. Cranwell, 1988. "Performance Assessment of Radioactive Waste Repositories," *SCIENCE,* Volume 239, p. 1389-1392.

Cooper, J.B., and V.M. Glanzman, 1971. "Geohydrology of Project GNOME Site, Eddy County, New Mexico," in *Hydrology of Nuclear Test Sites,* USGS Prof. Paper 712-A.

Cranwell, R.M., and E.J. Bonano, 1987. "Sources/Treatment of Uncertainties in the Performance Assessment of Geologic Radioactive Waste Repositories," *Proceedings of a Nuclear Energy Agency Workshop on Uncertainty Analysis of Performance Assessments of Radioactive Waste Disposal Systems, Seattle, WA,* Nuclear Energy Agency of the Organization for Economic and Cooperative Development (NEA), Paris.

Cranwell, R.M., and J.C. Helton, 1981. "Uncertainty Analysis for Geologic Disposal of Radioactive Waste," in D. C. Kocher, ed., *Proceedings of the Symposium on Uncertainties Associated with the Regulation of the Geologic Disposal of High-Level Radioactive Waste,* Gatlinburg, TN, March 9-13, 1981.

Cranwell, R.M., and J.C. Helton, 1980. "Uncertainty Analysis Associated with Radioactive Waste Disposal," *Proc. of 1980 DOE Statistical Symposium, October 29-31, 1980, Berkeley,* CA, pp 189-196. DOE CONF-80-1045.

Cranwell, R.M., R.V. Guzowski, J.E. Campbell, and N.E. Ortiz, 1982a. *Risk Methodology for Geologic Disposal of Radioactive Waste: Scenario Selection Procedure,* SAND80-1429, NUREG/CR-1667. Sandia National Laboratories, Albuquerque, NM. (Draft copy available from U.S. Nuclear Regulatory Commission Public Document Room; revised draft dated 1989 available through same source).

Cranwell, R.M., J.E. Campbell, J.C. Helton, R.L. Iman, D.E. Longsine, N.R. Ortiz, G.E. Runkle, and M.J. Shortencarier, 1982b. *Risk Methodology for Geologic Disposal of Radioactive Waste: Final Report,* NUREG/CR-2452, SAND81-2573. Sandia National Laboratories, Albuquerque, NM. (Draft report available through the U.S. Nuclear Regulatory Commission reading room, Washington, D.C.; revised report printed 1987).

Davies, P.B., 1989. *Variable-Density Ground-water Flow and Paleohydrology in the Region Surrounding the Waste Isolation Pilot Plant (WIPP), Southeastern New Mexico.* U.S. Geological Survey, Open-File Report 88-490.

Freeze, R.A., and J.A. Cherry, 1979. *Groundwater*, Englewood, NJ: Prentice-Hall, Inc., pp. 604.

Gilkey, A., 1988. *ALGEBRA: A Program that Algebraically Manipulates the Output of a Finite Element Analysis (Exodus Version)*, SAND88-1431. Sandia National Laboratories, Albuquerque, NM.

Gilkey, A., and J. H. Glick, III, 1989. *BLOT: A Mesh and Curve Plot Program for the Output of a Finite Element Analysis*, SAND88-1432. Sandia National Laboratories, Albuquerque, NM.

Harr, M.E., 1987. *Reliability-Based Design in Civil Engineering*, McGraw Hill, New York, NY.

Haug, A., V.A. Kelly, A.M. LaVenue, and J.F. Pickens, 1987. *Modeling of Groundwater Flow in the Culebra Dolomite at the Waste Isolation Pilot Plant (WIPP) Site: Interim Report*, SAND86-7167. Sandia National Laboratories, Albuquerque, NM.

Hunter, R.L., R.M. Cranwell, and M.S.Y. Chu, 1986. *Assessing Compliance with the EPA High-Level Waste Standard: An Overview*, NUREG/CR-4510, SAND86-0121. Sandia National Laboratories, Albuquerque, NM.

Hunter, R.L., 1989 (in preparation). *Events and Processes for Constructing Scenarios for Analysis of the Release of Transuranic Waste From Waste Isolation Pilot Plant, Southeastern New Mexico*, SAND89-2546, Sandia National Laboratories, Albuquerque, NM.

Iman, R.L., 1981. "Statistical Methods for Including Uncertainties Associated with the Geologic Isolation of Radioactive Waste Which Allow for a Comparison With Licensing Criteria." *Proceedings of the Symposium on Uncertainties Associated with the Regulation of the Geologic Disposal of High Level Radioactive Waste, Gatlinburg, TN, March 9-13, 1981.*

Iman, R.L., 1982. "Statistical Methods for Uncertainty Analysis and Sensitivity Analysis Associated with Computer Models." *Proceedings of Waste Management '82, Tucson, AZ, March 1982.*

Iman, R.L., J.M. Davenport, and D.K. Zeigler, 1980a. *Latin Hypercube Sampling (Program User's Guide)*, SAND79-1473. Sandia National Laboratories, Albuquerque, NM.

Iman, R.L., J.M. Davenport, E.L. Frost, and M.J. Shortencarier, 1980b. *Stepwise Regression with PRESS and Rank Regression (Program User's Guide)*, SAND79-1472. Sandia National Laboratories, Albuquerque, NM.

Iman, R.L., and J.C. Helton, 1985. *A Comparison of Uncertainty and Sensitivity Analysis Techniques for Computer Models*, SAND84-1461, NUREG/CR-3904. Sandia National Laboratories, Albuquerque, NM.

Iman, R.L., and M.J. Shortencarier, 1984. *A FORTRAN 77 Program and User's Guide for the Generation of Latin Hypercube and Random Samples for Use with Computer Models*, NUREG/CR-3624, SAND83-2365. Sandia National Laboratories, Albuquerque, NM.

Iman, R.L., M.J. Shortencarier, and J.D. Johnson, 1985. *A FORTRAN 77 Program and User's Manual for the Calculation of Partial Correlation and Standardized Regression Coefficients,* SAND85-0044, NUREG/CR. Sandia National Laboratories, Albuquerque, NM.

INTERA, 1986. *WIPP Hydrology Program, Waste Isolation Pilot Plant, SENM, Hydrologic Report No. 3,* SAND 86-7109. Sandia National Laboratories, Albuquerque, NM.

Kaplan and Yarrington, 1989. "Modeling the Uncertainties in the Parameter Values of a Layered, Variably Saturated Column of Volcanic Tuff Using the Beta Probability Distribution, in Solving Ground Water Problems with Models." *Proceedings of the Fourth International Conference on the Use of Models to Analyze and Find Working Solutions to Ground Water Problems, Feburary 7-9, 1989, Indianapolis, IN,* p. 111-128.

Kipp, 1987. HST3D: *Three Dimensional Hydrologic Solute Transport Code.* U.S. Geologic Survey, Denver, CO.

Kuchling, H., 1982. *Taschenbuch der Physik.* Verlag Harri Deutsch, Thun and Frankfurt, 678 p.

Lambert, S.J., 1983. *Dissolution of Evaporites in and around the Delaware Basin, Southeastern New Mexico and West Texas,* SAND82-0461. Sandia National Laboratories, Albuquerque, NM.

Langguth, H-R., and R. Voight, 1980. *Hydrogeologische Methoden,* Verlag, New York, 486 p.

Lappin, A.R., 1988. *Summary of Site-Characterization Studies Conducted from 1983 through 1987 at the Waste Isolation Pilot Plant (WIPP) Site, Southeastern New Mexico,* SAND88-0157. Sandia National Laboratories, Albuquerque, NM.

Lappin, A.R., R.L. Hunter, D.P. Garber, and P.B. Davies, eds., 1989. *Systems Analysis, Long-Term Radionuclide Transport, and Dose Assessments, Waste Isolation Pilot Plant (WIPP), Southeastern New Mexico; March 1989,* SAND89-0462. Sandia National Laboratories, Albuquerque, NM.

LaVenue, A.M., A. Haug, and V.A. Kelley, 1988. *Numerical Simulation of Groundwater Flow in the Culebra Dolomite at the Waste Isolation Pilot Plant (WIPP) Site; Second Interim Report,* SAND88-7002. Sandia National Laboratories, Albuquerque, NM.

Lerman, A., 1979. *Geochemical Processes,* John Wiley and Sons, Inc., New York, NY, 481 p.

Longsine, D.E., E.J. Bonano, and C.P. Harlan, 1987. *User's Manual for the NEFTRAN Computer Code,* SAND86-2405, NUREG/CR-4766. Sandia National Laboratories, Albuquerque, NM.

Marietta, M.G., and D.R. Anderson, in preparation. *Review of Parameter Sensitivity Studies for the WIPP Project through September, 1989,* SAND89-2028. Sandia National Laboratories, Albuquerque, NM.

Mercer, J.W., 1983. *Geohydrology of the Proposed Waste Isolation Pilot Plant Site, Los Medanos Area, Southeastern New Mexico.* U.S. Geological Survey, Water Resources Investigation 83-4016.

Mercer, J.W., and B.R. Orr, 1977. *Review and Analysis of Hydrogeologic Conditions Near the Site of a Potential Nuclear-Waste Repository, Eddy and Lea Counties, New Mexico,* U.S. Geological Survey, Open-File Report 77-123.

Mercer, J.W., and B.R. Orr, 1979. *Interim Data Report on the Geohydrology of the Proposed Waste Isolation Pilot Plant Site, Southeastern New Mexico.* U.S.G.S. Water-Resources Investigations 79-98, U.S. Geological Survey, Albuquerque, NM.

NEA, 1988. *Feasibility of Disposal of High-Level Radioactive Wastes into the Seabed, Volumes 1 - 8,* Nuclear Energy Agency of the Organization for Economic and Cooperative Development, Paris.

Pepping, R.E., M.S.Y. Chu, and M.D. Siegel, 1983. "A simplified analysis of a hypothetical repitory in a basalt formation, Volume 2," in *Technical Assistance for Regulatory Development: Review and Evaluation of the Draft EPA Standard 40 CFR 191 for Disposal of High-Level Waste,* SAND82-1557, NUREG/CR-3235, Sandia National Laboratories, Albuquerque, NM.

Rechard, R.P., 1989. *Review and Discussion of Code Linkage and Data Flow in Nuclear Waste Compliance Assessments,* SAND87-2833. Sandia National Laboratories, Albuquerque, NM.

Rechard, R.P., H.J. Iuzzolino, J.S. Rath, R.D. McCurley, and D.K. Rudeen, 1989. *User's Manual for CAMCON: Compliance Assessment Methodology Controller,* SAND88-1496. Sandia National Laboratories, Albuquerque, NM.

Rechard R.P., M.G. Marietta, R.D. McCurley, D.K. Rudeen, J. Bean, J. Schreiber, and W. Beyeler, 1990 (in preparation). *Parameter Sensitivity Studies of Selected Components of the WIPP Repository System,* SAND89-2030. Sandia National Laboratories, Albuquerque, NM.

Reeves, M., D.S. Ward, N.D. Johns, and R.M. Cranwell, 1986a. *Data Input Guide for SWIFT II, the Sandia Waste-Isolation Flow and Transport Model for Fractured Media, Release 4.84,* SAND83-0242, NUREG/CR-3162. Sandia National Laboratories, Albuquerque, NM.

Reeves, M., D.S. Ward, N.D. Johns and R.M. Cranwell, 1986b. *Theory and Implementation for SWIFT II, the Sandia Waste-Isolation Flow and Transport Model for Fractured Media, Release 4.84,* SAND83-1159, NUREG/CR-3328. Sandia National Laboratories, Albuquerque, NM.

Stormont, J.C., E.W. Peterson, and P.L. Lagus, 1987. *Summary of and Observations about WIPP Facility Horizon Flow Measurements through 1986,* SAND87-0176. Sandia National Laboratories, Albuquerque, NM.

The Earth Technology Corporation, 1988. *Final Report for Time Domain Electromagnetic (TDEM) Surveys at the WIPP Site,* SAND87-7144. Sandia National Laboratories, Albuquerque, NM.

Tyler, L.D., R.V. Matalucci, M.A. Molecke, D.E. Munson, E.J. Nowak, and J.C. Stormont, 1988. *Summary Report for the WIPP Technology Development Program for Isolation of Radioactive Waste*, SAND88-0844. Sandia National Laboratories, Albuquerque, NM.

U.S. DOE, 1988. *Geotechnical Field Data and Analysis Report,* DOE-WIPP-87-017. U.S. Department of Energy, Carlsbad, NM.

U.S. DOE, 1989a. *Draft Supplemental Environmental Impact Statement, Waste Isolation Pilot Plant,* DOE/EIS-0026-DS, Volume 1 of 2. U.S. Department of Energy, Washington, DC.

U.S. DOE, 1989b. *Waste Isolation Pilot Plant Compliance Strategy for 40 CFR Part 191,* WIPP-DOE-86-013. U.S. Department of Energy, Carlsbad, NM.

U.S. EPA, 1985. *Environmental Standards for the Management and Disposal of Spent Nuclear Fuel, High-Level and Transuranic Radioactive Waste; Final Rule,* 40 CFR Part 191, *Federal Register,* Volume 50, p. 38066-38089.

Vine, J.D., 1963. "Surface Geology of the Nash Draw Quadrangle, Eddy County, New Mexico," *USGS Bulletin* 1141-B.

Voss, C., 1984. *SUTRA: Saturated-Unsaturated Transport Code,* U.S. Geological Survey, Reston, VA.

Ward, D.S., M. Reeves, and L.E. Duda, Jr., 1984. *Verification and Field Comparison of the Sandia Waste-Isolation Flow and Transport Model* (SWIFT), SAND83-1154, NUREG/CR-3316. Sandia National Laboratories, Albuquerque, NM.

APPENDIX A:
SUPPLEMENTARY SENSITIVITY CALCULATIONS ON REPOSITORY/SHAFT SYSTEM

APPENDIX A: SUPPLEMENTARY SENSITIVITY CALCULATIONS ON REPOSITORY/SHAFT SYSTEM

Appendix A presents three sets of preliminary calculations performed on the repository/shaft system. These calculations are part of a more extensive (but still preliminary) sensitivity analysis [Rechard et al., 1990 (in preparation)].

The three sets of calculations, which focus on the repository and shafts, are an extension of earlier calculations (Lappin et al., 1989). In the earlier work, boundary conditions for models were selected to maximize releases without consideration of consistency from problem to problem. For example, to analyze undisturbed conditions, lithostatic pressure was assumed for the room and hydrostatic pressure was assumed elsewhere. For disturbed conditions, lithostatic pressure was assumed for the far field (Salado Formation) and hydrostatic pressure was assumed for the room. The same inconsistency appears in the following calculations that are meant, in part, to illuminate problems with using assumptions that always maximize release.

These three sets of calculations use SUTRA, a finite-element flow and transport code (Voss, 1984). Subsequent sections describe the three sets of calculations: (1) comparison of SUTRA and NEFTRAN (Longsine et al., 1987; Campbell et al., 1981) simulations of undisturbed conditions; (2) SUTRA simulations of permeability effects on brine flow into an intrusion borehole; and (3) estimates of the fraction of waste accessed (i.e., volume fraction of a saturated panel that is drained into an intrusion borehole in a specified time interval) using SUTRA flow simulations.

The SUTRA simulation of undisturbed conditions verifies that the MB139 pathway is more important than the drift pathway for NEFTRAN simulations. It also indicates that fluxes calculated by NEFTRAN within the repository/shaft system are reasonable when compared with two-dimensional SUTRA simulations. The second and third calculations begin to define the volume within a panel that may be drained into an intrusion borehole during different time periods of interest, given boundary conditions assumed in the earlier calculation (Lappin et al., 1989). Although the volume of an entire waste panel was previously assumed to be accessed, the following simulations show that only about one-fifth of this volume can be accessed. Simulations using more realistic boundary conditions may show that the fraction of the waste panel accessed is even less.

COMPARISON OF SUTRA AND NEFTRAN SIMULATIONS OF UNDISTURBED PERFORMANCE

A series of two-dimensional SUTRA simulations of undisturbed performance are compared with NEFTRAN results [Lappin et al., 1989, Appendix D, Case I, and Undisturbed Performance (Chapter IV, this report)]. This comparison has three objectives: (1) confirm that the pathway along MB139 and up through the shaft seals is an important migration pathway, from the room to the Culebra Dolomite Member, (2) confirm that fluid fluxes resulting from a difference between lithostatic pressure in the room and hydrostatic pressure in the Culebra Dolomite, calculated by NEFTRAN along this pathway, are reasonable compared to a two-dimensional SUTRA simulation of the same conditions, and (3) illustrate conceptual difficulties with assumptions intended to maximize releases.

NEFTRAN was used to model the repository/shaft system's response in terms of a series of discrete one-dimensional paths (Chapter III, this report and Figure A-1). SUTRA was used to calculate two-dimensional flow and solute transport in a region around the repository/shaft system. Several parameters are varied to assess each parameter's influence on flow and transport within the repository, lower shafts, and surrounding host rock. Those parameters include numerical parameters, such as size of material zones and time step, and material properties, such as porosity, permeability, and out-of-plane thickness of MB139. The effect of seals that also seal MB139 is examined. SUTRA simulations using reference data (Appendix B; also see Lappin et al., 1989) for steady-state conditions are described below for parameters that most closely match the NEFTRAN simulations. Transient calculations are described elsewhere [Rechard et al., 1990 (in preparation)]. Mass fluxes through the seal, seal-drift, seal-MB139, Salado-drift, and Salado-MB139 interfaces are reported. The last two fluxes estimate the flow around the seal.

A two-dimensional, finite-element mesh (Figure A-2) that is finer around the shaft-drift intersection (Figure A-3) and the seal-drift-MB139 interfaces (Figure A-4) is used. The mesh starts at a depth of 400 m (1,320 ft) with the drift located at a depth of 650 m (2150 ft). Horizontal distances are measured from the shaft (Figures A-2 through A-4). The shaft and MB139 are modeled with three elements of constant thickness. The thickness of the drift, room, and seal, modeled with six elements, increases geometrically away from MB139. The seal has three elements along its length and the room has 10. The mesh along the drift is variable, extending from fine near the shaft to coarse near the seal. The out-of-plane thickness (third dimension) is 5.0 m (16.0 ft) for the shaft, drift, and seal, and 1.0 m (3.3 ft) for the MB139; the remaining Salado material is 100 m (330 ft) thick.

The boundary pressures (Figure A-5) are hydrostatic and are based on a water table at 100 m (330 ft) depth. Hydrostatic conditions result in a 1 MPa

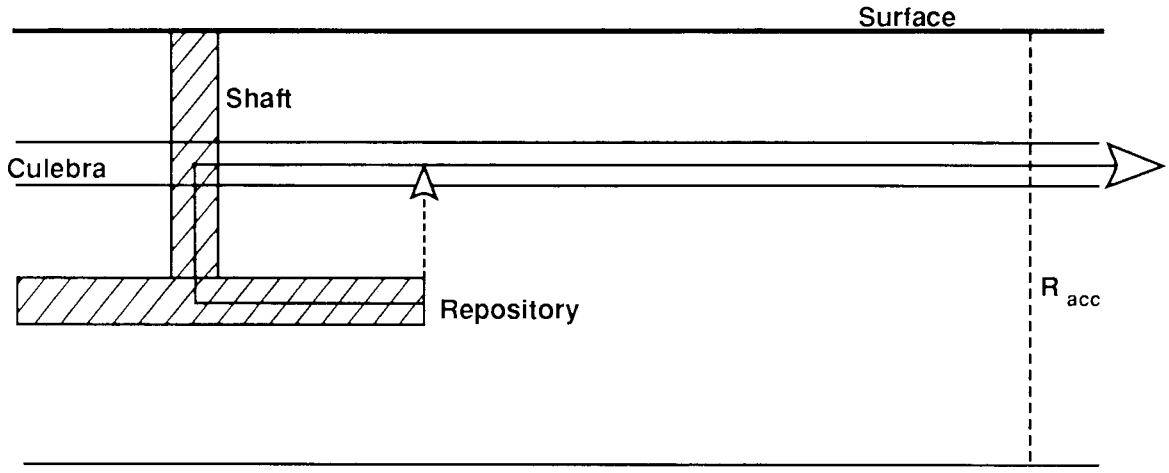

Conceptual Model

R_{acc} = Release at the Subsurface Boundary of the Accessible Environment

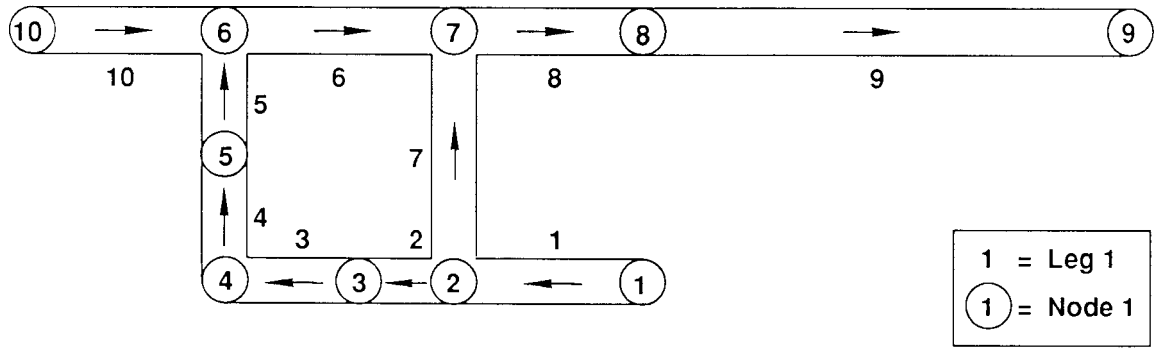

Flow Network

TRI-6342-199-0

Figure A-1. Conceptual Model and Network for the Undisturbed Disposal System (after Lappin et al., 1989).

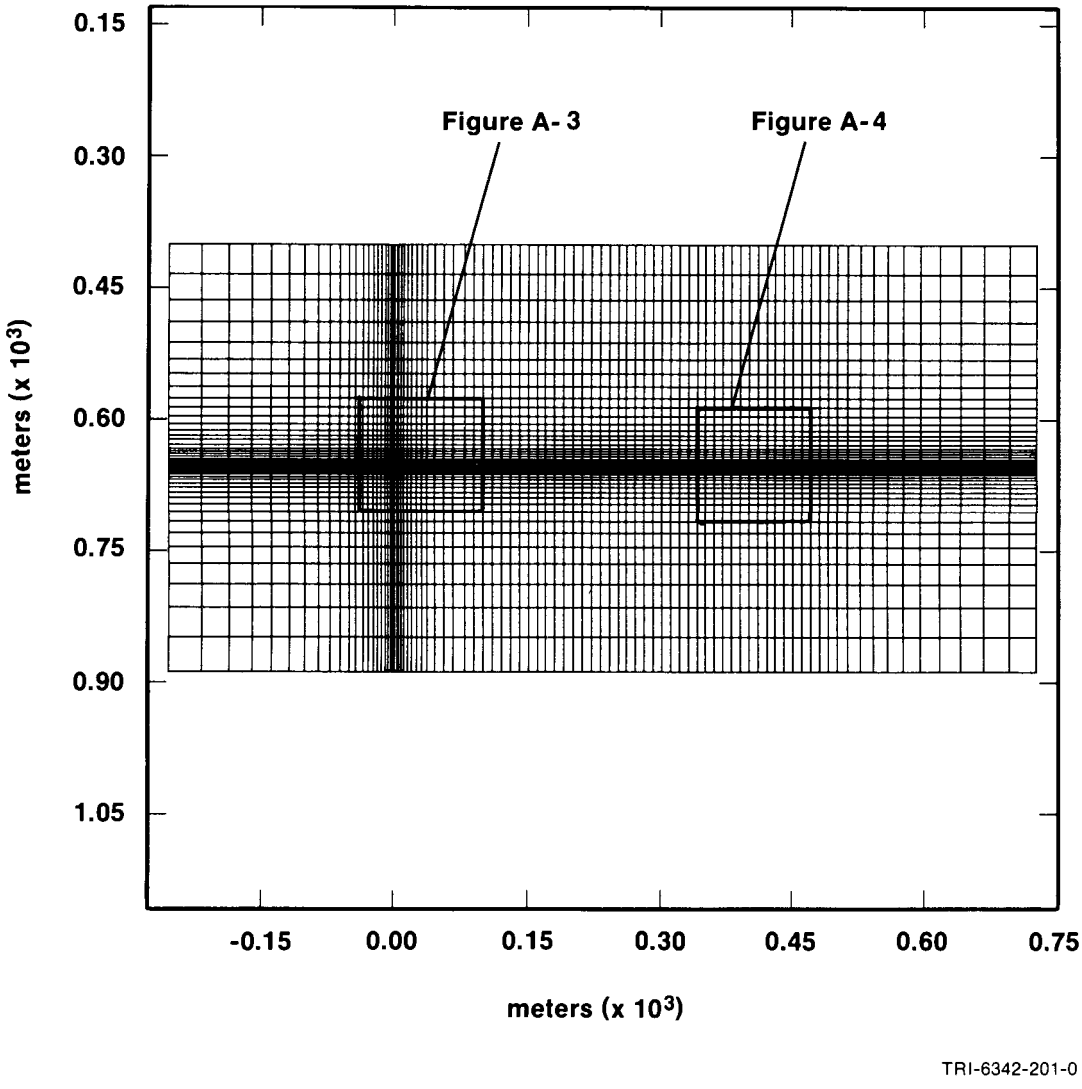

Figure A-2. Mesh of SUTRA Calculation of Undisturbed Repository/Shaft System, Showing Regions Illustrated in Figures A-3 and A-4.

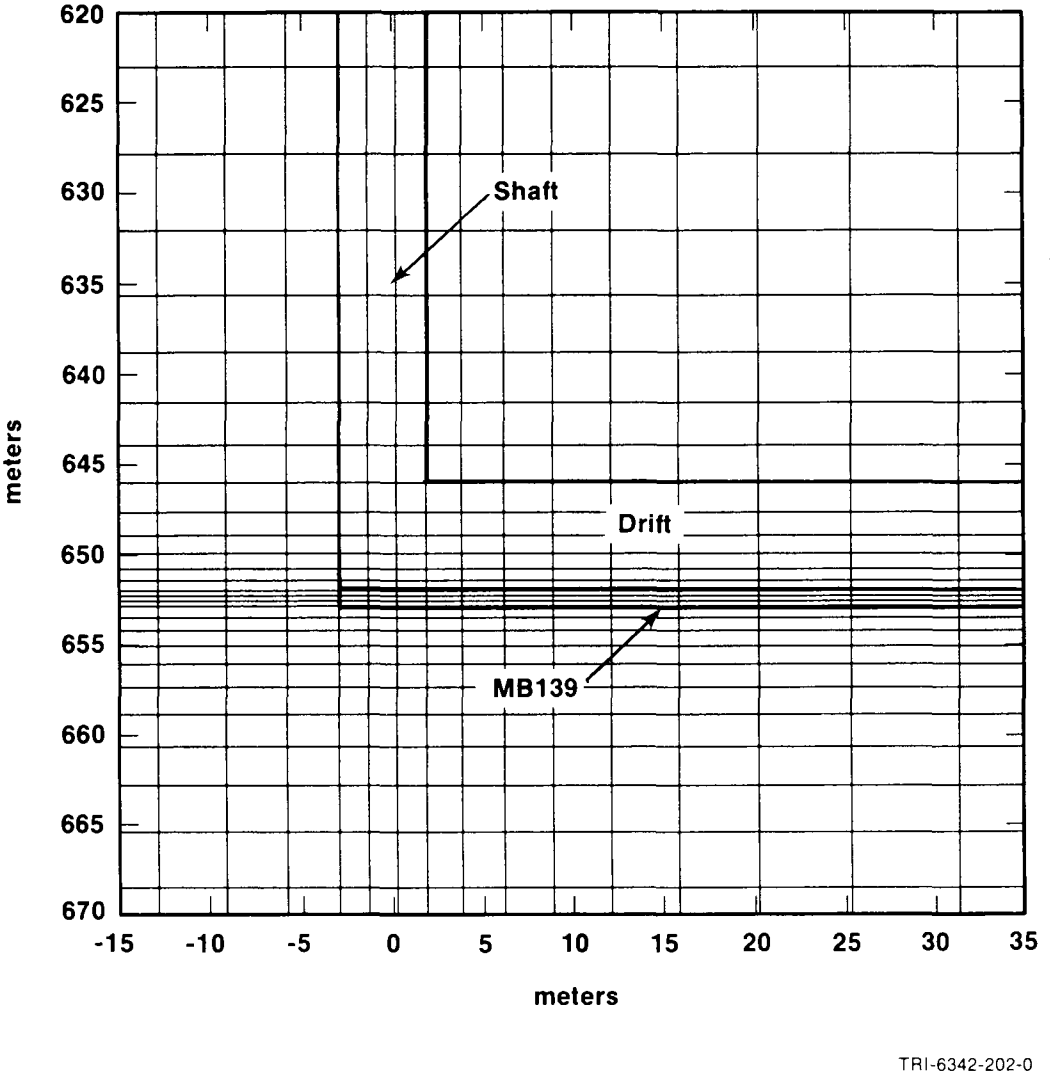

Figure A-3. Closeup of SUTRA Mesh at Shaft-Drift Intersection.

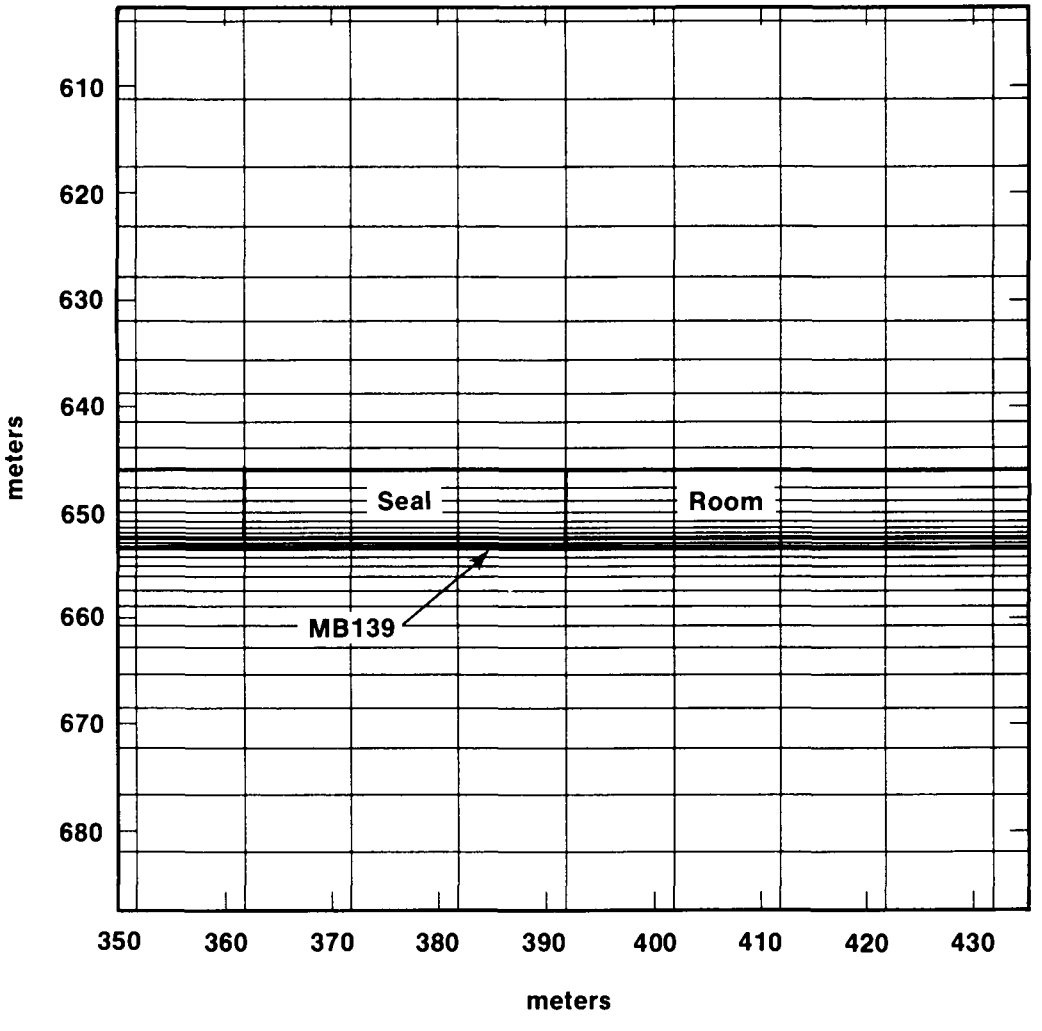

Figure A-4. Closeup of SUTRA Mesh at Panel Seal and Storage Room.

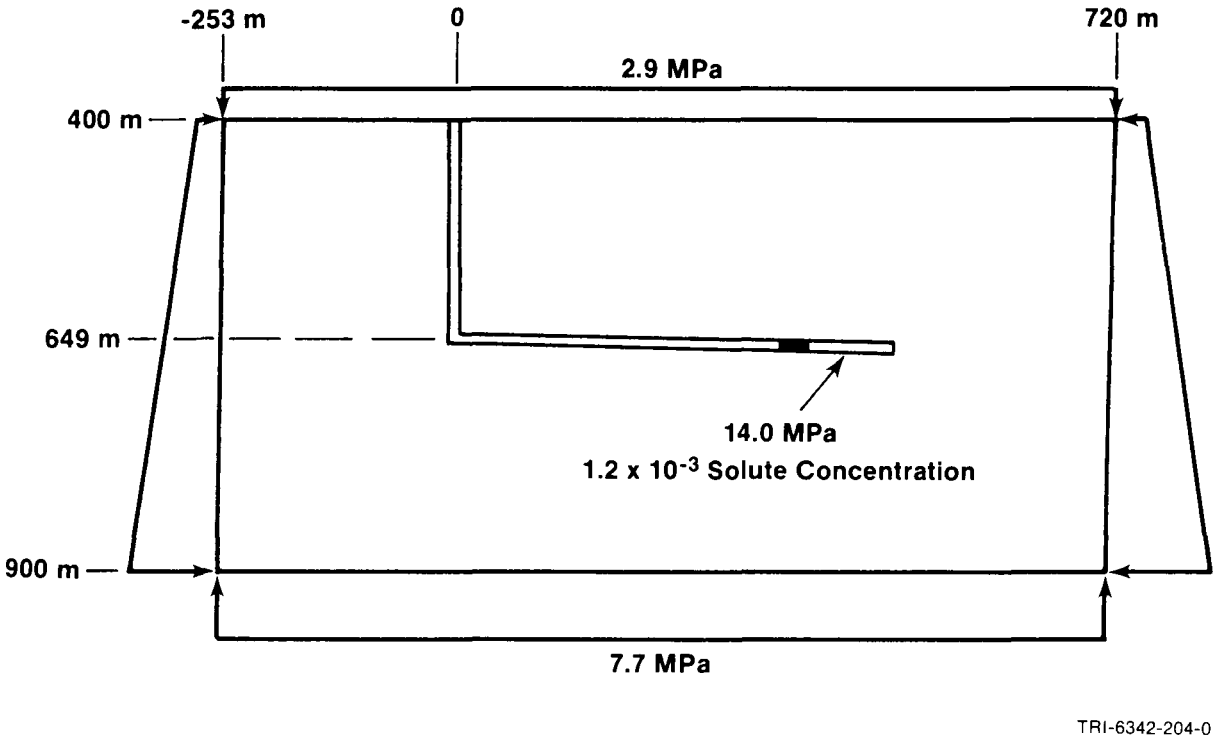

Figure A-5. SUTRA Boundary Conditions for Simulation of Undisturbed Conditions.

pressure at the Culebra Dolomite Member (not modeled) and 6.3 MPa at the repository horizon in the Salado Formation. Similarly, the boundary conditions at 400 and 800 m (1,320 and 2,640 ft) depth are 2.9 and 7.7 MPa, respectively. The fluid flow is driven by setting the pressure at four nodes in the center of the room to 14.0 MPa based on an assumption of lithostatic pressure caused by overburden weight after final consolidation (Lappin et al., 1989, Table D-2). Maintaining this pressure during the simulation implies that a fluid source exists in the room. Though not realistic, this assumption is required to simulate the same calculation performed with NEFTRAN so fluxes through the repository can be compared.

There are two categories of material properties (Table A-1): the first is represented by constant parameter values over the fluid and solid matrix and the second by parameter values that change among zones of different material. Porosities and out-of-plane thicknesses shown by material are actually stored in the calculation at nodes because of the hybrid (integrated finite-difference/finite-element) numerical technique in SUTRA. At material boundaries, porosities and thickness are the averages of the element values around the nodes.

Although the permeability of MB139 used in NEFTRAN calculations corresponds to coarse gravel (3.0×10^{-7} m^2), a value corresponding to silty sand (3.0×10^{-13} m^2) is used in SUTRA. The NEFTRAN value, 12 to 14 orders of magnitude larger than permeabilities for other materials such as rock salt, caused roundoff errors in SUTRA. The largest permeability value (3.0×10^{-13} m^2) giving accurate results for steady-state conditions was selected for the comparison. Values between 3.0×10^{-11} and 3.0×10^{-13} m^2 resulted in relatively small variations in flux along MB139 during the sensitivity analysis because this flux is controlled not only by MB139 properties but also by surrounding rock permeability which is 8 to 10 orders of magnitude smaller.

RESULTS

The steady-state results of the SUTRA simulation most closely matching the NEFTRAN simulation of Case IA are presented here (Figure A-6) along with interstitial velocities near the storage room (Figure A-7). Mass fluxes at selected locations in and around the seal were calculated for the two cases considered in the earlier analyses (Figure A-8) (Lappin et al., 1989).

The interstitial-velocity vectors (Figure A-7) show distinctly different behavior above and below the room. Above the room, flow is away from the pressure nodes in the center of the room (only the left half of the room is shown in the figure). Below the room the flow is into and along MB139, through and around the seal, and down MB139 to the shaft. Because of the large permeability difference between the seal and MB139, flow is diverted

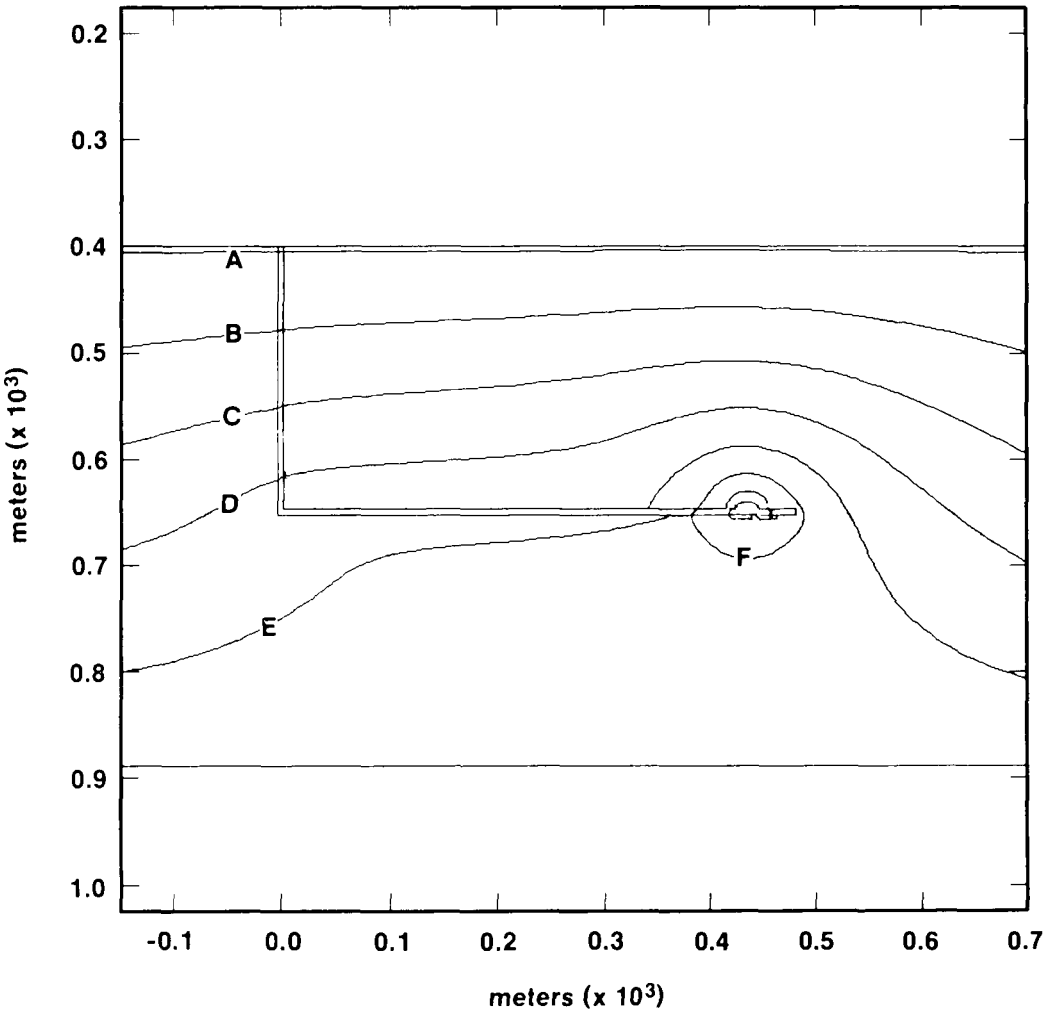

Figure A-6. SUTRA Steady-State Pressure Contours.

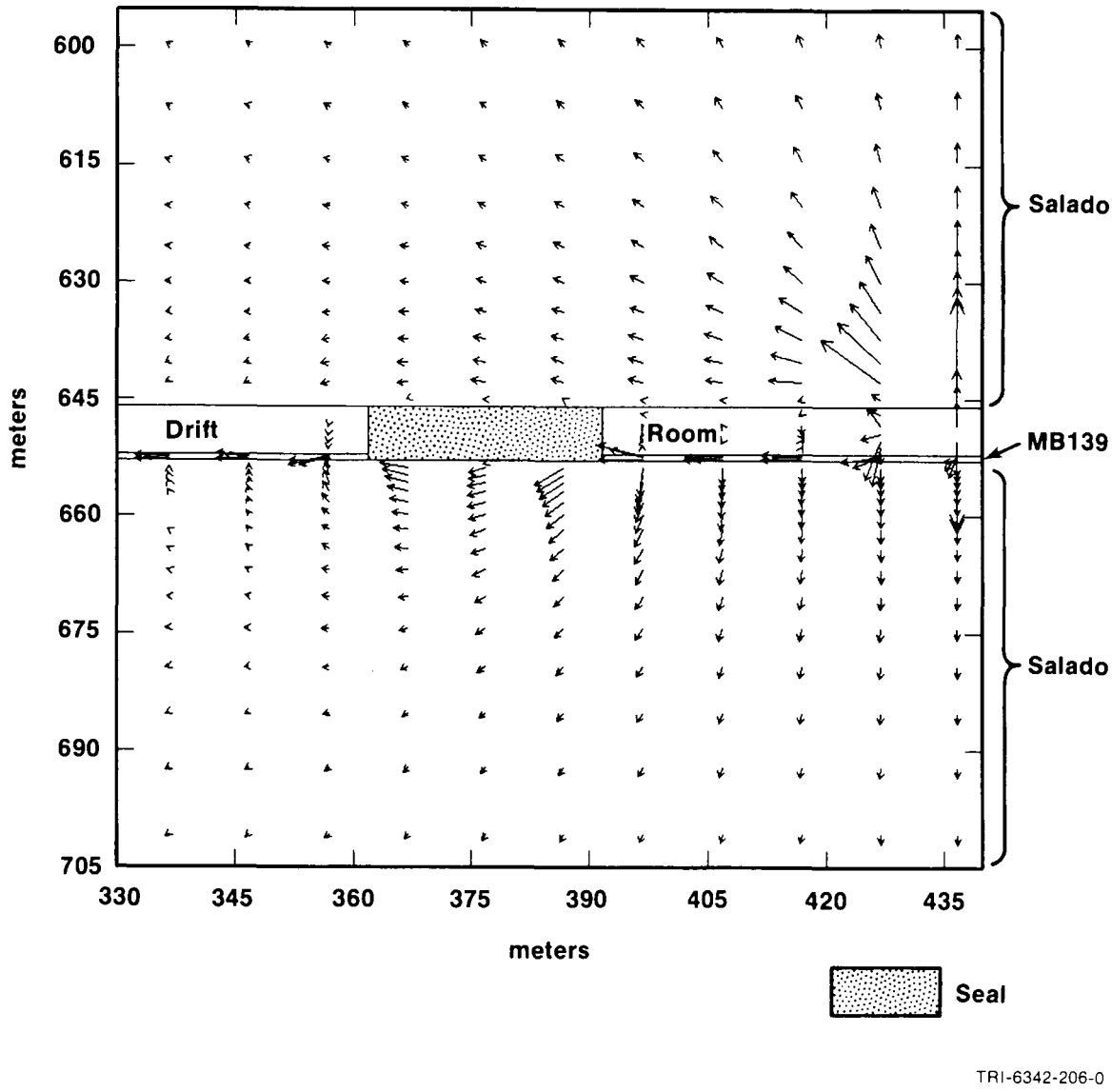

Figure A-7. Interstitial Velocities at Room Seal. Vectors in the Seal are not Shown, but Point to the Marker Bed-Seal Interface. Subdomain Shown Corresponds to Figure A-3.

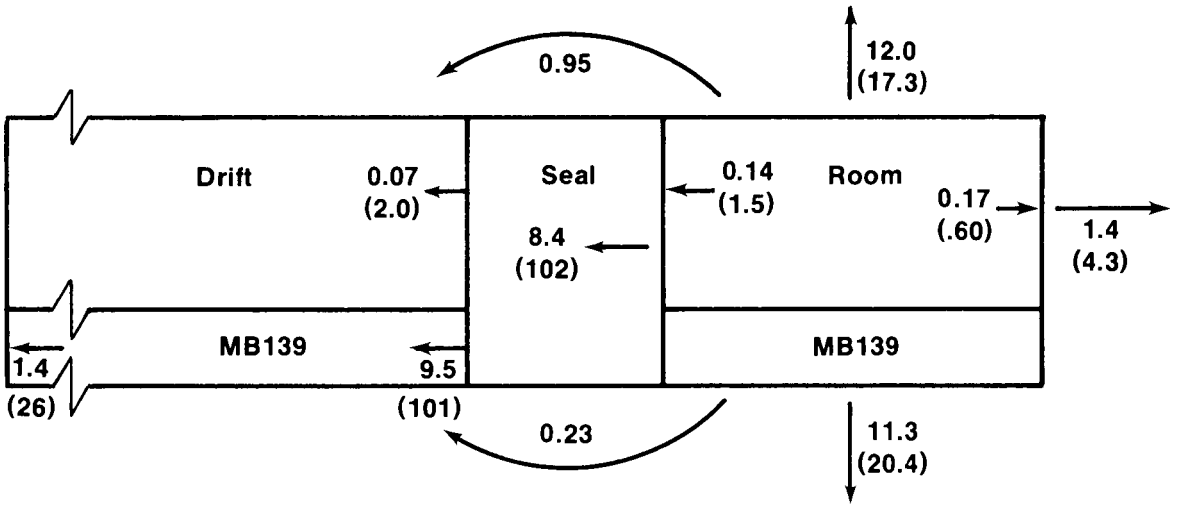

Flux x 10^{-7} kg/s - Case IA

(Flux x 10^{-7} kg/s - Case IB)

TRI-6342-207-0

Figure A-8. Brine Fluxes In and Around the Seal and Across Boundaries Around a Storage Room as Calculated by SUTRA. In Case IB, Flow from Room does not Re-Enter the Drift or MB139 on the Shaft Side of the Seal.

TABLE A-1. MATERIAL PROPERTIES (after Lappin et al., 1989)

Material	Permeability (m^2)	Porosity	Dispersivity	Thickness (m)
Drift/ Shaft	1.0×10^{-20}	0.05	15.2	5.0
MB139	3.0×10^{-13} - 3.0×10^{-7}*	1.0 - 0.2*	15.2	1.0 -5.0
Salado	3.0×10^{-21}	0.001	15.2	100.0
Seal	4.0×10^{-19}	0.03	15.2	5.0
Waste	1.0×10^{-13}	0.18		

Fluid and Solid Matrix Constants

Compressibility of Fluid	4.53×10^{-10} Pa^{-1}
Compressibility of Matrix	2.69×10^{-11} Pa^{-1}
Fluid Viscosity	0.0016 kg/m/s
Density of Solid	2300 kg/m^3
Fluid Base Density	1200 kg/m^3
Molecular Diffusivity	1.0×10^{-9} m^2/s

* An effective hydraulic conductivity was derived for the fractures in MB139 using $K = b^2 \rho g / 12 \mu$ with b = fracture aperture, ρ = fluid density, and μ = fluid viscosity. A fracture aperture of 2 mm was used, and to be consistent with the treatment of flow through fractures in NEFTRAN, a porosity of 1.0 was used (from Table D-2, Lappin et al., 1989).

beneath the seal. However, very little fluid returns to MB139 in Case IA and none returns in Case IB because of degraded properties. Vectors in the seal which would show flow out of and back into MB139 were not plotted because they would mask nearby vectors. All along MB139 (except near the seal in Case IA) fluid flows away (up and down) from MB139. Though not clearly visible in the figure, there is flow around the top of the seal. In fact, slightly more fluid re-enters the drift around the top than around the bottom. In Case IB with degraded properties, no fluid re-enters the drift or MB139 after flowing around the seal.

Comparing fluid fluxes between the drift and MB139 (Figure A-8) shows that the pathway through MB139 to the base of the shaft is more important for both Cases IA and IB than for the pathway through the drift. These fluxes provide partial confirmation of the similar NEFTRAN result from one-dimensional simulations using the same pressure difference assumptions.

SUTRA and NEFTRAN agree fairly well quantitatively on the flux entering the Salado Formation for Cases IA and IB (Table A-2). However, for Case IA, SUTRA and NEFTRAN substantially differ on the flux through MB139 and the partitioning of the total flow. However, in the SUTRA calculation, MB139 flux decreases by a factor of seven as fluid migrates down MB139. This difference is caused by differences in modeling techniques between SUTRA and NEFTRAN. NEFTRAN models MB139 as a one-dimensional pipe. SUTRA is two-dimensional consequently flow into surrounding host rock and down MB139 are both included, accounting for the larger fluxes at the seal-MB139 interface. NEFTRAN does not include fluid flow out the top or bottom of MB139 into surrounding host rock. Also apparent is the partitioning of the fluid flow between the drift and MB139 (Figure A-8). Flux through MB139 is roughly an order of magnitude larger than through the drift. The apparent imbalance of fluxes into, through and out of the seal has two causes. One, the SUTRA code performs flux-balance calculations at nodes and does not actually generate flux as an output. Reported fluxes are calculated from element velocities, which are averages of four Gauss-point velocities, and areas calculated from zone dimensions and out-of-plane thicknesses with the additional problem of averaged properties at interfaces. The second cause is that only specific components of flux are shown, giving flow the appearance of being one-dimensional. In the seal there is flow in and out the top and bottom (see velocities in Figure A-7) contributing to horizontal flux.

Summing the fluxes out of the room provides an estimate of the artificial fluid source at the pressure nodes. For Case IA the total inflow, including all components of flux, required to maintain the pressure is 3.3×10^{-6} kg/s (0.087 m^3/yr), and 1.4×10^{-5} kg/s (0.38 m^3/yr) for the degraded Case IB. These values are compared to brine inflow of 1.3 m^3/yr and 0.1 m^3/yr used for earlier analyses of disturbed cases (Table 1-2 in Lappin et al., 1989). Though the values are for two distinctly different problems, they produce flows representative of the properties and behavior of the disposal system.

For undisturbed conditions with an assumed pressure difference between lithostatic in the room and hydrostatic in the Culebra Dolomite Member, fluid migration occurs in all directions from the repository, but an important pathway for transport to the Culebra Dolomite is through MB139 and shaft seals as modeled by NEFTRAN. Comparison of fluid fluxes (Table A-2) between the two codes at the base of the shaft is within a factor of three for Case IB, which represents degraded properties that are representative of least favorable parameter values sampled during uncertainty analysis. Therefore, the NEFTRAN simulations are considered reasonable compared to the two-dimensional SUTRA simulation. Of course, this code/code comparison does not validate either model.

TABLE A-2. COMPARISON OF FLUXES BETWEEN NEFTRAN AND SUTRA

	IA		IB	
	SUTRA	NEFTRAN	SUTRA	NEFTRAN
Flux from room into Salado (kg/s)	2.5×10^{-6}	2.6×10^{-6}	4.2×10^{-6}	3.7×10^{-6}
Flux down MB139 (kg/s)				
start (seal)	9.5×10^{-7}		1.0×10^{-5}	
end (bottom of shaft)	1.4×10^{-7}	1.1×10^{-8}	2.6×10^{-6}	1.1×10^{-6}

Assumption of lithostatic pressure in the room and hydrostatic pressure in the host rock (with an implied fluid source within the room to maintain that assumed pressure gradient) is not meant to be realistic. These assumptions represent an artificial test problem intended only for comparison with the NEFTRAN simulation.

SUTRA SIMULATIONS OF WASTE PERMEABILITY EFFECTS ON FLOW INTO AN EXPLORATORY BOREHOLE

This preliminary axisymmetric simulation of one WIPP panel examines the influence of waste permeability on flow to a borehole at several pressure gradients and permeabilities for both transient and steady-state conditions. Flow into an intrusion borehole is a performance measure which is useful for ranking potential engineered modifications to the waste, and will help to determine the radionuclide source term for transport out of the repository. The results were used to adjust the distributions of room conductivity and porosity for sensitivity analyses of possible engineered modifications to the waste or repository.

For the axisymmetric simulation, one WIPP panel is modeled as a disk 4.0 m (13.0 ft) high (thickness prior to consolidation) and 48.6 m (160.4 ft) in radius. This radius preserves the exterior surface area of an actual panel. The boundaries are 165 m (545 ft) above and below the disk and 206 m (680 ft) out from the axis of symmetry (Figure A-9). A variable mesh is used, proceeding from fine to coarse in both the vertical and radial directions (Figure A-10).

The assumed boundary conditions are the following: (1) pressures of 14.8 (lithostatic), 10.5, and 8.4 MPa at the 206-m (680-ft) boundary; (2)

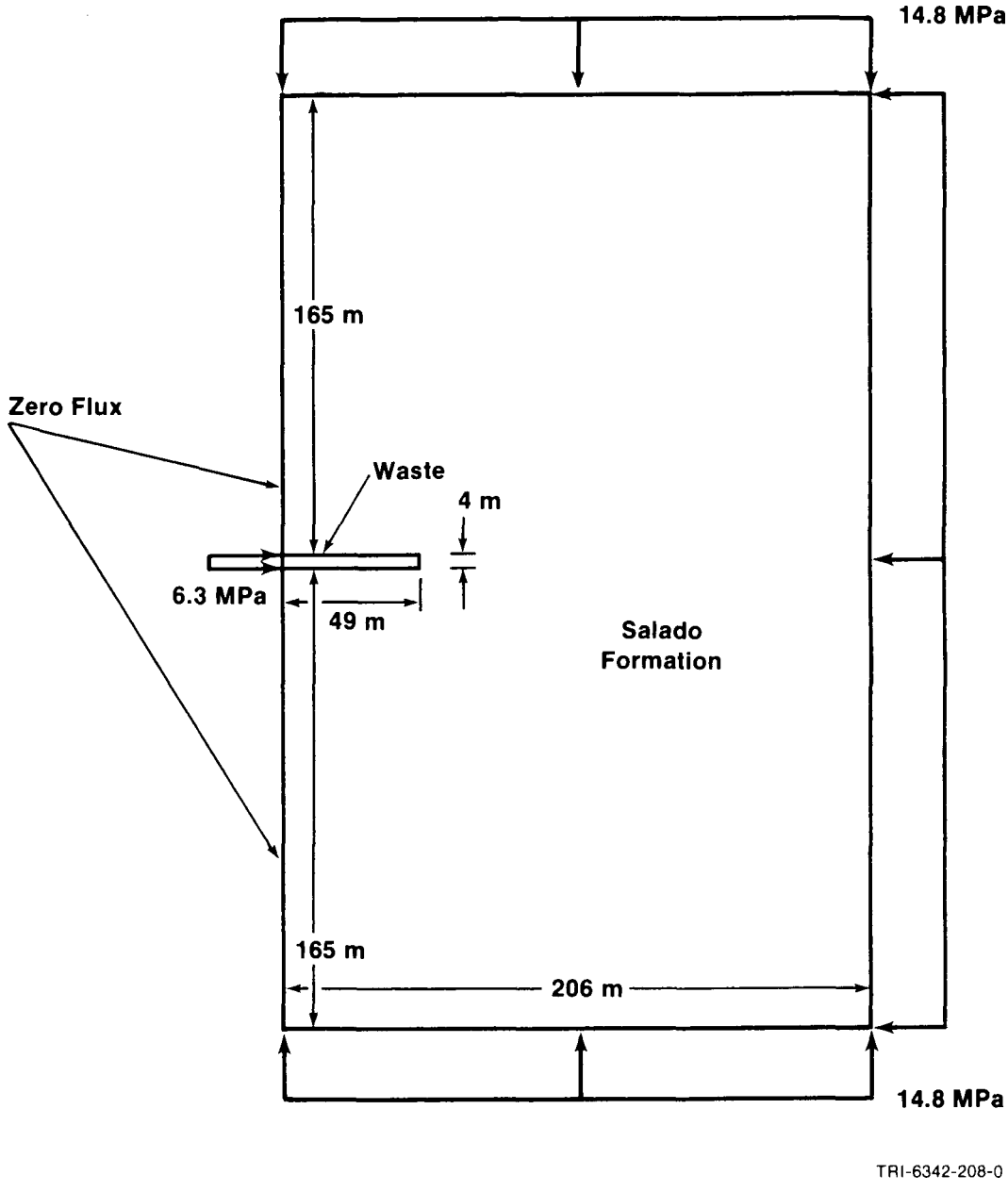

Figure A-9. Boundary Conditions Applied in Borehole Model (Elevation View).

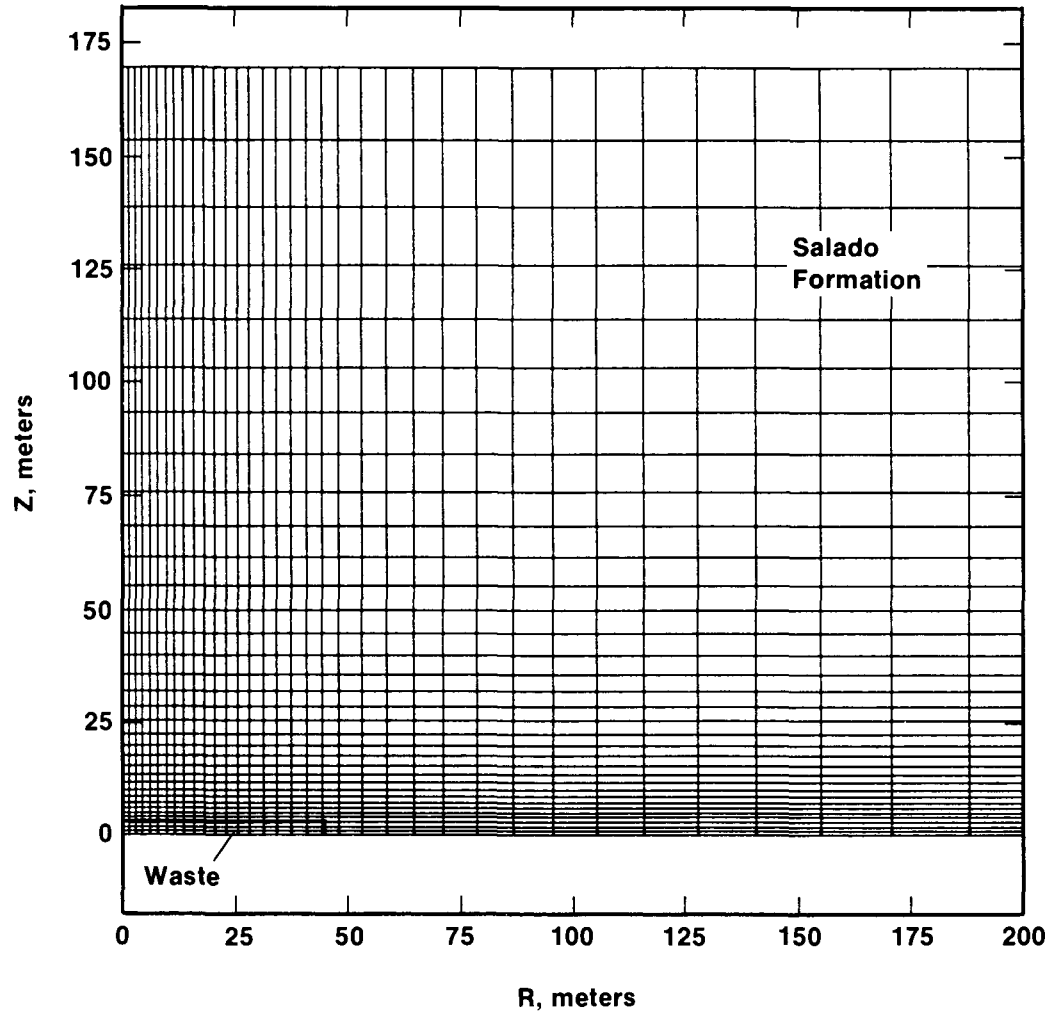

Figure A-10. Axisymmetric Mesh for SUTRA Calculation of an Intrusion Borehole through a Waste Panel (Upper Half).

hydrostatic pressure of 6.3 MPa in the borehole within the panel; and (3) no flow enters the borehole outside the panel in the Salado Formation (Figure A-9).

MATERIAL PROPERTIES

The fluid and solid matrix properties are the same as for the simulation of undisturbed conditions (Table A-1); however, only the Salado Formation and waste are modeled here. Waste permeability varies between 10^{-23} and 10^{-13} m^2. Although porosity may vary directly with permeability in some porous media, it was kept constant at 0.18 for these simulations.

RESULTS

Under steady-state conditions, mass flux to the borehole varies with permeability when the permeability of the waste is less than three orders of magnitude above the permeability of the Salado Formation (Figure A-11). Under transient conditions, mass flux varies when the permeability difference is less than five orders of magnitude (Figure A-12). Flow out of the borehole varies linearly with the changes in pressure gradient (Figure A-11).

If the pressure gradients specified for this simulation are valid (instead of those for the preceding simulation), modifications that reduce the waste permeability to within five orders of magnitude (and preferably three orders) of the Salado Formation permeability can significantly reduce the potential brine flux into an intrusion borehole and shift the CCDF downward well within EPA limits.

WASTE PERMEABILITY EFFECTS ON AMOUNT OF WASTE ACCESSED

Earlier analyses (Lappin et al., 1989) assumed the radionuclide source is solubility-limited until the inventory is depleted. The time of depletion depends upon the volume of waste accessed. As a very conservative assumption, those analyses assume an entire panel could be accessed in 10,000 years. This set of simulations refines that access fraction to a more realistic value, and begins development of a source term that accounts for rate of brine flow. The effect of adding salt dikes is evaluated. The access fraction can be used as a performance measure for ranking engineered modifications of the waste.

SUTRA is used to estimate the access fraction using a two-dimensional model in the horizontal plane. Vertical flux from the Salado Formation into the panel is included using a source of brine within each element to account for brine leakage within the waste panel. The uniform brine flux (2.7×10^{-6} kg/s) divided equally among these sources is from the above simulation of

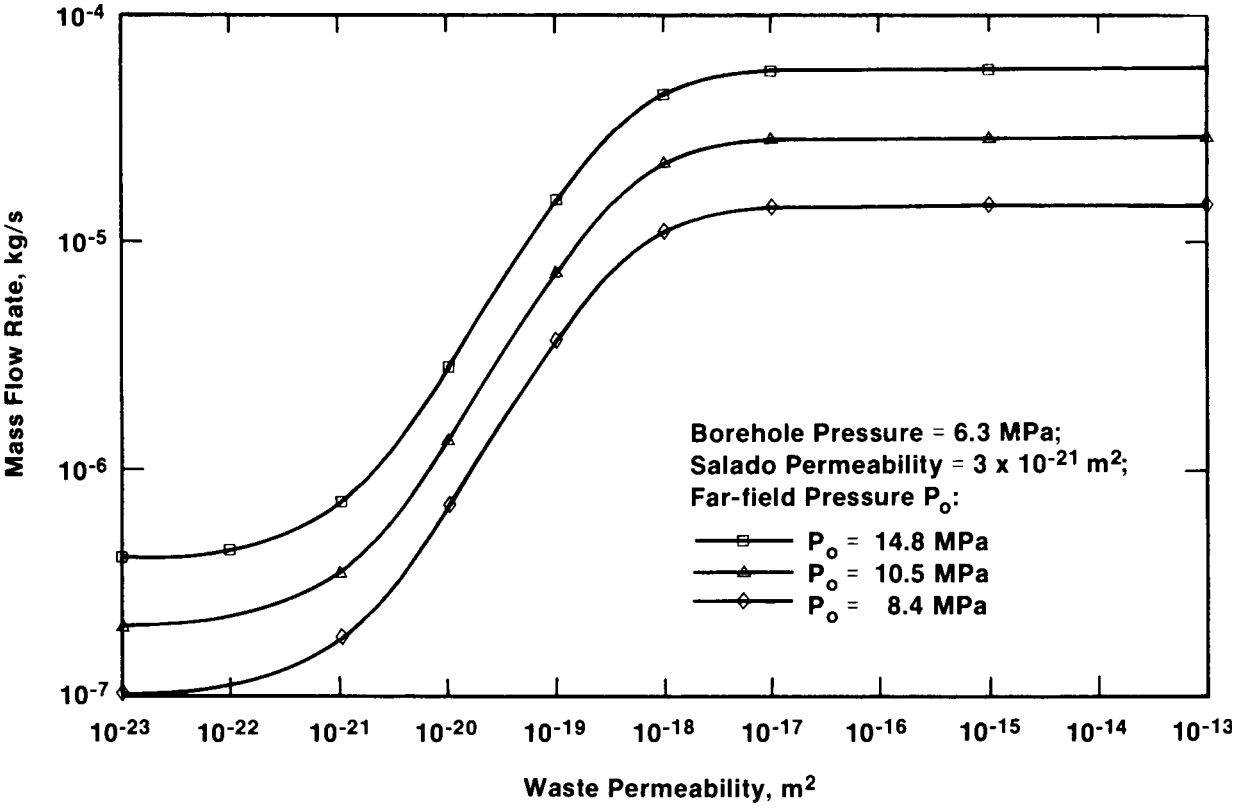

Figure A-11. Variation of Steady Mass Flux to a Borehole as a Function of Waste Permeability at Several Pressure Gradients.

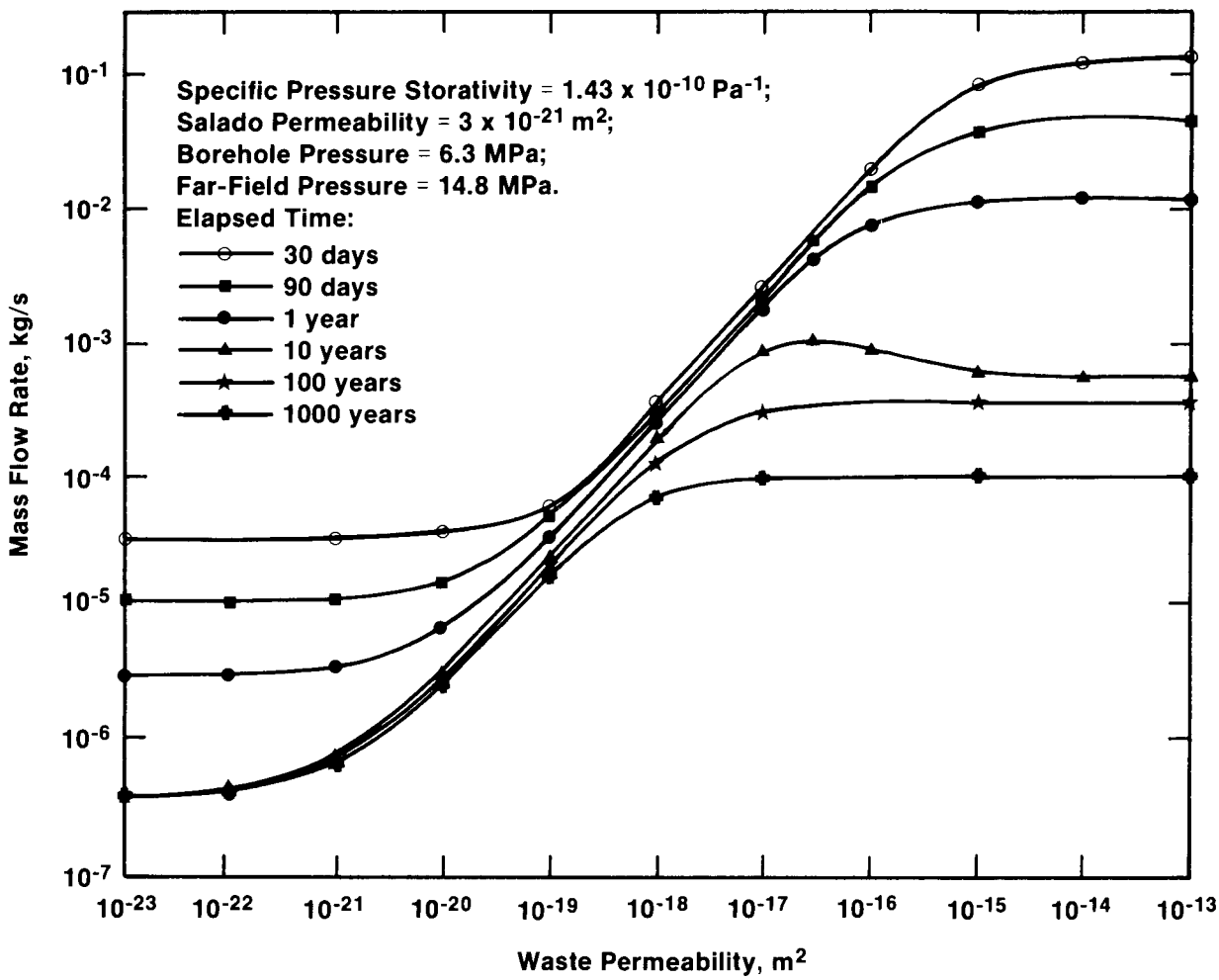

Figure A-12. Variation of Transient Mass Flux to a Borehole as a Function of Waste Permeability.

axisymmetric flow into a borehole with open boundary conditions along the borehole through the Salado Formation. Radial variation of brine flux is not considered when distributing these sources among elements.

These simulations are for long-term steady-flow conditions with the far-field Salado Formation providing the fluid source. They do not simulate the transient response following the intrusion event. Transient calculations are reported elsewhere [Rechard et al., 1990; (in preparation)]. The results presented here are intended to provide long-term realistic bounds for the volume of waste that can be used for defining radionuclide-source terms for scenarios with intrusion boreholes.

Constructing salt dikes within rooms and drifts diminishes flow into an intruding borehole. Although the effectiveness of salt dikes is not equivalent to uniformly changing waste permeability over a whole panel, the modification can be evaluated using this approach. The estimated vertical flux from the Salado Formation is revised by repeating the axisymmetric simulation with the salt dike included.

Using panel symmetry, only one-fourth of a panel is modeled (Figure A-13). The panel is 4 m (13 ft) high. The boundary conditions use the maximum conceivable pressure gradient, 6.3 MPa in the borehole and 14.8 MPa at the far boundary (Figure A-14). To simulate the relative effect of salt dikes, the intrusion borehole was located midway between proposed salt-dike locations [50 m (165 ft) from salt dikes] in a room. No flow boundary conditions are applied along planes of symmetry. Waste permeability varies between 10^{-19} and 10^{-13} m^2. The salt dike permeability, porosity, and width are 10^{-20} m^2, 0.10, and 2 m (7 ft), respectively. Additional cases varied the salt dike permeability and porosity, and confirmed the axisymmetric results (Figures A-11 and A-12) described above.

RESULTS

If waste permeability (10^{-13} m^2) is not modified, about one-half of the volume of a panel can be accessed by a single borehole [earlier analyses (Lappin et al., 1989) assumed conservatively that a borehole could access an entire panel]. A reduction in waste permeability to 10^{-19} m^2 reduces the volume of a panel that can be accessed in 10,000 yr to less than one-sixth (Figure A-15). About one fifth of the volume of a panel can be accessed if the rooms are isolated by salt dikes without modifying waste permeability. With a permeability of 10^{-20} m^2, the salt-dike would be as effective as a panel seal. Flow through MB139 is not included so these calculations also assume effective sealing in the MB139.

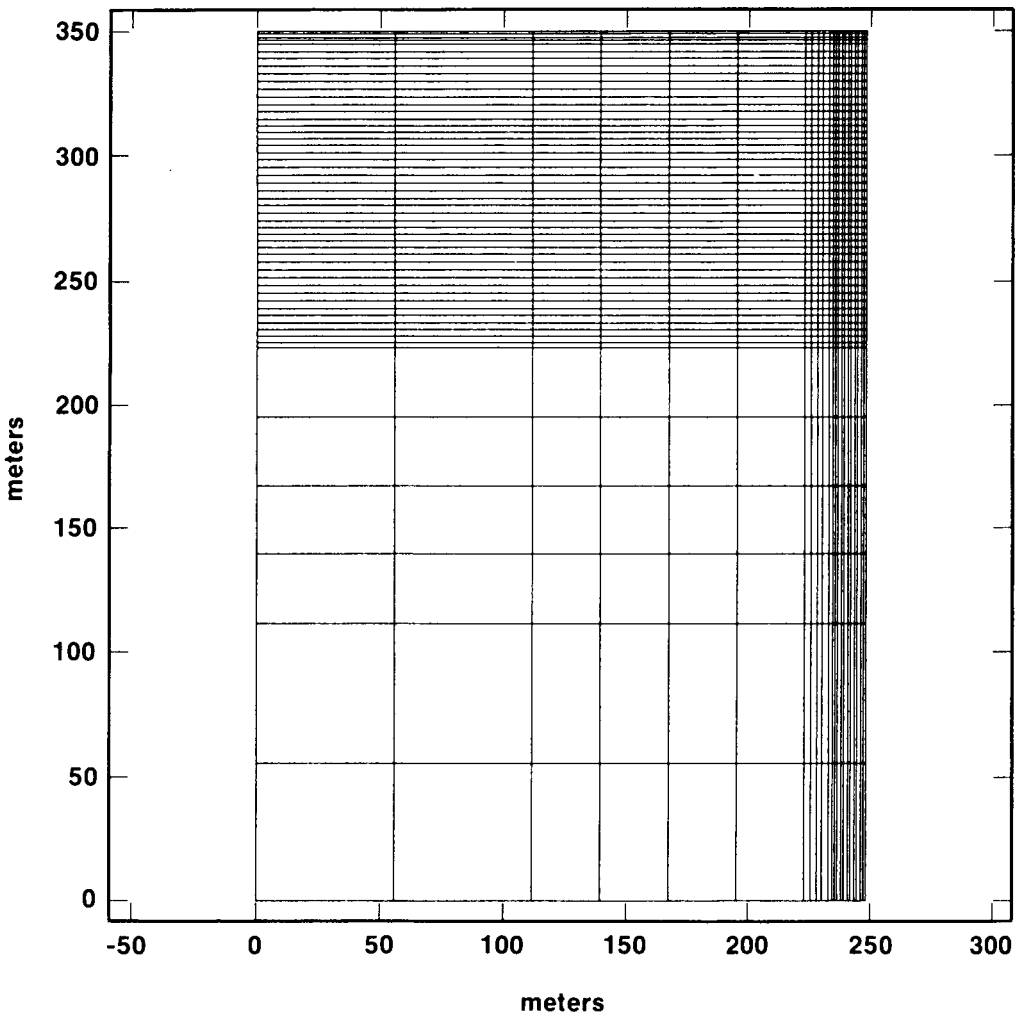

TRI-6342-212-0

Figure A-13. Quarter Panel Mesh for SUTRA Calculation.

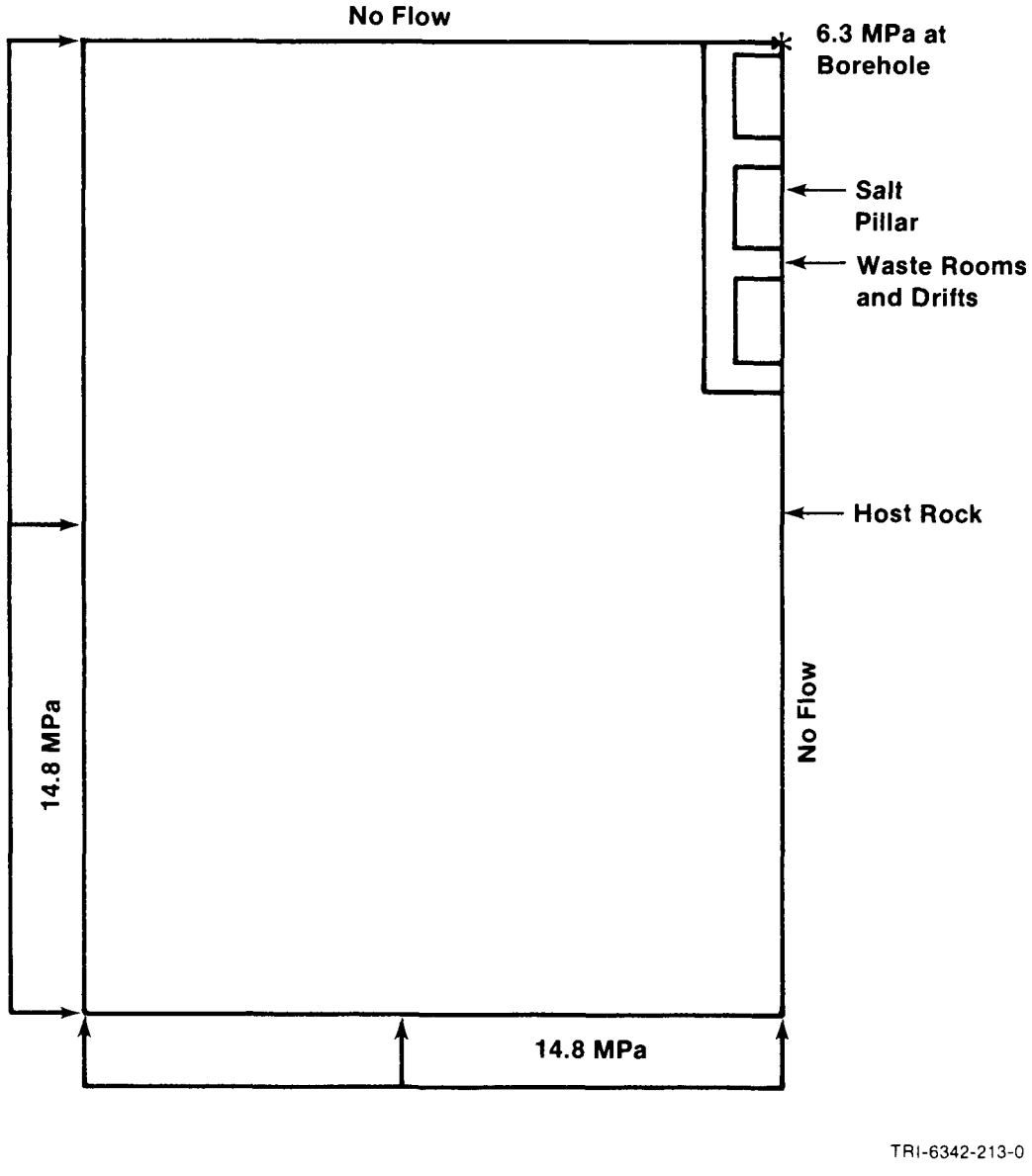

Figure A-14. Boundary Conditions for Quarter Panel SUTRA Model.

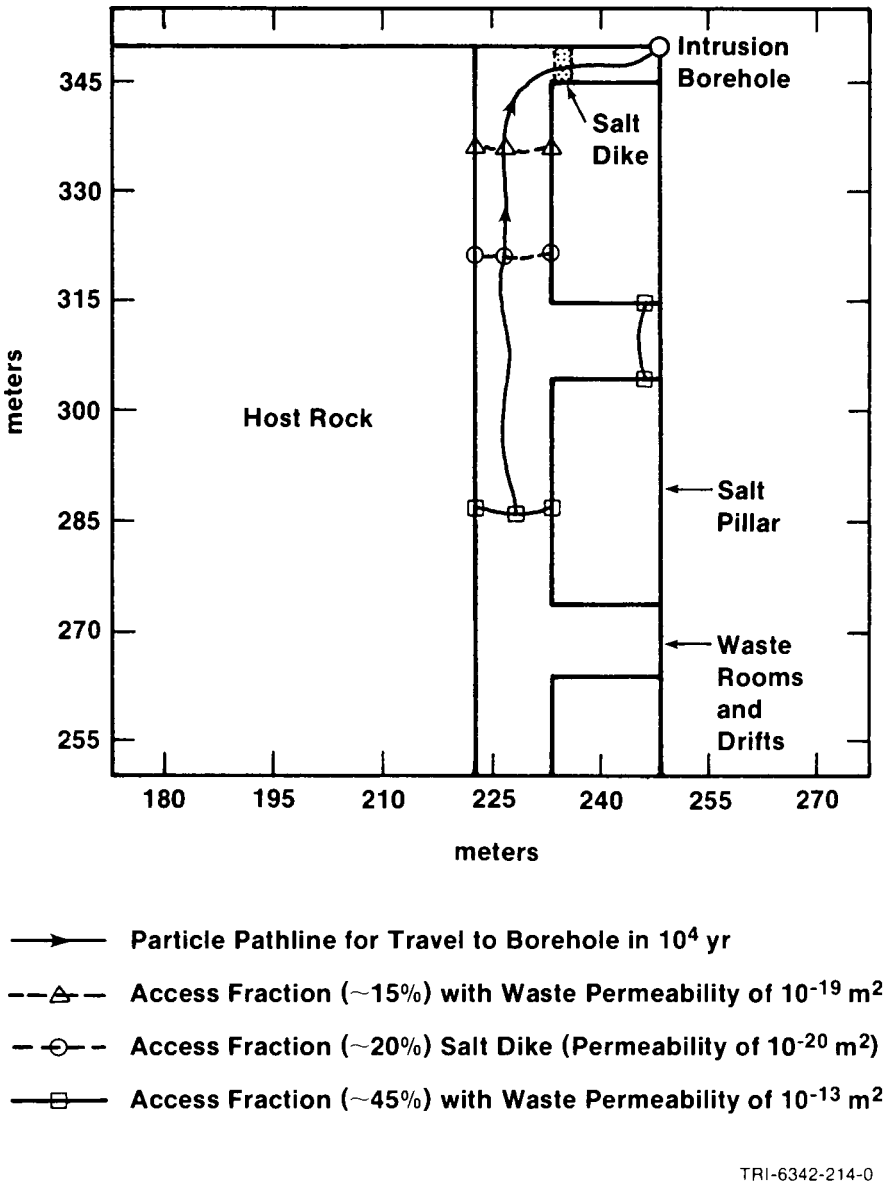

Figure A-15. Fraction of Waste Accessed in 10,000 yr with Waste Permeabilities of 10^{-13} and 10^{-19} m^2 and with a Salt-Dike Steady-State Condition.

Therefore, these salt-dike calculations indicate that steady-state flow into an intrusion borehole may only be decreased by about a factor of two if effective drift/MB139 seals are placed at room-drift boundaries.

An important result of the simulations is that assuming an entire panel is accessible in 10,000 yr to an intrusion borehole (Lappin et al., 1989 and this report) is conservative. Estimates from the axisymmetric simulations indicate that one-third, not one-half, of a panel volume is drained. Therefore, the previous assumption that an entire panel is drained is probably conservative by a factor of two or more. More accurate three-dimensional simulations for estimating these fractions are reported elsewhere [Rechard et al., 1990 (in preparation)].

REFERENCES

Campbell, J.E., D.E. Longsine, and R.M. Cranwell, 1981. *Risk Methodology for Geologic Disposal of Radioactive Waste: The NWFT/DVM Computer Code User's Manual,* SAND81-0886, NUREG/CR-2081. Sandia National Laboratories, Albuquerque, NM.

Lappin, A.R., R.L. Hunter, D.P. Garber, and P.B. Davies, eds., 1989. *Systems Analysis, Long-Term Radionuclide Transport, and Dose Assessments, Waste Isolation Pilot Plant (WIPP), Southeastern New Mexico; March 1989,* SAND89-0462. Sandia National Laboratories, Albuquerque, NM.

Longsine, D.E., E.J. Bonano, and C.P. Harlan, 1987. *User's Manual for the NEFTRAN Computer Code,* SAND86-2405, NUREG/CR-4766. Sandia National Laboratories, Albuquerque, NM.

Rechard R.P., M.G. Marietta, R.D. McCurley, D.K. Rudeen, J. Bean, J. Schreiber, and W. Beyeler, 1990 (in preparation). *Parameter Sensitivity Studies of Selected Components of the WIPP Repository System,* SAND89-2030. Sandia National Laboratories, Albuquerque, NM.

Voss, C., 1984. *SUTRA: Saturated-Unsaturated Transport Code,* U.S. Geological Survey, Reston, VA.

APPENDIX B:
REFERENCE DATA CASES IA, IB, IIA, AND IIC
(from Lappin et al., 1989)

APPENDIX B:
REFERENCE DATA CASES IA, IB, IIA, AND IIC
(from Lappin et al., 1989)

Two reference sets of calculations (Lappin et al., 1989) examined performance of the WIPP disposal system under undisturbed conditions (Table B-1). The calculations include expected behavior (Case IA) and behavior in which radionuclide solubility and repository-seal permeability are increased from expected values (Case IB). These calculations assume both that the repository is saturated with brine 2,000 years after closure and that any migration or release of gases prior to this time does not affect the subsequent permeability of the repository sealing system by more than two orders of magnitude.

Two additional reference sets of calculations (Lappin et al., 1989) (Cases IIA and IIC) examined response of the WIPP disposal system to a human intrusion through the repository into underlying pressurized brine within the Castile Formation.

The parameter values in the four reference cases provided reference data for the Methodology Demonstration. The following descriptions and Table are from the earlier work.

> Case IIA assumes "expected" or "representative" characteristics for the repository, the breaching well, and the Culebra Dolomite. Critical variables include radionuclide solubility, waste permeability, borehole permeability, and transport properties within the Culebra Dolomite (matrix porosity, fracture spacing, matrix tortuosity, free-water diffusivity of radionuclides, and radionuclide distribution coefficient, K_d). The waste permeability enters directly into these calculations only to the extent that the assigned permeability for Cases IIA and IIC (10^{-13} m^2) is assumed to allow mixing of Castile brine near the borehole, sufficient for these brines to reach the same radionuclide concentration as already exists within the repository. Thus, the radionuclide source term to the Culebra Dolomite for Cases IIA and IIC results from contamination of the entire Castile-brine and Salado-brine volumes by a full complement of radionuclides ....

Case IIC assumes that

> flow and transport properties in the repository and geosphere are degraded. Specifically, radionuclide solubility is increased by two orders of magnitude, and borehole-plug permeability is increased by

one order of magnitude. Analogous changes are made in the model of the Culebra Dolomite, which decrease the effectiveness of radionuclide retardation and increase the importance of fracture flow; i.e., matrix porosity, matrix tortuosity, free-water diffusivity, and distribution coefficients (K_ds) are all decreased, and fracture spacing is increased. This combination of changes results in increased flow and transport within the Culebra Dolomite ....

Case IIC ... assumes sufficient waste permeability to allow brine mixing within the repository. Thus, the differences between Case IIA and Case IIC are that radionuclide solubilities and flow and transport behavior outside the repository have been degraded in Case IIC and that brines are assumed to mix within the repository ....

TABLE B-1. DESCRIPTION OF AND INPUT PARAMETERS FOR CASES ANALYZED (taken from Lappin et al., 1989)

Case	Description	Repository Parameters	Transport Parameter
IA	Undisturbed Performance	EXPECTED Radionuclide Solubility 10^{-6} M	EXPECTED Lower-Shaft Permeability 10^{-20} m^2 Culebra Permeability 5×10^{-15} to 3×10^{-13} m^2 Culebra Matrix Porosity 0.16
IB	Undisturbed Performance	DEGRADED Radionuclide Solubility 10^{-4} M	DEGRADED Lower-Shaft Permeability 10^{-20} m^2 Marker Bed 139 Seal Permeability 4×10^{-17} m^2 Culebra Permeability 5×10^{-15} to 5×10^{-17} m^2 Culebra Matrix Porosity 0.07
IIA	Response to Breach of Castile Brine Reservoir	EXPECTED Radionuclide Solubility 10^{-6} M Waste/Backfill Permeability 10^{-13} m^2 Sufficient For Mixing[a] Salado Brine Inflow 1.3 m^3/panel/year	EXPECTED Long-Term Plug Permeability 10^{-12} m^2 Culebra Matrix Porosity 0.16 Culebra Fracture Porosity 0.0015 Culebra Fracture Spacing 2 m Culebra Free-Water Diffusivity 1×10^{-6} cm^2/s Culebra K_d's Range 0.1 to 200 mL/g Culebra Matrix Tortuosity 0.15
IIC	Response to Breach of Castile Brine Reservoir	DEGRADED Radionuclide Solubility 10^{-4} M Waste/Backfill Permeability 10^{-13} m^2 Sufficient for Mixing[a] Salado Brine Inflow 1.3 m^3/panel/year	DEGRADED Long-term Plug Permeability 10^{-11} m^2 Culebra Matrix Porosity 0.07 Culebra Fracture Porosity 0.0015 Culebra Fracture Spacing 7 m Culebra Free-Water Diffusivity 5×10^{-7} cm^2/s Culebra K_d's Range 0.05 to 100 mL/g Culebra Matrix Tortuosity 0.03

a. Sufficient for mixing: it is assumed that Castile brine equilibrates to same radionuclide concentration as in repository at each time step.

REFERENCES

Lappin, A.R., R.L. Hunter, D.P. Garber, and P.B. Davies, eds., 1989. *Systems Analysis, Long-Term Radionuclide Transport, and Dose Assessments, Waste Isolation Pilot Plant (WIPP), Southeastern New Mexico; March 1989*, SAND89-0462. Sandia National Laboratories, Albuquerque, NM.

APPENDIX C:
PROBABILITY DENSITY FUNCTIONS USED IN THE METHODOLOGY DEMONSTRATION

APPENDIX C:
PROBABILITY DENSITY FUNCTIONS USED IN THE METHODOLOGY DEMONSTRATION

This appendix contains the probability density functions (pdfs) necessary for uncertainty analysis in the WIPP performance assessment methodology demonstration. The philosophy for constructing pdfs for the parameters included in the uncertainty analysis depends upon available data (Lappin et al., 1989). If minimum, maximum, expected, or median values are available,

- For porosity, a normal distribution was tried; if the normal distribution was an inadequate fit, a lognormal or beta distribution was used.

- For hydraulic conductivity, a lognormal distribution was tried; if it was an inadequate fit, then a beta distribution was used.

- For solubility, a loguniform distribution was selected because estimates of the minimum, maximum and median values were only available on a decadal log scale.

In addition,

- For time of intrusion, a uniform distribution was selected only as an example.

- For all sampled radionuclide retardations, beta distributions were required to fit the available data.

- For radionuclide retardations that were not sampled, the expected value was too close to the minimum value to adequately fit any distribution.

The pdfs for the final performance assessment must be selected by expert judgment from the data available at that time. Project scientists and engineers and external experts will provide that expertise.

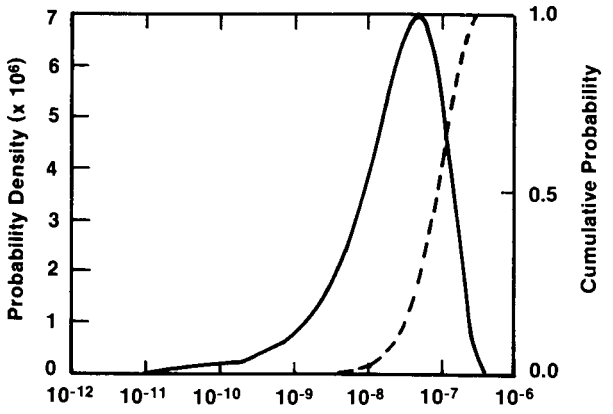

(a) Conductivity: Beta Distribution Function (p = 1.73639, q = 15.629) for Undisturbed Conditions, Cases El_a, El_b, El_c, and El_f, and Reference Design.

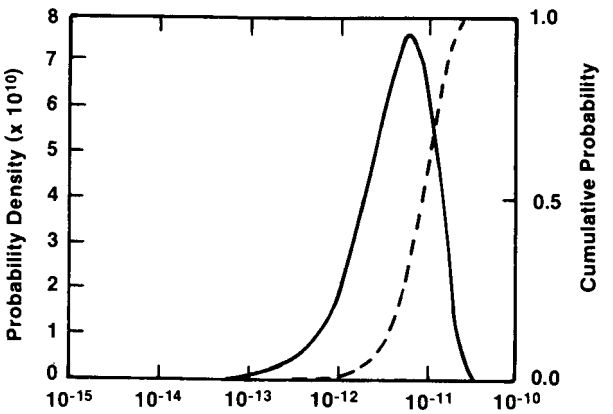

(b) Conductivity: Beta Distribution Function (p = 2.3953, q = 21.580) for Cases El_d and El_e, and Modified Design.

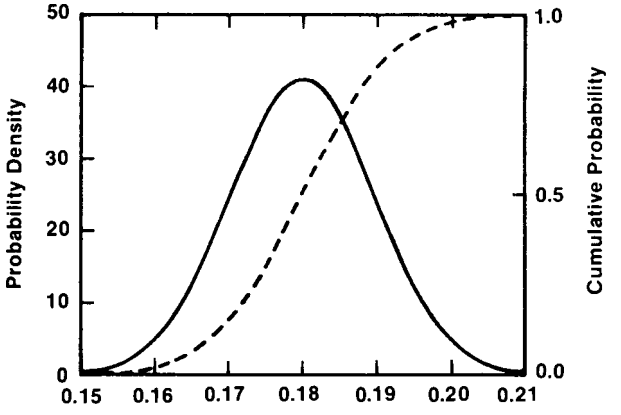

(c) Porosity: Normal Distribution Function for Cases El_a, El_b, El_c, and El_f, and Reference Design.

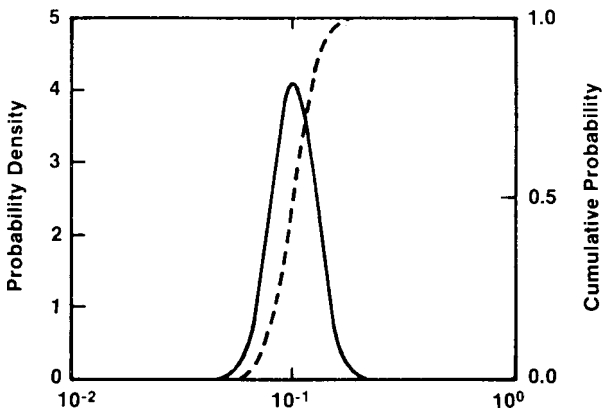

(d) Porosity: Lognormal Distribution Function for Cases El_d and El_e, and Modified Design.

TRI-6342-34-0

Figure C-1. Probability Density and Cumulative Probability Curves for Room Content Conductivity (m/s) and Porosity.

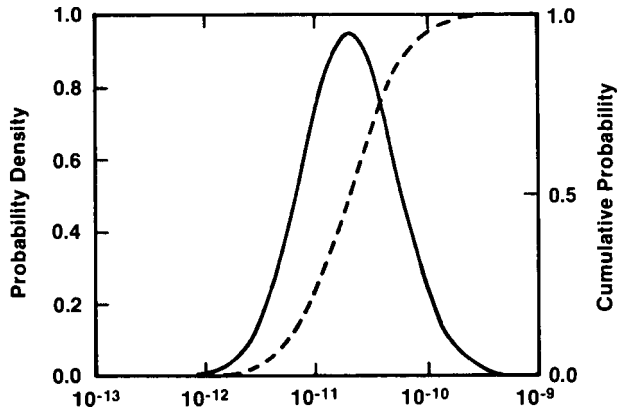

(a) MB139 Seal Conductivity (m/s): Lognormal Distribution Function.

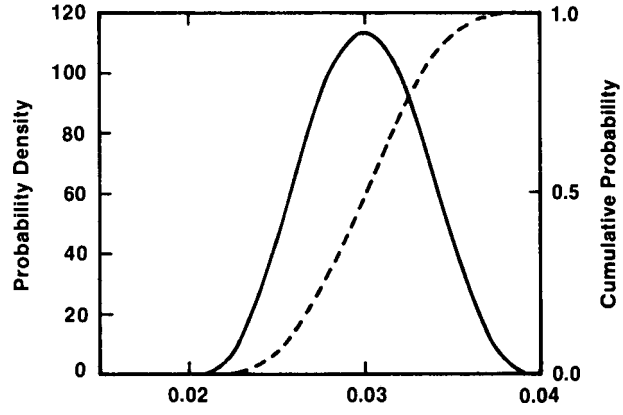

(b) MB139 Seal Porosity: Normal Distribution Function.

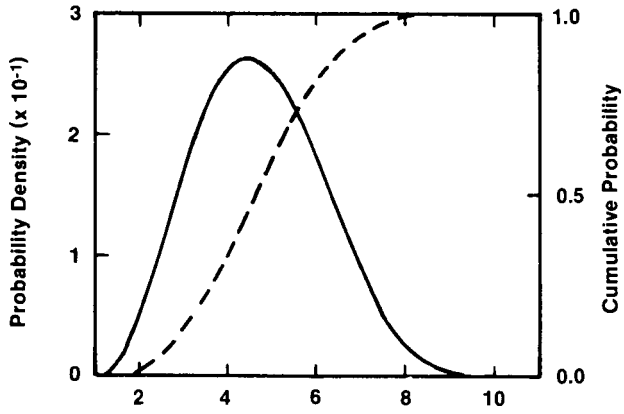

(c) MB139 Retardation: Beta Distribution Function (p = 3.644, q = 5.2197) for Plutonium and Thorium.

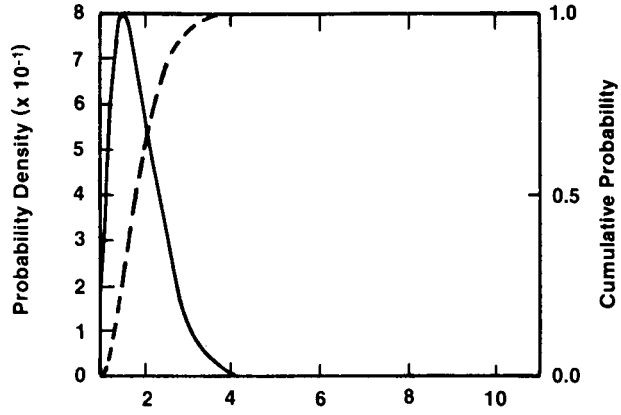

(d) MB139 Retardation: Beta Distribution Function (p = 2.06, q = 19.185) for Americium.

TRI-6342-35-0

Figure C-2. MB139 Probability Density and Cumulative Probability Curves for Marker Bed and Marker Bed Seal Parameters, for Undisturbed Conditions.

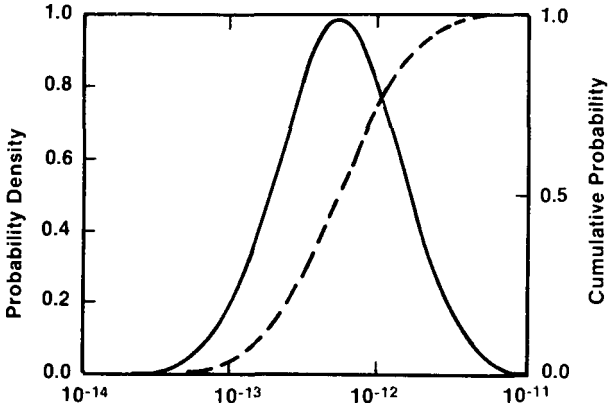

(a) Conductivity (m/s): Lognormal Distribution Function.

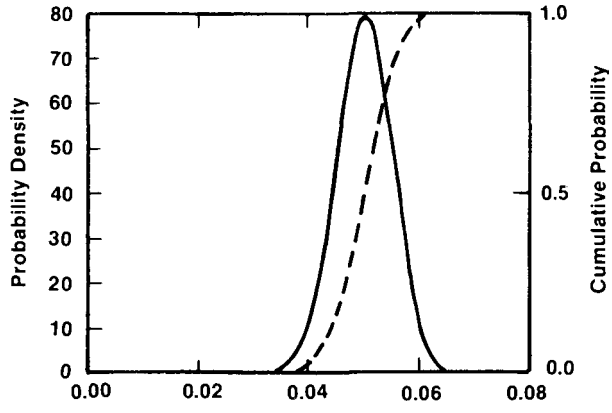

(b) Porosity: Beta Distribution Function (p = 35.8506, q = 21.949).

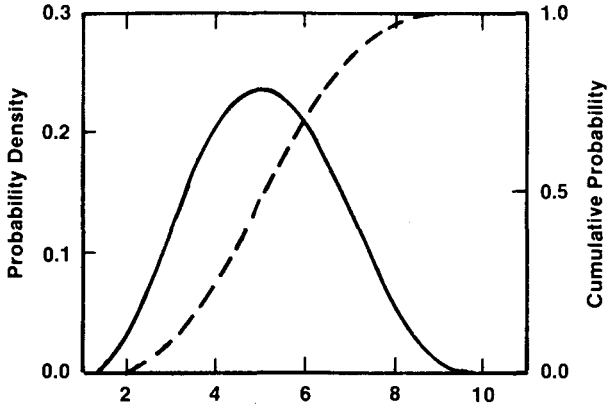

(c) Retardation: Beta Distribution Function (p = 3.21, q = 3.981) for Plutonium, Thorium, and Americium.

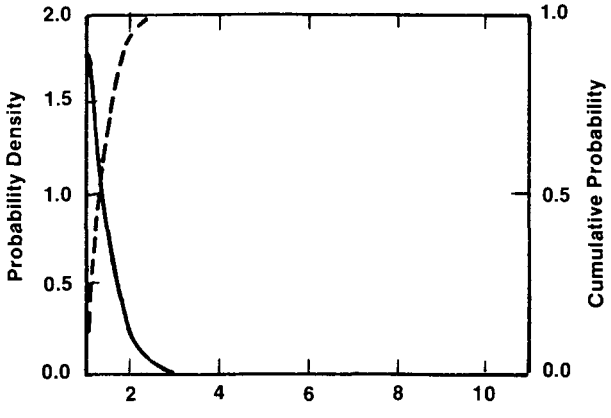

(d) Retardation: Beta Distribution Function (p = 1.2877, q =26.3) for Neptunium.

TRI-6342-36-0

Figure C-3. Probability Density and Cumulative Probability Curves for Lower Shaft Seal Parameters, for Undisturbed Conditions.

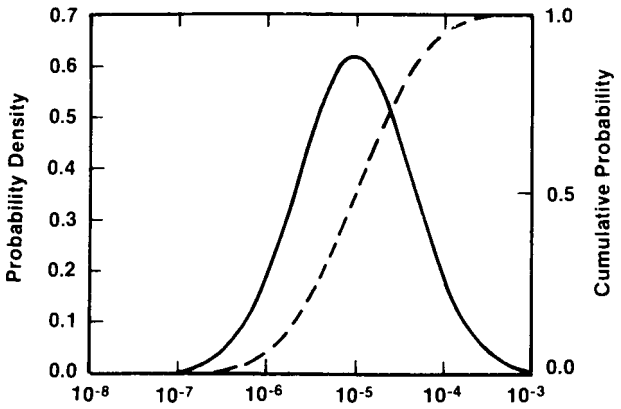

(a) Conductivity (m/s): Lognormal Distribution Function.

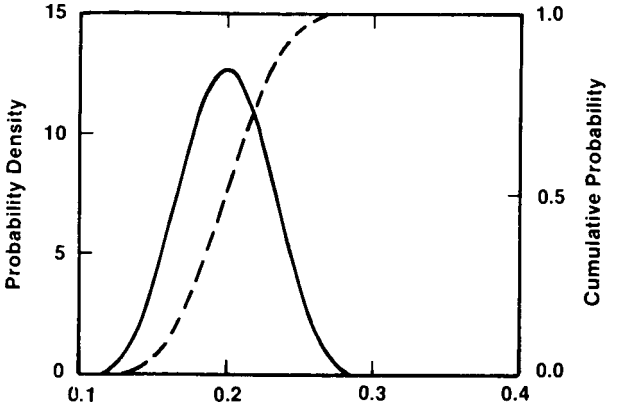

(b) Porosity: Normal Distribution Function.

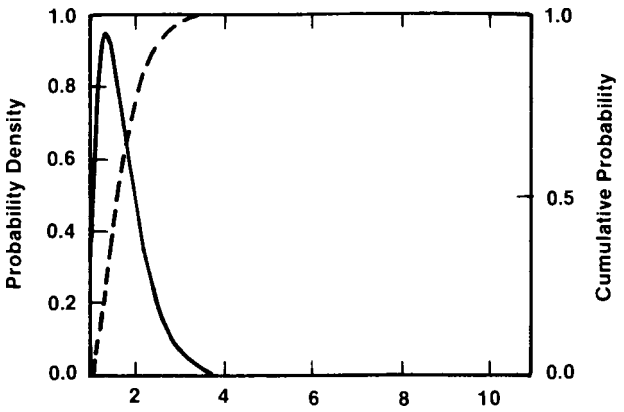

(c) Retardation: Beta Distribution Function (p = 1.762, q = 19.67) for Plutonium, Thorium, and Americium.

TRI-6342-37-0

Figure C-4. Probability Density and Cumulative Probability Curves for Upper Shaft Seal Parameters, for Undisturbed Conditions.

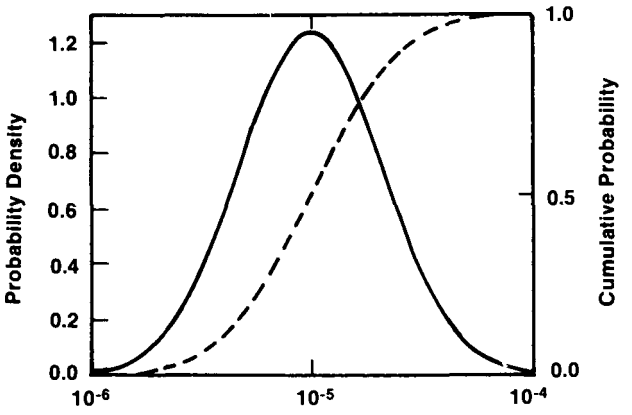

(a) Conductivity (m/s): Lognormal Distribution Function.

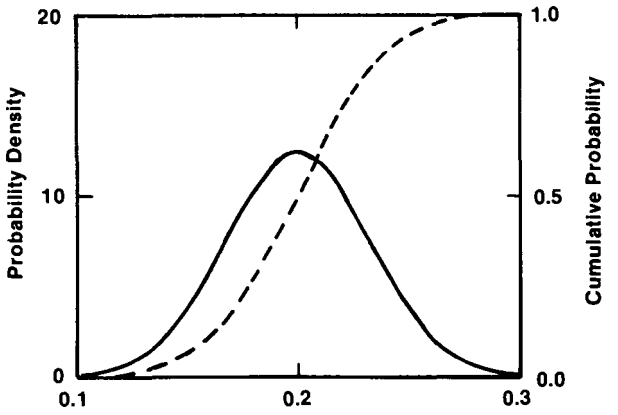

(b) Porosity: Normal Distribution Function.

TRI-6342-38-0

Figure C-5. Probability Density and Cumulative Probability Curves for Intrusion Borehole Parameters for Cases El_a through El_g, and Reference Design and Modified Design.

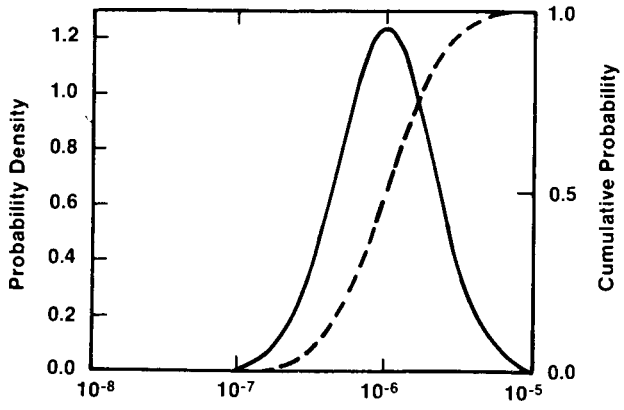

(a) Conductivity (m/s): Lognormal Distribution Function for Leg 4.

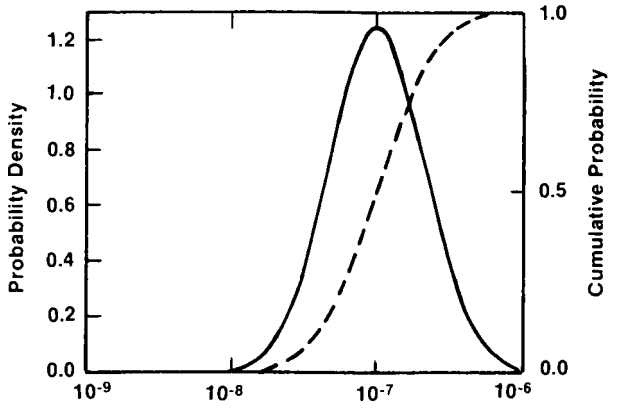

(b) Conductivity (m/s): Lognormal Distribution Fucntion for Legs 5 and 6.

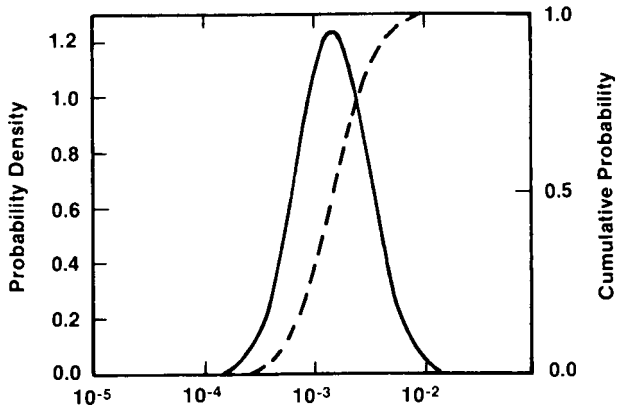

(c) Porosity: Lognormal Distribution Function for Legs 4, 5, and 6.

TRI-6342-39-0

Figure C-6. Probability Density and Cumulative Probability Curves for Culebra Dolomite Member Parameters for Cases El_a through El_e, and Reference Design and Modified Design.

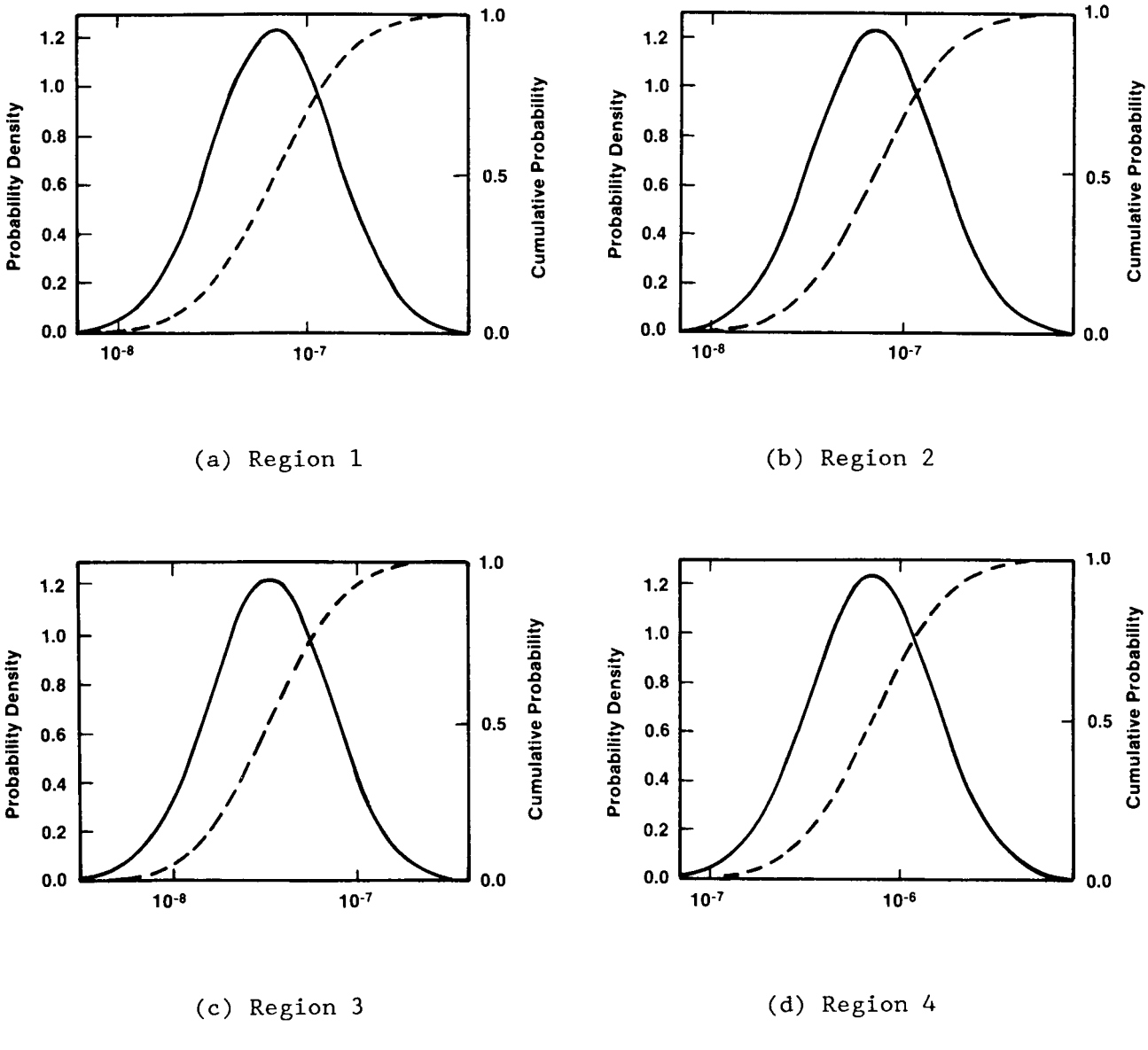

Figure C-7. Probability Density and Cumulative Probability Curves for Culebra Dolomite Member Conductivities for Cases El_f and El_g.

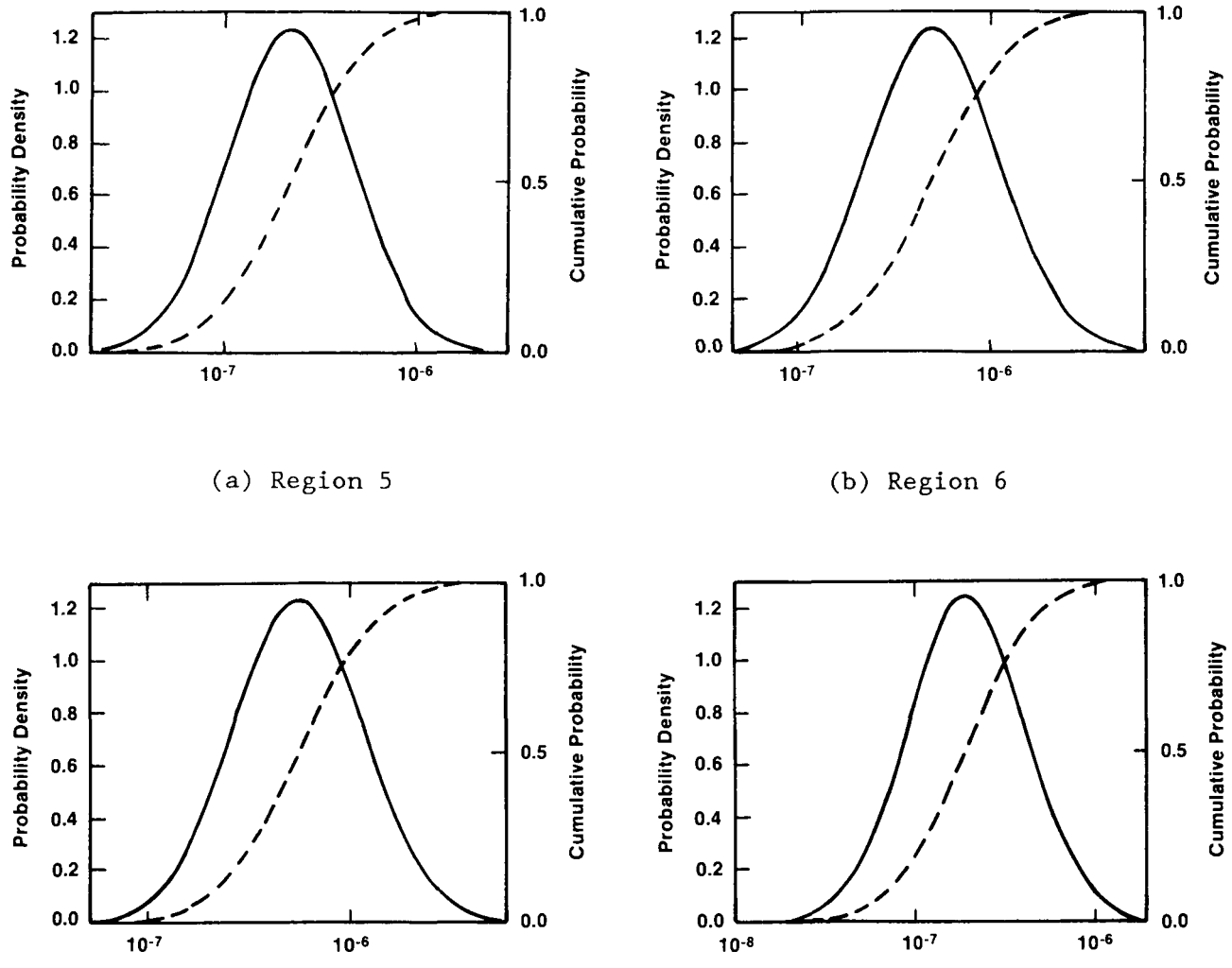

Figure C-8. Probability Density and Cumulative Probability Curves for Culebra Dolomite Member Conductivities for Cases El_f and El_g.

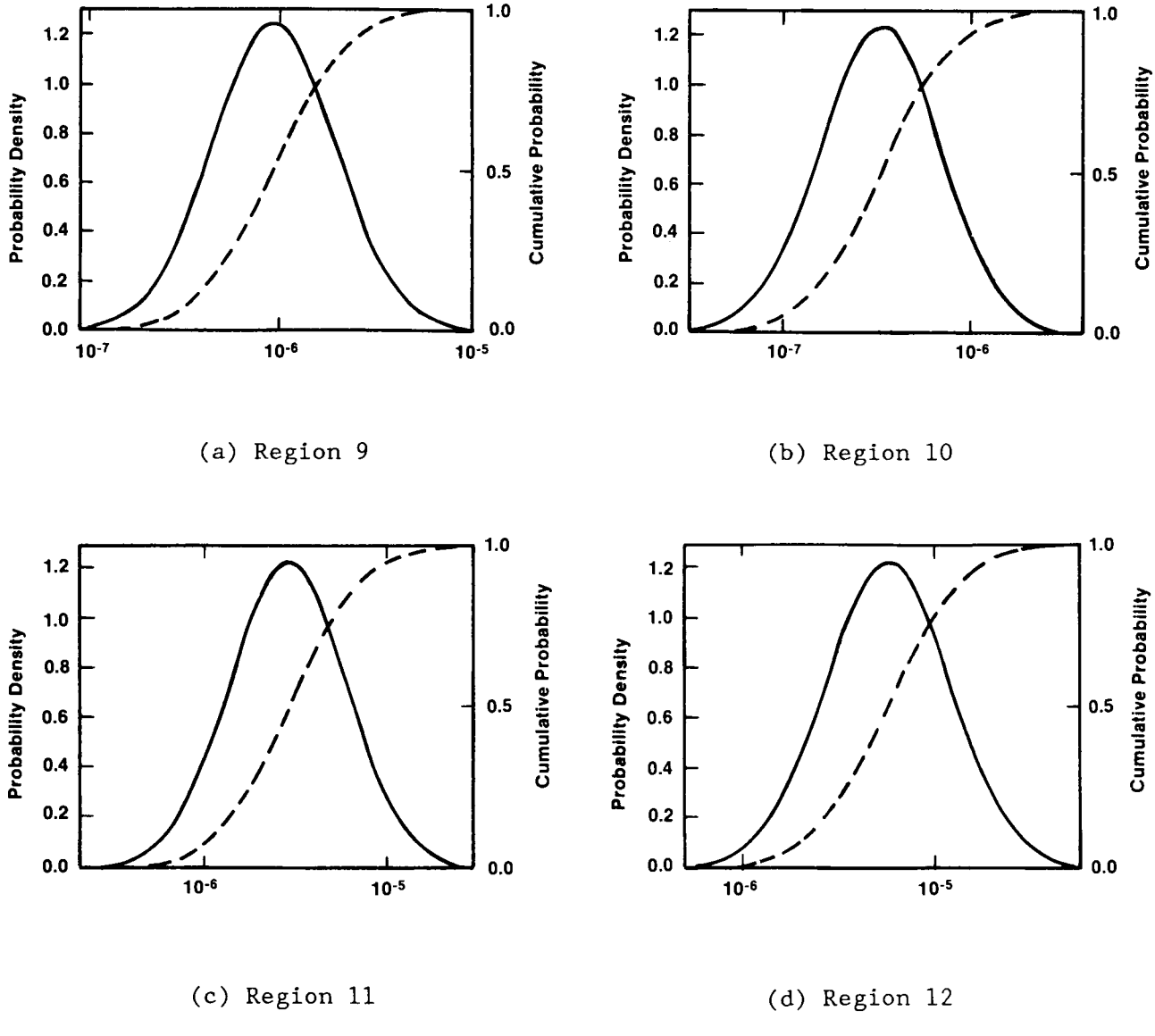

Figure C-9. Probability Density and Cumulative Probability Curves for Culebra Dolomite Member Conductivities for Cases El_f and El_g.

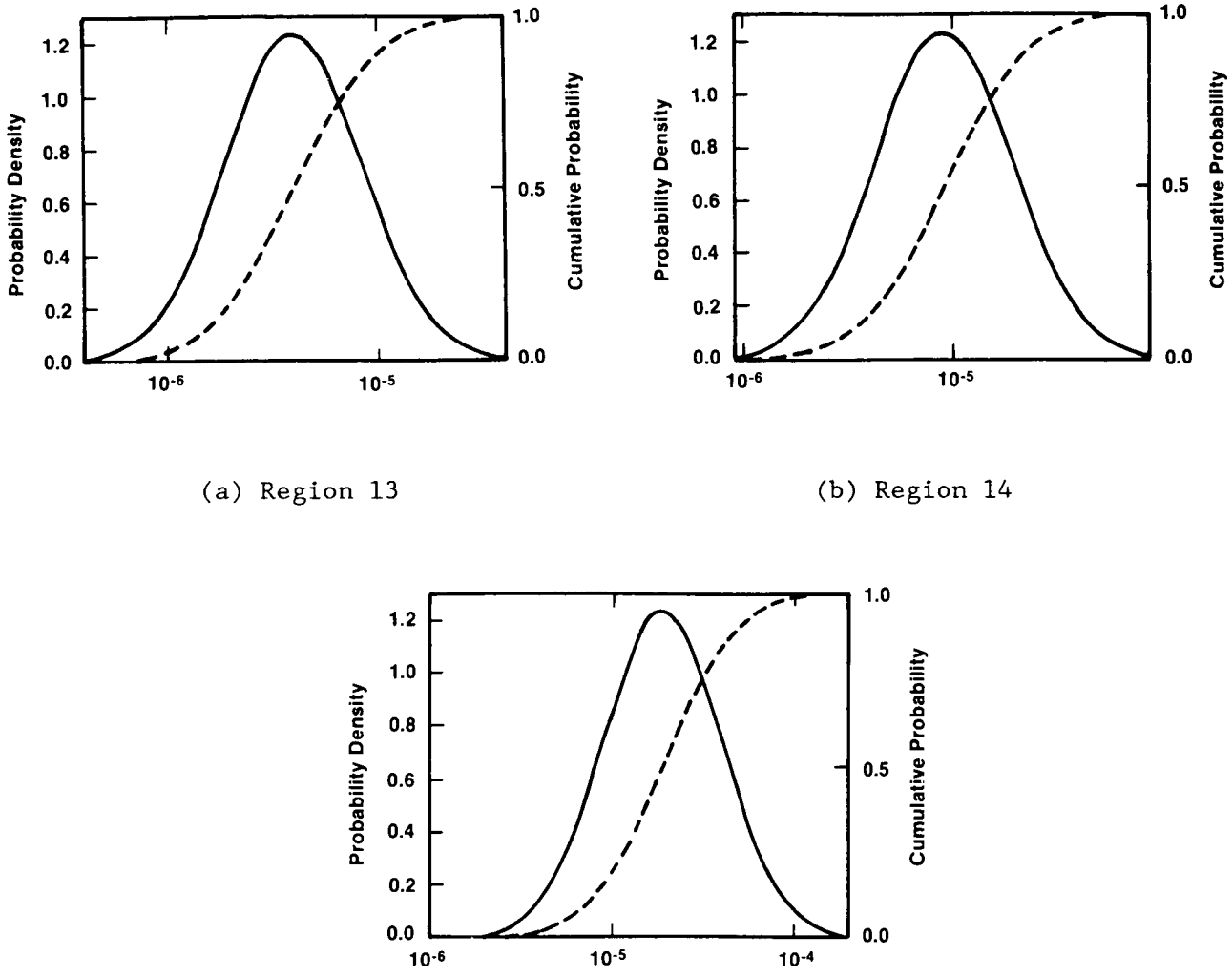

(a) Region 13

(b) Region 14

(c) Region 15

TRI-6342-43-0

Figure C-10. Probability Density and Cumulative Probability Curves for Culebra Dolomite Member Conductivities for Cases El_f and El_g.

REFERENCES

Lappin, A.R., R.L. Hunter, D.P. Garber, and P.B. Davies, eds., 1989. *Systems Analysis, Long-Term Radionuclide Transport, and Dose Assessments, Waste Isolation Pilot Plant (WIPP), Southeastern New Mexico; March 1989,* SAND89-0462. Sandia National Laboratories, Albuquerque, NM.

APPENDIX D:
LATIN HYPERCUBE SAMPLES

APPENDIX D:
LATIN HYPERCUBE SAMPLES

Within each scenario case, 50 sets (vectors) of sampled values were generated using a latin hypercube sampling technique. For undisturbed conditions (base case), 14 parameters were sampled (Table D-1).

In the human-intrusion-scenario cases, the borehole passes through a waste panel, so the marker bed and marker-bed seal are absent from the radionuclide migration path used in the simulations. The legs in the Culebra differ in size and location from those in the undisturbed scenario. For the human-intrusion scenario, twelve parameters were sampled (Table D-2).

The table presents the values used in Cases El_a and El_b. In Cases El_c and El_e, the solubility was sampled (Table D-3) from a narrower distribution. The values are used for each of the twelve nuclides in the simplified inventory. In Cases El_d and El_e, the repository conductivity and porosity were sampled from different distributions that are representative of engineered modifications (Table D-4).

Two Cases, El_f and El_g, were run using a more realistic sampling of the Culebra Dolomite Member conductivities. The Culebra Dolomite surrounding the WIPP site was divided into 15 regions or zones, with each region having its own probability density function. The SWIFT code was used to determine the flow field in the Culebra for the 50 vectors of each case. Although the same pdf was used for the solubility of each radionuclide, solubility was sampled independently for each radionuclide. For these cases, 28 parameters were sampled (Tables D-5 and D-6).

TABLE D-1. SAMPLED VALUES FOR THE UNDISTURBED PERFORMANCE SCENARIO

Parameters

- x(1) nuclide solubility (molar)
- x(2) pressure (Pa) driving flow through the repository
- x(3) repository hydraulic conductivity (m/s)
- x(4) MB139 seal hydraulic conductivity (m/s)
- x(5) MB139 seal porosity
- x(6) plutonium and thorium retardations in MB139
- x(7) americium retardation in MB139
- x(8) lower-shaft seal hydraulic conductivity (m/s)
- x(9) lower-shaft seal porosity
- x(10) plutonium, thorium, and americium retardations in the lower shaft seal
- x(11) neptunium retardation in the lower shaft seal
- x(12) upper shaft seal hydraulic conductivity (m/s)
- x(13) upper shaft seal porosity
- x(14) plutonium, thorium, and americium retardations in the upper shaft seal

TABLE D-1. SAMPLED VALUES FOR THE UNDISTURBED PERFORMANCE SCENARIO

Simulation	x(1)	x(2)	x(3)	x(4)	x(5)	x(6)	x(7)
1	3.840×10^{-7}	7.726×10^{6}	3.709×10^{-8}	6.188×10^{-12}	3.351×10^{-2}	5.56	1.67
2	3.766×10^{-6}	1.135×10^{7}	3.741×10^{-8}	2.067×10^{-11}	2.704×10^{-2}	2.92	2.00
3	5.746×10^{-9}	7.356×10^{6}	8.721×10^{-9}	1.029×10^{-11}	2.634×10^{-2}	3.59	1.91
4	1.862×10^{-7}	6.472×10^{6}	1.245×10^{-7}	1.258×10^{-11}	2.644×10^{-2}	6.20	1.89
5	3.064×10^{-6}	6.135×10^{6}	7.494×10^{-8}	6.956×10^{-12}	3.146×10^{-2}	6.02	1.22
6	2.164×10^{-8}	1.372×10^{7}	1.116×10^{-8}	3.411×10^{-11}	2.620×10^{-2}	7.09	1.94
7	2.294×10^{-7}	1.438×10^{7}	8.761×10^{-8}	2.387×10^{-11}	3.028×10^{-2}	3.61	1.62
8	2.634×10^{-5}	9.184×10^{6}	6.730×10^{-8}	1.369×10^{-11}	2.936×10^{-2}	6.00	1.88
9	2.170×10^{-6}	9.545×10^{6}	1.155×10^{-7}	9.793×10^{-12}	3.322×10^{-2}	5.06	1.85
10	2.650×10^{-7}	9.079×10^{6}	8.248×10^{-8}	1.415×10^{-11}	2.605×10^{-2}	6.02	2.36
11	3.976×10^{-6}	7.331×10^{6}	2.084×10^{-7}	1.548×10^{-11}	2.845×10^{-2}	4.88	2.06
12	3.956×10^{-9}	1.123×10^{7}	3.611×10^{-8}	1.038×10^{-11}	2.878×10^{-2}	5.46	2.67
13	3.142×10^{-7}	7.870×10^{6}	8.955×10^{-8}	3.502×10^{-11}	2.701×10^{-2}	4.66	2.45
14	1.777×10^{-5}	1.017×10^{7}	1.008×10^{-7}	1.389×10^{-11}	3.338×10^{-2}	4.56	1.12
15	8.686×10^{-5}	8.090×10^{6}	1.224×10^{-7}	3.942×10^{-11}	2.433×10^{-2}	3.24	1.38
16	3.621×10^{-9}	1.419×10^{7}	1.853×10^{-7}	3.996×10^{-11}	3.615×10^{-2}	4.34	2.08
17	1.052×10^{-8}	1.212×10^{7}	5.931×10^{-8}	1.650×10^{-11}	2.856×10^{-2}	5.94	1.31
18	1.248×10^{-5}	1.328×10^{7}	3.305×10^{-7}	6.764×10^{-12}	3.290×10^{-2}	5.24	1.77
19	4.779×10^{-5}	1.495×10^{7}	9.050×10^{-8}	1.272×10^{-11}	3.020×10^{-2}	4.59	1.31
20	9.886×10^{-4}	9.244×10^{6}	4.670×10^{-9}	2.756×10^{-11}	3.359×10^{-2}	4.47	1.28
21	1.363×10^{-9}	6.817×10^{6}	3.943×10^{-8}	2.527×10^{-11}	3.444×10^{-2}	3.99	1.73
22	2.996×10^{-4}	1.398×10^{7}	8.365×10^{-8}	2.479×10^{-11}	3.210×10^{-2}	5.44	2.23
23	1.975×10^{-5}	7.952×10^{6}	5.282×10^{-8}	1.583×10^{-11}	3.060×10^{-2}	3.98	1.09
24	5.260×10^{-5}	8.795×10^{6}	1.552×10^{-7}	2.974×10^{-11}	3.108×10^{-2}	2.54	2.19
25	5.975×10^{-5}	1.318×10^{7}	9.950×10^{-9}	5.270×10^{-11}	3.528×10^{-2}	5.97	1.95
26	3.075×10^{-6}	1.206×10^{7}	2.415×10^{-7}	7.370×10^{-12}	3.323×10^{-2}	3.37	1.87
27	3.278×10^{-8}	1.168×10^{7}	5.018×10^{-8}	1.029×10^{-11}	3.746×10^{-2}	7.76	2.85
28	4.592×10^{-4}	8.895×10^{6}	3.924×10^{-8}	8.140×10^{-11}	2.769×10^{-2}	3.33	1.40
29	2.362×10^{-5}	9.494×10^{6}	8.909×10^{-9}	2.487×10^{-11}	3.201×10^{-2}	5.08	1.96
30	8.282×10^{-5}	1.381×10^{7}	1.401×10^{-7}	1.991×10^{-11}	3.004×10^{-2}	4.43	1.52
31	1.065×10^{-6}	1.454×10^{7}	2.917×10^{-8}	3.647×10^{-11}	3.077×10^{-2}	3.45	1.22
32	5.979×10^{-9}	1.396×10^{7}	1.098×10^{-7}	3.129×10^{-11}	2.717×10^{-2}	6.05	3.39
33	9.885×10^{-5}	1.015×10^{7}	1.345×10^{-7}	5.228×10^{-12}	3.104×10^{-2}	5.06	1.68
34	8.736×10^{-7}	1.227×10^{7}	1.467×10^{-7}	4.036×10^{-11}	3.044×10^{-2}	6.05	1.58
35	4.700×10^{-5}	9.754×10^{6}	1.126×10^{-7}	1.996×10^{-11}	3.385×10^{-2}	2.56	2.13
36	2.308×10^{-7}	9.439×10^{6}	2.966×10^{-8}	4.006×10^{-11}	3.248×10^{-2}	4.79	2.26
37	1.302×10^{-7}	9.068×10^{6}	1.029×10^{-8}	1.564×10^{-11}	3.127×10^{-2}	5.01	2.13
38	4.049×10^{-5}	1.041×10^{7}	1.031×10^{-7}	1.353×10^{-11}	3.349×10^{-2}	1.47	2.94
39	8.677×10^{-4}	8.706×10^{6}	1.475×10^{-7}	1.076×10^{-11}	2.851×10^{-2}	2.90	1.30
40	1.387×10^{-6}	1.428×10^{7}	1.074×10^{-7}	2.179×10^{-11}	3.143×10^{-2}	3.50	1.88
41	7.520×10^{-6}	6.017×10^{6}	5.639×10^{-8}	5.932×10^{-12}	3.014×10^{-2}	6.31	1.73
42	3.308×10^{-6}	1.487×10^{7}	7.924×10^{-8}	2.339×10^{-11}	2.642×10^{-2}	3.13	1.31
43	3.603×10^{-4}	1.452×10^{7}	1.015×10^{-7}	2.752×10^{-11}	3.009×10^{-2}	4.74	1.32
44	5.508×10^{-5}	1.388×10^{7}	1.421×10^{-7}	4.659×10^{-12}	2.524×10^{-2}	2.38	1.27
45	8.441×10^{-9}	7.078×10^{6}	1.150×10^{-7}	6.239×10^{-12}	2.833×10^{-2}	4.02	1.81
46	3.514×10^{-5}	1.390×10^{7}	6.470×10^{-8}	1.366×10^{-11}	2.428×10^{-2}	4.10	3.01
47	1.219×10^{-5}	6.382×10^{6}	4.751×10^{-8}	2.997×10^{-11}	2.795×10^{-2}	2.76	1.39
48	1.607×10^{-6}	1.031×10^{7}	4.650×10^{-8}	2.116×10^{-11}	2.382×10^{-2}	3.47	2.57
49	1.050×10^{-4}	1.042×10^{7}	1.543×10^{-7}	4.238×10^{-11}	2.889×10^{-2}	6.49	1.83
50	1.756×10^{-9}	8.316×10^{6}	3.608×10^{-8}	1.538×10^{-11}	2.782×10^{-2}	4.46	1.99

TABLE D-1. SAMPLED VALUES FOR THE UNDISTURBED PERFORMANCE SCENARIO (Concluded)

Simulation	x(8)	x(9)	x(10)	x(11)	x(12)	x(13)	x(14)
1	1.234×10^{-12}	4.559×10^{-2}	6.26	1.74	1.146×10^{-6}	0.183	2.70
2	2.584×10^{-13}	4.276×10^{-2}	5.57	1.73	3.709×10^{-5}	0.224	1.49
3	1.479×10^{-12}	4.865×10^{-2}	3.76	1.05	1.461×10^{-5}	0.173	1.56
4	1.866×10^{-13}	5.367×10^{-2}	4.97	1.08	4.560×10^{-5}	0.169	2.84
5	2.737×10^{-13}	5.301×10^{-2}	1.90	1.23	4.018×10^{-6}	0.162	1.15
6	1.610×10^{-12}	5.012×10^{-2}	5.91	1.35	7.056×10^{-7}	0.250	2.22
7	2.493×10^{-13}	5.410×10^{-2}	7.20	1.38	7.971×10^{-6}	0.197	1.13
8	2.269×10^{-13}	5.858×10^{-2}	7.52	2.87	4.784×10^{-6}	0.167	1.19
9	3.409×10^{-13}	4.994×10^{-2}	6.94	1.11	4.558×10^{-7}	0.174	1.11
10	1.028×10^{-12}	5.321×10^{-2}	5.51	1.43	8.351×10^{-5}	0.252	1.54
11	4.320×10^{-13}	4.280×10^{-2}	6.57	1.23	1.362×10^{-6}	0.184	1.50
12	1.430×10^{-12}	4.590×10^{-2}	8.01	1.30	3.592×10^{-6}	0.160	2.05
13	7.117×10^{-13}	4.071×10^{-2}	6.40	1.03	9.098×10^{-7}	0.207	1.27
14	1.294×10^{-12}	5.168×10^{-2}	6.46	1.75	8.554×10^{-6}	0.219	1.28
15	1.712×10^{-12}	4.085×10^{-2}	2.17	1.52	3.958×10^{-5}	0.140	1.14
16	7.330×10^{-13}	5.422×10^{-2}	6.57	1.62	4.618×10^{-5}	0.230	1.32
17	8.494×10^{-13}	4.854×10^{-2}	6.34	1.27	4.342×10^{-6}	0.203	1.42
18	2.980×10^{-13}	5.290×10^{-2}	5.81	1.53	7.251×10^{-7}	0.154	1.79
19	2.466×10^{-13}	5.396×10^{-2}	1.34	1.20	9.600×10^{-6}	0.190	1.36
20	1.469×10^{-12}	5.340×10^{-2}	5.19	2.37	4.268×10^{-5}	0.220	1.22
21	9.075×10^{-13}	4.275×10^{-2}	5.55	1.55	1.741×10^{-5}	0.180	2.30
22	2.326×10^{-12}	3.812×10^{-2}	5.29	1.73	6.944×10^{-6}	0.224	1.83
23	5.617×10^{-13}	5.365×10^{-2}	3.28	1.15	6.350×10^{-6}	0.247	1.58
24	1.245×10^{-13}	3.912×10^{-2}	6.07	1.30	4.983×10^{-6}	0.216	1.75
25	2.738×10^{-13}	5.134×10^{-2}	5.80	1.57	5.112×10^{-6}	0.173	2.13
26	4.234×10^{-13}	5.084×10^{-2}	6.12	1.29	2.229×10^{-6}	0.157	1.36
27	1.231×10^{-12}	5.447×10^{-2}	6.04	1.95	2.972×10^{-6}	0.192	1.15
28	9.053×10^{-13}	4.069×10^{-2}	4.02	1.18	2.898×10^{-5}	0.165	1.89
29	9.678×10^{-13}	5.325×10^{-2}	5.65	1.49	1.038×10^{-6}	0.241	1.83
30	3.203×10^{-13}	4.638×10^{-2}	7.01	1.57	4.231×10^{-5}	0.234	1.07
31	1.375×10^{-12}	4.566×10^{-2}	2.89	1.17	3.047×10^{-6}	0.210	2.86
32	3.295×10^{-13}	5.297×10^{-2}	6.22	1.79	9.435×10^{-6}	0.125	2.01
33	1.491×10^{-13}	5.286×10^{-2}	4.55	1.01	2.038×10^{-5}	0.216	2.30
34	3.422×10^{-13}	4.671×10^{-2}	6.67	1.22	6.236×10^{-6}	0.157	1.16
35	2.104×10^{-12}	4.903×10^{-2}	6.39	1.62	8.049×10^{-5}	0.175	1.47
36	7.322×10^{-13}	5.339×10^{-2}	5.43	1.28	1.424×10^{-5}	0.223	1.04
37	9.451×10^{-13}	6.109×10^{-2}	7.72	1.36	2.760×10^{-5}	0.205	2.86
38	7.042×10^{-13}	5.316×10^{-2}	8.13	1.10	3.642×10^{-5}	0.190	1.11
39	4.705×10^{-13}	5.162×10^{-2}	6.12	1.24	8.713×10^{-5}	0.164	1.04
40	2.980×10^{-13}	5.946×10^{-2}	6.59	1.13	1.798×10^{-5}	0.165	2.63
41	7.457×10^{-13}	5.566×10^{-2}	7.15	1.82	1.707×10^{-5}	0.186	1.08
42	4.032×10^{-13}	5.356×10^{-2}	4.76	1.14	9.796×10^{-6}	0.199	1.21
43	5.682×10^{-12}	4.538×10^{-2}	2.28	1.63	6.856×10^{-6}	0.192	1.32
44	4.052×10^{-13}	5.742×10^{-2}	5.63	1.26	3.338×10^{-5}	0.183	2.43
45	4.843×10^{-13}	4.845×10^{-2}	5.00	1.21	1.838×10^{-5}	0.229	1.75
46	2.171×10^{-12}	5.598×10^{-2}	6.90	1.43	3.949×10^{-6}	0.196	1.85
47	6.854×10^{-13}	5.543×10^{-2}	4.84	1.22	9.012×10^{-5}	0.260	1.63
48	9.609×10^{-13}	5.179×10^{-2}	3.76	1.88	5.632×10^{-5}	0.206	1.10
49	2.143×10^{-13}	4.907×10^{-2}	7.04	1.43	3.919×10^{-6}	0.204	2.80
50	1.755×10^{-13}	5.480×10^{-2}	2.83	1.92	4.146×10^{-6}	0.239	2.17

TABLE D-2. SAMPLED VALUES FOR THE HUMAN INTRUSION SCENARIO (CASES $E1_a$ AND $E1_b$)

Parameters

- x(1) intrusion time (years)
- x(2) nuclide solubility (molar)
- x(3) repository hydraulic conductivity (m/s)
- x(4) repository porosity
- x(5) borehole hydraulic conductivity (m/s)
- x(6) borehole porosity
- x(7) Culebra hydraulic conductivity (m/s) for the first 300 m from the intrusion borehole
- x(8) Culebra Dolomite Member porosity for the first 300 m
- x(9) Culebra Dolomite Member hydraulic conductivity (m/s) for the next 2140 m
- x(10) Culebra Dolomite Member porosity for the next 2140 m
- x(11) Culebra Dolomite Member hydraulic conductivity (m/s) for the final 2400 m
- x(12) Culebra Dolomite Member porosity for the final 2400 m

TABLE D-2. SAMPLED VALUES FOR THE HUMAN INTRUSION SCENARIO (CASES $E1_a$ AND $E1_b$)

Simulation	x(1)	x(2)	x(3)	x(4)	x(5)	x(6)
1	7.961×10^{3}	1.393×10^{-4}	3.611×10^{-8}	0.182	7.098×10^{-6}	0.149
2	7.868×10^{3}	1.110×10^{-7}	1.421×10^{-7}	0.187	2.284×10^{-5}	0.177
3	9.992×10^{3}	3.184×10^{-7}	1.345×10^{-7}	0.185	1.283×10^{-5}	0.173
4	5.960×10^{3}	1.797×10^{-9}	5.639×10^{-8}	0.176	1.149×10^{-5}	0.239
5	5.343×10^{3}	2.025×10^{-4}	1.401×10^{-7}	0.173	1.589×10^{-5}	0.209
6	6.810×10^{3}	2.001×10^{-8}	1.126×10^{-7}	0.190	2.099×10^{-5}	0.143
7	5.237×10^{3}	7.486×10^{-7}	1.098×10^{-7}	0.183	1.032×10^{-5}	0.229
8	4.162×10^{3}	1.834×10^{-4}	8.955×10^{-8}	0.173	4.118×10^{-5}	0.194
9	1.704×10^{3}	2.064×10^{-9}	1.475×10^{-7}	0.182	6.242×10^{-6}	0.199
10	7.902×10^{3}	8.019×10^{-9}	9.050×10^{-8}	0.176	2.411×10^{-6}	0.229
11	5.561×10^{3}	8.657×10^{-7}	8.721×10^{-9}	0.165	2.709×10^{-6}	0.174
12	5.999×10^{3}	3.506×10^{-9}	1.029×10^{-8}	0.186	1.341×10^{-5}	0.269
13	7.679×10^{3}	3.676×10^{-6}	1.155×10^{-7}	0.176	5.059×10^{-6}	0.159
14	4.0×10^{2}	1.414×10^{-8}	7.924×10^{-8}	0.168	6.049×10^{-6}	0.160
15	8.231×10^{3}	1.505×10^{-5}	2.917×10^{-8}	0.186	1.010×10^{-5}	0.177
16	5.810×10^{3}	1.206×10^{-5}	8.248×10^{-8}	0.187	4.164×10^{-6}	0.208
17	7.368×10^{3}	2.308×10^{-7}	1.015×10^{-7}	0.183	7.171×10^{-6}	0.149
18	2.225×10^{3}	2.474×10^{-8}	1.150×10^{-7}	0.182	7.743×10^{-6}	0.252
19	9.95×10^{2}	3.875×10^{-4}	1.224×10^{-7}	0.184	4.404×10^{-6}	0.228
20	5.813×10^{3}	5.991×10^{-7}	6.470×10^{-8}	0.178	2.175×10^{-5}	0.205
21	7.799×10^{3}	1.326×10^{-7}	1.008×10^{-7}	0.170	1.270×10^{-5}	0.233
22	7.576×10^{3}	1.455×10^{-7}	5.282×10^{-8}	0.178	1.622×10^{-5}	0.175
23	4.902×10^{3}	8.198×10^{-4}	2.084×10^{-7}	0.184	3.375×10^{-5}	0.186
24	2.526×10^{3}	3.059×10^{-6}	5.931×10^{-8}	0.187	7.002×10^{-6}	0.196
25	8.369×10^{3}	2.884×10^{-4}	9.950×10^{-9}	0.181	7.556×10^{-6}	0.186
26	6.460×10^{3}	4.928×10^{-4}	1.074×10^{-7}	0.168	1.391×10^{-5}	0.187
27	4.039×10^{3}	5.229×10^{-9}	1.853×10^{-7}	0.180	5.572×10^{-5}	0.235
28	9.437×10^{3}	2.134×10^{-7}	1.245×10^{-7}	0.188	2.106×10^{-5}	0.229
29	7.159×10^{3}	7.108×10^{-5}	3.741×10^{-8}	0.182	6.806×10^{-6}	0.165
30	3.783×10^{3}	1.129×10^{-7}	3.709×10^{-8}	0.184	2.780×10^{-5}	0.227
31	1.544×10^{3}	4.794×10^{-4}	4.650×10^{-8}	0.180	1.951×10^{-5}	0.209
32	9.897×10^{3}	1.230×10^{-9}	7.494×10^{-8}	0.174	4.381×10^{-6}	0.196
33	3.524×10^{3}	3.497×10^{-8}	4.670×10^{-9}	0.176	5.869×10^{-6}	0.198
34	2.24×10^{2}	6.129×10^{-6}	3.608×10^{-8}	0.167	8.623×10^{-6}	0.217
35	1.266×10^{3}	1.027×10^{-9}	2.966×10^{-8}	0.173	1.020×10^{-5}	0.217
36	4.307×10^{3}	1.764×10^{-8}	1.031×10^{-7}	0.194	4.026×10^{-6}	0.202
37	7.289×10^{3}	7.719×10^{-9}	3.943×10^{-8}	0.173	3.344×10^{-6}	0.213
38	6.827×10^{3}	3.311×10^{-4}	1.552×10^{-7}	0.169	1.193×10^{-5}	0.171
39	9.261×10^{3}	5.849×10^{-7}	3.305×10^{-7}	0.177	5.207×10^{-6}	0.228
40	8.325×10^{3}	1.616×10^{-4}	2.415×10^{-7}	0.175	2.678×10^{-6}	0.229
41	9.128×10^{3}	1.787×10^{-4}	6.730×10^{-8}	0.177	2.429×10^{-5}	0.196
42	5.866×10^{3}	7.299×10^{-8}	1.543×10^{-7}	0.187	1.048×10^{-5}	0.170
43	3.939×10^{3}	8.506×10^{-8}	8.761×10^{-8}	0.175	2.243×10^{-5}	0.155
44	7.083×10^{3}	1.960×10^{-7}	3.924×10^{-8}	0.177	1.067×10^{-5}	0.209
45	5.046×10^{3}	9.244×10^{-4}	1.116×10^{-8}	0.178	1.107×10^{-5}	0.203
46	8.197×10^{3}	1.096×10^{-5}	8.365×10^{-8}	0.181	1.770×10^{-5}	0.168
47	7.787×10^{3}	6.368×10^{-8}	4.751×10^{-8}	0.169	4.308×10^{-6}	0.101
48	9.31×10^{2}	6.147×10^{-5}	1.467×10^{-7}	0.182	1.401×10^{-5}	0.200
49	1.294×10^{3}	8.885×10^{-7}	8.909×10^{-9}	0.180	5.027×10^{-6}	0.219
50	3.934×10^{3}	2.093×10^{-4}	5.018×10^{-8}	0.168	2.233×10^{-5}	0.188

TABLE D-2. SAMPLED VALUES FOR THE HUMAN INTRUSION SCENARIO (CASES $E1_a$ AND $E1_b$) (Concluded)

Simulation	x(7)	x(8)	x(9)	x(10)	x(11)	x(12)
1	1.460×10^{-6}	3.297×10^{-3}	3.491×10^{-8}	2.627×10^{-3}	2.767×10^{-7}	9.508×10^{-4}
2	1.616×10^{-6}	9.257×10^{-4}	4.313×10^{-7}	3.476×10^{-3}	1.779×10^{-7}	3.560×10^{-3}
3	1.084×10^{-6}	1.243×10^{-3}	1.930×10^{-7}	2.415×10^{-3}	7.534×10^{-8}	1.242×10^{-3}
4	1.378×10^{-6}	8.037×10^{-4}	2.595×10^{-8}	1.419×10^{-3}	6.362×10^{-8}	3.085×10^{-3}
5	2.095×10^{-7}	2.124×10^{-3}	3.466×10^{-8}	9.120×10^{-4}	4.414×10^{-7}	4.503×10^{-3}
6	1.070×10^{-6}	1.846×10^{-3}	5.717×10^{-7}	1.772×10^{-3}	7.922×10^{-8}	8.281×10^{-4}
7	2.277×10^{-6}	1.888×10^{-3}	3.726×10^{-7}	6.310×10^{-3}	7.778×10^{-8}	2.492×10^{-3}
8	1.353×10^{-6}	8.269×10^{-4}	1.794×10^{-8}	2.113×10^{-3}	1.500×10^{-7}	1.979×10^{-3}
9	9.325×10^{-7}	9.258×10^{-4}	1.705×10^{-7}	1.712×10^{-3}	2.109×10^{-7}	2.034×10^{-3}
10	1.239×10^{-6}	1.223×10^{-3}	7.945×10^{-8}	1.866×10^{-3}	2.253×10^{-7}	1.250×10^{-3}
11	1.557×10^{-6}	2.851×10^{-3}	2.030×10^{-7}	2.463×10^{-4}	7.465×10^{-8}	1.059×10^{-3}
12	3.193×10^{-7}	4.470×10^{-3}	1.263×10^{-7}	2.018×10^{-3}	1.753×10^{-7}	3.203×10^{-3}
13	4.511×10^{-6}	7.458×10^{-4}	1.200×10^{-7}	2.549×10^{-3}	5.855×10^{-8}	5.537×10^{-4}
14	1.787×10^{-7}	8.654×10^{-4}	9.750×10^{-8}	3.719×10^{-3}	2.338×10^{-7}	4.524×10^{-4}
15	3.759×10^{-7}	2.342×10^{-3}	5.196×10^{-8}	2.830×10^{-3}	1.079×10^{-7}	7.082×10^{-4}
16	4.014×10^{-7}	2.472×10^{-3}	3.469×10^{-8}	1.500×10^{-4}	1.549×10^{-7}	2.984×10^{-3}
17	4.229×10^{-7}	8.657×10^{-4}	5.243×10^{-8}	6.298×10^{-4}	1.623×10^{-7}	1.339×10^{-3}
18	6.363×10^{-7}	3.703×10^{-3}	1.283×10^{-7}	1.608×10^{-3}	4.534×10^{-8}	2.553×10^{-3}
19	9.940×10^{-7}	5.346×10^{-4}	1.821×10^{-7}	1.321×10^{-3}	7.173×10^{-7}	4.256×10^{-3}
20	1.103×10^{-6}	3.210×10^{-3}	1.781×10^{-7}	3.819×10^{-3}	6.701×10^{-8}	9.659×10^{-4}
21	4.081×10^{-7}	4.720×10^{-3}	2.585×10^{-8}	2.695×10^{-3}	9.149×10^{-8}	2.862×10^{-3}
22	8.257×10^{-7}	4.635×10^{-4}	1.113×10^{-7}	3.106×10^{-4}	9.461×10^{-8}	2.141×10^{-3}
23	4.808×10^{-7}	1.330×10^{-3}	5.038×10^{-8}	4.884×10^{-4}	2.663×10^{-7}	9.390×10^{-4}
24	1.194×10^{-6}	3.112×10^{-3}	2.443×10^{-7}	2.959×10^{-3}	8.673×10^{-8}	4.428×10^{-3}
25	3.715×10^{-7}	7.128×10^{-4}	1.532×10^{-7}	3.534×10^{-3}	2.770×10^{-8}	4.039×10^{-4}
26	1.852×10^{-6}	6.086×10^{-4}	1.855×10^{-7}	8.051×10^{-4}	4.097×10^{-8}	4.335×10^{-3}
27	1.039×10^{-6}	2.356×10^{-3}	5.816×10^{-8}	1.543×10^{-3}	2.545×10^{-7}	1.185×10^{-3}
28	1.122×10^{-6}	3.527×10^{-3}	1.002×10^{-7}	3.301×10^{-3}	5.486×10^{-8}	9.426×10^{-4}
29	2.899×10^{-6}	1.360×10^{-3}	1.599×10^{-7}	2.852×10^{-3}	2.073×10^{-7}	8.991×10^{-4}
30	4.971×10^{-7}	1.003×10^{-3}	1.542×10^{-7}	1.816×10^{-3}	7.077×10^{-8}	3.202×10^{-4}
31	2.018×10^{-6}	1.033×10^{-3}	1.677×10^{-7}	1.887×10^{-3}	1.064×10^{-7}	1.790×10^{-3}
32	7.095×10^{-7}	2.856×10^{-3}	1.517×10^{-7}	4.982×10^{-3}	5.636×10^{-8}	1.037×10^{-3}
33	1.023×10^{-6}	2.234×10^{-3}	2.239×10^{-7}	1.400×10^{-3}	7.758×10^{-8}	5.078×10^{-4}
34	7.512×10^{-7}	1.181×10^{-3}	1.576×10^{-7}	2.011×10^{-3}	5.017×10^{-8}	9.884×10^{-4}
35	2.491×10^{-6}	1.030×10^{-3}	1.699×10^{-7}	5.052×10^{-4}	1.264×10^{-7}	2.011×10^{-3}
36	4.070×10^{-7}	3.279×10^{-3}	6.099×10^{-8}	2.459×10^{-3}	1.484×10^{-8}	1.813×10^{-3}
37	1.453×10^{-6}	1.831×10^{-3}	5.428×10^{-8}	1.160×10^{-3}	3.426×10^{-8}	1.387×10^{-3}
38	1.675×10^{-6}	1.916×10^{-3}	1.250×10^{-7}	1.800×10^{-3}	1.624×10^{-7}	4.833×10^{-4}
39	1.170×10^{-6}	1.890×10^{-3}	8.531×10^{-8}	3.364×10^{-3}	1.129×10^{-7}	1.470×10^{-3}
40	8.130×10^{-7}	1.177×10^{-3}	1.637×10^{-7}	8.022×10^{-4}	2.079×10^{-7}	2.741×10^{-3}
41	8.802×10^{-7}	1.530×10^{-3}	2.644×10^{-8}	2.318×10^{-3}	2.121×10^{-7}	8.177×10^{-4}
42	3.111×10^{-7}	6.389×10^{-4}	1.633×10^{-7}	2.263×10^{-3}	9.466×10^{-8}	3.985×10^{-4}
43	1.256×10^{-6}	7.969×10^{-4}	3.075×10^{-7}	4.488×10^{-3}	8.828×10^{-8}	1.195×10^{-3}
44	1.179×10^{-6}	2.965×10^{-3}	1.507×10^{-7}	1.278×10^{-3}	1.752×10^{-7}	1.457×10^{-3}
45	3.337×10^{-6}	2.312×10^{-3}	8.076×10^{-8}	2.831×10^{-3}	1.401×10^{-7}	1.485×10^{-3}
46	4.094×10^{-7}	1.792×10^{-3}	7.847×10^{-8}	5.861×10^{-3}	1.474×10^{-7}	3.099×10^{-3}
47	1.083×10^{-6}	9.805×10^{-4}	2.069×10^{-8}	2.611×10^{-3}	1.260×10^{-7}	1.960×10^{-3}
48	3.131×10^{-6}	4.359×10^{-3}	2.322×10^{-7}	3.370×10^{-4}	7.312×10^{-8}	1.072×10^{-3}
49	8.855×10^{-7}	9.582×10^{-3}	8.581×10^{-8}	2.235×10^{-3}	8.558×10^{-8}	3.223×10^{-3}
50	5.023×10^{-7}	2.238×10^{-3}	1.590×10^{-7}	2.312×10^{-3}	1.242×10^{-7}	2.889×10^{-3}

TABLE D-3. ALTERNATE SOLUBILITY SAMPLING (Cases $E1_c$ and $E1_e$)

SIMULATION	X(2) SOLUBILITY (MOLAR)
1	2.687×10^{-5}
2	2.309×10^{-7}
3	4.663×10^{-7}
4	1.478×10^{-8}
5	3.449×10^{-5}
6	7.371×10^{-8}
7	8.245×10^{-7}
8	3.228×10^{-5}
9	1.621×10^{-8}
10	4.006×10^{-8}
11	9.083×10^{-7}
12	2.308×10^{-8}
13	2.382×10^{-6}
14	5.847×10^{-8}
15	6.096×10^{-6}
16	5.258×10^{-6}
17	3.762×10^{-7}
18	8.490×10^{-8}
19	5.315×10^{-5}
20	7.106×10^{-7}
21	2.600×10^{-7}
22	2.766×10^{-7}
23	8.759×10^{-5}
24	2.107×10^{-6}
25	4.365×10^{-5}
26	6.239×10^{-5}
27	3.013×10^{-8}
28	3.571×10^{-7}
29	1.716×10^{-5}
30	2.336×10^{-7}
31	6.125×10^{-5}
32	1.148×10^{-8}
33	1.069×10^{-7}
34	3.349×10^{-6}
35	1.018×10^{-8}
36	6.776×10^{-8}
37	3.906×10^{-8}
38	4.786×10^{-5}
39	6.994×10^{-7}
40	2.967×10^{-5}
41	3.173×10^{-5}
42	1.747×10^{-7}
43	1.934×10^{-7}
44	3.375×10^{-7}
45	9.489×10^{-5}
46	4.934×10^{-6}
47	1.595×10^{-7}
48	1.558×10^{-5}
49	9.242×10^{-7}
50	3.525×10^{-5}

TABLE D-4. ALTERNATE SAMPLING ON ROOM CONDUCTIVITY AND POROSITY (Cases $E1_d$ and $E1_e$)

SIMULATION	X(3) ROOM CONDUCTIVITY	X(4) ROOM POROSITY
1	4.450×10^{-12}	1.06×10^{-1}
2	1.374×10^{-11}	1.17×10^{-1}
3	1.311×10^{-11}	1.13×10^{-1}
4	6.363×10^{-12}	9.160×10^{-2}
5	1.358×10^{-11}	8.575×10^{-2}
6	1.127×10^{-11}	1.25×10^{-1}
7	1.104×10^{-11}	1.08×10^{-1}
8	9.305×10^{-12}	8.593×10^{-2}
9	1.420×10^{-11}	1.04×10^{-1}
10	9.387×10^{-12}	9.135×10^{-2}
11	1.485×10^{-12}	7.138×10^{-2}
12	1.682×10^{-12}	1.14×10^{-1}
13	1.152×10^{-11}	9.191×10^{-2}
14	8.408×10^{-12}	7.549×10^{-2}
15	3.759×10^{-12}	1.15×10^{-1}
16	8.691×10^{-12}	1.18×10^{-1}
17	1.033×10^{-11}	1.08×10^{-1}
18	1.148×10^{-11}	1.04×10^{-1}
19	1.211×10^{-11}	1.11×10^{-1}
20	7.117×10^{-12}	9.473×10^{-2}
21	1.027×10^{-11}	7.937×10^{-2}
22	6.035×10^{-12}	9.447×10^{-2}
23	1.918×10^{-11}	1.10×10^{-1}
24	6.630×10^{-12}	1.17×10^{-1}
25	1.640×10^{-12}	1.02×10^{-1}
26	1.083×10^{-11}	7.637×10^{-2}
27	1.730×10^{-11}	1.01×10^{-1}
28	1.228×10^{-11}	1.19×10^{-1}
29	4.576×10^{-12}	1.05×10^{-1}
30	4.546×10^{-12}	1.10×10^{-1}
31	5.446×10^{-12}	9.990×10^{-2}
32	8.029×10^{-12}	8.664×10^{-2}
33	9.306×10^{-13}	9.156×10^{-2}
34	4.447×10^{-12}	7.331×10^{-2}
35	3.809×10^{-12}	8.575×10^{-2}
36	1.047×10^{-11}	1.38×10^{-1}
37	4.772×10^{-12}	8.477×10^{-2}
38	1.483×10^{-11}	7.832×10^{-2}
39	2.910×10^{-11}	9.411×10^{-2}
40	2.188×10^{-11}	8.982×10^{-2}
41	7.351×10^{-12}	9.424×10^{-2}
42	1.476×10^{-11}	1.17×10^{-1}
43	9.137×10^{-12}	9.006×10^{-2}
44	4.754×10^{-12}	9.230×10^{-2}
45	1.790×10^{-12}	9.565×10^{-2}
46	8.793×10^{-12}	1.01×10^{-1}
47	5.541×10^{-12}	7.781×10^{-2}
48	1.413×10^{-11}	1.05×10^{-1}
49	1.509×10^{-12}	9.995×10^{-2}
50	5.790×10^{-12}	7.623×10^{-2}

TABLE D-5. SAMPLED VALUES FOR INTRUSION SCENARIO CASE $E1_f$

Parameters

x(1)	hydraulic conductivity (m/s) in Culebra Dolomite Member region 1
x(2)	hydraulic conductivity (m/s) in Culebra Dolomite Member region 2
x(3)	hydraulic conductivity (m/s) in Culebra Dolomite Member region 3
x(4)	hydraulic conductivity (m/s) in Culebra Dolomite Member region 4
x(5)	hydraulic conductivity (m/s) in Culebra Dolomite Member region 5
x(6)	hydraulic conductivity (m/s) in Culebra Dolomite Member region 6
x(7)	hydraulic conductivity (m/s) in Culebra Dolomite Member region 7
x(8)	hydraulic conductivity (m/s) in Culebra Dolomite Member region 8
x(9)	hydraulic conductivity (m/s) in Culebra Dolomite Member region 9
x(10)	hydraulic conductivity (m/s) in Culebra Dolomite Member region 10
x(11)	hydraulic conductivity (m/s) in Culebra Dolomite Member region 11
x(12)	hydraulic conductivity (m/s) in Culebra Dolomite Member region 12
x(13)	hydraulic conductivity (m/s) in Culebra Dolomite Member region 13
x(14)	hydraulic conductivity (m/s) in Culebra Dolomite Member region 14
x(15)	hydraulic conductivity (m/s) in Culebra Dolomite Member region 15
x(16)	plutonium solubility (molar)
x(17)	uranium solubility (molar)
x(18)	americium solubility (molar)
x(19)	neptunium solubility (molar)
x(20)	thorium solubility (molar)
x(21)	radium solubility (molar)
x(22)	lead solubility (molar)
x(23)	repository hydraulic conductivity (m/s)
x(24)	repository porosity
x(25)	borehole hydraulic conductivity (m/s)
x(26)	borehole porosity
x(27)	pressure (Pa) driving for flow through the repository
x(28)	intrusion time (years)

TABLE D-5. SAMPLED VALUES FOR INTRUSION SCENARIO CASE $E1_f$

Simulation	x(1)	x(2)	x(3)	x(4)	x(5)	x(6)	x(7)
1	3.006×10^{-8}	1.332×10^{-8}	1.703×10^{-8}	4.178×10^{-7}	1.185×10^{-7}	3.218×10^{-7}	3.877×10^{-7}
2	5.418×10^{-8}	5.279×10^{-8}	3.876×10^{-8}	1.348×10^{-6}	2.727×10^{-7}	8.163×10^{-7}	5.211×10^{-7}
3	3.497×10^{-8}	2.761×10^{-8}	1.844×10^{-8}	3.371×10^{-7}	8.009×10^{-8}	2.892×10^{-7}	2.791×10^{-7}
4	3.139×10^{-8}	2.636×10^{-8}	1.580×10^{-8}	4.778×10^{-7}	2.705×10^{-7}	3.955×10^{-7}	5.249×10^{-7}
5	2.446×10^{-7}	2.385×10^{-7}	8.661×10^{-8}	5.944×10^{-7}	1.406×10^{-7}	3.701×10^{-7}	4.366×10^{-7}
6	5.024×10^{-8}	6.081×10^{-8}	3.319×10^{-8}	7.665×10^{-7}	2.350×10^{-7}	5.363×10^{-7}	3.916×10^{-7}
7	5.117×10^{-8}	7.133×10^{-8}	2.981×10^{-8}	2.056×10^{-6}	4.023×10^{-7}	1.210×10^{-6}	7.522×10^{-7}
8	6.455×10^{-8}	1.271×10^{-7}	5.123×10^{-8}	1.888×10^{-7}	1.033×10^{-7}	1.986×10^{-7}	2.010×10^{-7}
9	1.660×10^{-7}	3.507×10^{-7}	9.445×10^{-8}	1.342×10^{-6}	3.057×10^{-7}	5.111×10^{-7}	5.119×10^{-7}
10	1.808×10^{-8}	2.034×10^{-8}	1.426×10^{-8}	8.200×10^{-7}	2.664×10^{-7}	5.414×10^{-7}	5.548×10^{-7}
11	1.493×10^{-7}	3.345×10^{-7}	8.419×10^{-8}	2.268×10^{-6}	1.281×10^{-6}	2.344×10^{-6}	1.277×10^{-6}
12	5.646×10^{-8}	7.184×10^{-8}	3.246×10^{-8}	1.624×10^{-6}	4.140×10^{-7}	1.287×10^{-6}	9.002×10^{-7}
13	3.657×10^{-8}	2.717×10^{-8}	1.616×10^{-8}	6.385×10^{-7}	2.390×10^{-7}	4.845×10^{-7}	4.641×10^{-7}
14	1.844×10^{-8}	2.032×10^{-8}	1.696×10^{-8}	8.239×10^{-7}	3.119×10^{-7}	5.122×10^{-7}	6.244×10^{-7}
15	1.405×10^{-7}	3.312×10^{-7}	7.821×10^{-8}	4.728×10^{-7}	2.345×10^{-7}	3.443×10^{-7}	4.187×10^{-7}
16	8.498×10^{-8}	9.619×10^{-8}	3.483×10^{-8}	2.341×10^{-6}	1.320×10^{-6}	3.617×10^{-6}	1.833×10^{-6}
17	8.507×10^{-8}	7.426×10^{-8}	6.724×10^{-8}	1.239×10^{-6}	3.704×10^{-7}	8.469×10^{-7}	7.210×10^{-7}
18	9.228×10^{-8}	7.302×10^{-8}	3.161×10^{-8}	1.440×10^{-6}	3.492×10^{-7}	6.160×10^{-7}	7.018×10^{-7}
19	4.453×10^{-8}	5.329×10^{-8}	3.158×10^{-8}	1.500×10^{-6}	5.416×10^{-7}	2.076×10^{-6}	7.723×10^{-7}
20	7.326×10^{-8}	8.669×10^{-8}	5.083×10^{-8}	2.773×10^{-7}	1.912×10^{-7}	2.850×10^{-7}	3.099×10^{-7}
21	9.848×10^{-8}	1.382×10^{-7}	5.330×10^{-8}	5.940×10^{-7}	1.450×10^{-7}	4.213×10^{-7}	4.756×10^{-7}
22	5.410×10^{-8}	4.373×10^{-8}	2.304×10^{-8}	1.982×10^{-6}	6.977×10^{-7}	1.226×10^{-6}	1.110×10^{-6}
23	1.187×10^{-7}	1.871×10^{-7}	7.937×10^{-8}	1.711×10^{-7}	6.592×10^{-8}	1.619×10^{-7}	1.919×10^{-7}
24	4.812×10^{-8}	5.053×10^{-8}	2.367×10^{-8}	2.969×10^{-7}	8.549×10^{-8}	1.221×10^{-7}	2.366×10^{-7}
25	3.263×10^{-8}	3.646×10^{-8}	2.301×10^{-8}	7.938×10^{-7}	2.595×10^{-7}	8.021×10^{-7}	4.666×10^{-7}
26	9.247×10^{-8}	1.045×10^{-7}	3.960×10^{-8}	2.067×10^{-6}	5.793×10^{-7}	1.473×10^{-6}	9.241×10^{-7}
27	1.056×10^{-7}	1.206×10^{-7}	7.158×10^{-8}	2.569×10^{-7}	9.470×10^{-8}	2.023×10^{-7}	2.880×10^{-7}
28	6.769×10^{-9}	1.880×10^{-8}	9.905×10^{-9}	9.249×10^{-7}	2.421×10^{-7}	4.164×10^{-7}	5.301×10^{-7}
29	3.569×10^{-8}	3.149×10^{-8}	2.205×10^{-8}	1.693×10^{-6}	3.909×10^{-7}	9.768×10^{-7}	7.056×10^{-7}
30	7.649×10^{-8}	1.329×10^{-7}	4.270×10^{-8}	4.498×10^{-7}	1.136×10^{-7}	3.208×10^{-7}	3.370×10^{-7}
31	1.448×10^{-7}	3.230×10^{-7}	8.296×10^{-8}	7.764×10^{-7}	2.956×10^{-7}	8.783×10^{-7}	7.268×10^{-7}
32	4.338×10^{-8}	3.275×10^{-8}	1.966×10^{-8}	2.318×10^{-7}	8.160×10^{-8}	3.001×10^{-7}	2.575×10^{-7}
33	6.996×10^{-8}	9.749×10^{-8}	3.501×10^{-8}	5.215×10^{-7}	2.026×10^{-7}	3.037×10^{-7}	4.041×10^{-7}
34	7.561×10^{-8}	1.129×10^{-7}	6.156×10^{-8}	9.798×10^{-7}	3.251×10^{-7}	5.665×10^{-7}	6.620×10^{-7}
35	1.098×10^{-7}	1.060×10^{-7}	5.639×10^{-8}	1.805×10^{-7}	7.693×10^{-8}	2.299×10^{-7}	2.673×10^{-7}
36	4.763×10^{-8}	3.855×10^{-8}	2.780×10^{-8}	4.982×10^{-7}	2.144×10^{-7}	5.999×10^{-7}	5.624×10^{-7}
37	6.045×10^{-8}	7.243×10^{-8}	2.860×10^{-8}	3.357×10^{-7}	1.202×10^{-7}	2.849×10^{-7}	3.582×10^{-7}
38	9.797×10^{-8}	7.987×10^{-8}	4.770×10^{-8}	4.106×10^{-7}	1.084×10^{-7}	2.996×10^{-7}	2.922×10^{-7}
39	3.397×10^{-8}	3.649×10^{-8}	2.322×10^{-8}	1.195×10^{-6}	2.647×10^{-7}	4.622×10^{-7}	5.241×10^{-7}
40	2.152×10^{-8}	7.887×10^{-9}	1.118×10^{-8}	2.558×10^{-7}	1.024×10^{-7}	2.587×10^{-7}	2.483×10^{-7}
41	9.106×10^{-8}	1.231×10^{-7}	4.230×10^{-8}	6.995×10^{-7}	2.059×10^{-7}	4.022×10^{-7}	6.168×10^{-7}
42	6.404×10^{-8}	7.311×10^{-8}	2.657×10^{-8}	2.097×10^{-6}	6.963×10^{-7}	1.538×10^{-6}	9.908×10^{-7}
43	5.018×10^{-8}	2.734×10^{-8}	2.540×10^{-8}	1.077×10^{-6}	3.804×10^{-7}	8.848×10^{-7}	7.416×10^{-7}
44	1.263×10^{-7}	1.529×10^{-7}	7.926×10^{-8}	9.625×10^{-7}	2.543×10^{-7}	5.232×10^{-7}	4.889×10^{-7}
45	8.984×10^{-8}	7.387×10^{-8}	3.359×10^{-8}	1.516×10^{-6}	2.770×10^{-7}	1.126×10^{-6}	7.927×10^{-7}
46	1.290×10^{-7}	1.338×10^{-7}	7.425×10^{-8}	2.925×10^{-7}	1.357×10^{-7}	2.336×10^{-7}	2.953×10^{-7}
47	2.529×10^{-8}	2.171×10^{-8}	1.362×10^{-8}	2.554×10^{-7}	9.822×10^{-8}	2.569×10^{-7}	1.749×10^{-7}
48	1.004×10^{-7}	1.253×10^{-7}	3.982×10^{-8}	1.760×10^{-7}	5.034×10^{-8}	1.086×10^{-7}	1.610×10^{-7}
49	3.479×10^{-7}	6.239×10^{-7}	1.303×10^{-7}	4.679×10^{-7}	2.082×10^{-7}	3.547×10^{-7}	3.058×10^{-7}
50	2.748×10^{-8}	2.853×10^{-8}	1.704×10^{-8}	7.309×10^{-7}	1.268×10^{-7}	3.216×10^{-7}	4.927×10^{-7}

TABLE D-5. SAMPLED VALUES FOR INTRUSION SCENARIO CASE $E1_f$ (Continued)

Simulation	x(8)	x(9)	x(10)	x(11)	x(12)	x(13)	x(14)
1	1.107×10^{-7}	6.643×10^{-7}	1.644×10^{-7}	2.201×10^{-6}	6.421×10^{-6}	4.040×10^{-6}	6.440×10^{-6}
2	1.896×10^{-7}	1.368×10^{-6}	3.998×10^{-7}	1.529×10^{-6}	4.891×10^{-6}	1.966×10^{-6}	8.023×10^{-6}
3	8.624×10^{-8}	5.535×10^{-7}	1.448×10^{-7}	3.135×10^{-6}	4.965×10^{-6}	4.633×10^{-6}	1.055×10^{-5}
4	1.329×10^{-7}	9.920×10^{-7}	3.548×10^{-7}	4.905×10^{-6}	1.002×10^{-5}	1.067×10^{-5}	1.915×10^{-5}
5	9.113×10^{-8}	9.826×10^{-7}	2.679×10^{-7}	8.880×10^{-7}	2.634×10^{-6}	1.257×10^{-6}	5.267×10^{-6}
6	1.662×10^{-7}	7.838×10^{-7}	3.218×10^{-7}	4.282×10^{-6}	9.331×10^{-6}	5.539×10^{-6}	1.322×10^{-5}
7	3.153×10^{-7}	1.808×10^{-6}	7.847×10^{-7}	1.046×10^{-6}	2.490×10^{-6}	1.733×10^{-6}	3.447×10^{-6}
8	5.745×10^{-8}	4.432×10^{-7}	1.007×10^{-7}	5.218×10^{-6}	1.313×10^{-5}	7.784×10^{-6}	2.678×10^{-5}
9	2.371×10^{-7}	1.675×10^{-6}	5.490×10^{-7}	1.363×10^{-6}	5.637×10^{-6}	2.971×10^{-6}	5.773×10^{-6}
10	2.021×10^{-7}	1.071×10^{-6}	3.557×10^{-7}	9.838×10^{-7}	2.303×10^{-6}	9.794×10^{-7}	1.371×10^{-6}
11	7.945×10^{-7}	3.483×10^{-6}	9.513×10^{-7}	9.930×10^{-7}	2.587×10^{-6}	1.426×10^{-6}	4.863×10^{-6}
12	3.282×10^{-7}	1.912×10^{-6}	7.084×10^{-7}	3.439×10^{-6}	1.062×10^{-5}	5.539×10^{-6}	2.077×10^{-5}
13	1.531×10^{-7}	1.010×10^{-6}	3.228×10^{-7}	1.800×10^{-6}	4.380×10^{-6}	2.219×10^{-6}	6.021×10^{-6}
14	2.126×10^{-7}	1.450×10^{-6}	3.863×10^{-7}	4.498×10^{-7}	1.921×10^{-6}	6.350×10^{-7}	1.170×10^{-6}
15	1.208×10^{-7}	9.430×10^{-7}	3.071×10^{-7}	4.162×10^{-6}	8.341×10^{-6}	5.312×10^{-6}	1.250×10^{-5}
16	7.948×10^{-7}	3.802×10^{-6}	9.930×10^{-7}	3.639×10^{-6}	1.102×10^{-5}	7.907×10^{-6}	1.765×10^{-5}
17	2.516×10^{-7}	2.015×10^{-6}	6.675×10^{-7}	1.091×10^{-5}	1.627×10^{-5}	1.622×10^{-5}	2.751×10^{-5}
18	4.014×10^{-7}	1.891×10^{-6}	4.015×10^{-7}	2.938×10^{-6}	4.550×10^{-6}	2.822×10^{-6}	5.879×10^{-6}
19	7.929×10^{-7}	2.509×10^{-6}	8.014×10^{-7}	1.645×10^{-6}	3.949×10^{-6}	2.523×10^{-6}	8.205×10^{-6}
20	8.893×10^{-8}	4.846×10^{-7}	1.473×10^{-7}	8.303×10^{-7}	2.729×10^{-6}	1.416×10^{-6}	2.310×10^{-6}
21	1.757×10^{-7}	6.954×10^{-7}	2.748×10^{-7}	2.733×10^{-6}	7.600×10^{-6}	5.425×10^{-6}	9.905×10^{-6}
22	5.892×10^{-7}	1.768×10^{-6}	4.432×10^{-7}	3.459×10^{-6}	7.731×10^{-6}	4.159×10^{-6}	1.249×10^{-5}
23	3.914×10^{-8}	3.683×10^{-7}	3.255×10^{-8}	1.115×10^{-6}	2.816×10^{-6}	1.045×10^{-6}	3.441×10^{-6}
24	5.103×10^{-8}	3.773×10^{-7}	1.419×10^{-7}	3.819×10^{-6}	7.933×10^{-6}	6.810×10^{-6}	1.627×10^{-5}
25	1.593×10^{-7}	9.108×10^{-7}	2.951×10^{-7}	2.537×10^{-6}	4.503×10^{-6}	1.776×10^{-6}	9.152×10^{-6}
26	6.761×10^{-7}	3.219×10^{-6}	6.477×10^{-7}	5.050×10^{-6}	1.129×10^{-5}	8.510×10^{-6}	2.383×10^{-5}
27	7.399×10^{-8}	3.455×10^{-7}	7.834×10^{-8}	3.377×10^{-6}	5.942×10^{-6}	4.174×10^{-6}	1.028×10^{-5}
28	1.996×10^{-7}	1.348×10^{-6}	5.298×10^{-7}	2.608×10^{-6}	8.196×10^{-6}	5.284×10^{-6}	1.221×10^{-5}
29	3.443×10^{-7}	1.899×10^{-6}	5.602×10^{-7}	1.558×10^{-6}	3.886×10^{-6}	2.305×10^{-6}	1.061×10^{-5}
30	1.083×10^{-7}	9.717×10^{-7}	1.633×10^{-7}	3.578×10^{-6}	5.072×10^{-6}	5.436×10^{-6}	1.348×10^{-5}
31	2.222×10^{-7}	1.753×10^{-6}	4.204×10^{-7}	3.349×10^{-6}	8.043×10^{-6}	4.571×10^{-6}	1.516×10^{-5}
32	6.448×10^{-8}	4.782×10^{-7}	1.468×10^{-7}	5.336×10^{-6}	1.143×10^{-5}	1.104×10^{-5}	2.347×10^{-5}
33	1.300×10^{-7}	5.878×10^{-7}	2.223×10^{-7}	1.585×10^{-6}	3.700×10^{-6}	3.950×10^{-6}	8.433×10^{-6}
34	2.087×10^{-7}	1.459×10^{-6}	2.966×10^{-7}	2.428×10^{-6}	5.925×10^{-6}	3.152×10^{-6}	9.275×10^{-6}
35	6.539×10^{-8}	2.515×10^{-7}	1.218×10^{-7}	1.381×10^{-6}	3.675×10^{-6}	1.179×10^{-6}	7.877×10^{-6}
36	1.706×10^{-7}	9.601×10^{-7}	3.610×10^{-7}	1.239×10^{-6}	3.494×10^{-6}	3.584×10^{-6}	5.711×10^{-6}
37	1.134×10^{-7}	5.403×10^{-7}	2.164×10^{-7}	4.317×10^{-6}	9.705×10^{-6}	4.907×10^{-6}	1.406×10^{-5}
38	9.545×10^{-8}	8.081×10^{-7}	2.116×10^{-7}	4.186×10^{-6}	9.307×10^{-6}	5.569×10^{-6}	1.594×10^{-5}
39	1.400×10^{-7}	1.103×10^{-6}	4.187×10^{-7}	1.401×10^{-6}	6.261×10^{-6}	2.199×10^{-6}	5.688×10^{-6}
40	7.230×10^{-8}	4.520×10^{-7}	1.426×10^{-7}	4.876×10^{-6}	1.198×10^{-5}	1.333×10^{-5}	3.186×10^{-5}
41	1.625×10^{-7}	9.726×10^{-7}	2.464×10^{-7}	4.749×10^{-6}	1.593×10^{-5}	1.158×10^{-5}	1.896×10^{-5}
42	6.774×10^{-7}	3.149×10^{-6}	8.471×10^{-7}	7.119×10^{-6}	1.404×10^{-5}	7.298×10^{-6}	2.390×10^{-5}
43	3.515×10^{-7}	1.730×10^{-6}	5.926×10^{-7}	2.438×10^{-6}	7.035×10^{-6}	4.036×10^{-6}	9.712×10^{-6}
44	1.353×10^{-7}	8.904×10^{-7}	2.355×10^{-7}	2.056×10^{-6}	4.213×10^{-6}	2.599×10^{-6}	5.302×10^{-6}
45	3.459×10^{-7}	1.471×10^{-6}	4.307×10^{-7}	3.471×10^{-6}	4.658×10^{-6}	2.429×10^{-6}	6.464×10^{-6}
46	8.693×10^{-8}	4.657×10^{-7}	2.082×10^{-7}	7.011×10^{-7}	2.454×10^{-6}	1.390×10^{-6}	2.042×10^{-6}
47	6.440×10^{-8}	2.770×10^{-7}	7.230×10^{-8}	4.530×10^{-6}	1.139×10^{-5}	9.787×10^{-6}	2.158×10^{-5}
48	4.146×10^{-8}	2.014×10^{-7}	6.664×10^{-8}	6.199×10^{-7}	2.066×10^{-6}	8.295×10^{-7}	1.360×10^{-6}
49	1.495×10^{-7}	6.692×10^{-7}	2.514×10^{-7}	1.256×10^{-5}	3.154×10^{-5}	1.753×10^{-5}	5.840×10^{-5}
50	1.536×10^{-7}	8.830×10^{-7}	2.336×10^{-7}	9.462×10^{-6}	2.346×10^{-5}	1.358×10^{-5}	3.855×10^{-5}

TABLE D-5. SAMPLED VALUES FOR INTRUSION SCENARIO CASE $E1_f$ (Continued)

Simulation	x(15)	x(16)	x(17)	x(18)	x(19)	x(20)	x(21)
1	2.108×10^{-5}	1.767×10^{-8}	1.757×10^{-6}	2.595×10^{-6}	6.153×10^{-8}	2.035×10^{-9}	8.164×10^{-7}
2	1.498×10^{-5}	5.821×10^{-7}	9.933×10^{-6}	6.429×10^{-9}	2.203×10^{-6}	8.235×10^{-8}	2.029×10^{-7}
3	3.398×10^{-5}	5.258×10^{-8}	1.884×10^{-8}	4.136×10^{-8}	1.354×10^{-7}	1.378×10^{-7}	1.866×10^{-9}
4	1.074×10^{-5}	1.118×10^{-6}	1.158×10^{-7}	8.244×10^{-7}	1.706×10^{-7}	3.138×10^{-7}	4.467×10^{-8}
5	1.517×10^{-5}	3.506×10^{-6}	1.712×10^{-8}	6.377×10^{-8}	6.322×10^{-9}	1.949×10^{-8}	2.610×10^{-7}
6	2.062×10^{-5}	5.271×10^{-7}	1.395×10^{-6}	8.152×10^{-7}	1.450×10^{-7}	9.115×10^{-9}	5.090×10^{-7}
7	1.310×10^{-5}	9.743×10^{-8}	2.652×10^{-5}	2.387×10^{-6}	1.590×10^{-7}	3.279×10^{-8}	8.417×10^{-6}
8	9.347×10^{-6}	1.673×10^{-6}	6.368×10^{-8}	3.333×10^{-8}	1.374×10^{-6}	1.280×10^{-9}	3.268×10^{-8}
9	1.409×10^{-5}	1.535×10^{-7}	1.013×10^{-7}	2.701×10^{-6}	1.935×10^{-6}	1.384×10^{-6}	1.576×10^{-7}
10	2.989×10^{-6}	6.060×10^{-7}	4.103×10^{-7}	2.321×10^{-8}	1.570×10^{-6}	2.926×10^{-7}	3.623×10^{-7}
11	4.105×10^{-6}	7.372×10^{-8}	1.392×10^{-6}	5.469×10^{-6}	2.931×10^{-7}	1.158×10^{-7}	1.128×10^{-8}
12	2.747×10^{-5}	9.302×10^{-6}	1.256×10^{-7}	1.029×10^{-6}	1.793×10^{-7}	3.063×10^{-5}	5.165×10^{-6}
13	1.737×10^{-5}	2.673×10^{-6}	5.070×10^{-8}	6.388×10^{-8}	6.197×10^{-8}	9.521×10^{-7}	2.830×10^{-7}
14	2.516×10^{-5}	3.602×10^{-7}	1.035×10^{-6}	4.107×10^{-7}	2.425×10^{-7}	1.485×10^{-7}	2.673×10^{-8}
15	6.647×10^{-6}	8.544×10^{-9}	8.566×10^{-8}	9.091×10^{-7}	2.232×10^{-6}	2.119×10^{-8}	9.388×10^{-7}
16	7.645×10^{-6}	1.369×10^{-7}	3.241×10^{-7}	3.442×10^{-7}	2.539×10^{-7}	4.239×10^{-9}	1.083×10^{-6}
17	3.056×10^{-5}	1.063×10^{-5}	8.134×10^{-7}	8.012×10^{-7}	1.430×10^{-6}	4.065×10^{-9}	3.264×10^{-7}
18	1.935×10^{-5}	3.568×10^{-6}	9.742×10^{-8}	2.899×10^{-8}	1.354×10^{-5}	1.311×10^{-8}	1.377×10^{-7}
19	1.323×10^{-5}	5.156×10^{-7}	2.300×10^{-9}	1.967×10^{-7}	6.953×10^{-8}	1.159×10^{-6}	1.989×10^{-7}
20	2.911×10^{-5}	9.458×10^{-8}	1.201×10^{-7}	3.246×10^{-8}	4.906×10^{-8}	1.111×10^{-6}	1.852×10^{-7}
21	5.966×10^{-5}	2.385×10^{-5}	6.059×10^{-6}	3.352×10^{-8}	6.362×10^{-9}	1.511×10^{-7}	2.786×10^{-7}
22	6.110×10^{-6}	2.470×10^{-6}	8.094×10^{-9}	1.819×10^{-7}	2.704×10^{-9}	1.810×10^{-8}	3.175×10^{-6}
23	8.890×10^{-6}	4.633×10^{-7}	1.470×10^{-6}	4.866×10^{-6}	7.856×10^{-9}	2.407×10^{-8}	6.112×10^{-7}
24	1.155×10^{-5}	5.050×10^{-7}	5.219×10^{-8}	2.122×10^{-7}	7.891×10^{-6}	2.371×10^{-7}	2.387×10^{-5}
25	3.925×10^{-5}	3.490×10^{-8}	2.980×10^{-8}	3.185×10^{-6}	6.738×10^{-7}	1.417×10^{-8}	2.882×10^{-7}
26	1.754×10^{-5}	1.503×10^{-6}	1.243×10^{-6}	2.509×10^{-5}	2.051×10^{-6}	2.908×10^{-7}	9.126×10^{-9}
27	1.567×10^{-5}	3.313×10^{-7}	6.359×10^{-8}	9.625×10^{-6}	1.962×10^{-6}	2.454×10^{-7}	2.310×10^{-7}
28	1.908×10^{-5}	5.272×10^{-9}	3.479×10^{-8}	3.785×10^{-7}	8.193×10^{-8}	2.642×10^{-8}	2.919×10^{-7}
29	1.088×10^{-5}	2.987×10^{-7}	3.735×10^{-8}	1.430×10^{-7}	1.933×10^{-6}	2.652×10^{-8}	7.683×10^{-9}
30	8.284×10^{-5}	4.432×10^{-7}	2.513×10^{-7}	5.891×10^{-7}	5.170×10^{-7}	2.171×10^{-7}	2.713×10^{-6}
31	2.510×10^{-5}	1.097×10^{-8}	1.409×10^{-5}	2.512×10^{-8}	7.512×10^{-7}	5.421×10^{-8}	1.300×10^{-7}
32	9.806×10^{-6}	3.118×10^{-8}	1.395×10^{-7}	4.563×10^{-7}	9.213×10^{-7}	2.228×10^{-6}	5.777×10^{-8}
33	1.089×10^{-5}	4.376×10^{-7}	1.666×10^{-7}	4.763×10^{-7}	6.733×10^{-7}	6.511×10^{-8}	5.743×10^{-8}
34	2.033×10^{-5}	8.307×10^{-8}	1.401×10^{-6}	1.676×10^{-5}	2.672×10^{-8}	6.985×10^{-7}	2.864×10^{-7}
35	6.881×10^{-6}	3.469×10^{-7}	1.233×10^{-7}	3.704×10^{-8}	2.402×10^{-5}	4.413×10^{-6}	1.532×10^{-5}
36	2.366×10^{-5}	2.976×10^{-6}	2.101×10^{-8}	1.122×10^{-5}	1.845×10^{-5}	1.294×10^{-9}	2.446×10^{-9}
37	4.103×10^{-5}	1.020×10^{-7}	2.229×10^{-6}	2.236×10^{-7}	1.607×10^{-7}	2.173×10^{-7}	1.098×10^{-7}
38	1.141×10^{-5}	3.775×10^{-7}	9.478×10^{-8}	1.351×10^{-7}	3.686×10^{-8}	2.704×10^{-6}	4.729×10^{-8}
39	7.239×10^{-6}	2.157×10^{-7}	8.989×10^{-8}	1.183×10^{-8}	1.230×10^{-8}	4.221×10^{-8}	7.740×10^{-8}
40	1.469×10^{-5}	2.759×10^{-7}	1.674×10^{-5}	9.513×10^{-8}	1.855×10^{-6}	2.716×10^{-9}	1.897×10^{-8}
41	1.532×10^{-5}	4.046×10^{-8}	9.996×10^{-9}	3.016×10^{-8}	7.832×10^{-6}	1.007×10^{-8}	2.746×10^{-6}
42	9.341×10^{-5}	2.995×10^{-8}	3.219×10^{-8}	5.595×10^{-7}	1.739×10^{-7}	2.140×10^{-7}	3.389×10^{-7}
43	2.630×10^{-5}	4.984×10^{-10}	1.394×10^{-7}	1.879×10^{-6}	8.435×10^{-7}	4.964×10^{-7}	2.093×10^{-6}
44	5.692×10^{-5}	2.619×10^{-8}	7.033×10^{-8}	6.403×10^{-9}	2.089×10^{-6}	3.081×10^{-6}	4.529×10^{-9}
45	1.160×10^{-5}	1.282×10^{-7}	2.140×10^{-6}	7.485×10^{-8}	1.116×10^{-7}	1.012×10^{-7}	2.606×10^{-7}
46	3.557×10^{-5}	1.523×10^{-7}	1.967×10^{-6}	3.398×10^{-7}	5.232×10^{-8}	7.976×10^{-8}	1.120×10^{-8}
47	2.006×10^{-5}	5.134×10^{-7}	1.008×10^{-6}	1.699×10^{-6}	3.004×10^{-8}	2.510×10^{-7}	7.025×10^{-7}
48	1.470×10^{-5}	2.738×10^{-6}	3.682×10^{-8}	1.681×10^{-5}	4.238×10^{-7}	3.519×10^{-9}	2.473×10^{-7}
49	6.051×10^{-6}	7.042×10^{-9}	4.787×10^{-8}	3.396×10^{-8}	2.934×10^{-9}	2.955×10^{-8}	1.027×10^{-7}
50	4.988×10^{-6}	1.628×10^{-6}	1.953×10^{-6}	9.146×10^{-6}	5.971×10^{-8}	2.284×10^{-6}	1.477×10^{-9}

TABLE D-5. SAMPLED VALUES FOR INTRUSION SCENARIO CASE $E1_f$ (Concluded)

Simulation	x(22)	x(23)	x(24)	x(25)	x(26)	x(27)	x(28)
1	4.562×10^{-9}	1.519×10^{-7}	0.186	9.530×10^{-6}	0.197	1.416×10^{7}	7.844×10^{3}
2	1.081×10^{-6}	5.213×10^{-8}	0.179	8.530×10^{-6}	0.201	9.592×10^{6}	9.599×10^{3}
3	1.131×10^{-6}	6.623×10^{-8}	0.197	1.641×10^{-5}	0.217	6.479×10^{6}	2.239×10^{3}
4	2.917×10^{-6}	6.394×10^{-8}	0.185	1.645×10^{-5}	0.168	1.329×10^{7}	6.898×10^{3}
5	5.335×10^{-7}	5.327×10^{-8}	0.177	5.628×10^{-6}	0.236	7.959×10^{6}	6.730×10^{3}
6	3.671×10^{-8}	7.682×10^{-8}	0.202	2.606×10^{-6}	0.256	1.278×10^{7}	2.181×10^{3}
7	7.049×10^{-8}	6.431×10^{-8}	0.183	3.282×10^{-6}	0.176	6.471×10^{6}	2.48×10^{2}
8	3.120×10^{-9}	1.609×10^{-7}	0.180	2.656×10^{-6}	0.229	1.283×10^{7}	8.789×10^{3}
9	2.220×10^{-7}	9.884×10^{-8}	0.203	8.232×10^{-6}	0.209	7.549×10^{6}	8.512×10^{3}
10	6.086×10^{-8}	4.262×10^{-8}	0.186	2.953×10^{-5}	0.256	1.047×10^{7}	4.642×10^{3}
11	1.530×10^{-5}	9.655×10^{-8}	0.168	5.182×10^{-6}	0.257	1.178×10^{7}	2.619×10^{3}
12	2.217×10^{-8}	2.189×10^{-7}	0.189	9.598×10^{-6}	0.217	1.096×10^{7}	7.32×10^{2}
13	3.242×10^{-9}	1.056×10^{-7}	0.169	3.147×10^{-6}	0.207	6.156×10^{6}	7.278×10^{3}
14	1.563×10^{-7}	7.916×10^{-8}	0.181	1.690×10^{-6}	0.177	8.093×10^{6}	1.221×10^{3}
15	2.975×10^{-9}	4.707×10^{-8}	0.179	7.238×10^{-6}	0.189	1.015×10^{7}	6.917×10^{3}
16	3.364×10^{-7}	4.874×10^{-8}	0.174	8.463×10^{-6}	0.235	6.639×10^{6}	6.838×10^{3}
17	1.648×10^{-6}	1.094×10^{-7}	0.169	3.329×10^{-5}	0.232	6.813×10^{6}	5.508×10^{3}
18	1.687×10^{-7}	5.722×10^{-8}	0.183	1.494×10^{-5}	0.198	1.415×10^{7}	3.58×10^{2}
19	2.283×10^{-6}	1.085×10^{-7}	0.187	2.646×10^{-6}	0.121	7.593×10^{6}	8.494×10^{3}
20	1.419×10^{-8}	2.185×10^{-8}	0.164	5.917×10^{-6}	0.211	7.328×10^{6}	2.020×10^{3}
21	6.670×10^{-8}	9.487×10^{-8}	0.163	5.234×10^{-6}	0.136	1.063×10^{7}	5.765×10^{3}
22	2.877×10^{-8}	5.797×10^{-8}	0.190	3.934×10^{-6}	0.224	1.020×10^{7}	5.343×10^{3}
23	1.371×10^{-4}	1.100×10^{-7}	0.184	5.374×10^{-6}	0.176	8.440×10^{6}	6.760×10^{3}
24	5.311×10^{-7}	1.127×10^{-7}	0.153	5.136×10^{-6}	0.193	1.144×10^{7}	3.812×10^{3}
25	1.554×10^{-6}	4.245×10^{-8}	0.170	1.754×10^{-5}	0.188	1.042×10^{7}	8.62×10^{2}
26	4.217×10^{-8}	3.225×10^{-8}	0.178	1.895×10^{-6}	0.146	1.397×10^{7}	8.885×10^{3}
27	5.206×10^{-7}	2.386×10^{-7}	0.171	9.688×10^{-6}	0.159	6.830×10^{6}	7.635×10^{3}
28	2.693×10^{-7}	1.393×10^{-7}	0.165	5.796×10^{-6}	0.224	8.845×10^{6}	9.232×10^{3}
29	3.999×10^{-7}	1.745×10^{-7}	0.179	7.872×10^{-6}	0.165	1.195×10^{7}	2.392×10^{3}
30	1.077×10^{-7}	2.292×10^{-8}	0.191	5.181×10^{-6}	0.224	8.386×10^{6}	6.913×10^{3}
31	6.408×10^{-8}	1.193×10^{-7}	0.178	2.394×10^{-5}	0.143	1.360×10^{7}	9.32×10^{2}
32	7.356×10^{-9}	1.619×10^{-7}	0.177	6.529×10^{-6}	0.238	7.135×10^{6}	2.60×10^{2}
33	1.074×10^{-7}	1.092×10^{-7}	0.193	3.740×10^{-5}	0.199	7.577×10^{6}	3.917×10^{3}
34	1.015×10^{-7}	1.147×10^{-7}	0.170	3.038×10^{-5}	0.200	6.844×10^{6}	2.89×10^{2}
35	2.941×10^{-7}	1.121×10^{-8}	0.188	8.294×10^{-6}	0.181	9.850×10^{6}	5.637×10^{3}
36	2.045×10^{-8}	9.116×10^{-9}	0.169	1.460×10^{-5}	0.223	7.996×10^{6}	2.939×10^{3}
37	1.840×10^{-5}	6.902×10^{-8}	0.180	1.956×10^{-6}	0.260	1.312×10^{7}	1.749×10^{3}
38	6.139×10^{-7}	9.674×10^{-8}	0.165	7.835×10^{-6}	0.221	1.296×10^{7}	1.195×10^{3}
39	2.528×10^{-7}	4.320×10^{-8}	0.177	1.812×10^{-5}	0.131	1.413×10^{7}	1.595×10^{3}
40	4.909×10^{-7}	5.057×10^{-8}	0.183	4.980×10^{-6}	0.158	6.089×10^{6}	1.029×10^{3}
41	3.857×10^{-6}	1.188×10^{-7}	0.187	2.482×10^{-6}	0.154	7.019×10^{6}	6.77×10^{2}
42	3.450×10^{-8}	5.665×10^{-8}	0.188	2.274×10^{-5}	0.186	8.014×10^{6}	1.991×10^{3}
43	9.177×10^{-8}	6.018×10^{-8}	0.173	7.035×10^{-6}	0.205	1.172×10^{7}	6.571×10^{3}
44	4.137×10^{-8}	1.107×10^{-7}	0.176	5.417×10^{-6}	0.217	1.059×10^{7}	6.770×10^{3}
45	1.188×10^{-8}	1.266×10^{-7}	0.176	1.828×10^{-5}	0.172	6.369×10^{6}	9.662×10^{3}
46	3.773×10^{-7}	1.205×10^{-7}	0.184	1.097×10^{-5}	0.198	6.844×10^{6}	8.806×10^{3}
47	2.259×10^{-6}	3.315×10^{-8}	0.181	2.950×10^{-5}	0.205	1.366×10^{7}	9.326×10^{3}
48	7.045×10^{-9}	1.081×10^{-7}	0.177	8.899×10^{-6}	0.178	1.218×10^{7}	6.59×10^{2}
49	4.314×10^{-8}	2.617×10^{-8}	0.180	6.516×10^{-6}	0.176	1.023×10^{7}	1.011×10^{3}
50	3.412×10^{-8}	3.853×10^{-8}	0.178	8.160×10^{-6}	0.178	7.490×10^{6}	3.188×10^{3}

TABLE D-6. SAMPLED VALUES FOR INTRUSION SCENARIO CASE $E1_g$

Parameters

x(1)	hydraulic conductivity (m/s) in Culebra Dolomite Member region 1
x(2)	hydraulic conductivity (m/s) in Culebra Dolomite Member region 2
x(3)	hydraulic conductivity (m/s) in Culebra Dolomite Member region 3
x(4)	hydraulic conductivity (m/s) in Culebra Dolomite Member region 4
x(5)	hydraulic conductivity (m/s) in Culebra Dolomite Member region 5
x(6)	hydraulic conductivity (m/s) in Culebra Dolomite Member region 6
x(7)	hydraulic conductivity (m/s) in Culebra Dolomite Member region 7
x(8)	hydraulic conductivity (m/s) in Culebra Dolomite Member region 8
x(9)	hydraulic conductivity (m/s) in Culebra Dolomite Member region 9
x(10)	hydraulic conductivity (m/s) in Culebra Dolomite Member region 10
x(11)	hydraulic conductivity (m/s) in Culebra Dolomite Member region 11
x(12)	hydraulic conductivity (m/s) in Culebra Dolomite Member region 12
x(13)	hydraulic conductivity (m/s) in Culebra Dolomite Member region 13
x(14)	hydraulic conductivity (m/s) in Culebra Dolomite Member region 14
x(15)	hydraulic conductivity (m/s) in Culebra Dolomite Member region 15
x(16)	plutonium solubility (molar)
x(17)	uranium solubility (molar)
x(18)	americium solubility (molar)
x(19)	neptunium solubility (molar)
x(20)	thorium solubility (molar)
x(21)	radium solubility (molar)
x(22)	lead solubility (molar)
x(23)	repository hydraulic conductivity (m/s)
x(24)	repository porosity
x(25)	borehole hydraulic conductivity (m/s)
x(26)	borehole porosity
x(27)	pressure (Pa) driving for flow through the repository
x(28)	intrusion time (years)

TABLE D-6. SAMPLED VALUES FOR INTRUSION SCENARIO CASE $E1_g$

Simulation	x(1)	x(2)	x(3)	x(4)	x(5)	x(6)	x(7)
1	3.006×10^{-8}	1.332×10^{-8}	1.703×10^{-8}	4.178×10^{-7}	1.185×10^{-7}	3.218×10^{-7}	3.877×10^{-7}
2	5.418×10^{-8}	5.279×10^{-8}	3.876×10^{-8}	1.348×10^{-6}	2.727×10^{-7}	8.163×10^{-7}	5.211×10^{-7}
3	3.497×10^{-8}	2.761×10^{-8}	1.844×10^{-8}	3.371×10^{-7}	8.009×10^{-8}	2.892×10^{-7}	2.791×10^{-7}
4	3.139×10^{-8}	2.636×10^{-8}	1.580×10^{-8}	4.778×10^{-7}	2.705×10^{-7}	3.955×10^{-7}	5.249×10^{-7}
5	2.446×10^{-7}	2.385×10^{-7}	8.661×10^{-8}	5.944×10^{-7}	1.406×10^{-7}	3.701×10^{-7}	4.366×10^{-7}
6	5.024×10^{-8}	6.081×10^{-8}	3.319×10^{-8}	7.665×10^{-7}	2.350×10^{-7}	5.363×10^{-7}	3.916×10^{-7}
7	5.117×10^{-8}	7.133×10^{-8}	2.981×10^{-8}	2.056×10^{-6}	4.023×10^{-7}	1.210×10^{-6}	7.522×10^{-7}
8	6.455×10^{-8}	1.271×10^{-7}	5.123×10^{-8}	1.888×10^{-7}	1.033×10^{-7}	1.986×10^{-7}	2.010×10^{-7}
9	1.660×10^{-7}	3.507×10^{-7}	9.445×10^{-8}	1.342×10^{-6}	3.057×10^{-7}	5.111×10^{-7}	5.119×10^{-7}
10	1.808×10^{-8}	2.034×10^{-8}	1.426×10^{-8}	8.200×10^{-7}	2.664×10^{-7}	5.414×10^{-7}	5.548×10^{-7}
11	1.493×10^{-7}	3.345×10^{-7}	8.419×10^{-8}	2.268×10^{-6}	1.281×10^{-6}	2.344×10^{-6}	1.277×10^{-6}
12	5.646×10^{-8}	7.184×10^{-8}	3.246×10^{-8}	1.624×10^{-6}	4.140×10^{-7}	1.287×10^{-6}	9.002×10^{-7}
13	3.657×10^{-8}	2.717×10^{-8}	1.616×10^{-8}	6.385×10^{-7}	2.390×10^{-7}	4.845×10^{-7}	4.641×10^{-7}
14	1.844×10^{-8}	2.032×10^{-8}	1.696×10^{-8}	8.239×10^{-7}	3.119×10^{-7}	5.122×10^{-7}	6.244×10^{-7}
15	1.405×10^{-7}	3.312×10^{-7}	7.821×10^{-8}	4.728×10^{-7}	2.345×10^{-7}	3.443×10^{-7}	4.187×10^{-7}
16	8.498×10^{-8}	9.619×10^{-8}	3.483×10^{-8}	2.341×10^{-6}	1.320×10^{-6}	3.617×10^{-6}	1.833×10^{-6}
17	8.507×10^{-8}	7.426×10^{-8}	6.724×10^{-8}	1.239×10^{-6}	3.704×10^{-7}	8.469×10^{-7}	7.210×10^{-7}
18	9.228×10^{-8}	7.302×10^{-8}	3.161×10^{-8}	1.440×10^{-6}	3.492×10^{-7}	6.160×10^{-7}	7.018×10^{-7}
19	4.453×10^{-8}	5.329×10^{-8}	3.158×10^{-8}	1.500×10^{-6}	5.416×10^{-7}	2.076×10^{-6}	7.723×10^{-7}
20	7.326×10^{-8}	8.669×10^{-8}	5.083×10^{-8}	2.773×10^{-7}	1.912×10^{-7}	2.850×10^{-7}	3.099×10^{-7}
21	9.848×10^{-8}	1.382×10^{-7}	5.330×10^{-8}	5.940×10^{-7}	1.450×10^{-7}	4.213×10^{-7}	4.756×10^{-7}
22	5.410×10^{-8}	4.373×10^{-8}	2.304×10^{-8}	1.982×10^{-6}	6.977×10^{-7}	1.226×10^{-6}	1.110×10^{-6}
23	1.187×10^{-7}	1.871×10^{-7}	7.937×10^{-8}	1.711×10^{-7}	6.592×10^{-8}	1.619×10^{-7}	1.919×10^{-7}
24	4.812×10^{-8}	5.053×10^{-8}	2.367×10^{-8}	2.969×10^{-7}	8.549×10^{-8}	1.221×10^{-7}	2.366×10^{-7}
25	3.263×10^{-8}	3.646×10^{-8}	2.301×10^{-8}	7.938×10^{-7}	2.595×10^{-7}	8.021×10^{-7}	4.666×10^{-7}
26	9.247×10^{-8}	1.045×10^{-7}	3.960×10^{-8}	2.067×10^{-6}	5.793×10^{-7}	1.473×10^{-6}	9.241×10^{-7}
27	1.056×10^{-7}	1.206×10^{-7}	7.158×10^{-8}	2.569×10^{-7}	9.470×10^{-8}	2.023×10^{-7}	2.880×10^{-7}
28	6.769×10^{-9}	1.880×10^{-8}	9.905×10^{-9}	9.249×10^{-7}	2.421×10^{-7}	4.164×10^{-7}	5.301×10^{-7}
29	3.569×10^{-8}	3.149×10^{-8}	2.205×10^{-8}	1.693×10^{-6}	3.909×10^{-7}	9.768×10^{-7}	7.056×10^{-7}
30	7.649×10^{-8}	1.329×10^{-7}	4.270×10^{-8}	4.498×10^{-7}	1.136×10^{-7}	3.208×10^{-7}	3.370×10^{-7}
31	1.448×10^{-7}	3.230×10^{-7}	8.296×10^{-8}	7.764×10^{-7}	2.956×10^{-7}	8.783×10^{-7}	7.268×10^{-7}
32	4.338×10^{-8}	3.275×10^{-8}	1.966×10^{-8}	2.318×10^{-7}	8.160×10^{-8}	3.001×10^{-7}	2.575×10^{-7}
33	6.996×10^{-8}	9.749×10^{-8}	3.501×10^{-8}	5.215×10^{-7}	2.026×10^{-7}	3.037×10^{-7}	4.041×10^{-7}
34	7.561×10^{-8}	1.129×10^{-7}	6.156×10^{-8}	9.798×10^{-7}	3.251×10^{-7}	5.665×10^{-7}	6.620×10^{-7}
35	1.098×10^{-7}	1.060×10^{-7}	5.639×10^{-8}	1.805×10^{-7}	7.693×10^{-8}	2.299×10^{-7}	2.673×10^{-7}
36	4.763×10^{-8}	3.855×10^{-8}	2.780×10^{-8}	4.982×10^{-7}	2.144×10^{-7}	5.999×10^{-7}	5.624×10^{-7}
37	6.045×10^{-8}	7.243×10^{-8}	2.860×10^{-8}	3.357×10^{-7}	1.202×10^{-7}	2.849×10^{-7}	3.582×10^{-7}
38	9.797×10^{-8}	7.987×10^{-8}	4.770×10^{-8}	4.106×10^{-7}	1.084×10^{-7}	2.996×10^{-7}	2.922×10^{-7}
39	3.397×10^{-8}	3.649×10^{-8}	2.322×10^{-8}	1.195×10^{-6}	2.647×10^{-7}	4.622×10^{-7}	5.241×10^{-7}
40	2.152×10^{-8}	7.887×10^{-9}	1.118×10^{-8}	2.558×10^{-7}	1.024×10^{-7}	2.587×10^{-7}	2.483×10^{-7}
41	9.106×10^{-8}	1.231×10^{-7}	4.230×10^{-8}	6.995×10^{-7}	2.059×10^{-7}	4.022×10^{-7}	6.168×10^{-7}
42	6.404×10^{-8}	7.311×10^{-8}	2.657×10^{-8}	2.097×10^{-6}	6.963×10^{-7}	1.538×10^{-6}	9.908×10^{-7}
43	5.018×10^{-8}	2.734×10^{-8}	2.540×10^{-8}	1.077×10^{-6}	3.804×10^{-7}	8.848×10^{-7}	7.416×10^{-7}
44	1.263×10^{-7}	1.529×10^{-7}	7.926×10^{-8}	9.625×10^{-7}	2.543×10^{-7}	5.232×10^{-7}	4.889×10^{-7}
45	8.984×10^{-8}	7.387×10^{-8}	3.359×10^{-8}	1.516×10^{-6}	2.770×10^{-7}	1.126×10^{-6}	7.927×10^{-7}
46	1.290×10^{-7}	1.338×10^{-7}	7.425×10^{-8}	2.925×10^{-7}	1.357×10^{-7}	2.336×10^{-7}	2.953×10^{-7}
47	2.529×10^{-8}	2.171×10^{-8}	1.362×10^{-8}	2.554×10^{-7}	9.822×10^{-8}	2.569×10^{-7}	1.749×10^{-7}
48	1.004×10^{-7}	1.253×10^{-7}	3.982×10^{-8}	1.760×10^{-7}	5.034×10^{-8}	1.086×10^{-7}	1.610×10^{-7}
49	3.479×10^{-7}	6.239×10^{-7}	1.303×10^{-7}	4.679×10^{-7}	2.082×10^{-7}	3.547×10^{-7}	3.058×10^{-7}
50	2.748×10^{-8}	2.853×10^{-8}	1.704×10^{-8}	7.309×10^{-7}	1.268×10^{-7}	3.216×10^{-7}	4.927×10^{-7}

TABLE D-6. SAMPLED VALUES FOR INTRUSION SCENARIO CASE $E1_g$ (Continued)

Simulation	x(8)	x(9)	x(10)	x(11)	x(12)	x(13)	x(14)
1	1.107×10^{-7}	6.643×10^{-7}	1.644×10^{-7}	2.201×10^{-6}	6.421×10^{-6}	4.040×10^{-6}	6.440×10^{-6}
2	1.896×10^{-7}	1.368×10^{-6}	3.998×10^{-7}	1.529×10^{-6}	4.891×10^{-6}	1.966×10^{-6}	8.023×10^{-6}
3	8.624×10^{-8}	5.535×10^{-7}	1.448×10^{-7}	3.135×10^{-6}	4.965×10^{-6}	4.633×10^{-6}	1.055×10^{-5}
4	1.329×10^{-7}	9.920×10^{-7}	3.548×10^{-7}	4.905×10^{-6}	1.002×10^{-5}	1.067×10^{-5}	1.915×10^{-5}
5	9.113×10^{-8}	9.826×10^{-7}	2.679×10^{-7}	8.880×10^{-7}	2.634×10^{-6}	1.257×10^{-6}	5.267×10^{-6}
6	1.662×10^{-7}	7.838×10^{-7}	3.218×10^{-7}	4.282×10^{-6}	9.331×10^{-6}	5.539×10^{-6}	1.322×10^{-5}
7	3.153×10^{-7}	1.808×10^{-6}	7.847×10^{-7}	1.046×10^{-6}	2.490×10^{-6}	1.733×10^{-6}	3.447×10^{-6}
8	5.745×10^{-8}	4.432×10^{-7}	1.007×10^{-7}	5.218×10^{-6}	1.313×10^{-5}	7.784×10^{-6}	2.678×10^{-5}
9	2.371×10^{-7}	1.675×10^{-6}	5.490×10^{-7}	1.363×10^{-6}	5.637×10^{-6}	2.971×10^{-6}	5.773×10^{-6}
10	2.021×10^{-7}	1.071×10^{-6}	3.557×10^{-7}	9.838×10^{-7}	2.303×10^{-6}	9.794×10^{-7}	1.371×10^{-6}
11	7.945×10^{-7}	3.483×10^{-6}	9.513×10^{-7}	9.930×10^{-7}	2.587×10^{-6}	1.426×10^{-6}	4.863×10^{-6}
12	3.282×10^{-7}	1.912×10^{-6}	7.084×10^{-7}	3.439×10^{-6}	1.062×10^{-5}	5.539×10^{-6}	2.077×10^{-5}
13	1.531×10^{-7}	1.010×10^{-6}	3.228×10^{-7}	1.800×10^{-6}	4.380×10^{-6}	2.219×10^{-6}	6.021×10^{-6}
14	2.126×10^{-7}	1.450×10^{-6}	3.863×10^{-7}	4.498×10^{-7}	1.921×10^{-6}	6.350×10^{-7}	1.170×10^{-6}
15	1.208×10^{-7}	9.430×10^{-7}	3.071×10^{-7}	4.162×10^{-6}	8.341×10^{-6}	5.312×10^{-6}	1.250×10^{-5}
16	7.948×10^{-7}	3.802×10^{-6}	9.930×10^{-7}	3.639×10^{-6}	1.102×10^{-5}	7.907×10^{-6}	1.765×10^{-5}
17	2.516×10^{-7}	2.015×10^{-6}	6.675×10^{-7}	1.091×10^{-5}	1.627×10^{-5}	1.622×10^{-5}	2.751×10^{-5}
18	4.014×10^{-7}	1.891×10^{-6}	4.015×10^{-7}	2.938×10^{-6}	4.550×10^{-6}	2.822×10^{-6}	5.879×10^{-6}
19	7.929×10^{-7}	2.509×10^{-6}	8.014×10^{-7}	1.645×10^{-6}	3.949×10^{-6}	2.523×10^{-6}	8.205×10^{-6}
20	8.893×10^{-8}	4.846×10^{-7}	1.473×10^{-7}	8.303×10^{-7}	2.729×10^{-6}	1.416×10^{-6}	2.310×10^{-6}
21	1.757×10^{-7}	6.954×10^{-7}	2.748×10^{-7}	2.733×10^{-6}	7.600×10^{-6}	5.425×10^{-6}	9.905×10^{-6}
22	5.892×10^{-7}	1.768×10^{-6}	4.432×10^{-7}	3.459×10^{-6}	7.731×10^{-6}	4.159×10^{-6}	1.249×10^{-5}
23	3.914×10^{-8}	3.683×10^{-7}	3.255×10^{-8}	1.115×10^{-6}	2.816×10^{-6}	1.045×10^{-6}	3.441×10^{-6}
24	5.103×10^{-8}	3.773×10^{-7}	1.419×10^{-7}	3.819×10^{-6}	7.933×10^{-6}	6.810×10^{-6}	1.627×10^{-5}
25	1.593×10^{-7}	9.108×10^{-7}	2.951×10^{-7}	2.537×10^{-6}	4.503×10^{-6}	1.776×10^{-6}	9.152×10^{-6}
26	6.761×10^{-7}	3.219×10^{-6}	6.477×10^{-7}	5.050×10^{-6}	1.129×10^{-5}	8.510×10^{-6}	2.383×10^{-5}
27	7.399×10^{-8}	3.455×10^{-7}	7.834×10^{-8}	3.377×10^{-6}	5.942×10^{-6}	4.174×10^{-6}	1.028×10^{-5}
28	1.996×10^{-7}	1.348×10^{-6}	5.298×10^{-7}	2.608×10^{-6}	8.196×10^{-6}	5.284×10^{-6}	1.221×10^{-5}
29	3.443×10^{-7}	1.899×10^{-6}	5.602×10^{-7}	1.558×10^{-6}	3.886×10^{-6}	2.305×10^{-6}	1.061×10^{-5}
30	1.083×10^{-7}	9.717×10^{-7}	1.633×10^{-7}	3.578×10^{-6}	5.072×10^{-6}	5.436×10^{-6}	1.348×10^{-5}
31	2.222×10^{-7}	1.753×10^{-6}	4.204×10^{-7}	3.349×10^{-6}	8.043×10^{-6}	4.571×10^{-6}	1.516×10^{-5}
32	6.448×10^{-8}	4.782×10^{-7}	1.468×10^{-7}	5.336×10^{-6}	1.143×10^{-5}	1.104×10^{-5}	2.347×10^{-5}
33	1.300×10^{-7}	5.878×10^{-7}	2.223×10^{-7}	1.585×10^{-6}	3.700×10^{-6}	3.950×10^{-6}	8.433×10^{-6}
34	2.087×10^{-7}	1.459×10^{-6}	2.966×10^{-7}	2.428×10^{-6}	5.925×10^{-6}	3.152×10^{-6}	9.275×10^{-6}
35	6.539×10^{-8}	2.515×10^{-7}	1.218×10^{-7}	1.381×10^{-6}	3.675×10^{-6}	1.179×10^{-6}	7.877×10^{-6}
36	1.706×10^{-7}	9.601×10^{-7}	3.610×10^{-7}	1.239×10^{-6}	3.494×10^{-6}	3.584×10^{-6}	5.711×10^{-6}
37	1.134×10^{-7}	5.403×10^{-7}	2.164×10^{-7}	4.317×10^{-6}	9.705×10^{-6}	4.907×10^{-6}	1.406×10^{-5}
38	9.545×10^{-8}	8.081×10^{-7}	2.116×10^{-7}	4.186×10^{-6}	9.307×10^{-6}	5.569×10^{-6}	1.594×10^{-5}
39	1.400×10^{-7}	1.103×10^{-6}	4.187×10^{-7}	1.401×10^{-6}	6.261×10^{-6}	2.199×10^{-6}	5.688×10^{-6}
40	7.230×10^{-8}	4.520×10^{-7}	1.426×10^{-7}	4.876×10^{-6}	1.198×10^{-5}	1.333×10^{-5}	3.186×10^{-5}
41	1.625×10^{-7}	9.726×10^{-7}	2.464×10^{-7}	4.749×10^{-6}	1.593×10^{-5}	1.158×10^{-5}	1.896×10^{-5}
42	6.774×10^{-7}	3.149×10^{-6}	8.471×10^{-7}	7.119×10^{-6}	1.404×10^{-5}	7.298×10^{-6}	2.390×10^{-5}
43	3.515×10^{-7}	1.730×10^{-6}	5.926×10^{-7}	2.438×10^{-6}	7.035×10^{-6}	4.036×10^{-6}	9.712×10^{-6}
44	1.353×10^{-7}	8.904×10^{-7}	2.355×10^{-7}	2.056×10^{-6}	4.213×10^{-6}	2.599×10^{-6}	5.302×10^{-6}
45	3.459×10^{-7}	1.471×10^{-6}	4.307×10^{-7}	3.471×10^{-6}	4.658×10^{-6}	2.429×10^{-6}	6.464×10^{-6}
46	8.693×10^{-8}	4.657×10^{-7}	2.082×10^{-7}	7.011×10^{-7}	2.454×10^{-6}	1.390×10^{-6}	2.042×10^{-6}
47	6.440×10^{-8}	2.770×10^{-7}	7.230×10^{-8}	4.530×10^{-6}	1.139×10^{-5}	9.787×10^{-6}	2.158×10^{-5}
48	4.146×10^{-8}	2.014×10^{-7}	6.664×10^{-8}	6.199×10^{-7}	2.066×10^{-6}	8.295×10^{-7}	1.360×10^{-6}
49	1.495×10^{-7}	6.692×10^{-7}	2.514×10^{-7}	1.256×10^{-5}	3.154×10^{-5}	1.753×10^{-5}	5.840×10^{-5}
50	1.536×10^{-7}	8.830×10^{-7}	2.336×10^{-7}	9.462×10^{-6}	2.346×10^{-5}	1.358×10^{-5}	3.855×10^{-5}

TABLE D-6. SAMPLED VALUES FOR INTRUSION SCENARIO CASE $E1_g$ (Continued)

Simulation	x(15)	x(16)	x(17)	x(18)	x(19)	x(20)	x(21)
1	2.108×10^{-5}	4.215×10^{-8}	9.049×10^{-7}	1.174×10^{-6}	9.686×10^{-8}	9.981×10^{-9}	5.428×10^{-7}
2	1.498×10^{-5}	4.332×10^{-7}	2.872×10^{-6}	2.149×10^{-8}	1.052×10^{-6}	1.176×10^{-7}	2.146×10^{-7}
3	3.398×10^{-5}	8.722×10^{-8}	4.401×10^{-8}	7.432×10^{-8}	1.639×10^{-7}	1.658×10^{-7}	9.419×10^{-9}
4	1.074×10^{-5}	6.694×10^{-7}	1.476×10^{-7}	5.464×10^{-7}	1.912×10^{-7}	2.870×10^{-7}	7.824×10^{-8}
5	1.517×10^{-5}	1.434×10^{-6}	4.128×10^{-8}	9.919×10^{-8}	2.125×10^{-8}	4.501×10^{-8}	2.538×10^{-7}
6	2.062×10^{-5}	4.055×10^{-7}	7.758×10^{-7}	5.423×10^{-7}	1.715×10^{-7}	2.712×10^{-8}	3.962×10^{-7}
7	1.310×10^{-5}	1.316×10^{-7}	5.527×10^{-6}	1.110×10^{-6}	1.824×10^{-7}	6.366×10^{-8}	2.571×10^{-6}
8	9.347×10^{-6}	8.759×10^{-7}	9.910×10^{-8}	6.436×10^{-8}	7.680×10^{-7}	7.327×10^{-9}	6.352×10^{-8}
9	1.409×10^{-5}	1.782×10^{-7}	1.351×10^{-7}	1.205×10^{-6}	9.649×10^{-7}	7.717×10^{-7}	1.813×10^{-7}
10	2.989×10^{-6}	4.450×10^{-7}	3.432×10^{-7}	5.056×10^{-8}	8.394×10^{-7}	2.739×10^{-7}	3.158×10^{-7}
11	4.105×10^{-6}	1.093×10^{-7}	7.748×10^{-7}	1.929×10^{-6}	2.742×10^{-7}	1.477×10^{-7}	3.126×10^{-8}
12	2.747×10^{-5}	2.749×10^{-6}	1.559×10^{-7}	6.333×10^{-7}	1.976×10^{-7}	6.084×10^{-6}	1.857×10^{-6}
13	1.737×10^{-5}	1.197×10^{-6}	8.513×10^{-8}	9.930×10^{-8}	9.731×10^{-8}	6.014×10^{-7}	2.679×10^{-7}
14	2.516×10^{-5}	3.146×10^{-7}	6.359×10^{-7}	3.434×10^{-7}	2.417×10^{-7}	1.743×10^{-7}	5.556×10^{-8}
15	6.647×10^{-6}	2.597×10^{-8}	1.208×10^{-7}	5.832×10^{-7}	1.061×10^{-6}	4.758×10^{-8}	5.958×10^{-7}
16	7.645×10^{-6}	1.651×10^{-7}	2.932×10^{-7}	3.052×10^{-7}	2.492×10^{-7}	1.628×10^{-8}	6.554×10^{-7}
17	3.056×10^{-5}	3.004×10^{-6}	5.415×10^{-7}	5.361×10^{-7}	7.888×10^{-7}	1.583×10^{-8}	2.946×10^{-7}
18	1.935×10^{-5}	1.451×10^{-6}	1.316×10^{-7}	5.864×10^{-8}	3.531×10^{-6}	3.456×10^{-8}	1.657×10^{-7}
19	1.323×10^{-5}	3.996×10^{-7}	1.083×10^{-8}	2.102×10^{-7}	1.051×10^{-7}	6.858×10^{-7}	2.118×10^{-7}
20	2.911×10^{-5}	1.290×10^{-7}	1.513×10^{-7}	6.324×10^{-8}	8.328×10^{-8}	6.668×10^{-7}	2.019×10^{-7}
21	5.966×10^{-5}	5.149×10^{-6}	2.065×10^{-6}	6.460×10^{-8}	2.134×10^{-8}	1.763×10^{-7}	2.651×10^{-7}
22	6.110×10^{-6}	1.136×10^{-6}	2.505×10^{-8}	1.995×10^{-7}	1.206×10^{-8}	4.283×10^{-8}	1.342×10^{-6}
23	8.890×10^{-6}	3.721×10^{-7}	8.035×10^{-7}	1.785×10^{-6}	2.456×10^{-8}	5.181×10^{-8}	4.476×10^{-7}
24	1.155×10^{-5}	3.941×10^{-7}	8.679×10^{-8}	2.211×10^{-7}	2.463×10^{-6}	2.381×10^{-7}	5.153×10^{-6}
25	3.925×10^{-5}	6.637×10^{-8}	5.974×10^{-8}	1.345×10^{-6}	4.776×10^{-7}	3.640×10^{-8}	2.711×10^{-7}
26	1.754×10^{-5}	8.156×10^{-7}	7.184×10^{-7}	5.326×10^{-6}	1.003×10^{-6}	2.728×10^{-7}	2.714×10^{-8}
27	1.567×10^{-5}	2.975×10^{-7}	9.901×10^{-8}	2.812×10^{-6}	9.739×10^{-7}	2.436×10^{-7}	2.340×10^{-7}
28	1.908×10^{-5}	1.882×10^{-8}	6.622×10^{-8}	3.252×10^{-7}	1.172×10^{-7}	5.512×10^{-8}	2.735×10^{-7}
29	1.088×10^{-5}	2.777×10^{-7}	6.944×10^{-8}	1.699×10^{-7}	9.644×10^{-7}	5.526×10^{-8}	2.420×10^{-8}
30	8.284×10^{-5}	3.613×10^{-7}	2.474×10^{-7}	4.367×10^{-7}	4.003×10^{-7}	2.245×10^{-7}	1.209×10^{-6}
31	2.510×10^{-5}	3.068×10^{-8}	3.626×10^{-6}	5.330×10^{-8}	5.135×10^{-7}	8.902×10^{-8}	1.594×10^{-7}
32	9.806×10^{-6}	6.157×10^{-8}	1.672×10^{-7}	3.683×10^{-7}	5.884×10^{-7}	1.060×10^{-6}	9.287×10^{-8}
33	1.089×10^{-5}	3.582×10^{-7}	1.882×10^{-7}	3.790×10^{-7}	4.774×10^{-7}	1.006×10^{-7}	9.250×10^{-8}
34	2.033×10^{-5}	1.183×10^{-7}	7.783×10^{-7}	4.070×10^{-6}	5.554×10^{-8}	4.892×10^{-7}	2.700×10^{-7}
35	6.881×10^{-6}	3.068×10^{-7}	1.540×10^{-7}	6.906×10^{-8}	5.174×10^{-6}	1.672×10^{-6}	3.834×10^{-6}
36	2.366×10^{-5}	1.286×10^{-6}	4.732×10^{-8}	3.115×10^{-6}	4.340×10^{-6}	7.381×10^{-9}	1.128×10^{-8}
37	4.103×10^{-5}	1.356×10^{-7}	1.060×10^{-6}	2.289×10^{-7}	1.837×10^{-7}	2.246×10^{-7}	1.425×10^{-7}
38	1.141×10^{-5}	3.246×10^{-7}	1.292×10^{-7}	1.636×10^{-7}	6.883×10^{-8}	1.206×10^{-6}	8.126×10^{-8}
39	7.239×10^{-6}	2.235×10^{-7}	1.247×10^{-7}	3.227×10^{-8}	3.312×10^{-8}	7.534×10^{-8}	1.129×10^{-7}
40	1.469×10^{-5}	2.634×10^{-7}	4.067×10^{-6}	1.295×10^{-7}	9.381×10^{-7}	1.210×10^{-8}	4.420×10^{-8}
41	1.532×10^{-5}	7.324×10^{-8}	2.884×10^{-8}	6.022×10^{-8}	2.451×10^{-6}	2.899×10^{-8}	1.219×10^{-6}
42	9.341×10^{-5}	5.993×10^{-8}	6.288×10^{-8}	4.219×10^{-7}	1.936×10^{-7}	2.224×10^{-7}	3.021×10^{-7}
43	2.630×10^{-5}	3.907×10^{-9}	1.671×10^{-7}	9.464×10^{-7}	5.548×10^{-7}	3.896×10^{-7}	1.017×10^{-6}
44	5.692×10^{-5}	5.481×10^{-8}	1.059×10^{-7}	2.143×10^{-8}	1.016×10^{-6}	1.316×10^{-6}	1.701×10^{-8}
45	1.160×10^{-5}	1.580×10^{-7}	1.032×10^{-6}	1.104×10^{-7}	1.440×10^{-7}	1.349×10^{-7}	2.535×10^{-7}
46	3.557×10^{-5}	1.772×10^{-7}	9.755×10^{-7}	3.026×10^{-7}	8.693×10^{-8}	1.151×10^{-7}	3.111×10^{-8}
47	2.006×10^{-5}	3.985×10^{-7}	6.246×10^{-7}	8.850×10^{-7}	6.006×10^{-8}	2.473×10^{-7}	4.911×10^{-7}
48	1.470×10^{-5}	1.216×10^{-6}	6.878×10^{-8}	4.079×10^{-6}	3.506×10^{-7}	1.438×10^{-8}	2.449×10^{-7}
49	6.051×10^{-6}	2.283×10^{-8}	8.193×10^{-8}	6.516×10^{-8}	1.274×10^{-8}	5.939×10^{-8}	1.363×10^{-7}
50	4.988×10^{-6}	8.602×10^{-7}	9.710×10^{-7}	2.718×10^{-6}	9.494×10^{-8}	1.078×10^{-6}	8.058×10^{-9}

TABLE D-6. SAMPLED VALUES FOR INTRUSION SCENARIO CASE $E1_g$ (Concluded)

Simulation	x(22)	x(23)	x(24)	x(25)	x(26)	x(27)	x(28)
1	1.709×10^{-8}	1.456×10^{-11}	1.16×10^{-1}	9.530×10^{-6}	0.197	1.416×10^{7}	7.844×10^{3}
2	6.546×10^{-7}	5.972×10^{-12}	9.757×10^{-2}	8.530×10^{-6}	0.201	9.592×10^{6}	9.599×10^{3}
3	6.745×10^{-7}	7.255×10^{-12}	1.48×10^{-1}	1.641×10^{-5}	0.217	6.479×10^{6}	2.239×10^{3}
4	1.269×10^{-6}	7.048×10^{-12}	1.11×10^{-1}	1.645×10^{-5}	0.168	1.329×10^{7}	6.898×10^{3}
5	4.088×10^{-7}	6.076×10^{-12}	9.239×10^{-2}	5.628×10^{-6}	0.236	7.959×10^{6}	6.730×10^{3}
6	6.864×10^{-8}	8.195×10^{-12}	1.67×10^{-1}	2.606×10^{-6}	0.256	1.278×10^{7}	2.181×10^{3}
7	1.060×10^{-7}	7.082×10^{-12}	1.07×10^{-1}	3.282×10^{-6}	0.176	6.471×10^{6}	2.48×10^{2}
8	1.327×10^{-8}	1.530×10^{-11}	9.992×10^{-2}	2.656×10^{-6}	0.229	1.283×10^{7}	8.789×10^{3}
9	2.278×10^{-7}	1.010×10^{-11}	1.70×10^{-1}	8.232×10^{-6}	0.209	7.549×10^{6}	8.512×10^{3}
10	9.615×10^{-8}	5.078×10^{-12}	1.15×10^{-1}	2.953×10^{-5}	0.256	1.047×10^{7}	4.642×10^{3}
11	3.829×10^{-6}	9.909×10^{-12}	7.591×10^{-2}	5.182×10^{-6}	0.257	1.178×10^{7}	2.619×10^{3}
12	4.904×10^{-8}	2.004×10^{-11}	1.24×10^{-1}	9.598×10^{-6}	0.217	1.096×10^{7}	7.32×10^{2}
13	1.361×10^{-8}	1.068×10^{-11}	7.690×10^{-2}	3.147×10^{-6}	0.207	6.156×10^{6}	7.278×10^{3}
14	1.803×10^{-7}	8.401×10^{-12}	1.03×10^{-1}	1.690×10^{-6}	0.177	8.093×10^{6}	1.221×10^{3}
15	1.286×10^{-8}	5.500×10^{-12}	9.706×10^{-2}	7.238×10^{-6}	0.189	1.015×10^{7}	6.917×10^{3}
16	3.006×10^{-7}	5.656×10^{-12}	8.669×10^{-2}	8.463×10^{-6}	0.235	6.639×10^{6}	6.838×10^{3}
17	8.669×10^{-7}	1.100×10^{-11}	7.689×10^{-2}	3.329×10^{-5}	0.232	6.813×10^{6}	5.508×10^{3}
18	1.897×10^{-7}	6.439×10^{-12}	1.06×10^{-1}	1.494×10^{-5}	0.198	1.415×10^{7}	3.58×10^{2}
19	1.077×10^{-6}	1.093×10^{-11}	1.18×10^{-1}	2.646×10^{-6}	0.121	7.593×10^{6}	8.494×10^{3}
20	3.643×10^{-8}	2.999×10^{-12}	6.880×10^{-2}	5.917×10^{-6}	0.211	7.328×10^{6}	2.020×10^{3}
21	1.022×10^{-7}	9.764×10^{-12}	6.816×10^{-2}	5.234×10^{-6}	0.136	1.063×10^{7}	5.765×10^{3}
22	5.835×10^{-8}	6.508×10^{-12}	1.26×10^{-1}	3.934×10^{-6}	0.224	1.020×10^{7}	5.343×10^{3}
23	1.652×10^{-5}	1.106×10^{-11}	1.11×10^{-1}	5.374×10^{-6}	0.176	8.440×10^{6}	6.760×10^{3}
24	4.076×10^{-7}	1.128×10^{-11}	5.349×10^{-2}	5.136×10^{-6}	0.193	1.144×10^{7}	3.812×10^{3}
25	8.338×10^{-7}	5.062×10^{-12}	8.013×10^{-2}	1.754×10^{-5}	0.188	1.042×10^{7}	8.62×10^{2}
26	7.529×10^{-8}	4.069×10^{-12}	9.621×10^{-2}	1.895×10^{-6}	0.146	1.397×10^{7}	8.885×10^{3}
27	4.022×10^{-7}	2.164×10^{-11}	8.076×10^{-2}	9.688×10^{-6}	0.159	6.830×10^{6}	7.635×10^{3}
28	2.591×10^{-7}	1.351×10^{-11}	7.085×10^{-2}	5.796×10^{-6}	0.224	8.845×10^{6}	9.232×10^{3}
29	3.373×10^{-7}	1.642×10^{-11}	9.818×10^{-2}	7.872×10^{-6}	0.165	1.195×10^{7}	2.392×10^{3}
30	1.406×10^{-7}	3.113×10^{-12}	1.30×10^{-1}	5.181×10^{-6}	0.224	8.386×10^{6}	6.913×10^{3}
31	9.951×10^{-8}	1.184×10^{-11}	9.657×10^{-2}	2.394×10^{-5}	0.143	1.360×10^{7}	9.32×10^{2}
32	2.351×10^{-8}	1.538×10^{-11}	9.399×10^{-2}	6.529×10^{-6}	0.238	7.135×10^{6}	2.60×10^{2}
33	1.404×10^{-7}	1.098×10^{-11}	1.37×10^{-1}	3.740×10^{-5}	0.199	7.577×10^{6}	3.917×10^{3}
34	1.352×10^{-7}	1.145×10^{-11}	8.024×10^{-2}	3.038×10^{-5}	0.200	6.844×10^{6}	2.89×10^{2}
35	2.748×10^{-7}	1.796×10^{-12}	1.21×10^{-1}	8.294×10^{-6}	0.181	9.850×10^{6}	5.637×10^{3}
36	4.648×10^{-8}	1.535×10^{-12}	7.758×10^{-2}	1.460×10^{-5}	0.223	7.996×10^{6}	2.939×10^{3}
37	4.331×10^{-6}	7.504×10^{-12}	1.00×10^{-1}	1.956×10^{-6}	0.260	1.312×10^{7}	1.749×10^{3}
38	4.489×10^{-7}	9.925×10^{-12}	7.118×10^{-2}	7.835×10^{-6}	0.221	1.296×10^{7}	1.195×10^{3}
39	2.484×10^{-7}	5.134×10^{-12}	9.228×10^{-2}	1.812×10^{-5}	0.131	1.413×10^{7}	1.595×10^{3}
40	3.867×10^{-7}	5.827×10^{-12}	1.07×10^{-1}	4.980×10^{-6}	0.158	6.089×10^{6}	1.029×10^{3}
41	1.528×10^{-6}	1.179×10^{-11}	1.17×10^{-1}	2.482×10^{-6}	0.154	7.019×10^{6}	6.77×10^{2}
42	6.585×10^{-8}	6.387×10^{-12}	1.19×10^{-1}	2.274×10^{-5}	0.186	8.014×10^{6}	1.991×10^{3}
43	1.264×10^{-7}	6.709×10^{-12}	8.480×10^{-2}	7.035×10^{-6}	0.205	1.172×10^{7}	6.571×10^{3}
44	7.434×10^{-8}	1.112×10^{-11}	9.215×10^{-2}	5.417×10^{-6}	0.217	1.059×10^{7}	6.770×10^{3}
45	3.236×10^{-8}	1.245×10^{-11}	9.223×10^{-2}	1.828×10^{-5}	0.172	6.369×10^{6}	9.662×10^{3}
46	3.245×10^{-7}	1.195×10^{-11}	1.11×10^{-1}	1.097×10^{-5}	0.198	6.844×10^{6}	8.806×10^{3}
47	1.070×10^{-6}	4.158×10^{-12}	1.02×10^{-1}	2.950×10^{-5}	0.205	1.366×10^{7}	9.326×10^{3}
48	2.284×10^{-8}	1.089×10^{-11}	9.431×10^{-2}	8.899×10^{-6}	0.178	1.218×10^{7}	6.59×10^{2}
49	7.644×10^{-8}	3.452×10^{-12}	9.911×10^{-2}	6.516×10^{-6}	0.176	1.023×10^{7}	1.011×10^{3}
50	6.537×10^{-8}	4.686×10^{-12}	9.573×10^{-2}	8.160×10^{-6}	0.178	7.490×10^{6}	3.188×10^{3}

APPENDIX E:
ESTIMATES OF RADIONUCLIDE CONCENTRATIONS IN BRINES

APPENDIX E: ESTIMATES OF RADIONUCLIDE CONCENTRATIONS IN BRINES

DATE: February 14, 1989
TO: B. M. Butcher, 6332
FROM: L. H. Brush and D. R. Anderson, 6334
SUBJECT: Estimates of Gas Production Rates, Potentials, and Periods, and Dissolved Radionuclide Concentrations for the WIPP Supplemental Environmental Impact Statement

GAS PRODUCTION RATES, POTENTIALS, AND PERIODS

The gas and water (H_2O) contents of WIPP disposal rooms will affect the long-term performance of the repository, especially in the event of human intrusion. Because chemical reactions can produce or consume large amounts of gas and H_2O, quantification of repository chemistry is necessary to predict repository gas and H_2O budgets. During the last year, the WIPP Performance Assessment (PA) Source-Term Group (STG) has: (1) reviewed relevant investigations carried out by the WIPP Project, as well as for other applications; (2) identified additional laboratory studies required for the quantification of repository gas and H_2O budgets; (3) assigned priorities to these studies; (4) developed a conceptual design for them. Brush and Anderson (1988a, 1988b, 1988c) have described these activities in detail. Unfortunately, data from the laboratory investigations recommended by the STG will not be available for several months.

The STG concluded, however, that several processes could affect repository gas and H_2O budgets. The air trapped in WIPP disposal rooms at the time they are filled and sealed will comprise mostly nitrogen (N_2) and oxygen (O_2). The Salado Fm. will release brine and will initially release gas, mostly N_2. Eventually, the Salado will serve as a sink for all gases, except perhaps N_2. Microbial activity, either aerobic or anaerobic, halophilic or nonhalophilic, will consume cellulosic and perhaps other materials in the waste and will produce carbon dioxide (CO_2) in potentially significant amounts, as well as other gases under certain conditions. These other gases could include hydrogen sulfide (H_2S), methane (CH_4), and N_2. The net effect of microbial activity on the H_2O budget of the repository, however, is unclear. Corrosion, either oxic or anoxic, of drums, metal boxes, and metallic constituents of the waste, will consume significant quantities of H_2O, and (in the case of anoxic corrosion) produce significant amounts of hydrogen (H_2). Microbial consumption of H_2

during sulfate (SO_4^{2-}) reduction might remove one of these gases. The reaction of H_2S with drums, metal boxes, metallic constituents of the waste, or their corrosion products to form pyrite (FeS_2) will probably remove another. The formation of FeS_2, however, will release the H_2 consumed during SO_4^{2-} reduction and perhaps produce additional H_2, and release any H_2O consumed during oxic or anoxic corrosion. Radiolysis of brines, cellulosics, plastics, and rubbers will consume H_2O and produce carbon monoxide (CO), CO_2, H_2, and O_2. Brush and Anderson (1988a, 1988b, 1988c) have described these reactions in detail.

The laboratory investigations recommended by the STG will provide detailed information on several of the processes described above. In lieu of these results, the best available data are those reviewed by Molecke (1979). Based on an extensive literature review and experimental program, Molecke (1979) concluded that the "most probable overall average" gas production rate for TRU waste in WIPP disposal rooms will be 0.3 to 1.4 moles per drum per year, with 0.0005 as the lower limit and 2.8 as the upper limit. This estimate comprised four processes, microbial degradation (the most important process), chemical corrosion, radiolysis, and thermal degradation, and was based on estimated properties of the TRU waste existing at the Idaho National Engineering Laboratory (INEL) at that time. Sandia National Laboratories (1979) also estimated a "worst case" gas production rate of 5 moles per drum per year for 400 years. To calculate this "worst case" gas production rate and gas production period, Molecke (personal communication) estimated that the total gas production potential of a typical TRU waste drum is 5,600 moles, but that the actual gas production potential under the conditions expected for the WIPP is 2,000 moles per drum.

The National Academy of Sciences reviewed these estimates (see National Research Council Panel on the Waste Isolation Pilot Plant, 1984), and accepted Molecke's (1979) "most probable overall average" estimate of 0.3 to 1.4 moles per drum per year for the gas production rate, as well as Sandia National Laboratories' (1979) estimate of 2,000 moles per drum for the gas production potential under expected WIPP conditions. We propose a "best estimate" (expected or most realistic value) of 0.85 moles per drum per year for the gas production rate. This rate is the arithmetic mean of 0.3 and 1.4 moles per drum per year, the range estimated by Molecke (1979). This gas production rate does not include the H_2 produced by anoxic corrosion of drums, metal boxes, and metallic constituents of the waste (see below). We do not recommend, however, the gas production potential of 2,000 moles per drum estimated by Sandia National Laboratories (1979); instead, we propose a total gas production potential of 1,480 moles per drum.

We calculated a gas production potential of 1,480 moles per drum with the same assumptions used by Molecke (personal communication) for the estimate of 2,000 moles per drum proposed by Sandia National Laboratories (1979), but with new

estimates by Drez (personal communication) of the quantities of some of the nonradioactive constituents of the WIPP inventory, as well as an estimate of the H_2 production potential from anoxic corrosion of drums, metal boxes, and metallic constituents of the waste. Our gas production potential of 1,480 moles per drum does not include radiolysis, which is probably a minor component of the total gas production potential for most of the nonradioactive constituents of TRU waste.

To calculate a gas production potential of 2,000 moles per drum for Sandia National Laboratories (1979), Molecke (personal communication) assumed that 100% of the cellulosic materials and 50% of the Neoprene and Hypalon (two types of rubber) in the waste will be converted to gas by microbial degradation. Furthermore, Molecke (personal communication) assumed that the yields for the conversion of these materials by microbial degradation will be 37.1 moles of carbon oxides (CO_X) and 30.9 moles of H_2 per kg of cellulosics; 4.16 moles of chlorine gas (Cl_2), 28.8 moles of CO_X, 24.9 moles of H_2, and 4.81 moles of sulfur oxides (SO_X) per kg of Hypalon; and 8.05 moles of Cl_2, 45.2 moles of CO_X, and 28.3 moles of H_2 per kg of Neoprene

Drez (personal communication) estimated that there are 253,000 kg of cloth, 66,600 kg of treated lumber, 56,700 kg of untreated lumber, 3,280,000 kg of paper, and 93,700 kg of plywood in the TRU waste that will be emplaced in the WIPP. Furthermore, Drez (personal communication) estimated that 4,500 of the "old" boxes which contain TRU waste (see below) are made of plywood. For these boxes, the average mass of plywood per box (excluding any plywood in the waste) is 158 kg. Because neither the "new" boxes nor the drums contain any plywood (excluding any plywood in the waste), the total quantity of plywood in containers is 711,000 kg. We used these estimates to calculate that the total quantity of cellulosic materials in the WIPP will be 4,461,000 kg.

Drez (personal communication) also estimated that there are 118,000 kg of Hypalon, 135,000 kg of Neoprene, 591,000 kg of surgical gloves, and 80,000 kg of miscellaneous rubbers in the WIPP inventory. We prorated the 671,000 kg of surgical gloves and miscellaneous rubbers between Hypalon and Neoprene to obtain revised estimates of 313,000 kg of Hypalon and 358,000 kg of Neoprene in the waste.

Based on estimates by Drez (personal communication) that there are 385,000 drums of TRU waste in the WIPP inventory, 6,000 "old" boxes of TRU waste in the WIPP inventory, the equivalent of 15 drums of waste per "old" box, 13,500 "new" boxes of TRU waste in the WIPP inventory, and the equivalent of 6 drums of TRU waste per "new" box, we calculated that the equivalent of 556,000 drums of TRU waste will be emplaced in the WIPP.

We divided the estimates of the total quantities of cellulosic materials, Hypalon, and Neoprene given above by 556,000 drums to calculate that there are 8.02 kg of cellulosic materials, 0.563 kg of Hypalon, and 0.644 kg of Neoprene per drum. Clearly, the quantities of these materials per "old" or "new" box are higher, but our objective is to calculate the gas production potential of a drum of waste. We then applied the same microbial conversion factors and yields (see above) assumed by Molecke (personal communication) for Sandia National Laboratories (1979) to these quantities of materials, and calculated gas production potentials of 545 moles per drum for cellulosic materials, 17.6 moles per drum for Hypalon, and 26.3 moles per drum for Neoprene. The total gas production potential is then 589 moles per drum for these materials. Molecke's (1979) gas production rate of 0.85 moles per drum per year and our gas production potential of 589 moles per drum imply a gas production period of 693 years, but these estimates do not include the H_2 that will be produced by anoxic corrosion of drums, metal boxes, and metallic constituents of the waste (see below).

Although Molecke (1979) considered chemical corrosion for his estimate of the "most probable overall average" gas production rate, he assumed that corrosion of drums, metal boxes, and metallic constituents of the waste will only occur prior to filling and sealing of WIPP disposal rooms. Such corrosion will consume O_2 from the mine air. After sealing, the depletion of this O_2 and any O_2 produced by radiolysis, and the resaturation of the repository by magnesium (Mg^{2+})-bearing brine, anoxic corrosion of drums, metal boxes, and metallic constituents of the waste will consume H_2O and produce H_2. An estimate of the H_2 production rate must therefore be added to the value of 0.85 moles per drum per year for those scenarios in which resaturation of WIPP disposal rooms is assumed.

We calculated the H_2 production rate due to anoxic corrosion of drums, metal boxes, and metallic constituents of the waste as follows. Data reviewed by Molecke (1979) provide the most pessimistic estimate of the H_2 production rate. These data, which were obtained from a laboratory study of the corrosion of 1018 mild steel (the same alloy used for the drums) in sodium-chloride-saturated brine at 25°C, imply that anoxic corrosion will produce 2 moles of H_2 per drum per year for 336 years, after which all of the drums will be consumed. In addition, Brush and Anderson (1988a) extrapolated data reported by Haberman and Frydrych (1988) from a laboratory study of the corrosion of A216 Grade WCA mild steel in Permian Basin brines at 90, 150, and 200°C to expected WIPP temperatures of about 30°C and the lower Mg^{2+} concentrations of intergranular Salado-Fm. brines. Based on these extrapolations, they concluded that anoxic corrosion will consume all of the drums in 500 to 2,000 years. The most optimistic estimate of the H_2 production rate is therefore based on a corrosion period of 2,000 years, and is 0.262 moles per drum per year. For our "best estimate" of the H_2 production rate, we propose the arithmetic mean of the most

optimistic and the most pessimistic rates, 1.13 moles per drum per year. Note that Molecke (1979) calculated an H_2 production potential of 672 moles per drum, but Brush and Anderson (1988a) calculated an H_2 production potential of 524 moles per drum. We therefore propose an H_2 production potential that is the mean of the two values cited above, or 598 moles per drum. The use of these mean values implies that anoxic drum corrosion will produce 1.13 moles of H_2 per drum per year for a period of 529 years, but these estimates do not include the H_2 that will be produced by anoxic corrosion of metal boxes and metallic constituents of the waste.

Because much of the waste will be emplaced in metal boxes, we must correct our estimates of the H_2 production potential and the H_2 production period given above to account for the fact that the quantities of steel per equivalent drum of waste in the metal boxes are different from the mass of steel per 55-gallon drum used by Brush and Anderson (1988a), 29.3 kg. (Because we have no corrosion data for the metal boxes, we must assume that the H_2 production rates for the metal boxes are identical to the rate for the drums.) Drez (personal communication) estimated that 1,500 of the 6,000 "old" boxes and all of the 13,500 "new" boxes will be made of steel. He also estimated that each "old" metal box contains 236 kg of steel and that each "new" box contains 341 kg of steel. Because each "old" box contains the equivalent of 15 drums of waste and each "new" box contains the equivalent of 6 drums of waste, there are 15.8 kg of steel per equivalent drum of waste in the "old" boxes and 56.8 kg of steel per equivalent drum of waste in the "new" boxes. We therefore calculated a weighted average for the mass of steel per equivalent drum of waste in the WIPP inventory by adding the product of the number of 55-gallon drums (385,000) and the mass of steel per 55-gallon drum (29.3 kg), the product of the number of equivalent drums of waste in "old" metal boxes (22,500) and the mass of steel per equivalent drum of waste in "old" metal boxes (15.8 kg), and the product of the number of equivalent drums of waste in "new" boxes (81,000) and the mass of steel per equivalent drum of waste in "new" boxes (56.8 Kg), and dividing this sum by the total number of equivalent drums of waste in the WIPP inventory (556,000). The result, 29.2 kg of steel per equivalent drum, is virtually identical to 29.3 kg per 55-gallon drum, the value used by Brush and Anderson (1988a). We nevertheless reduced our estimate of the H_2 production potential from 598 moles per drum to 596 moles per equivalent drum, and our estimate of the H_2 production period from 529 years to 527 years.

In addition to the H_2 produced by anoxic corrosion of drums and metal boxes, anoxic corrosion of various iron (Fe) and steel alloys in the waste will also produce H_2. Drez (personal communication) estimated that there are 5,110,000 kg of stainless steel alloys and 3,002,000 kg of miscellaneous Fe-based alloys in the WIPP inventory. We used these estimates to calculate that there are 14.6 kg of Fe and steel per equivalent drum of waste. Because each equivalent drum of waste contains 14.6 kg of Fe or steel in addition to the 29.2 kg of steel used

to fabricate the drum or metal box, we increased the H_2 production potential by 50% from 596 moles per drum to 894 moles per drum. If sufficient brine were present (see below), anoxic corrosion of drums, metal boxes, and Fe-bearing constituents of the waste would occur simultaneously; we therefore estimate that the H_2 production rate will increase by 50% from 1.13 moles per drum per year to 1.70 moles per drum per year, but this rate will still be applicable for 527 years. Because we have no information to evaluate the possibility of H_2 production by anoxic corrosion of other metals in the waste, we cannot correct the estimate described above for these metals. About 64% of metallic constituents of the waste, however, comprise Fe-based alloys (Butcher, personal communication). Other metallic constituents are lead, 7%; tantalum, 4%; and others (mainly aluminum and copper), 25%.

Brush and Anderson (1988a) calculated that 102 m^3 of brine will be consumed by anoxic corrosion of all of the drums in a WIPP disposal room, but this value was based on the assumptions that there will be 6,750 drums per room and that the mass of steel per drum is 29.3 kg. Assuming 7,000 drums per room and 29.2 kg of steel per equivalent drum, 105 m^3 of brine would be required. Furthermore, this value must be increased by an additional 50% to 158 m^3 to account for Fe-bearing constituents of the waste. If all of the brine that enters the rooms were consumed by absorption by bentonite or crushed salt in the backfill, or by other processes such as microbial hydrolysis of cellulosic materials or radiolysis, anoxic corrosion of drums, metal boxes, and metallic constituents of the waste might not occur and H_2 might not be produced by this process. (It is possible that anoxic corrosion could proceed using H_2O vapor present in WIPP disposal rooms after they are sealed and O_2 is depleted, or using H_2O previously absorbed by bentonite in contact with drums, metal boxes, and metallic constituents of the waste, but we have no evidence yet that anoxic corrosion will actually occur in the absence of condensed H_2O.) If sufficient brine were present for anoxic corrosion to occur, the total gas production rate would be the sum of 0.85 and 1.70 moles per drum per year, or 2.55 moles per drum per year. Furthermore, the total gas production potential would be the sum of 589 and 894 moles per drum, or 1,480 moles per drum.

Although the chemical reactions discussed above will also affect the H_2O budget of the repository, we do not know yet whether they will consume or produce H_2O. In lieu of results from the laboratory investigations proposed by the STG, we will assume that these reactions have no net effect on the repository H_2O budget.

The estimates of the gas production rates and the gas production potentials discussed above both raise concerns about the long-term performance of the WIPP. We must therefore justify our reasons for proposing these estimates, especially with respect to the possible choice of lower values for these parameters.

Drez (personal communication) calculated gas consumption and production rates based on the results of analyses by Clements and Kudera (1985) of head-space gases from drums of Rocky Flats TRU waste stored at INEL. Drez concluded that both the gas consumption and production rates decrease to very low values after a few years. This conclusion might be applicable to waste in WIPP disposal rooms prior to filling and sealing, but is probably inapplicable thereafter because: (1) the low relative humidity during near-surface storage at INEL probably prevented significant microbial degradation of the waste at that time, but microbial activity will occur once the rooms are sealed, the drums are crushed, and the repository resaturates (even without resaturation, the relative humidity of WIPP disposal rooms will be significantly higher after sealing than it was during near-surface storage at INEL, and could be high enough for significant microbial activity, albeit at slow rates); (2) in the event of resaturation of the repository, anoxic corrosion of drums, metal boxes, and metallic constituents of the waste will produce copious quantities of H_2 (even without resaturation, anoxic corrosion could proceed using H_2O vapor, and the relative humidity of WIPP disposal rooms will probably be significantly higher than it was at INEL).

Recently, critics of the laboratory studies reviewed by Molecke (1979) have stated that these experiments yielded microbial gas production rates greater than those expected for actual repository conditions because they were carried out under conditions optimized for microbial activity. Molecke (1979) pointed out, however, that experiments conducted under saline or asaline conditions, brine-saturated or moist conditions, and with glucose or less bioavailable waste simulants as the substrate (food) all yielded similar gas production rates. Critics have also suggested that Molecke's (1979) "most probable overall average" gas production rate of 0.85 moles per drum per year is actually a "worst case" estimate because his experiments were short relative to the period of interest to the WIPP PA, and the microbial gas production rate will probably decrease significantly with time. Such a decrease could indeed occur as microorganisms turn to less efficient metabolic pathways upon depletion of electron acceptors (oxidants) that yield more free energy per mole of organic carbon consumed (see Brush and Anderson, 1988a). Molecke (1979), however, reviewed the results of both aerobic and anaerobic microbiological experiments and concluded that the gas production rates were similar. Our proposed rate of 0.85 moles per drum per year thus probably already reflects the expected decrease in microbial gas production rates with time. It is still possible, of course, that additional laboratory or underground studies will yield microbial gas production rates lower than those reviewed by Molecke (1979). Whether or not these studies will yield gas production rates low enough to preclude significant pressurization of the repository, however, is unclear. (Bixler and Chu, personal communication, believe that the total gas production rate would have to be lower than about 0.1 to 1 mole per drum per year to prevent the achievemnt of lithostatic pressure.) In any case, it would be very difficult at

this time to justify any rate lower than 0.85 moles per drum per year for microbial and radiolytic gas production.

The use of a gas production potential less than our current estimate of 1,480 moles per drum is also appealing. Brush and Anderson (1988a), for example, calculated a microbial gas production potential of 690 moles per drum based on the assumption that the only substrate used by microorganisms would be cellulosic materials, a previous estimate of 6.90 kg of cellulosics per drum from Drez (personal communication), and the assumptions that microorganisms would consume all of the cellulosics by using SO_4^{2-} as the electron acceptor and that none of the CO_2 or H_2S produced would dissolve in any brine present and/or react with drums, metal boxes, metallic constituents of the waste, or their corrosion products. The estimate of 690 moles per drum from Brush and Anderson (1988a) must now be revised for several reasons. First, the previous estimate of 6.90 kg of cellulosics per drum (Drez, personal communication) did not include the plywood boxes in which much of the waste will be emplaced. Plywood boxes have been included in our current estimate of the gas production potential (see above). Second, microorganisms could well consume waste constituents in addition to cellulosics. The most important potential additions are plastics, which we did not include in our current estimate, and rubbers, of which we assumed 50% will be be converted to gas in our current estimate. Although microorganisms will almost certainly consume cellulosics in preference to plastics, they could turn to plastics after depletion of the cellulosics. Furthermore, radiolysis of plastics could transform them into more bioavailable materials. Third, the stoichiometry of the microbial reactions proposed by Brush and Anderson (1988a) must be revised to include factors such as the hydrolysis of cellulosics and the synthesis of cellular material (biomass) by microorganisms. Fourth, the microbial gas production potential will also depend on estimates of the quantities of waste constituents in addition to cellulosics, such as NO_3- (a potential electron acceptor) and plastics. Fifth, the estimate of 690 moles per drum did not include the H_2 production potential from anoxic corrosion of drums, metal boxes, and metallic constituents of the waste. Anoxic corrosion has been included in our current estimate of the total gas production potential, 1,480 moles per drum. Based on these considerations, we will revise our current estimate of the gas production potential in the next few months. The revised estimate, however, might not be significantly lower than our current estimate, at least not with respect to its implications for repository pressurization. Furthermore, it could even be higher than our current estimate

The backfill additives proposed by Brush and Anderson (1988a) might remove much of the microbially produced gas from WIPP disposal rooms. Backfill additives such as calcium carbonate ($CaCO_3$), calcium oxide (CaO), potassium hydroxide (KOH), and sodium hydroxide (NaOH) might remove most of the CO_2, probably the most abundant microbial gas under most conditions. ($CaCO_3$ would remove CO_2 only if brine were present; CaO, KOH, and NaOH might remove CO_2 in the absence of

brine, but if brine subsequently entered the rooms its pH would increase significantly after the dissolution of these backfill additives or their CO_2-bearing reaction products.) Brush and Anderson (1988a) calculated that about 87,000 kg of KOH or 62,000 kg of NaOH per room would be required to remove all of the microbially produced CO_2. but did not calculate the required quantities of $CaCO_3$ or CaO because the stoichiometry of CO_2 uptake by these compounds has not been defined yet for expected WIPP conditions. Because the required quantity of any backfill additive for the removal of CO_2 depends critically on how much of the microbially produced gas is in fact CO_2, which is unknown at present, the quantities of these backfill additives cannot be estimated. The quantities of KOH and NaOH calculated by Brush and Anderson (1988a) will therefore have to be revised during the next several months as data from additional laboratory studies of microbial gas production become available.

It might be possible to reduce the microbial gas production rate and the microbial gas production potential by storing sludges containing nitrate (NO_3-) separately from waste with cellulosic materials. This might prevent denitrification, microbial N_2 production resulting from the use of NO_3- as an electron acceptor (see Brush and Anderson, 1988a; 1988c). Storage of sludges in separate rooms, however, might not preclude denitrification; NO_3- is very soluble, diffuses rapidly in aqueous solutions, and could well diffuse from room to room through brine-saturated fractures in Marker Bed 139 during the period of interest to the WIPP PA.

Addition of manganese dioxide (MnO_2) to the backfill might prevent SO_4^{2-} reduction, the concomitant production of H_2S, the reaction of H_2S with drums, metal boxes, metallic constituents of the waste, or their corrosion products to form FeS_2, and the concomitant production of H_2. The use of MnO_2 as a backfill additive, however, has two potential problems. First, it must be demonstrated that there are halophilic or halotolerant bacteria that can use MnO_2 as an electron acceptor under expected WIPP conditions, and that they would survive in the repository until conditions conducive to MnO_2 reduction occur, or throughout the period during which MnO_2 reduction would be required. Second, MnO_2 is extremely insoluble and thus might not migrate through any brine present fast enough to prevent significant SO_4^{2-} reduction in isolated locations within the rooms. Even if it could be demonstrated that MnO_2 were effective, it would be impossible to calculate the quantity required to prevent SO_4^{2-} reduction in the absence of an estimate of the quantity of NO_3- in the WIPP inventory (microorganisms would use all available NO_3- as an electron acceptor prior to turning to MnO_2, thus reducing the quantity of MnO_2 required to prevent SO_4^{2-} reduction).

Finally, the proposed backfill additive copper sulfate ($CuSO_4$), an oxidant, might corrode drums, metal boxes, and Fe-bearing constituents of the waste without producing H_2. $CuSO_4$ will only be effective if brine is present, but

anoxic corrosion might not occur in the absence of brine anyway. Assuming that 1 mole of $CuSO_4$ would be required to corrode 1 mole of Fe in drums, metal boxes, or the waste without producing H_2, the total quantity of $CuSO_4$ required per WIPP disposal room would equal the quantity of Fe per room. Brush and Anderson (1988a) calculated that there will be 3,540,000 moles of Fe per room, but this value was based on the assumption that there will be 6,750 drums per room and did not include the metal boxes or the Fe-bearing constituents of the waste. Assuming 7,000 drums per room and an Fe content of 29.2 kg per equivalent drum (see above), there will be 3,660,000 moles of Fe per room. Furthermore, this value should be increased by an additional 50% to 5,490,000 moles of Fe per room to account for the Fe in the waste. Assuming that 5,490,000 moles per room of $CuSO_4$ will be required and a molecular weight of 160 g for $CuSO_4$, 878,000 kg per room of $CuSO_4$ would be required. Finally, assuming a particle density of 3.60 g per cm^3, a bulk density that is 60% of the particle density, and 1,000,000 cm^3 per m^3, the total volume of $CuSO_4$ required would be 244 m^3 per room.

Unfortunately, any of the backfill additives discussed above could inhibit the closure of WIPP disposal rooms by increasing the strength of the materials in the rooms. This could in turn increase the quantities of radionuclides released in the event of human intrusion by promoting fluid flow and particle suspension.

RADIONUCLIDE CONCENTRATIONS IN BRINES

The WIPP PA STG recently attempted to estimate the solubilities of some of the actinide elements in likely WIPP brines under the conditions expected for WIPP disposal rooms. The STG attempted these estimates to provide input for the calculations for the upcoming forecast of the comparison to the Environmental Protection Agency standard and methodology demonstration by Bertram-Howery et al. (in prep.). A detailed description of this exercise appears in Brush and Anderson (1988b).

For this exercise, Brush and Anderson (1988b) defined two standard brines, an average, intergranular brine from the Salado Fm. now referred to as PAB 1, and a representative fluid from a brine reservoir in the Castile Fm. Brush and Anderson (1988b) assumed that three possible quantities of brine could eventually resaturate WIPP disposal rooms, and used these quantities, along with estimates by Drez (personal communication) of the total quantities of four organic ligands in the WIPP inventory, to estimate the possible concentrations of these ligands in the brines. Choppin (personal communication) then attempted to calculate the speciation and solubilities of Am, Np, Pu, U, and Th in both the Salado and Castile brines with the estimated concentrations of four organic ligands.

Choppin (personal communication) concluded that there are no thermodynamic data (solubility products for solid phases, or stability constants for dissolved organic or inorganic complexes) for these elements in solutions with ionic strengths (I) equal to those of the standard Salado and Castile brines defined by Brush and Anderson (1988b) (I = 7.66 and 6.14 M, respectively). Most existing data apply to solutions with I less than or equal to 1 M, and only a few pertain to values of I as high as 2 or 3 M. Furthermore, most of the data are for 1:1 (metal:ligand) or 1:2 complexes; very few data exist for 1:3 or 1:4 complexes, which could be important species in these brines. Choppin (personal communication) therefore attempted to estimate thermodynamic data for the actinides listed above by: (1) extrapolating existing data to the ionic strengths of likely WIPP Brines; (2) in those cases in which the availability of data at lower values of I is so limited that extrapolation is impossible, using these data directly for the WIPP brines or arbitrarily adding one log unit to them; (3) in those cases in which there are no data at all for the appropriate complex, extrapolating data for chemically analogous organoactinide or organolanthanide complexes.

Unfortunately, these procedures result in order-of-magnitude uncertainties in any estimates of thermodynamic data for WIPP brines. Furthermore, it is not yet possible to predict how processes such as microbial activity, anoxic corrosion of drums, metal boxes, and metallic constituents of the waste, or radiolysis will affect the Eh of the repository, and to what extent these processes will influence the oxidation states of Np, Pu, and U. Finally, the values of pH reported for the Salado and Castile brines could differ significantly from the actual values because of problems associated with pH measurements in concentrated brines. Even if the reported values are accurate, the dissolution of microbially produced CO_2 or reactions between the brines and nonradioactive constituents of the waste such as cements could change the pH significantly. Because Eh and pH affect the speciation and solubilities of the actinides significantly, these problems increase the uncertainties associated with the estimation of thermodynamic data at high ionic strengths.

Preliminary results from an ongoing sensitivity study suggest that, in addition to the solubilities of radionuclide-bearing solids, the sorption of radionuclides by bentonite and/or Fe oxides formed by anoxic corrosion of drums, metal boxes, and Fe-bearing constituents of the waste will also affect the source term significantly. Unfortunately, there are also virtually no data on the sorption of radionuclides by bentonite and Fe oxides under the wide-ranging conditions expected for WIPP disposal rooms.

Laboratory experiments will eventually provide data on the solubilities and sorption of radionuclides under expected repository conditions. In lieu of such data, we propose a "best estimate" of 10^{-6} M for the concentration of Pu and Am, the important actinide elements in TRU waste, in any brine that resaturates WIPP

disposal rooms. This is the intermediate value (on a logarithmic scale) of the range of dissolved radionuclide concentrations (10^{-3} to 10^{-9} M) that we have been and are using for sensitivity studies of the source term. Neither the intermediate value nor the range can be justified on the basis of experimental data or modeling studies. The STG feels, however, that it is unlikely that the concentrations of radionuclides dissolved in likely WIPP brines will exceed this intermediate value significantly.

CONCLUSIONS

We propose a "best estimate" (expected or most realistic rate of 0.85 moles per drum per year for the gas production rate in WIPP disposal rooms. This estimate, which is based on the "most probable overall average" gas production rate of Molecke (1979), comprises mainly microbial degradation, but also includes chemical corrosion (oxic only), radiolysis, and thermal degradation. We also propose a "best estimate" of 589 moles per drum for the microbial gas production potential (radiolysis will probably not increase this estimate significantly). Taken together, these estimates imply a gas production period of 693 years.

In the event that brine resaturates the repository, we propose an additional 1.70 moles per drum per year of H_2 production from anoxic corrosion of drums, metal boxes, and the metallic constituents of the waste. and an additional 894 moles per drum of gas production potential. These "best estimates" are based on the arithmetic mean of the most pessimistic estimates from Molecke (1979), and the most optimistic estimates from extrapolations by Brush and Anderson (1988a) of data from Haberman and Frydrych (1988). Anoxic corrosion would occur for 527 years, and would require 158 m^3 of brine per room. Given this quantity of brine, the "best estimate" of the total gas production rate would be 2.55 moles per drum per year and the "best estimate" of the total gas production potential would be 1,480 moles per drum.

Several factors might reduce these estimates of the gas production rate and the gas production potential significantly, but such reductions cannot be justified in the absence of additional laboratory studies of these processes.

Finally, we propose a "best estimate? [sic] of 10^{-6} M for the concentration of Pu and Am in any brine that resaturates WIPP disposal rooms. This is the intermediate value (on a logarithmic scale) of the range of dissolved radionuclide concentrations (10^{-3} to 10^{-9} M) that we have been and are using for sensitivity studies of the source term.

REFERENCES

Bertram-Howery, S. G., M. G. Marietta, R. L. Hunter, M. S. Y. Chu, L. H. Brush, R. P. Rechard, and K. F. Brinster. Forecast of the Comparison to 40 CFR Part 191, Subpart B, and Methodology Demonstration for the Waste Isolation Pilot Plant. SAND88-1452, Sandia National Laboratories, Albuquerque, NM, in preparation.

Brush, L. H., and D. R. Anderson (1988a). Potential Effects of Chemical Reactions on WIPP Gas and Water Budgets. Memo to distribution dated 3/28/1988, Sandia National Laboratories, Albuquerque, NM.

Brush, L. H., and D. R. Anderson (1988b). First Meeting of the WIPP PA Source-Term Group. Memo to distribution dated 10/27/1988, Sandia National Laboratories, Albuquerque, NM.

Brush, L. H., and D. R. Anderson (1988c). Second Meeting of the WIPP PA Source-Term Group. Memo to distribution dated 12/09/1988, Sandia National Laboratories, Albuquerque, NM.

Clements, T. L., and D. E. Kudera (1985). TRU Waste Sampling Program: Volume II - Gas Generation Studies. EGG-WM-6503, Idaho National Engineering Laboratory, Idaho Falls, ID.

Haberman, J. H., and D. J. Frydrych (1988). Corrosion Studies of A216 Grade WCA Steel in Hydrothermal Magnesium-Containing Brines. In M. J. Apted and R. E. Westerman, Eds., Scientific Basis for Nuclear Waste Management XI, Materials Research Society, Pittsburgh, PA, pp. 761-772.

Molecke, M. A. (1979). Gas Generation from Transuranic Waste Degradation: Data Summary and Interpretation. SAND79-1245, Sandia National Laboratories, Albuquerque, NM.

National Research Council on the Waste Isolation Pilot Plant (1984). Review of the Scientific and Technical Criteria for the Waste Isolation Pilot Plant (WIPP). DOE/DP/48015-1, National Academy Press, Washington, DC.

Sandia National Laboratories (1979). Summary of Research and Development Activities in Support of Waste Acceptance Criteria for WIPP. SAND 79-1305, Sandia National Laboratories, Albuquerque, NM.

Distribution:

J. N. Butler, Harvard University
G. R. Choppin, Florida State University
P. E. Drez, IT Corporation
A. J. Francis, Brookhaven National Laboratory
D. Grbic-Galic, Stanford University
B. King, IT Corporation
J. K. Lanyi, UC Irvine
J. Myers, IT Corporation
1511 D. F. McTigue
6233 J. L. Krumhansl
6233 C. L. Stein
6300 R. W. Lynch
6322 N. N. Brown
6322 M. M. Warrant
6330 W. D. Weart
6331 A. R. Lappin
6331 R. L. Beauheim
6331 D. J. Borns
6331 P. B. Davies
6331 S. J. Lambert
6331 K. L. Robinson
6331 M. D. Siegel
6332 L. D. Tyler
6332 R. Beraun
6332 R. V. Matalucci
6332 M. A. Molecke
6332 D. E. Munson
6332 E. J. Nowak
6332 T. M. Torres
6333 T. M. Schultheis
6334 D. R. Anderson
6334 S. G. Bertram-Howery
6334 K. F. Brinster
6334 L. H. Brush
6334 M. S. Y. Chu
6334 L. S. Gomez
6334 R. Guzowski
6334 R. L. Hunter
6334 M. G. Marietta
6334 R. P. Rechard
6334 A. K. Rutledge

DISTRIBUTION LIST

Distribution:

U. S. Department of Energy (5)
Office of Defense Waste and
Transportation Management
Attn: J. E. Lytle ------ DP-10
L. D. Tyler ------ DP-10
T. B. Hindman----- DP-12
M. Duff --------- DP-123
A. Follett ------- DP-122
C. H. George ----- DP-124
J. Mathur -------- DP-123
Forrestal Bldg.
1000 Independence Ave.
Washington, DC 20545

U. S. Department of Energy (8)
Albuquerque Operations Office
Attn: Bruce G. Twining
J. E. Bickel
R. Marquez
Karen A. Griffith
Mary Wilson
D. Krenz
G. Runkle (EHD)
C. Soden (EHD)
P.O. Box 5400
Albuquerque, NM 87185-5400

U. S. Department of Energy (12)
WIPP Project Office (Carlsbad)
Attn: J. Arthur
A. Hunt
T. Lukow (2)
V. Daub
K. Hunter
M. McFadden
P.O. Box 3090
Carlsbad, NM 88221-3090

U.S. Department of Energy (2)
Deputy Assistant Secretary for
Environment, EH-20
Attn: Raymond P. Berube
John Tseng
1000 Independence Ave. SW
Washington, D.C. 20585

U. S. Department of Energy, (5)
Office of Civilian Radioactive Waste
Management
Attn: Deputy Director, RW-2
Associate Director, RW-10
Office of Program
Administration and
Resources Management
Associate Director, RW-20
Office of Facilities
Siting and
Development
Associate Director, RW-30
Office of Systems
Integration and
Regulations
Associate Director, RW-40
Office of External
Relations and Policy
Office of Geologic Repositories
Forrestal Building
Washington, DC 20585

U. S. Department of Energy
Attn: National Atomic Museum Library
Albuquerque Operations Office
P. O. Box 5400
Albuquerque, NM 87185

U. S. Department of Energy
Research & Waste Management Division
Attn: W. R. Bibb, Director
P. O. Box E
Oak Ridge, TN 37831

U. S. Department of Energy (2)
Idaho Operations Office
Fuel Processing and Waste
Management Division
Attn: J. E. Solecki
785 DOE Place
Idaho Falls, ID 83402

U.S. Department of Energy (3)
Savannah River Operations Office
Defense Waste Processing
Facility Project Office
Attn: S. Cowan
W. J. Brumley
M. G. O'Rear
P.O. Box A
Aiken, SC 29802

Distribution (Continued):

U.S. Department of Energy (2)
Attn: Marvin Furman
R. E. Gerton
Richland Operations Office
825 Jadwin Ave.
P.O. Box 550
Richland, WA 99352

U.S. Department of Energy (3)
Nevada Operations Office
Attn: J. R. Boland
D. Livingston
P. K. Fitzsimmons
2753 S. Highland Drive
Las Vegas, NV 87183-8518

U.S. Department of Energy (2)
Technical Information Center
P.O. Box 62
Oak Ridge, TN 37831

U.S. Department of Energy (2)
Chicago Operations Office
Attn: J. C. Haugen
David Dashavsky
9800 South Cass Avenue
Argonne, IL 60439

U.S. Department of Energy (2)
Los Alamos Area Office
Attn: J. D. Tillman
528 35th Street
Los Alamos, NM 87544

U.S. Department of Energy (3)
Rocky Flats Area Office
Attn: W. C. Rask
T. Anderson
P.O.Box 928
Golden, CO 80402-0928

U.S. Department of Energy
Dayton Area Office
Attn: R. Grandfield
P.O.Box 66
Maimisburg, OH 45343-0066

Charlie Armstrong, WIPP Panel
Secretary
National Research Council
Board on Radioactive Waste Management
HA462
2101 Constitution Avenue
Washington, DC 20418

U.S. Environmental Protection
Agency (5)
Office of Radiation Protection
Programs (ANR-460)
Attn: Daniel J. Egan, Jr.
Washington, D.C. 20460

Bureau of Land Management
101 E. Mermod
Carlsbad, NM 88220

Bureau of Land Management
New Mexico State Office
P.O. Box 1449
Santa Fe, NM 87507

U.S. Geological Survey
Branch of Regional Geology
Attn: R. Snyder
MS913, Box 25046
Denver Federal Center
Denver, CO 80225

U.S. Geological Survey
Conservation Division
Attn: W. Melton
P.O. Box 1857
Roswell, NM 88201

U.S. Geological Survey (2)
Water Resources Division
Attn: Cathy Peters
Suite 200
4501 Indian School, NE
Albuquerque, NM 87110

U.S. Nuclear Regulatory Commission
(4)
Division of Waste Management
Attn: Michael Bell
Hubart Miller
Jacob Philip
NRC Library
Mail Stop 623SS
Washington, DC 20555

Distribution (Continued):

Environmental Evaluation Group (5)
Attn: Robert Neill
Suite F-2
7007 Wyoming Blvd., N.E.
Albuquerque, NM 87109

New Mexico Bureau of Mines
and Mineral Resources (2)
Attn: F. E. Kottolowski, Director
J. Hawley
Socorro, NM 87801

NM Department of Energy & Minerals
Attn: Kasey LaPlante, Librarian
P.O. Box 2770
Santa Fe, NM 87501

Bob Forrest
Mayor, City of Carlsbad
P.O. Box 1569
Carlsbad, NM 88221

Chuck Bernard
Executive Director
Carlsbad Department of Development
P.O. Box 1090
Carlsbad, NM 88221

Tom Bahr (2)
Chairman, Radioactive Waste
Consultation Task Force
408 Galisteo
Santa Fe, NM 87503

Robert M. Hawk (2)
Chairman, Hazardous and Radioactive
Materials Committee
Room 334
State Capitol
Sante Fe, NM 87503

Kirkland Jones (2)
Department Director
New Mexico Environmental Improvement
Division
P.O. Box 968
1190 St. Francis Drive
Santa Fe, NM 87503-0968

Battelle Pacific Northwest
Laboratories (6)
Attn: D. J. Bradley
J. Relyea
R. E. Westerman
S. Bates
H. C. Burkholder
L. Pederson
Battelle Boulevard
Richland, WA 99352

Savannah River Laboratory (6)
Attn: N. Bibler
E. L. Albenisius
M. J. Plodinec
G. G. Wicks
C. Jantzen
J. A. Stone
Aiken, SC 29801

Savannah River Plant (2)
Attn: Richard G. Baxter
Building 704-S
K. W. Wierzbicki
Building 703-H
Aiken, SC 29808-0001

Los Alamos National Laboratory (2)
Attn: B. Erdal, CNC-11
Attn: J. L. Warren,
HSE-7, MS-ES16
P.O. Box 1663
Los Alamos, NM 87545

Los Alamos National Laboratories (3)
HSE-8
Attn: M. Enoris
L. Soholt
J. Wenzel
P.O. Box 1663
Los Alamos, NM 87544

Oak Ridge National Laboratory (4)
Attn: R. E. Blanko
E. Bondietti
C. Claiborne
G. H. Jenks
Box Y
Oak Ridge, TN 37830

Distribution (Continued):

Lawrence Livermore National
Laboratory
Attn: G. Mackanic
P.O. Box 808, MS L-192
Livermore, CA 94550

Martin Marietta Systems, Inc.
Oak Ridge National Labs
Attn: J. Setaro
P.O. Box 2008, Bldg. 3047
Oak Ridge, TN 37831-6019

Argonne National Labs
Attn: A. Smith
9700 South Cass, Bldg. 201
Argonne, IL 60439

INTERA Technologies, Inc. (4)
Attn: G. E. Grisak
J. F. Pickens
A. Haug
A. M. LeVenue
Suite #300
6850 Austin Center Blvd.
Austin, TX 78731

INTERA Technologies, Inc.
Attn: Wayne Stensrud
P.O. Box 2123
Carlsbad, NM 88221

IT Corporation
Attn: R. F. McKinney (2)
Regional Office - Suite 700
5301 Central Avenue, NE
Albuquerque, NM 87108

IT Corporation
R. J. Eastmond
825 Jadwin Ave.
Richland, WA 99352

IT Corporation
Attn: D. E. Deal
P.O. Box 2078
Carlsbad, NM 88221

RE/SPEC, Inc. (2)
Attn: W. Coons
P. F. Gnirk
P.O. Box 14984
Albuquerque NM 871[illegible]

RE/SPEC, Inc. (7)
Attn: L. L. Van Sambeek
D. B. Blankenship
G. Callahan
T. Pfeifle
J. L. Ratigan
P. O. Box 725
Rapid City, SD 57709

Reynolds Elect/Engr. Co., Inc.
Building 790, Warehouse Row
Attn: E. W. Kendall
P.O. Box 98521
Las Vegas, NV 89193-8521

Rockwell International (2)
Attn: C. E. Wickland
D. Reinhart
Rocky Flats Plant
Golden, CO 80401

Rockwell International (3)
Atomics International Division
Rockwell Hanford Operations
Attn: J. Nelson (HWVP)
P. Salter
W. W. Schultz
P.O. Box 800
Richland, WA 99352

Science Applications
International Corporation
Attn: Howard R. Pratt,
Senior Vice President
10260 Campus Point Drive
San Diego, CA 92121

Science Applications
International Corporation
Attn: Michael B. Gross
Ass't. Vice President
Suite 1250
160 Spear Street
San Francisco, CA 94105

Science Applications
International Corporation
George Dymmel
101 Convention Center Dr.
Las Vegas, NV 89109

Distribution (Continued):

Science Applications
International Corporation
Attn: J. Sandha
W. Beyeler
J. Schreiber
2109 Air Park Road, SE
Albuquerque, NM 87106

Systems, Science, and Software (2)
Attn: E. Peterson
P. Lagus
Box 1620
La Jolla, CA 92038

Westinghouse Electric Corporation (9)
Attn: Library
L. Trega
W. P. Poirer
W. R. Chiquelin
V. F. Likar
D. J. Moak
R. F. Kehrman
T. Campbell
T. Miller
T. Halverson
P. O. Box 2078
Carlsbad, NM 88221

E G & G Idaho (3)
1955 Fremont Street
Attn: C. Atwood
C. Hertzler
T. I. Clements
Idaho Falls, ID 83415

New Mexico Engineering Research
Institute (6)
Attn: J. Bean
A. Schreyer
R. McCurley
D. Morrison
J. Rath
D. Rudeen
P.O. Box 25
University Station
Albuquerque, New Mexico 87131

Geo-Centers, Inc.
Attn: H. J. Iuzzolino
2201 Buena Vista Dr., SE
Suite 300
Albuquerque, New Mexico 87106

Charles R. Hadlock
Arthur D. Little, Inc.
Acorn Park
Cambridge, MA 02140-2390

Kathleen Hain
BDM Corporation
7519 Jones Branch Drive
McLean, VA 22101

Bill Kennedy
Pacific Northwest Laboratory
Battelle Blvd.
P.O. Box 999
Richland, WA 99352

Don Wood
Westinghouse Hanford Company
P.O. Box 1970
Richland, WA 99352

K. Owens
Westinghouse/Hanford
2401 Stevens Road
Richland, WA 99352

R. Blauvelt
Monsanto Research Corp.
Mound Road
Miamisburg, OH 45432

University of Arizona
Attn: J. G. McCray
Department of Nuclear Engineering
Tucson, AZ 85721

University of New Mexico (2)
Geology Department
Attn: D. G. Brookins
Library
Albuquerque, NM 87131

Pennsylvania State University
Materials Research Laboratory
Attn: Della Roy
University Park, PA 16802

Texas A&M University
Center of Tectonophysics
College Station, TX 77840

Distribution (Continued):

Mechanical, Aerospace, and
Nuclear Engineering Department (2)
Attn: W. Kastenberg
D. Browne
5532 Boelter Hall
University of California
Los Angeles, CA 90024

Thomas Brannigan Library
Attn: Don Dresp, Head Librarian
106 W. Hadley St.
Las Cruces, NM 88001

Hobbs Public Library
Attn: Marcia Lewis, Librarian
509 N. Ship Street
Hobbs, NM 88248

New Mexico State Library
Attn: Ingrid Vollenhofer
P.O. Box 1629
Santa Fe, NM 87503

New Mexico Tech
Martin Speere Memorial Library
Campus Street
Socorro, NM 87810

Pannell Library
Attn: Ruth Hill
New Mexico Junior College
Lovington Highway
Hobbs, NM 88240

Roswell Public Library
Attn: Nancy Langston
301 N. Pennsylvania Avenue
Roswell, NM 88201

WIPP Public Reading Room
Attn: Lee Hubbard, Head Librarian
Carlsbad Municipal Library
101 S. Halagueno St.
Carlsbad, NM 88220

Government Publications Department
General Library
University of New Mexico
Albuquerque, NM 87131

Charles Fairhurst, Chairman
Department of Civil and
Mineral Engineering
University of Minnesota
500 Pillsbury Dr. SE
Minneapolis, MN 55455

John O. Blomeke
Route 3
Sandy Shore Drive
Lenoir City, TN 37771

John D. Bredehoeft
Western Region Hydrologist
Water Resources Division
U.S. Geological Survey (M/S 439)
345 Middlefield Road
Menlo Park, CA 94025

Karl P. Cohen
928 N. California Avenue
Palo Alto, CA 94303

Fred M. Ernsberger
250 Old Mill Road
Pittsburgh, PA 15238

Rodney C. Ewing
Department of Geology
University of New Mexico
200 Yale, NE
Albuquerque, NM 87131

George M. Hornberger
Department of Environmental Science
Clark Hall
University of Virginia
Charlottesville, VA 22903

Frank L. Parker
Department of Environmental
Engineering
Vanderbilt University
Nashville, TN 37235

D'Arcy A. Shock
233 Virginia
Ponca City, OK 74601

Distribution (Continued):

Peter B. Myers, Staff
Director (3)
National Research Council
Committee on Radioactive
Waste Management
2101 Constitution Avenue
Washington, DC 20418

Ina Alterman
Board on Radioactive Waste
Management
GF462
2101 Constitution Avenue
Washington, D. C. 20418

G. Ross Heath
College of Ocean
and Fishery Sciences
University of Washington
Seattle, WA 98195

Thomas H. Pigford
Department of Nuclear Engineering
4153 Etcheverry Hall
University of California
Berkeley, CA 94270

Patrick A. Domenico
Geology Department
Texas A & M
College Station, TX 77843-3115

Neville Cook
Rock Mechanics Engineering
Mine Engineering Dept.
University of California
Berkeley, CA 94270

Thomas A. Cotton
4429 Butterworth Place, NW
Washington, DC 20016

Robert J. Budnitz
President, Future Resources
Associates Inc.
2000 Center Street
Suite 418
Berkeley, CA 94704

C. John Mann
Department of Geology
245 Natural History Bldg.
1301 West Green Street
University of Illinois
Urbana, IL 61801

Charles D. Hollister
Dean for Studies
Woods Hole Oceanographic
Institute
Woods Hole, MA 02543

Benjamin Ross
Disposal Safety, Inc.
Suite 600
1629 K Street NW
Washington, D.C. 20006

Christopher Wipple
Electric Power Research Institute
3412 Hillview Avenue
Palo Alto, CA 94303

Tech. Reps., Inc. (2)
5000 Marble NE
Suite 222
Albuquerque, NM 87110
Attn: D. Medina
J. Stikar

Studiecentrum Voor Kernenergie (1)
Centre D'Energie Nucleaire
Attn: A. Bonne
SCK/CEN
Boeretang 200
B-2400 Mol
BELGIUM

Atomic Energy of Canada, Ltd. (2)
Whiteshell Research Estab.
Attn: Peter Haywood
John Tait
Pinewa, Manitoba, CANADA
ROE 1LO

D. K. Mukerjee
Ontario Hydro Research Lab
800 Kipling Avenue
Toronto, Ontario, CANADA
M8Z 5S4

Distribution (Continued):

Jean-Pierre Olivier
OECD Nuclear Energy Agency
Division of Radiation Protection
and Waste Management
38, Boulevard Suchet
75016 Paris, FRANCE

Claude Sombret
Centre D'Etudes Nucleaires
De La Vallee Rhone
CEN/VALRHO
S.D.H.A. BP 171
30205 Bagnols-Sur-Ceze
FRANCE

Bundesministerium fur Forschung und
Technologie
Postfach 200 706
5300 Bonn 2
FEDERAL REPUBLIC OF GERMANY

Bundesanstalt fur Geowissenschaften
und Rohstoffe
Attn: Michael Langer
Postfach 510 153
3000 Hannover 51
FEDERAL REPUBLIC OF GERMANY

Hahn-Mietner-Institut fur
Kernforschung (1)
Attn: Werner Lutze
Glienicker Strasse 100
100 Berlin 39
FEDERAL REPUBLIC OF GERMANY

Institut fur Tieflagerung (4)
Attn: K. Kuhn
Theodor-Heuss-Strasse 4
D-3300 Braunschweig
FEDERAL REPUPLIC OF GERMANY

Kernforschug Karlsruhe (1)
Attn: K. D. Closs
Postfach 3640
7500 Karlsruhe
FEDERAL REPUBLIC OF GERMANY

Physikalisch-Technische Bundesanstalt
Attn: Peter Brenneke
Postfach 33 45
D-3300 Braunschweig
FEDERAL REPUBLIC OF GERMANY

D. R. Knowles
British Nuclear Fuels, plc
Risley, Warrington, Cheshire WA3 6AS
1002607 GREAT BRITAIN

Shingo Tashiro
Japan Atomic Energy Research
Institute
Tokai-Mura, Ibaraki-Ken
319-11 JAPAN

Netherlands Energy Research
Foundation
ECN (2)
Attn: Tuen Deboer, Mgr.
L. H. Vons
3 Westerduinweg
P.O. Box 1
1755 ZG Petten, THE NETHERLANDS

Svensk Karnbransleforsorjning AB
Attn: Fred Karlsson
Project KBS
Karnbranslesakerhet
Box 5864
10248 Stockholm, SWEDEN

Internal Distribution:

1 A. Narath
20 O. E. Jones
1510 J. W. Nunziato
1511 D. K. Gartling
1511 N. Bixler
1511 R. R. Eaton
1511 M. Martinez
1511 P. Hopkins
1521 R. D. Krieg
1521 J. G. Arguello
1521 H. S. Morgan
1524 M. Stone
3200 N. R. Ortiz
6000 D. L. Hartley
6230 W. C. Luth
6232 W. R. Wawersik
6233 T. M. Gerlach
6233 J. L. Krumhansl
6300 R. W. Lynch
6310 T. O. Hunter
6310 G. E. Barr
6311 A. L. Stevens
6312 F. W. Bingham
6313 T. Blejwas
6315 P. C. Kaplan
6315 L. E. Shephard
6316 R. P. Sandoval
6317 S. Sinnock
6320 J. E. Stiegler
6340 W. D. Weart
6340 S. Y. Pickering
6341 D. P. Garber
6341 R. L. Hunter
6341 R. D. Klett
6341 R. C. Lincoln
6341 Sandia WIPP Central Files (100)
6342 D. R. Anderson (25)
6342 B. L. Baker
6342 S. Bertram-Howery (25)
6342 K. Brinster
6342 A. Gilkey
6342 L. S. Gomez
6342 R. Guzowski
6342 W. Harrison
6342 H. Iuzzolino
6342 M. G. Marietta (35)
6342 R. R. Rechard
6343 T. M. Schultheis
6344 R. L. Beauheim
6344 P. B. Davies
6344 E. Gorham-Bergeron
6344 S. J. Finley
6344 A. L. Jensen
6344 R. Z. Lawson
6344 M. D. Siegel
6345 L. Brush
6345 B. M. Butcher
6345 A. R. Lappin
6345 M. A. Molecke
6345 D. E. Munson
6345 K. L. Robinson
6346 D. J. Borns
6346 S. J. Lambert
6346 E. J. Nowak
6346 J. R. Tillerson
6346 T. M. Torres
6400 D. J. McCloskey
6415 J. Campbell
6415 R. M. Cranwell
6415 J. C. Helton
6415 R. L. Iman
6415 M. Tierney
6416 E. Bonano
6416 M. Piepho
6416 M.S.Y. Chu
7100 C. D. Broyles
7110 J. D. Plimpton
7120 M. J. Navratil
7125 R. L. Rutter
7125 J. T. McIlmoyle
7130 J. O. Kennedy
7133 O. Burchett
7133 J. W. Mercer
7135 P. D. Seward
8524 J. A. Wackerly (SNLL Library)
3141 S. A. Landenberger (5)
3151 W. I. Klein (3)
3154-1 C. L. Ward (8) for DOE/OSTI

DO NOT MICROFILM
COVER